ABSTRACT

Title of Document: Metabolic Acid Transport in Human Retinal Pigment Epithelium

Jeffrey Adijanto, Doctor of Philosophy, 2010

Directed By: Associate Professor Nam Sun Wang, Department of Chemical and Biomolecular Engineering

At the back of our eyes, photoreceptors capture light and convert it into electrical signals that we perceive in our brain as vision. Photoreceptor function is energy expensive, even more so than many other processes in the body. Furthermore, photoreceptor metabolism increases in the dark and releases more metabolic by-products (CO_2, lactic acid, and H_2O) into the photoreceptor extracellular space (SRS). The retinal pigment epithelium (RPE) maintains photoreceptor health by transporting these metabolic acids from the SRS to the choroidal blood supply. By using native and cultured fetal human RPE, we show that the apical membrane is significantly more permeable to CO_2 than the basolateral membrane. This feature traps CO_2 in the cell and drives carbonic anhydrase (CA)-mediated hydration of CO_2 into HCO_3^-, which is subsequently transported out of the basolateral membrane by a Na^+-linked HCO_3^- co-transporter (NBC). This process increases net steady-state fluid absorption, thus maintaining retinal adhesion to the RPE.

Oxidative metabolism generates significantly more ATP than glycolysis, but photoreceptors derive ≈ 50% of their total ATP consumed from glycolysis due to the low oxygen level at the photoreceptor inner segment. Furthermore, lactic acid production and release into the SRS almost doubles in the dark. We show that the RPE transports lactic acid from the SRS via a proton-linked monocarboxylate transporter (MCT1), and this process activates pH_i-regulatory mechanisms at the RPE apical membrane: Na^+/H^+ exchanger (NHE) and Na^+-linked HCO_3^- transporters (NBC1 & NBC3). These mechanisms also facilitate MCT1-mediated lactic acid transport by preventing buildup of a proton-gradient across the RPE apical membrane.

We show that an increase in SRS CO_2 or lactic acid level causes RPE cell swelling. The RPE alleviates swell-induced osmotic stress by activating apical membrane K^+-channel (Kir 7.1) and basolateral membrane Cl^--channel (ClC-2), which drives KCl (and fluid) out of the cell to decrease cell volume. In this study, we identified the cellular mechanisms in RPE that prevent acidosis and fluid accumulation in the SRS caused by increased photoreceptor metabolism in the dark. These homeostatic processes maintain the close anatomical relationship between photoreceptors and RPE, thus protecting photoreceptor health and preserving visual function.

METABOLIC ACID TRANSPORT IN HUMAN RETINAL PIGMENT EPITHELIUM

By

Jeffrey Adijanto

Dissertation submitted to the Faculty of the Graduate School of the
University of Maryland, College Park, in partial fulfillment
of the requirements for the degree of
Doctor of Philosophy
2010

Advisory Committee:
Professor Nam Sun Wang, Chair
Professor Sheryl H. Ehrman
Professor Srinivasa R. Raghavan
Professor Sheldon S. Miller
Professor Keith E. Herold, Dean's Representative

Dedication

This work is dedicated to my Mom and Dad, Rusuanti and Winoto,

to my brothers, Lawrence and Raymond,

and to the love of my life, Melissa.

Acknowledgements

This dissertation will not be complete without properly thanking my advisors, Dr. Sheldon Miller, Dr. Sarah Sohraby, Dr. Nancy Philp, and Dr. Nam Sun Wang, whose guidance, patience, and excellent mentorship have taught me what it takes to be a scientist. Many colleagues contributed significantly to this project: Dr. Wan Qin helped perform microelectrode experiments; Dr. Rong Li performed protein detection and localization experiments; Tina Banzon performed fluid transport experiments. In addition, Jing Zhao is responsible for the maintenance of the RPE cell cultures used in virtually all experiments presented in this dissertation. I've had many ups and downs throughout the projects, but in those tough times, I received solace from my colleagues, who somewhat willingly listened to my rants and raves. Finally, I want to extend a special thanks to Dr. Miller, who provided me my second home in his laboratory, who taught me proper English and worked tirelessly on my manuscripts.

Table of Contents

List of Tables

List of Figures

CHAPTER 1 FIGURES

CHAPTER 2 FIGURES

CHAPTER 3 FIGURES

CHAPTER 4 FIGURES

CHAPTER 5 FIGURES

CHAPTER 6 FIGURES

List of Abbreviations and Symbols

(Ap)	apical (bath)
(Ba)	basal (bath)
ABCC1	multi-drug resistance protein 1
ace	acetate
ADP	adenosine diphosphate
AE	anion exchanger (e.g., AE1, AE2, AE3)
AMD	age-related macular degeneration
AMP	adenosine monophosphate
AQP1	aquaporin 1 (water channel)
ATP	Adenosine triphosphate
BCECF	2',7'-bis-(2-carboxyethyl)-5-(and-6)-carboxyfluorescein
β_{HCO3}	CO_2/HCO_3 buffering capacity
β_i	intrinsic buffering capacity
β_{total}	total intracellular buffering capacity
BZA	benzolamide
CA	carbonic anhydrase
CD147	MCT accesory protein (also called basigin)
CFTR	cystic fibrosis transmembrane conductance regulator
cGMP	cyclic guanosine monophosphate
ClC-2	Chloride channel
CPE	choroid plexus epithelium
CSF	cerebrospinal fluid
D_{Apical}	diffusion coefficient of CO_2 across the apical membrane
D_{Basal}	diffusion coefficient of CO_2 across the basolateral membrane
DIDS	4,4'-Diisothiocyanatostilbene-2,2'-disulfonate
DZA	dorzolamide
E_A	apical membrane net reversal potential
E_B	basolateral membrane net reversal potential
EMT	epithelial-mesenchymal transition
EZA	ethoxyzolamide
g_A	apical membrane net conductance
g_B	basolateral membrane net conductance
HEPES	4-(2-hydroxyethyl)-1-piperazineethanesulfonic acid
hfRPE	human fetal retinal pigment epithelium
HIF-1α	hypoxia inducible factor 1 alpha
I_S	shunt current
JAM	junctional adhesion molecules
J_V	steady-state fluid absorption rate
Kir 7.1	inwardly rectifying potassium channel isoform 7.1
Lac	lactate
MCT	monocarboxylate transporter (e.g., MCT1, MCT3, MCT4)
MEM	minimum essential medium eagle (culture media)

mOsm	milliosmole
MRP1	multi-drug resistance protein 1
NBC	sodium bicarbonate co-transporter (e.g., NBC1, NBC3, NBC4)
NHE	sodium hydrogen exchanger
NKCC1	sodium potassium chloride co-transporter isoform 1
NMDG	N-methyl-D-glucamine
P	relative CO_2 permeability at the apical vs. basolateral membrane
P1	apical lactate induced V_A & V_B responses 1 (depolarization)
P2	apical lactate induced V_A & V_B responses 2 (hyperpolarization)
pCMBS	p-chloromercuribenzenesulfonic acid
PEDF	pigment epithelium-derived factor
pH_i	intracellular pH
pro	propionate
PVR	proliferative vitreoretinopathy
pyr	pyruvate
R1	apical lactate induced pH_i-response 1 (acidification)
R2	apical lactate induced pH_i-response 2 (alkalinization)
R_A	apical membrane resistance
R_B	basolateral membrane resistance
RPE	retinal pigment epithelium
R_S	shunt resistance (tight junction resistance)
R_T	total tissue resistance
siRNA	small interfering RNA
SMCT	sodium-coupled monocarboxylate transporter
SRS	subretinal space
TCA	tricarboxylic acid cycle (citric acid cycle)
TEP	transepithelial potential
TGF-β	transforming growth factor beta
TJ	tight junctions
V_A	apical membrane voltage
V_B	basolateral membrane voltage
VEGF	vascular endothelial growth factor
Zip	Zn^{2+} ion channels
ZO-1	zona occludens 1

CHAPTER 1: Introduction and Background

Section 1.1 – Overview

Our view of the external world begins at the photoreceptors, which capture light quanta and convert them into electrical signals that are transmitted to and interpreted in our brain as vision. This event involves a large amount of coordination between many different specialized cells within the retina, which continuously integrates, process, and transmit the visual signals to the brain (Yau, 1994; Lamb & Pugh, 2004; Stephen *et al.*, 2008). However, photoreceptor function requires a large amount of energy, even more so than the brain. Energy (as ATP) is generated by mitochondria that are densely packed at the junction between photoreceptor inner and outer segments (Stone *et al.*, 2008). As a result, metabolic waste-products (i.e., CO_2, lactic acid, and water) are released into the extracellular space that surrounds the photoreceptors – subretinal space (SRS). In the human eye, the SRS has a very small volume (≈ 10 μL), thus even small accumulations of metabolic acids within the SRS can cause acidosis and increased osmotic pressure – both of which can be detrimental to photoreceptor function. It has been hypothesized that the retinal pigment epithelium (RPE), a specialized monolayer of cells adjacent to the photoreceptors (Fig. 1-1), prevents these potentially catastrophic conditions by actively transporting these photoreceptor-generated metabolic by-products from the SRS into the choroid. However, the mechanisms involved in this process have been unclear.

The goal of this thesis is to identify and understand the various mechanisms involved in CO_2, lactic acid, and water transport in human RPE. We used a primary cell culture model of fetal human RPE (Chapter 1), which has been shown to closely mimic

physiological and morphological characteristics of the native tissue (Lin *et al.*, 1992; Quinn & Miller, 1992; la Cour *et al.*, 1994; Quinn *et al.*, 2001; Maminishkis *et al.*, 2006; Adijanto *et al.*, 2009; Wang *et al.*, 2010). To study RPE pH regulatory mechanisms involved in CO_2 and lactic acid transport, intracellular pH (pH_i) in human RPE was measured by using a pH_i-sensitive fluorescence dye (Chapter 2). The transepithelial potential (TEP) was recorded with a pair of calomel electrodes linked to agar bridges placed in apical and basal baths (Chapter 2). Recording TEP is a highly sensitive method to detect acute (millisecond) changes in apical or basolateral membrane voltage (V_A & V_B) that reflects ion channel or transporter activity. In some experiments, we placed a reference microelectrode within the cell to record changes in V_A & V_B independently (Chapter 2). Combining these recording techniques with pharmacological interventions (see Table 2-4) and other maneuvers allows us to produce unequivocal physiological data on human RPE transporters and channels (Chapters 3, 4, & 5). Understanding the normal physiological role of mechanisms involved in metabolic acid transport provides a first critical step in understanding the pathophysiology of human ocular diseases. This analysis is required for the development of appropriate animal models suitable for pre-clinical experiments that can lead to phase I clinical trails and facilitate the development of therapeutic interventions and strategies for disease prevention.

This new work is described in three main chapters: (1) CO_2/HCO_3 transport in RPE (Chapter 3); (2) lactate transport in the absence of CO_2/HCO_3 (Chapter 4); (3) lactate transport and its interactions with HCO_3-transport mechanisms (Chapter 5). In Chapter 6, we present ideas for future projects and describe some supporting preliminary data.

Section 1.2 - Behind every successful retina is an intact retinal pigment epithelium

In 2002, 2.5% (160 million) of the world's total human population was visually impaired, with 0.6% being completely blind (www.who.int/en/). The consequences of vision loss are severe: you lose a sense of yourself and the world around you. A reduced ability to independently perform essential daily functions diminishes an individual's quality of life and imposes a burden on one's family and the community. The RPE is involved in many vision-impairing diseases. For example, age-related macular degeneration (AMD) is the leading cause of blindness among the elderly (> 55 years) in the US and developed countries world-wide (Congdon *et al.*, 2004).

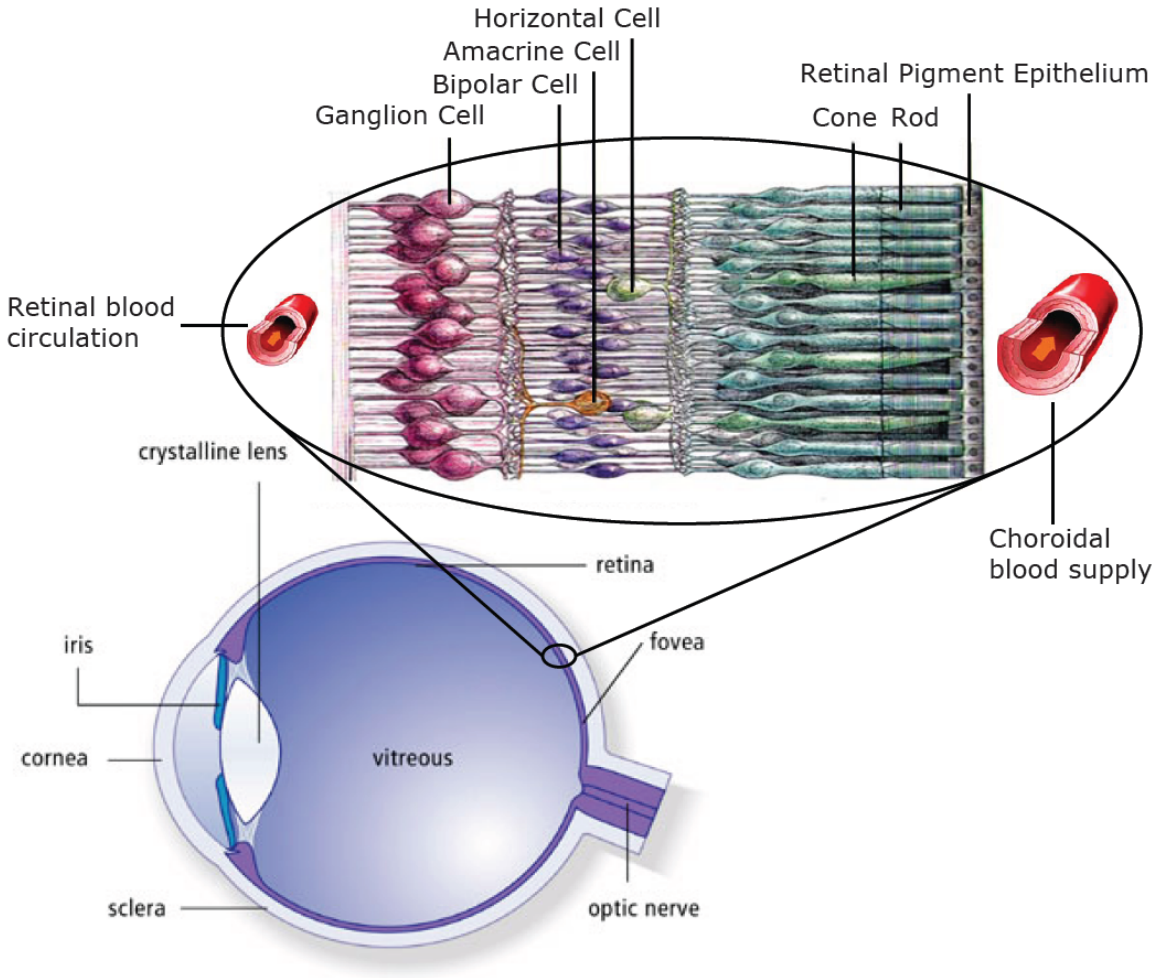

Fig. 1-1: Anatomy of the eye: the neural retina and retinal pigment epithelium.

Light enters the eye through the cornea and passes through the lens and vitreous onto the retina, where it is absorbed by the visual pigment within the photoreceptors (rods and cones) (Fig. 1-1). The capture of a photon by the visual pigment activates visual phototransduction; a cascade of events that induces a rapid change in photoreceptor membrane potential (Yau & Hardie, 2009). This response is subsequently transmitted across the retinal layers and out of the retinal ganglion cells into the brain (Fig. 1-1). The rest of the retina serves to fine-tune and regulate the electrical input from the photoreceptors (bipolar, amacrine, and horizontal cells), and to protect and nourish the retinal cells (Müller cells) (Oyster, 1999). The retinal pigment epithelium (RPE) separates the photoreceptor from its major blood supply (choroid) and provides critical support to retinal photoreceptor function (Gallemore *et al.*, 1998; Hughes *et al.*, 1998; Strauss, 2005).

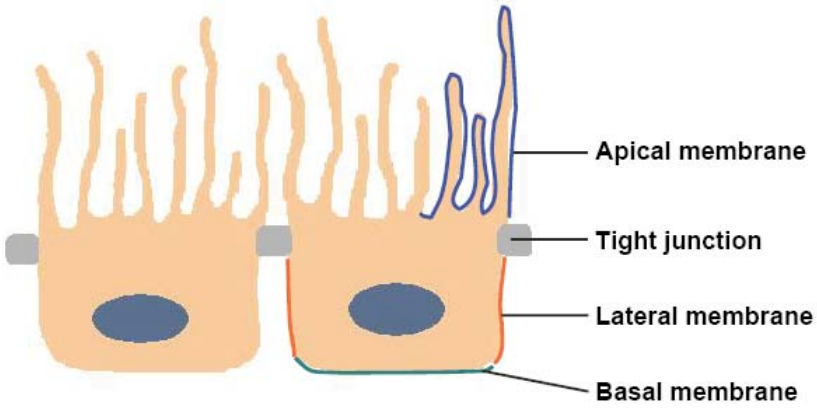

Fig. 1-2: Schematic of retinal pigment epithelium cells depicting apical and basolateral membrane separation by tight junctions.

Like other epithelia, the RPE is a polarized monolayer – its apical (facing photoreceptors) and basolateral (facing choroid) membranes are separated by tight and adherens junction

that link individual RPE cells to adjacent cells to form a confluent monolayer of cells (Fig. 1-2) (Nelson, 2003; Burke, 2008). The RPE apical and basolateral membranes are separated by tight junctions, which help establish cell polarity by acting as a "fence" that segregates the proteins that are trafficked to either the apical or basolateral membranes (Shin *et al.*, 2006; Terry *et al.*, 2010). RPE cell polarity is necessary for material (e.g., nutrients, metabolic by-products, growth factors) exchange and transport between photoreceptors, RPE, and choroid (Hughes *et al.*, 1998; Rizzolo, 2007).

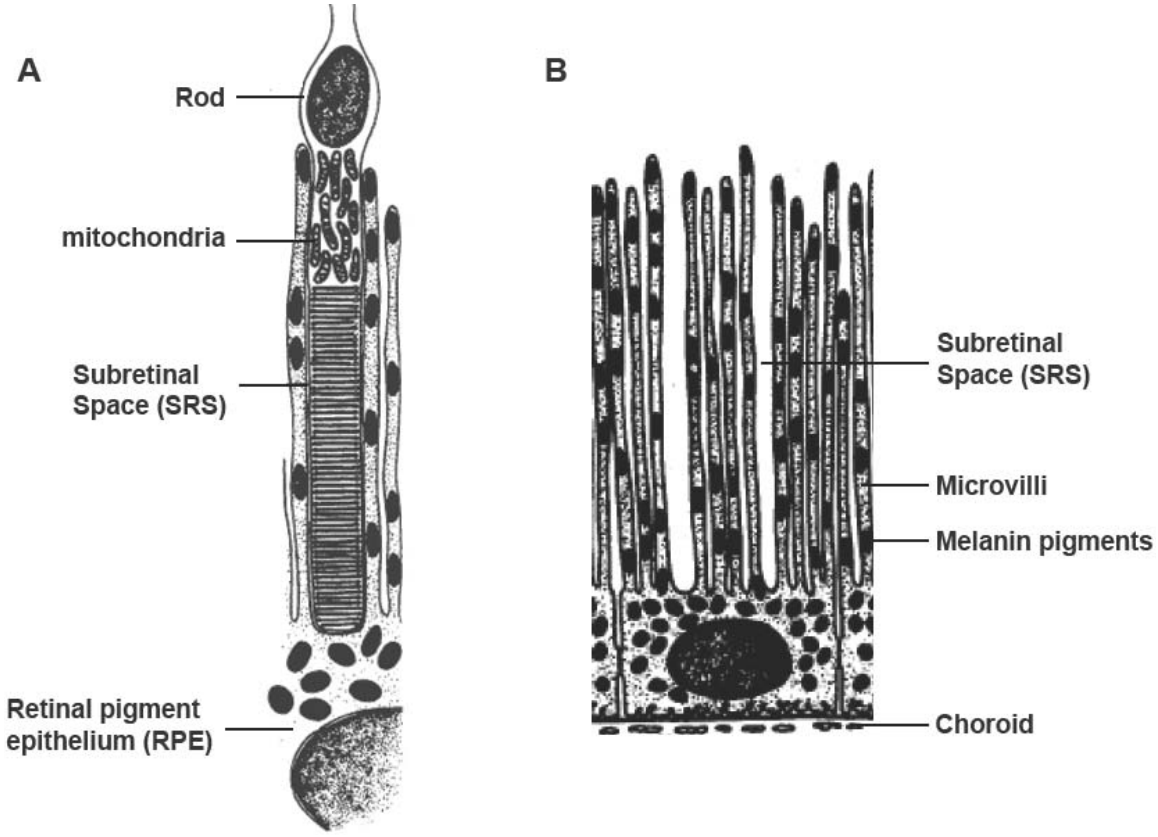

Fig. 1-3: Anatomical relationship between retinal pigment epithelium and photoreceptor (Miller & Steinberg, 1977).

To facilitate this process, the RPE apical membrane has numerous microvilli that ensheathes the outer segments of the photoreceptors (Fig. 1-3). This anatomical structure

increases the apical membrane surface area in contact with the SRS, thus facilitating RPE-photoreceptor interactions (e.g., material exchange and transport) due to the high surface/volume ratio. The RPE apical membrane and photoreceptors are not in physical contact; they are separated by a small volume (≈ 10 μL in human) of extracellular space (subretinal space; SRS), whose ionic and pH homeostasis is maintained by active and passive transport of solute and fluid across the RPE. The RPE basolateral membrane faces the Bruch's membrane and an extensive network of blood vessels (choriocapillaries) that form the choroidal blood supply (Fig. 1-4). The choroid has normally high blood flow rate; it accounts for ≈ 85% of blood supply to the eye (Alm & Bill, 1973; Bill, 1975). As such, it constitutes the sole blood supply for retinal photoreceptors; the RPE transports nutrients, ions, fluid, and metabolic byproducts between photoreceptors and choroid (Hughes *et al.*, 1998).

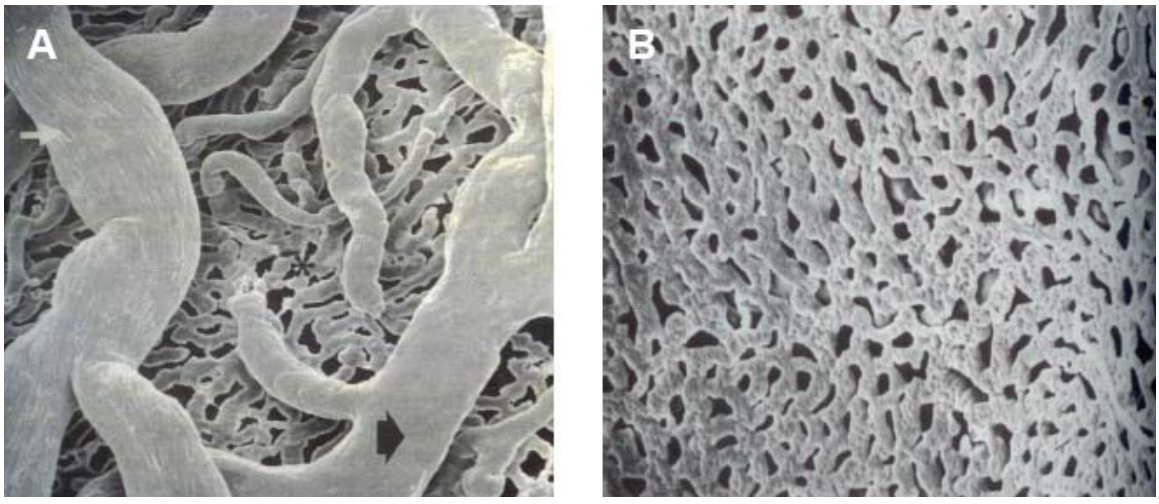

Fig. 1-4: The choroidal blood supply (Olver, 1990). (A) Choroidal vasculature viewed from the scleral side, showing arterioles (e.g., white arrow), venules (e.g., black arrow), and choriocapillaris (asterisk). (B) Choriocapillaris viewed from the retinal side.

Besides solute and fluid transport, the RPE also mediates important visual functions such as the retinal cycle (Rando, 1991; Lamb & Pugh, 2004), where retinal (vitamin A component of the visual pigment) is constantly cycled between the photoreceptors and the RPE to regenerate the visual pigment (rhodopsin) and maintain photoreceptor photoexitability. In addition, the photoreceptors are highly susceptible to photodamage, thus accumulating toxic amounts of oxidized proteins and lipids within the photoreceptor discs, which are continuously shed and replaced at a high turnover rate (Nguyen-Legros & Hicks, 2000; Kevany & Palczewski, 2010). The RPE phagocytose shed photoreceptor discs and recycle its components back to the photoreceptor cilium – where new photoreceptor discs are synthesized. Failure of the RPE to phagocytose photoreceptor discs results in photoreceptor degeneration in rats (Vollrath *et al.*, 2001) and in humans (Koenekoop, 2007). The RPE also secretes a wide variety of growth factors in a polarized manner to the neural retina (e.g., pigment epithelium-derived factor (PEDF)) and to the choroid (e.g., vascular endothelial growth factor (VEGF)); these growth factors help maintain the structural integrity of the neural retina and the choroidal vasculature (Ishida *et al.*, 1997; Blaauwgeers *et al.*, 1999; Jablonski *et al.*, 2000; King & Suzuma, 2000; Schlingemann, 2004; Marneros *et al.*, 2005). Loss of RPE function leads to photoreceptor degeneration and visual impairment; RPE damage leads to retina and choroid degeneration (Del Priore *et al.*, 1995; Litchfield *et al.*, 1997; Aramant & Seiler, 2004).

Section 1.3 – The retina and its high metabolism in light and in the dark

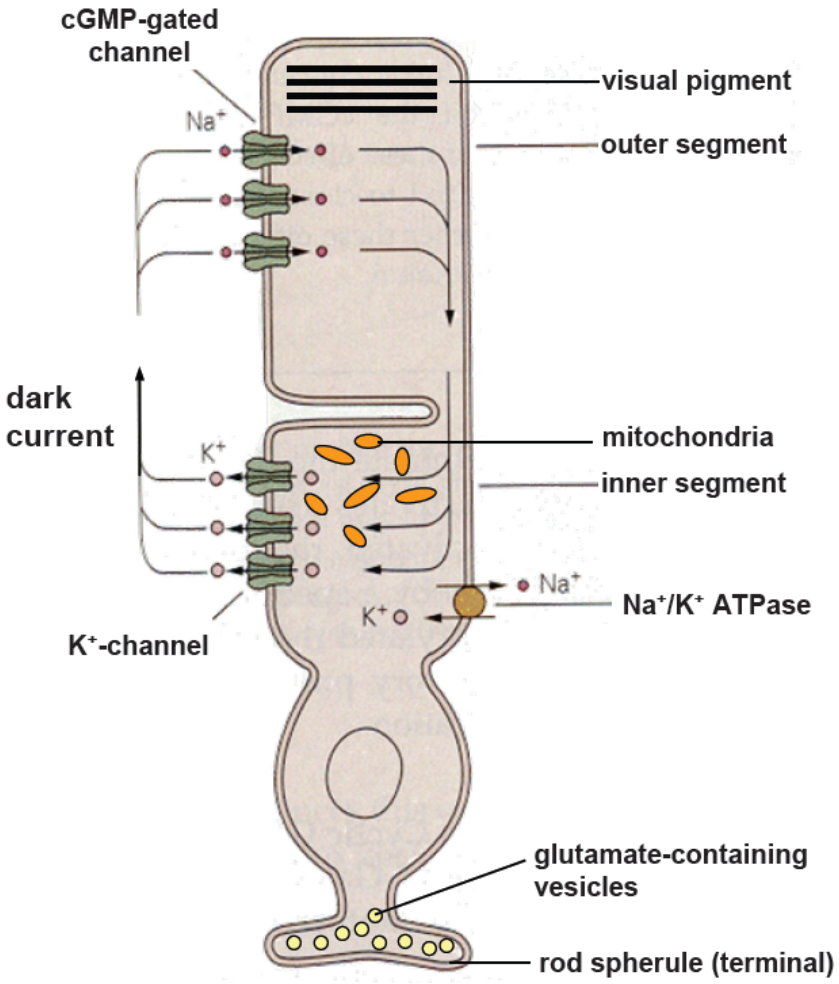

Fig. 1-5: Schematic of rod photoreceptor: The dark current circulates between the inner and outer segments.

Metabolic activity in the photoreceptors is among the highest of all human tissue (Wangsa-Wirawan & Linsenmeier, 2003); this energy is required to fuel phototransduction and to regenerate new photoreceptor discs (Kimble *et al.*, 1980; Yu & Cringle, 2001). The photoreceptor is a polarized cell (Fig. 1-5); it expresses cGMP-gated cation (85% Na^+ and 15% Ca^{2+}) channels at the outer segments and a K^+-selective channel and the electrogenic Na^+/K^+ ATPase at the inner segment. The polarized

distribution of these channels allows for the circulation of a current around the inner and outer segments. This current (also called the dark current) is maximal in the dark; in light, phototransduction events lead to the depletion of cGMP at the outer segment, which causes the cGMP-gated cation channels to close (Yau & Hardie, 2009). The closure of these channels hyperpolarizes the photoreceptor membrane potential, which inhibits the release of glutamate neurotransmitter at the photoreceptor terminal (rod spherule or cone pedicle) into the synaptic cleft, where it activates 2nd order neurons such as bipolar cells and horizontal cells (Oyster, 1999). These electrical signals are subsequently transmitted to the retinal ganglion cells and into the brain.

The dark current relies on the high Na^+ gradient (inward) and a high K^+ gradient (outward) across the photoreceptor plasma membrane. If these ionic gradients were not continuously sustained, the dark current eventually drives both Na^+ and K^+ gradients into equilibrium, and the photoreceptors would no longer respond to photoexcitation. The $3Na^+/2K^+$ ATPase at the inner segment maintains the Na^+ and K^+ gradients across the plasma membrane by using the energy of an ATP molecule to drive three Na^+ ions out of the cell in exchange for two K^+ ions. A recent study estimated that ATP consumption by rod photoreceptor increases ≈ 4-fold in the dark (Okawa *et al.*, 2008). In darkness, large amount of ATP is needed to maintain the dark-current, which requires a high $3Na^+/2K^+$ ATPase activity at the inner segments (Ames *et al.*, 1992). In addition, ATP is used by Ca^{2+}-ATPase to recycle Ca^{2+} out of the cell (Okawa *et al.*, 2008). Activity of these ATPase pumps increases [ATP], and increases [ADP], [inorganic phosphate], and [AMP], which in turn activates glycolysis, the TCA cycle, and oxidative phosphorylation.

Most of the ATP used by the photoreceptors is produced by oxidative phosphorylation in mitochondria located at the junction between the inner and outer segment of the photoreceptor (Fig. 1-5) (Stone *et al.*, 2008). A recent study also provides evidence of mitochondria-independent oxidative phosphorylation at the photoreceptor disks (Panfoli *et al.*, 2009). In the dark-adapted eye, photoreceptor O_2 consumption (oxidative metabolism) and energy production increases to meet the high ATP demand (Wangsa-Wirawan & Linsenmeier, 2003) – this depletes O_2 in the SRS. Consistent with this notion, *in vivo* O_2-sensitive microelectrode experiments on the cat eye show that SRS $[O_2]$ levels is ≈ 0 mm Hg in the dark vs. ≈ 20 mm Hg in light (Wangsa-Wirawan & Linsenmeier, 2003). The depletion of local O_2 forces the photoreceptors to rely more on glycolysis (with lactate production) as a source of energy (Linsenmeier, 1986). Increased photoreceptor metabolism (aerobic and anaerobic) in the dark increases CO_2, lactic acid, and water release into the SRS. Metabolic acid accumulation in the SRS can cause acidosis that inhibits photoreceptor activity (Liebman *et al.*, 1984) and is detrimental to the health of surrounding cells (i.e., Müller cells, photoreceptors, and RPE). In addition, pathological conditions that compromise the ability of RPE to clear fluid from the SRS can cause abnormal fluid accumulation, resulting in retinal detachment and photoreceptor death (Stone *et al.*, 1999; Wickham *et al.*, 2006; Nakazawa *et al.*, 2007). The RPE protects the photoreceptors from these potentially destructive conditions in part by regulating pH- and ion- homeostasis of the SRS. Among its many functions, the RPE is responsible for the removal and delivery of metabolites to the choroidal blood supply.

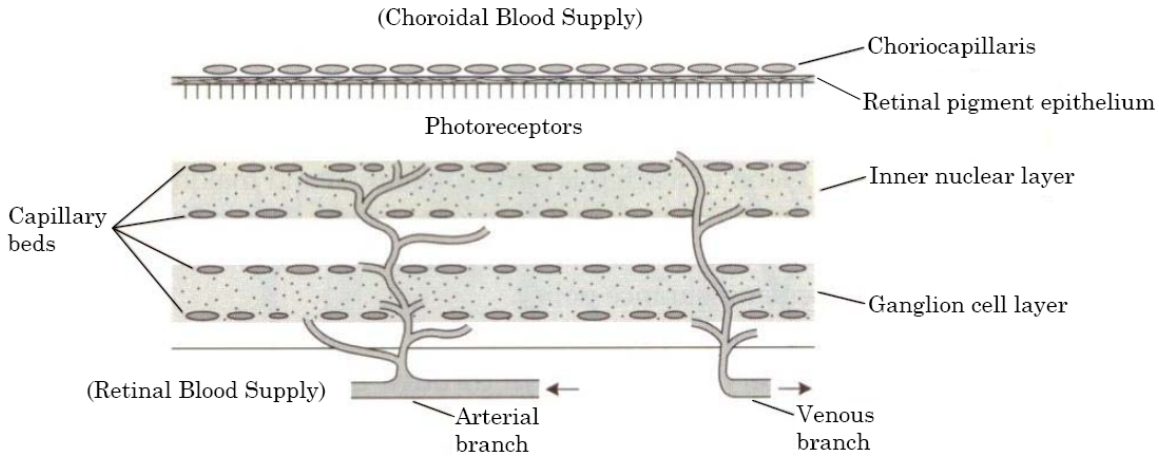

Fig. 1-6: Blood supply of the inner retina (Fig. 6-25 from Oyster, 1999).

The neural retina has two blood supplies (Fig. 1-6) (Oyster, 1999): (1) the retinal blood circulation is located at the inner retina; (2) the choroidal blood supply is located distally behind the RPE. Early studies demonstrated that choroidal circulation is the major blood supply for the photoreceptors; blocking choroidal circulation results in photoreceptor degeneration without affecting other retinal cells (Oyster, 1999). Studies in porcine eye also show that most lactate released from the retina is transported to the choroid by the RPE (Wang *et al.*, 1997b). The choroid is the main sink for the removal of most photoreceptor-generated metabolites: (1) blood flow rate in the choroid is significantly higher than in the retinal blood vessels (Alm & Bill, 1987); (2) metabolites released by the photoreceptor inner segments need to diffuse a shorter distance to the choroid (35 μm) than to the retinal capillary bed at the inner nuclear layer (70 μm) (Oyster, 1999).

Section 1.4 – Major ion and fluid transport mechanisms in RPE

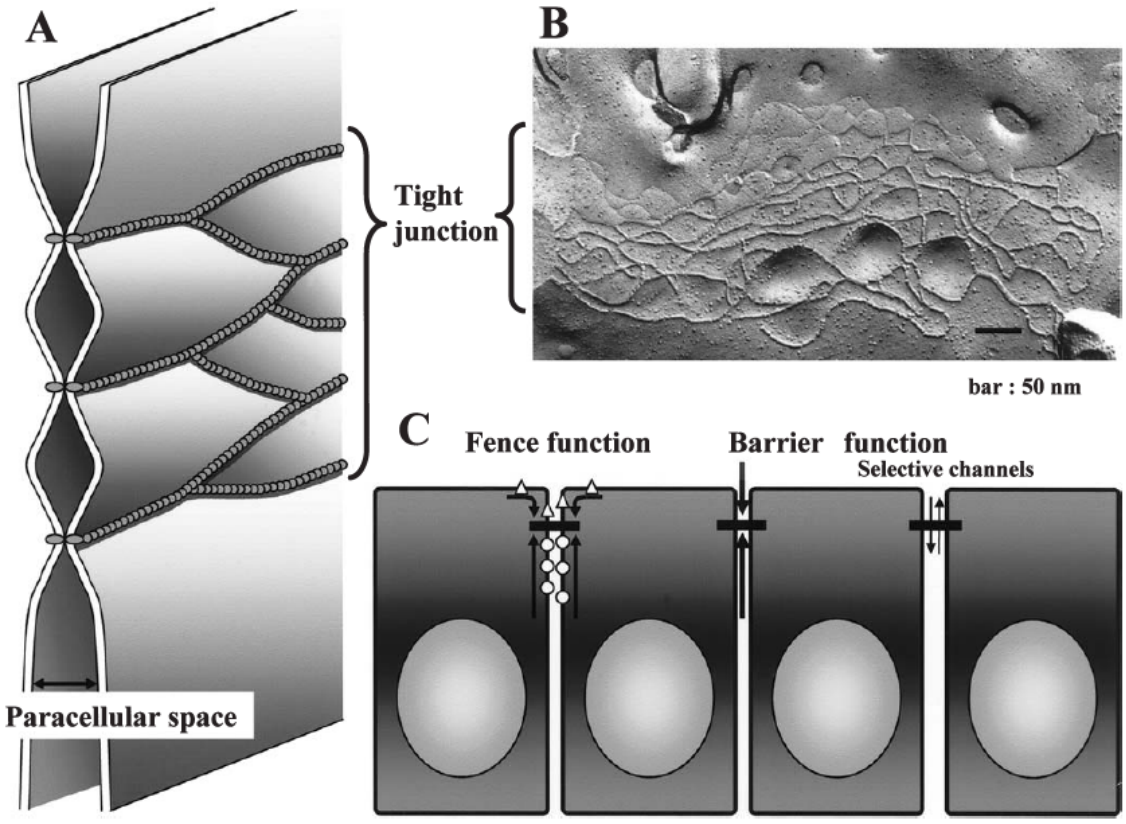

Fig. 1-7: Morphology and functions of tight junctions (Sawada *et al.*, 2003). (A) Schematic diagram of tight junction. (B) Tight junction strands on freeze-fracture replica. (C) The fence and barrier functions of tight junctions.

The RPE apical membrane is separated from the basolateral membrane by tight junctions (TJs) – TJs function as a fence that prevents intermixing of proteins and lipids between the apical and basolateral membrane domains (Fig. 1-7) (Rizzolo, 2007; Burke, 2008; Cereijido *et al.*, 2008). In addition, TJs also form a selectively permeable barrier at the intercellular spaces between epithelial cells and its adjacent neighbors, thus limiting free diffusion of certain ions and large molecules across the paracellular pathway. The TJ is mainly composed of three families of transmembrane proteins: (1) occludin; (2) claudins;

(3) junctional adhesion molecules (JAMs). These TJ proteins then associate with several peripheral membrane scaffolding proteins (e.g., ZO-1), which in turn interacts with the actin-cytoskeleton (Shin *et al.*, 2006). This interaction induces cytoskeleton assembly and reorganization within the cell and is critical for post-golgi protein delivery to its proper membrane domain (Etienne-Manneville & Hall, 2003; Nelson, 2003). These proteins allow the RPE to maintain a polarized distribution of ion channels, receptors, and transporters at its apical and basolateral membranes (Fig. 1-8) (Hughes *et al.*, 1989; Lin & Miller, 1994; Kenyon *et al.*, 1997; Hughes *et al.*, 1998; Yang *et al.*, 2008a; Adijanto *et al.*, 2009).

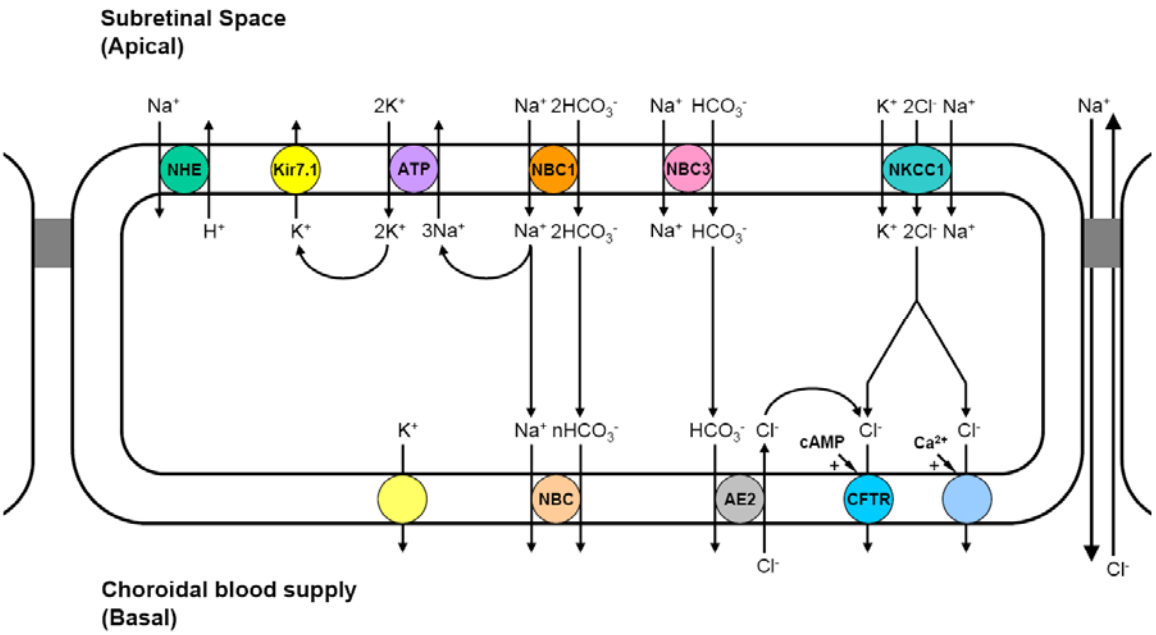

Fig. 1-8: Ion channels and transporters in retinal pigment epithelium.

The RPE is one of the two epithelia in the body that expresses the 3Na/2K ATPase (a classical marker of epithelial polarity) at the apical membrane (Okami *et al.*, 1990; Rizzolo, 1990; Gundersen *et al.*, 1991; Hughes *et al.*, 1998). The 3Na/2K ATPase is

essential for any transporting epithelium, because it maintains Na-gradient needed for vectorial (unidirectional) nutrient, ion, and fluid transport (Jaitovich & Bertorello, 2006). Besides the 3Na/2K ATPase, the RPE apical membrane contains a Na/H exchanger (NHE), an electrogenic $Na/2HCO_3$ co-transporter (NBC1), an electroneutral Na/HCO_3 co-transporter (NBC3), a Na/K/2Cl co-transporter (NKCC1), and an inwardly-rectifying K^+-channel (Kir 7.1). The basolateral membrane contains an electrogenic $Na/nHCO_3$ co-transporter (NBC; $n \geq 2$), a Cl/HCO_3 exchanger (AE2), a Ba^{2+}-sensitive K^+-channel, Ca^{2+}-activated Cl-channels, and cAMP-activated cystic fibrosis transmembrane conductance regulator (CFTR). This segregated arrangement of proteins on separate membranes allows the RPE to coordinate solute transport vectorially from one side of the tissue to another. The major ions in most biological systems are Na^+, K^+, Cl^-, and HCO_3^-. $[Na]_o$ (≈ 140 mM) and $[Cl]_o$ (≈ 120 mM) levels are high in the extracellular space, but are low in RPE cytosol ($[Na]_i \approx 15$ mM and $[Cl]_i \approx 70$ mM respectively). In contrast, [K] is high in RPE cytosol (≈ 85 mM), but low in the extracellular space (2-5 mM). $[HCO_3^-]$ is approximately equal inside and outside the cell (≈ 25 mM).

At the apical membrane, Cl is transported into the cell via the NKCC1, and Cl exits the basolateral membrane via Ca^{2+}-activated Cl-channels and CFTR. HCO_3 is transported across the apical membrane via NBC1 and NBC3 with the help of the strong Na-gradient. HCO_3 is transported out of the basolateral membrane via NBC and AE2 (a Cl/HCO_3 exchanger). Na enters the cell from the apical membrane via NKCC1 and NBC1. Although some of these Na is recycled out of the apical membrane via the 3Na/2K ATPase, the unrecycled Na leaves the basolateral membrane via the basolateral

membrane NBC. Na-channels or its activity has not been detected in the RPE, NBC is currently the only known Na-transport pathway at the basolateral membrane. K enters the cell from the apical membrane via NKCC1 and 3Na/2K ATPase, but most (if not all) K is recycled out of the apical membrane via Kir 7.1 K-channel. Other K-channels at the basolateral membrane provides K^+ as a counter-ion for Cl^- and HCO_3^- efflux from the RPE. Although ions are transported across the RPE plasma membrane via transporters and channels, some ions (i.e., Na^+ and Cl^-) can also diffuse across the tight junctions (see Fig. 1-8). In the paracellular pathway, Na is absorbed (from apical to basal) and Cl is secreted (from basal to apical). In the resting state, the RPE transports NaCl and $NaHCO_3$ from the apical side to the basal side to drive isoosmotic fluid transport across the epithelium. In addition to osmotically driven fluid transport, other mechanisms of fluid transport have also been described (Zeuthen, 2000).

Carbonic anhydrases (CAs) are zinc-metalloenzymes that catalyze the conversion between CO_2 and HCO_3^- according to the following equation: $CO_2 + H_2O \leftrightarrow H_2CO_3 \leftrightarrow HCO_3^- + H^+$. Several isozymes of CAs found in the RPE (CA II, CA IV, CA IX, and CA XIV) has been shown in other systems to functionally interact with HCO_3-transporters such as NBC1, NBC3, AE1, AE2, AE3 (Cl/HCO_3 exchangers) in a functional complex known as the bicarbonate-transport metabolon (Sterling *et al.*, 2001; Alvarez *et al.*, 2003; Loiselle *et al.*, 2004; Nagelhus *et al.*, 2005; Morgan *et al.*, 2007; Casey *et al.*, 2009; Svichar *et al.*, 2009). In support of this metabolon theory, binding sites on AE1 and CA II for physical interactions with each other has been found (Vince *et al.*, 2000; Vince & Reithmeier, 2000). Further, CA II is activated when it is physically bound to AE1

(Scozzafava & Supuran, 2002). In RPE, several membrane-bound CAs (CA IV, CA XII, and CA XIV) are expressed exclusively at the apical surface (Wolfensberger *et al.*, 1994; Nagelhus *et al.*, 2005; Zhi *et al.*, 2007), suggesting CA involvement in HCO_3-transport at the apical membrane. Since the RPE functionally expresses several different HCO_3-transport proteins (i.e., NBCs and AE2) at the apical and basolateral membranes, it is possible that their activities are dependent on CAs as illustrated in Fig. 1-9. Since HCO_3-transport is linked to Na and Cl transport, the interactions between CAs and HCO_3-transporters is indicative of the involvement of CAs in steady-state fluid transport across the RPE.

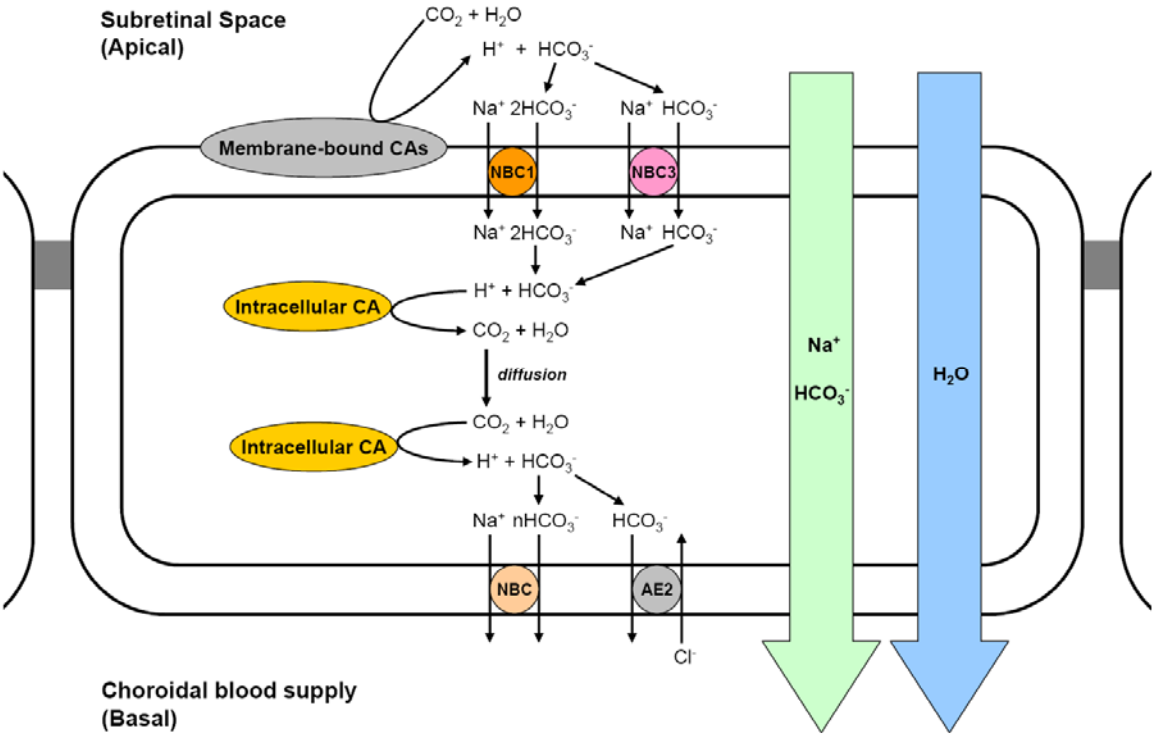

Fig. 1-9: Bicarbonate transport metabolon: HCO_3-transporters (i.e., NBCs) interact with carbonic anhydrases (CAs) to maximize HCO_3 transport across the RPE.

The close physiological relationship between HCO_3 and fluid-transport was demonstrated in frog RPE, where steady-state fluid-absorption was reduced by ≈ 70% following HCO_3-removal from the bathing solutions (Hughes *et al.*, 1984). Furthermore, the addition of a potent but non-specific CA-inhibitor, acetazolamide, has been shown to decrease steady-state fluid-transport in RPE. However, these *in vitro* results are in contrast to *in vivo* animal studies which suggest that acetazolamide (a non-specific CA-inhibitor) enhances retinal adhesion and SRS fluid clearance (Kita & Marmor, 1992; Wolfensberger *et al.*, 2000). In addition, clinical studies showed that some (but not all) patients with macular edema respond to acetazolamide treatment by increasing SRS fluid clearance (Cox et al., 1988; Fishman et al., 1989). This difference in the effect of CA inhibition on fluid transport *in vivo* and *in vitro* will be discussed (in section 3.8), but the underlying mechanisms remain to be determined.

There are a number of retinal degenerative diseases (e.g., uveitis, retinitis pigmentosa, diabetic retinopathy, age-related macular degeneration) that lead to abnormal accumulation of fluid within the retina and subsequent loss of visual acuity (Wolfensberger, 1999). Consequently, there is significant interest in identifying mechanisms by which small molecules such as acetazolamide can be utilized to activate the fluid transport "engine" of the RPE to eliminate this fluid. Its efficacy in the clinic depends on the extent to which the underlying disease damages the RPE or its transport capability.

Section 1.5 – Lactate transport in RPE

Lactate is generally considered as a metabolic waste by-product, which accumulates in organs within our body to cause lactic acidosis and muscle fatigue (Hermansen, 1981). Research over the past three decades demonstrate that lactate is an intermediate metabolic substrate that undergoes oxidative metabolism in cells (Gladden, 2004; Philp *et al.*, 2005; Kennedy & Dewhirst, 2010). The most well established example is the skeletal muscles, which contains type I oxidative fibers and type II glycolytic fibers. In this scheme, known as the lactate-shuttle model, type II fibers metabolize glucose into lactate upon exercise, which is directly taken up and oxidized by neighboring type I fibers (Peter *et al.*, 1971; Baldwin *et al.*, 1978). A similar lactate-shuttle mechanism was found between astrocytes and neurons in the brain, in which astrocytes generates lactate that is subsequently metabolized by the neighboring neurons to produce energy (Magistretti, 2006; Bergersen, 2007; Brown & Ransom, 2007; Pellerin *et al.*, 2007; Pellerin, 2008), but this relationship between astrocyte and neuron is controversial (Chih *et al.*, 2001; Gladden, 2004; Fillenz, 2005). In the retina, the lactate shuttling mechanism between Müller glia cells and photoreceptors has been described (Poitry-Yamate *et al.*, 1995; Poitry *et al.*, 2000): Müller cells metabolize glucose into lactate (Winkler *et al.*, 2000), which is taken up by photoreceptors to be used as substrate for oxidative metabolism. However this theory of metabolic coupling between Müller cells and photoreceptors is also controversial (Winkler *et al.*, 2004).

The retina is highly glycolytic. More than 80% of all glucose consumed by photoreceptors is converted to lactic acid (Wang *et al.*, 1997a; Wang *et al.*, 1997b;

Winkler *et al.*, 2008) indicating that the retina is highly dependent on glycolysis as a source of ATP, even in the presence of oxygen (Winkler *et al.*, 2000; Padnick-Silver & Linsenmeier, 2002; Winkler *et al.*, 2004). Therefore, regardless of whether lactate derives from glutamate-induced lactate release from Müller glia cells, or as a product of photoreceptor aerobic glycolysis (or both), large amounts of lactic acid are generated and released from the retina into the SRS in light and in dark. This is consistent with the high lactate concentration (≈ 4 - 13 mM) in the SRS compared to that in blood (≈ 1 mM) (Adler & Southwick, 1992).

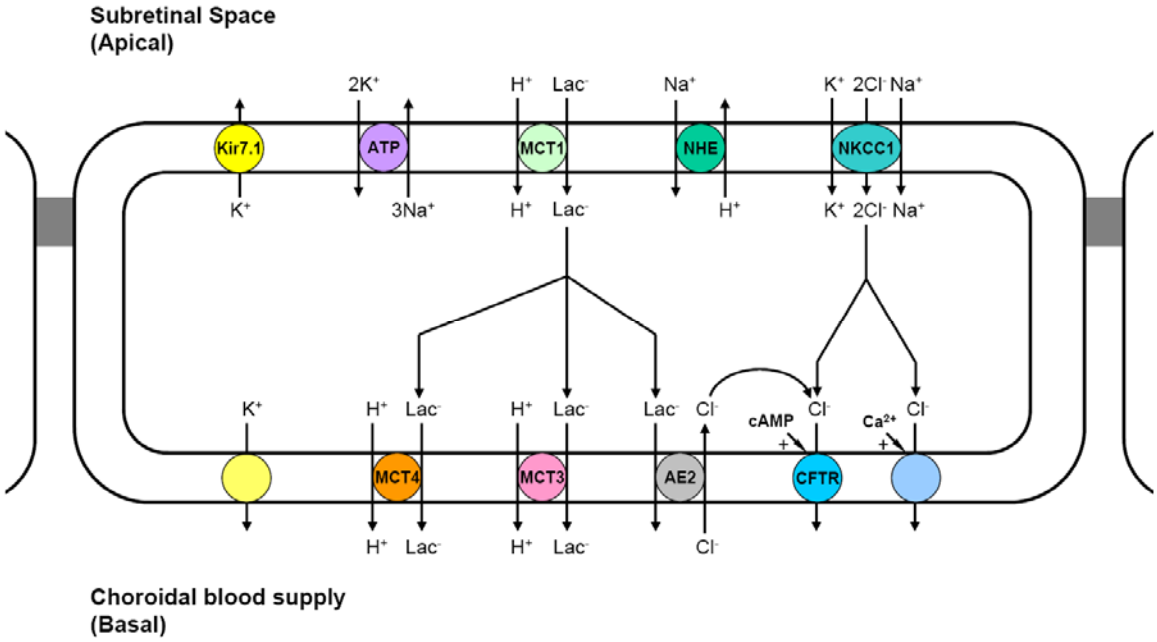

Fig. 1-10: Lactate transport in retinal pigment epithelium: MCT1 at the apical membrane mediates H^+-coupled lactate transport into the cell. At the basolateral membrane, lactate is transported out of the cell via MCT3, MCT4, and AE2.

Lactic acid has a low pKa (3.9) and it exists predominantly in ionic form at physiological pH (7.4). Thus although lactic acid may diffuse passively across the plasma membrane, lactate is transported much more quickly via H^+-coupled lactate transporters or anion-

exchangers. Early physiological studies showed that RPE expresses a proton-coupled lactate transporter (1:1 H^+:Lac^-) at the apical membrane in various native and cultured RPE preparations (bovine, porcine, frog, and human; see Fig. 1-10) (Kenyon *et al.*, 1994; la Cour *et al.*, 1994; Lin *et al.*, 1994; Zeuthen *et al.*, 1996). This apical membrane H/Lac co-transporter in RPE was identified as MCT1, the first member in the family of monocarboxylate transporters (Philp *et al.*, 2003b). Besides in RPE, MCT1 is also highly expressed in many other tissues in our body including skeletal muscle, heart, and brain (Bonen, 2001; Bonen *et al.*, 2006; Chiry *et al.*, 2006). At the RPE basolateral membrane, lactate is transported out of the cell via H/Lac co-transporters (MCT3 & MCT4) (Philp *et al.*, 2001; Philp *et al.*, 2003b) and a Cl/Lac anion exchanger (AE2) (Kenyon *et al.*, 1994).

The importance of lactate transport in the mammalian eye was demonstrated in mice lacking MCT1, MCT3, and MCT4 expression – these mice gradually lose photoreceptor function and were completely blind within two months after birth (Hori *et al.*, 2000; Philp *et al.*, 2003a). Further, the affliction of MCT3-null mice with altered visual function reaffirmed the importance of lactate transport in the eye, more specifically in the RPE (Daniele *et al.*, 2008).

CHAPTER 2: Materials and Methods

Section 2.1 – Human Fetal Retinal Pigment Epithelium (hfRPE) culture

Studying ion and fluid transport mechanisms of RPE using intact adult human RPE is highly impractical; adult human eyes are extremely difficult to obtain and are expensive if available (≈ $2000/pair). An alternative is to grow adult RPE cultures. However, culturing adult human RPE cells is complex and comes with many difficulties. For example, adult RPE cells are terminally differentiated and are non-mitotic, thus highly specialized culture media formulations supplemented with high levels of serum (10 – 20%) are needed to "coax" the RPE cells to proliferate (Valtink & Engelmann, 2009). In addition, culture conditions must also allow the RPE cultures to retain most of its *in vivo* characteristics. The development of RPE polarity and function *in vivo* are influenced by its interactions with the retina and the choroid (Rizzolo, 1991, 1999), which prompted the use of retinal or choroidal extracts in cell culture media to mimic *in vivo* conditions of the RPE (Hu & Bok, 2001; Engelmann & Valtink, 2004; Valtink & Engelmann, 2009). Nonetheless, typical RPE characteristics such as pigmentation and the cobblestone-like morphology are easily lost in cultures. Furthermore, RPE cell cultures have a tendency to dedifferentiate in a process called epithelial-mesenchymal transition into fibroblast-like cells with marked different morphological and physiological characteristics to that of RPE (MacDonald, 1994) (also see Chapter 6). There are also variations stemming from the production of retinal or choroid extracts and from the use of serum in the culture media. All these problems and complications results in large variations in the quality of human RPE cell cultures, which makes physiological studies with these cells difficult.

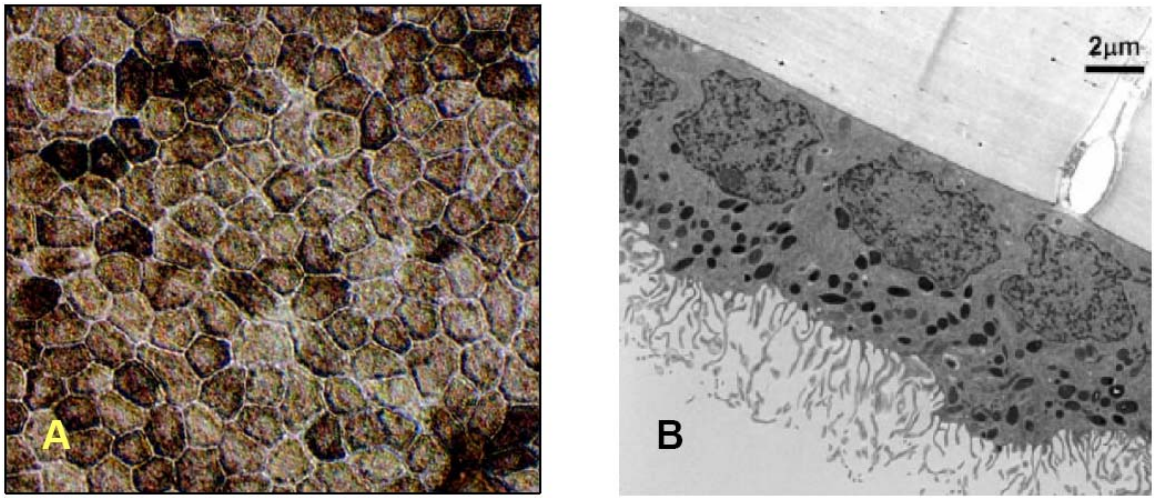

Fig. 2-1: Human fetal retinal pigment epithelium (hfRPE; 4 week old) cultured on porous plastic filter (Maminishkis *et al.*, 2006): (A) Micrograph of hfRPE. (B) Electron micrograph of hfRPE.

Early researchers observed that the success of human RPE culture decreases with increasing donor age (Engelmann & Valtink, 2004). Therefore, culturing RPE cells that are in the growth and development process should produce a more successful cell culture that is well-differentiated and retains *in vivo* characteristics. Indeed, the best characterized models of human RPE today are human fetal RPE cultures developed by Bok and Miller laboratories (Hu & Bok, 2001; Maminishkis *et al.*, 2006). Unlike Bok lab's hfRPE culture, the hfRPE culture developed by the Miller lab does not require any retinal extracts in the culture media. In their formulation, every component of the media is commercially available and well-defined. These culture conditions allows for the "mass production" of highly differentiated and confluent hfRPE monolayers (Fig. 2-1) that possess many characteristics found in native RPE such as steady-state fluid absorption, ion transport, CO_2/HCO_3 transport, tight-junction formation, and growth factor secretion (Maminishkis *et al.*, 2006; Li *et al.*, 2007; Economopoulou *et al.*, 2008;

Shi *et al.*, 2008; Adijanto *et al.*, 2009; Li *et al.*, 2009). A major disadvantage of using native adult RPE (bovine or human) in physiological studies is the occlusion of the basolateral membrane by the thick choroidal vasculature, which significantly reduces the accessibility of drugs or solutions to the basolateral membrane. Using cultured hfRPE monolayers eliminates this problem; hfRPE cells are grown on a thin polyethylene membrane with numerous pores (0.4 μm diameter).

Section 2.2 – Fluorescence imaging experiments

Cultured hfRPE monolayer was incubated (at room temperature and 5% CO_2) in control Ringer solution containing 8 μM BCECF-AM (30 minutes) for pH_i-imaging, or 8 μM Calcein-AM (30 minutes) for volume measurements, or 10 μM (1 hour) Fura-2-AM for calcium-imaging (Invitrogen Corp., CA). Following dye-incubation, the hfRPE was incubated for another 30 minutes in control Ringer for at least 30 min before mounting onto a modified Üssing chamber (surface-area = 7.1 mm^2). The Üssing chamber was mounted on the stage of a Zeiss axiovert-200 microscope equipped with a 20X plan-neofluar objective. The hfRPE was continuously perfused with Ringer solution (equilibrated with 5%/10%/85% $CO_2/O_2/N_2$ gas mixture at 34.5 ^oC) at a flow rate of 2 $ml \cdot min^{-1}$. Excitation photons (440/480 nm-for BCECF; 480 nm for Calcein; 350/380 nm for Fura-2) were generated by a xenon light source and the specific wavelengths were selected with a monochromator, Polychrome IV (Photonics, CA). The emission fluorescence (535 nm) was collected, amplified and converted into electrical signals by a photomultiplier tube (Thorn, EMI).

pH_i-calibrations were performed by perfusing high-K calibration solutions (at pH = 6.8, 7.2, and 7.6) containing 20 μM nigericin into both solution baths. The average calibration parameters were used to linearly correlate fluorescence intensity to intracellular pH (pH_i) for all pH-imaging experiments. Fig. 2-2 is a schematic representation of the fluorescence imaging set-up. Cell volume measurement with calcein was not a ratiometric, therefore the data was fitted and normalized to an exponential curve (fluorescence signal = Ke^{-bt}). Calibration was achieved by perfusing

control Ringer solutions (305 mOsm) with different osmolarities (i.e., 280 mOsm, 330 mOsm, and 355 mOsm) into both apical and basal baths. Fura-2 signals was calibrated by first perfusing both apical and basolateral membranes with Ca^{2+}-free Ringer solution (with 2 mM EGTA) before adding ionomycin (10 μM) into both solution baths. Next, control Ringer solution (1.8 mM Ca^{2+}) containing 10 μM ionomycin was added to both baths. After $[Ca^{2+}]_i$ reaches saturation, Ca^{2+}-free Ringer containing 5 mM $MnCl_2$ was added to quench Fura-2 fluorescence to reveal autofluorescence signals. For every experiment, autofluorescence levels were determined and subtracted from the data to obtain true Ca^{2+}-signals.

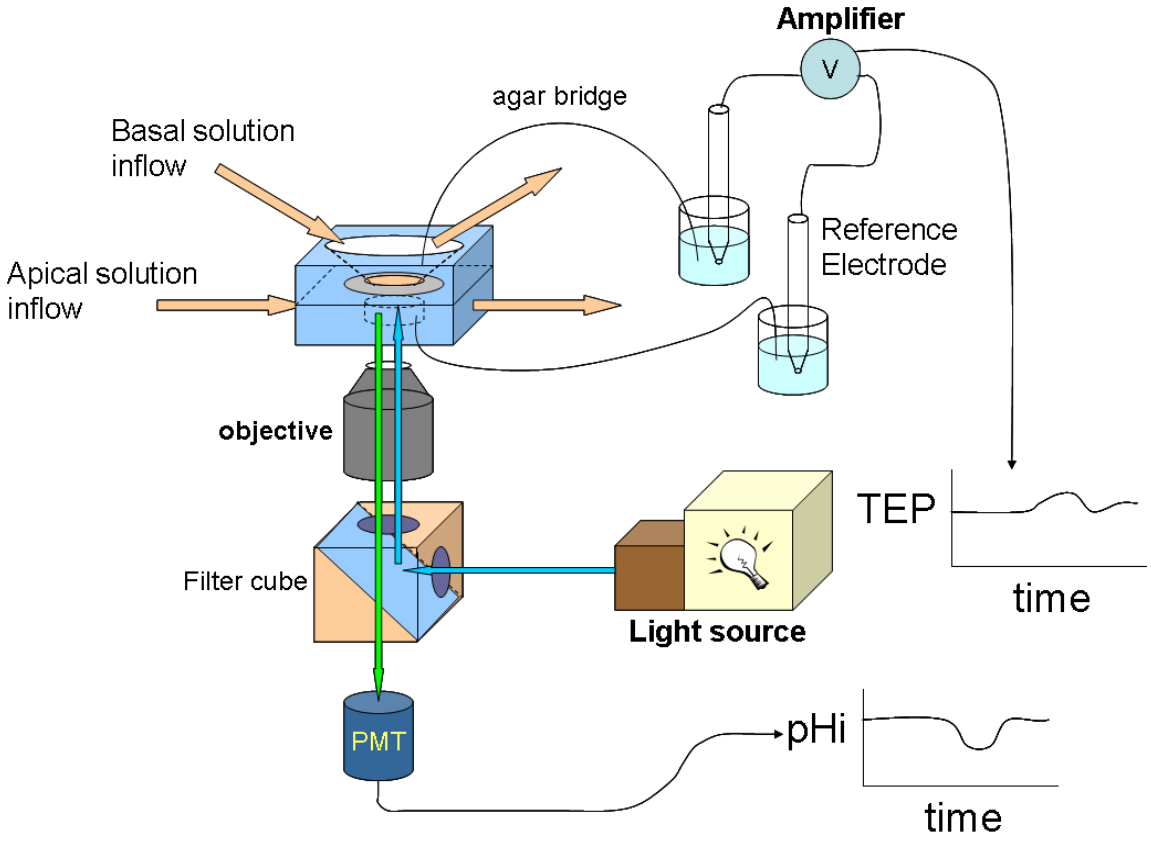

Fig. 2-2: Schematic of the fluorescence imaging and electrophysiology set-up.

Fluorescence dyes (i.e., BCECF, Fura-2, and calcein) are used in their ester-form (e.g., BCECF-AM), which are non-fluorescent but are cell permeable. The ester groups on BCECF-AM are cleaved by endogenous esterases within the cell, producing BCECF ions with multiple (4-5) negative charges. In its charged form, BCECF is membrane-impermeable. However, during the course of physiology experiments, fluorescence dye is lost through two main pathways: (1) photobleaching of the dye and (2) dye extrusion via an organic anion transporter (multi-drug resistant protein; MRP1 or ABCC1). Dye loss via photobleaching can be easily controlled by the following methods: (1) using a neutral-density filter (reduce light intensity); (2) controlling xenon-lamp intensity; (3) reducing exposure time and interval (20 ms exposure every 1.5 seconds). On the other hand, the control of dye extrusion via ABCC1 is more difficult and is the major cause of dye-loss in imaging experiments with hfRPE cells. This can be demonstrated by a simple test where excitation fluorescence was stopped for a long period of time (10 minutes) – fluorescence emission was reduced at the same rate with or without fluorescence excitation.

Fluorescence dye extrusion by ABCC1 is a function of two factors: (1) Ringer solution temperature (the higher the temperature, the faster the dye-leakage); (2) RPE viability (unhealthy or stressed RPE has a faster dye-leakage). Dye-loss is extremely fast at 37 ^{o}C. However, a low temperature reduces the activities of many proteins in the RPE – 34 ^{o}C strikes a good balance. When RPE cells experience prolonged periods of stress (e.g., alkalosis, acidosis, Na-free conditions), fluorescence dye-leakage was significantly faster. From these observations, it is tempting to speculate that either ABCC1 expression or

activity is upregulated by cell stress – alleviating cell stress should reduce dye-leakage. In support of this possibility, earlier pH_i-imaging experiments use Ringer solution supplemented with glutathione or glutaMAX™ (antioxidant) to help reduce dye-leakage. A more direct but effective method to prevent dye-leakage is the addition of probenecid, an ABCC1 inhibitor (Feller *et al.*, 1995; de Jong *et al.*, 2003), to all Ringer solution used in all imaging-experiments (Kenyon *et al.*, 1997). However, high concentrations of probenecid show slight inhibition of Cl/HCO_3 exchange (Zeidel *et al.*, 1986). Probenecid also inhibits SMCT (Coady *et al.*, 2004), a Na-linked lactate co-transporter expressed in RPE (Martin *et al.*, 2007). Therefore, a low concentration of probenecid (0.5 mM) is added to all Ringer solutions used in imaging experiments.

Section 2.3 – Intracellular buffering capacity

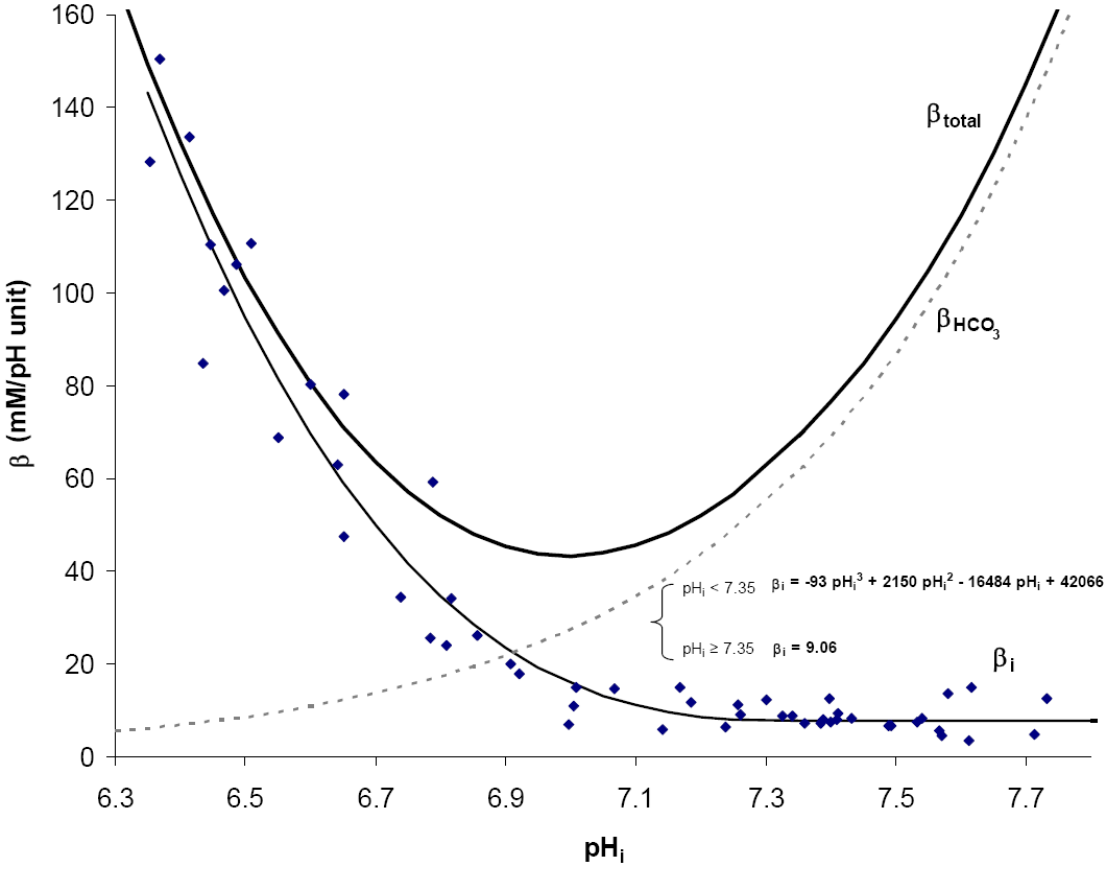

Fig. 2-3: Intrinsic buffering capacity of cultured hfRPE.

The intrinsic buffering capacity (β_i mM/pH units) of the hfRPE cells was determined by using a previously described method (Weintraub & Machen, 1989) and was fitted to a third-order polynomial: $\beta_i = -93.4\,pH_i^{\,3} + 2150.4\,pH_i^{\,2} + 16483.6\,pH_i + 42065.6$ for $pH_i < 7.35$, and for $7.35 \le pH_i \le 7.7$, $\beta_i = 9.06$. The total buffering capacity (β_{total}) was then calculated with the equation, $\beta_{total} = \beta_i + \beta_{HCO_3} = \beta_i + 2.3[HCO_3]_i$. $[HCO_3]_i$ was estimated from the Henderson-Hasselbalch equation with the assumption that intracellular CO_2 level is 5%. H^+-flux was determined by multiplying β_{total} by an estimate of the initial dpH_i/dt determined from the pH_i response.

Section 2.4 – Transepithelial potential and total tissue resistance

As described earlier, the RPE maintains a polarized distribution of different channels and transporters at its apical and basolateral membranes, which are separated by the tight junction. This results in different apical and basolateral membrane voltages (V_A and V_B), which gives rise to the transepithelial potential (TEP) of the RPE: TEP = $V_B - V_A$. Since V_A and V_B are directly affected by electrogenic (carrying net ionic charge) transport processes, the measurement of TEP provides a sensitive method to study ion channels and electrogenic transporters at the apical and basolateral membranes of the RPE. Early studies of epithelial electrophysiology showed that the electrical properties of the RPE can be simplified and analyzed in the form of an electrical circuit model as shown in Fig. 2-4 (Hughes *et al.*, 1998).

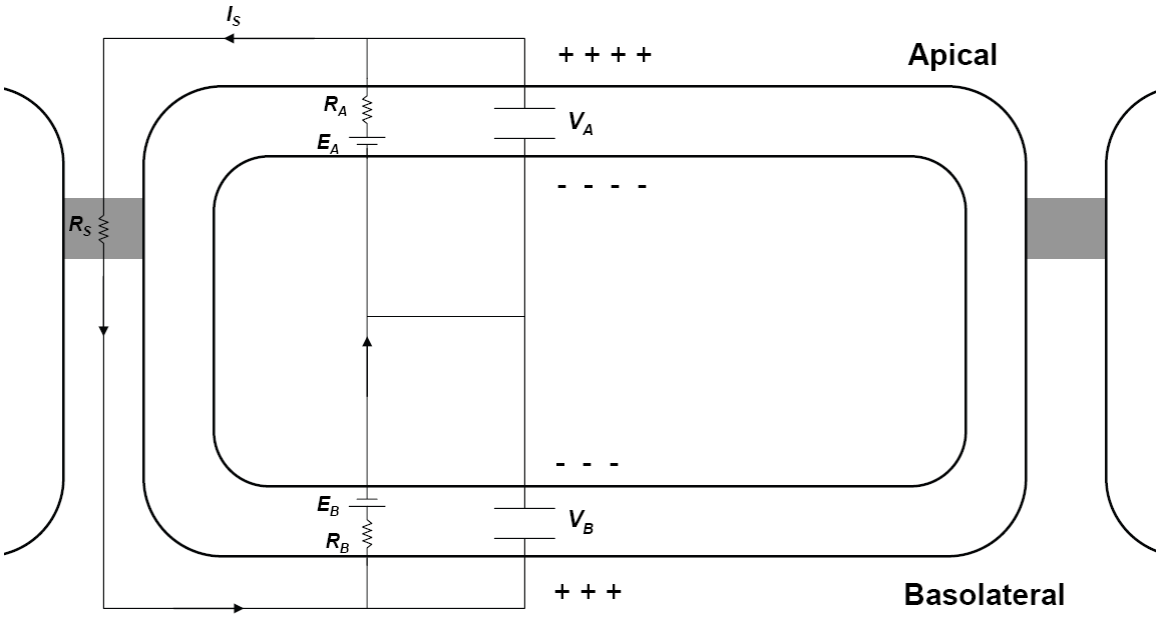

Fig. 2-4: Equivalent circuit of the retinal pigment epithelium.

From the circuit analysis, $V_A = E_A - I_S R_A$ and $V_B = E_B + I_S R_B$. E_A and E_B are the "batteries" of the apical membrane and basolateral membranes respectively. E_A is the combination of all potentials that derives from the ion concentration gradients and their respective ion channel conductivity at the apical membrane: $E_A = \frac{g_K E_K + g_{NBC1} E_{NBC1}}{g_K + g_{NBC1}}$.

g_K and g_{NBC1} are conductances of electrogenic processes (Kir7.1 and NBC1) at the apical membrane (conductance is the reciprocal of resistance). Similarly,

$E_B = \frac{g_K E_K + g_{NBC1} E_{NBC1} + g_{Cl} E_{Cl}}{g_K + g_{NBC1} + g_{Cl}}$. Since E_A and E_B have non-equivalent values, a current (I_S; shunt current) circulates around the epithelium. The shunt current, $I_S = \frac{E_A - E_B}{R_A + R_B + R_S}$, is carried mainly by Na^+ and Cl^- ions. R_A and R_B are apical and basolateral membrane resistances: $R_A = \frac{1}{g_A} = \frac{1}{g_K + g_{NBC1}}$; $R_B = \frac{1}{g_B} = \frac{1}{g_K + g_{NBC} + g_{Cl}}$.

I_S depolarizes (more positive) the apical and hyperpolarizes (more negative) the basolateral membrane. Conventionally, the shunt current has a negative value. Experimentally, TEP is measured with a pair of calomel electrodes in series with Ringer solution bridges (3 %wt/v agar) placed in the apical and basal baths of the Üssing chamber (Fig. 2-2).

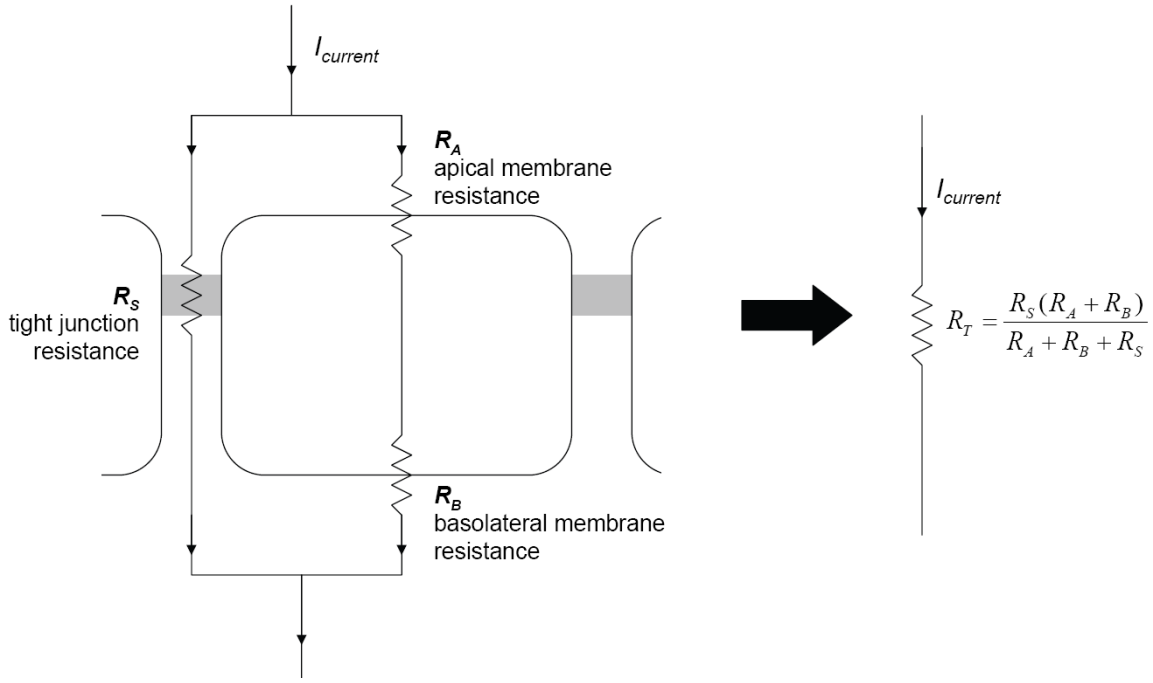

Fig. 2-5: Measuring total tissue resistance (R_T).

The total tissue resistance (R_T) is experimentally determined by passing a 2 µA *Current* across the hfRPE monolayer (once every 45 seconds) with Ag/AgCl electrodes placed at the apical and basal baths and measuring the voltage drop (i.e., ΔTEP) across the tissue. R_T is then calculated with Ohm's law: $R_T = \frac{\Delta TEP \cdot Area}{Current}$. *Area* is the cross-sectional surface area of the RPE that is exposed to the apical or basolateral baths. As shown in Fig. 2-5, R_T is a combination of apical and basolateral membrane resistances (R_A and R_B), and tight junction resistance (R_S; shunt resistance).

Section 2.5 – Intracellular microelectrode recordings

Although TEP recording allows for the detection of changes in V_A and V_B, a TEP response can have two different interpretations. For example, an increase in TEP can be interpreted as: (1) an increase in V_B, or (2) a decrease in V_A. By placing a microelectrode reference within the cell, V_A and V_B can be measured separately (Fig. 2-6). This method provides valuable information on ion-transport mechanism at the apical or basolateral membrane.

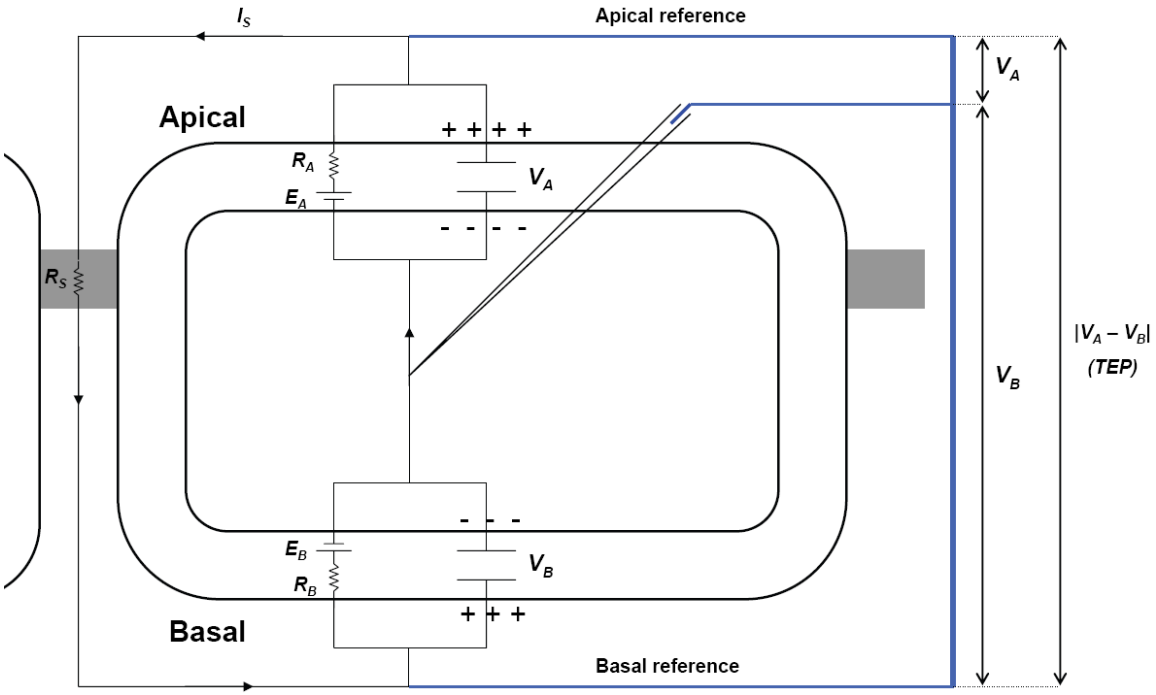

Fig. 2-6: Measuring apical and basolateral membrane voltages (V_A & V_B) with intracellular microelectrodes.

In addition to measuring V_A and V_B, when a current is passed across the tissue in the presence of an intracellular microelectrode, the ratio of R_A/R_B can be determined by measuring the current induced deflections in V_A and V_B.

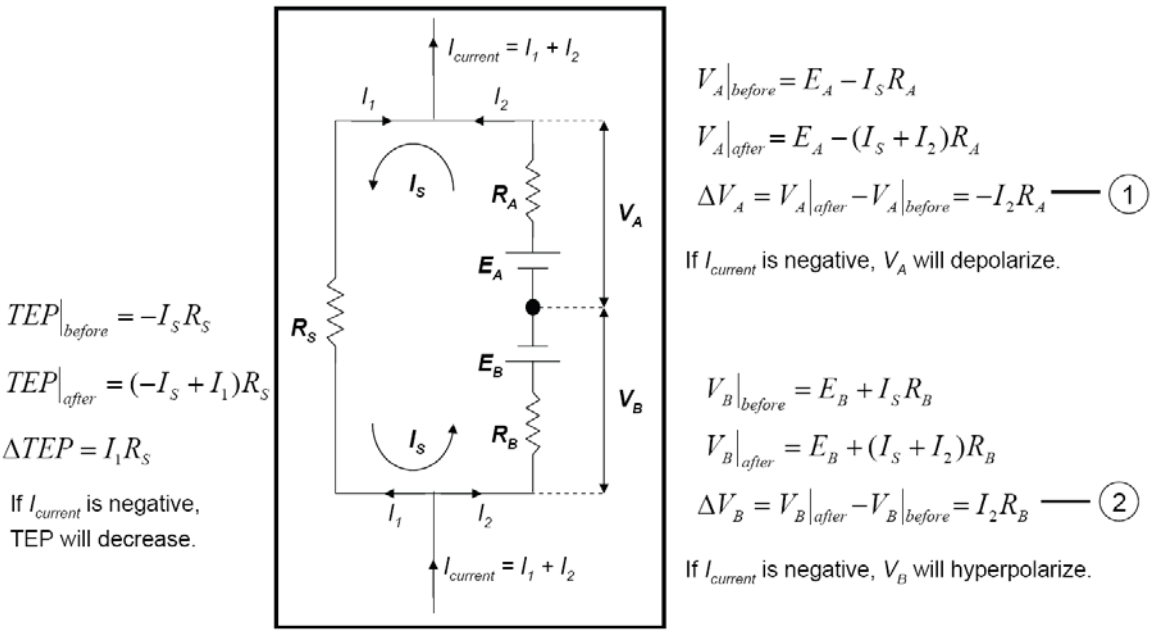

Fig. 2-7: Measuring and calculating R_A/R_B.

As shown in Fig. 2-7, the ratio of the current induced deflections in V_A and V_B (equations 1 and 2) is: $\frac{\Delta V_A}{\Delta V_B} = -\frac{R_A}{R_B}$.

Section 2.6 – Steady-state fluid-transport measurement

The polarized distribution of the various ion-transport mechanisms at the apical and basolateral membranes allow for vectorial transport of solute (Na, Cl, and HCO_3) and water from the apical side to the basal side. By measuring the capacitance between the probe and the basal bath (electrically grounded), we can monitor the steady increase in fluid level in the basal bath, which is directly proportional to the steady-state fluid transport rate of the RPE (Fig. 2-8). In this set-up, hfRPE monolayers were mounted in a modified Üssing chamber and the rate of transepithelial water flow (J_V; $\mu l \cdot cm^{-2} \cdot hr^{-1}$) was measured using a capacitance probe at the basal bath of the chamber (Hughes *et al.*, 1984). In addition, the TEP (mV) and R_T ($\Omega \cdot cm^2$) of the hfRPE monolayer were simultaneously measured by injecting a known current (5 μA) via Ag/AgCl electrodes that were connected to the solution baths with Ringer solution bridges (4 %wt agar). Fluid transport experiments were performed in a Steri-Cult™ CO_2 incubator (Thermo Electron Corp; OH, Marietta) set at 5%/10%/85% $CO_2/O_2/N_2$ and 37 ^oC.

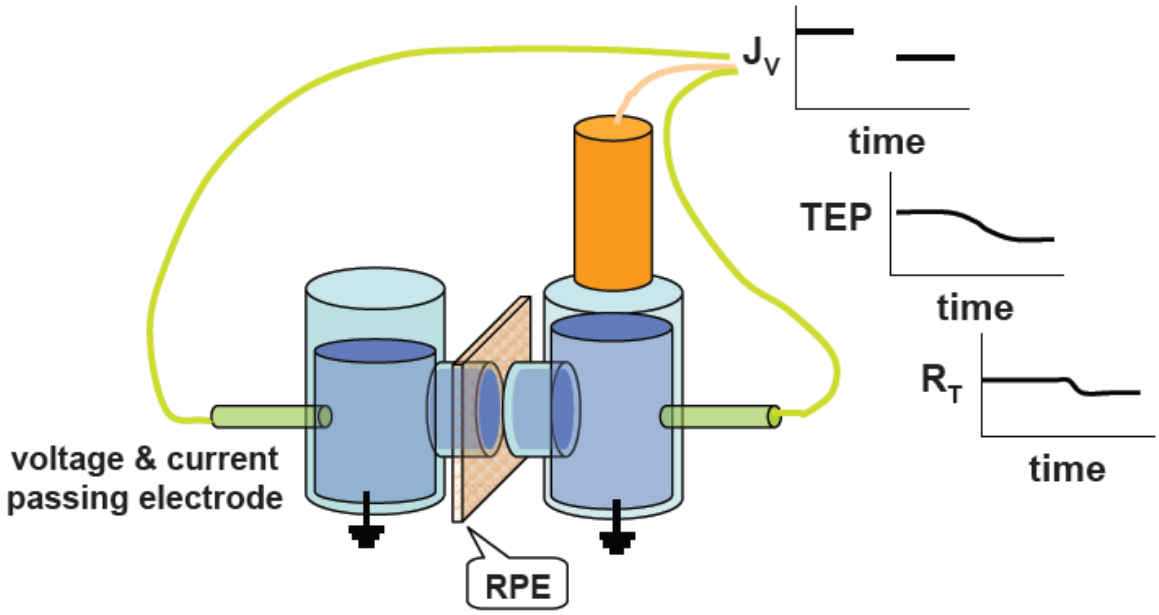

Fig. 2-8: Schematic of the fluid-transport measurement set-up.

Section 2.7 – Ringer solution composition, materials, and methods

Physiology experiments are performed with physiological saline solution (Ringer solution). Two main types of Ringer solution are used: (1) CO_2/HCO_3 buffered; (2) HEPES buffered. CO_2/HCO_3 buffered Ringer contains 26.2 mM of HCO_3 and requires continuous bubbling of 5% CO_2 (in a gas mixture containing 5%/10%/85% $CO_2/O_2/N_2$) to maintain a pH of 7.5 at 37 ^oC. On the other hand, HEPES buffered Ringer do not contain CO_2 or HCO_3, and is titrated to pH 7.5 (at 37 ^oC) with NMDG (base). CO_2/HCO_3 buffered Ringer is more physiologically relevant as CO_2/HCO_3 is the major buffer system used in our body to control cellular pH. In some cases CO_2/HCO_3-free Ringer (HEPES buffered) is very useful: (1) simplicity: HEPES buffered solutions do not require constant bubbling or incubation with 5% CO_2; (2) to study HCO_3-transport: CO_2/HCO_3-free condition eliminates HCO_3 transport activity; (3) removing the major intracellular buffering system in the cell: acid-coupled transport mechanisms (e.g., H^+/Lac co-transporter) can be easily studied.

For imaging and electrophysiology experiments involving hfRPE cultures, the Ringer solutions (Table 2-1) closely mimics the ionic composition and osmolarity of the cell culture media (Minimum Essential Medium Eagle; MEM), which has a final osmolarity of 310 mOsm (after addition of 5% serum, amino-acid supplements, antibiotics, and taurine). Control Ringer solution contains (in mM): 142.7 Na^+, 126.1 Cl^-, 26.2 HCO_3^-, 5 K^+, 0.5 Mg^{2+}, 1.8 Ca^{2+}, 2 Taurine, 5 Glucose. The solution is equilibrated with 5%/10%/85% $CO_2/O_2/N_2$. Sucrose was added to the Ringer to reach osmolarity of 305 mOsm. Low Cl (1 mM) Ringer (pH 7.5 when equilibrated with 5% CO_2) was prepared

by replacing all Cl-salts with gluconate-salts (except for $MgCl_2$). The high gluconate concentration (128.7 mM) in the low Cl Ringer requires consideration of the strong Ca^{2+} and Mg^{2+} chelating ability of gluconate. By using the stability constants of Ca-gluconate (16.22 $L \cdot mol^{-1}$) and Mg-gluconate (5.01 $L \cdot mol^{-1}$) (Furia, 1972; Abercrombie *et al.*, 1983), the estimated free [Ca^{2+}] and [Mg^{2+}] in the low Cl Ringer are 0.6 and 0.3 mM, respectively. Therefore, the low Cl Ringer was supplemented with additional Ca^{2+} (to 5.7 mM) and Mg^{2+} (to 0.84 mM) to give free [Ca^{2+}] and [Mg^{2+}] of 1.8 mM and 0.5 mM, respectively. Low HCO_3 Ringer (2.62 mM HCO_3; pH 6.5 when equilibrated with 5% CO_2) was prepared by replacing 23.58 mM $NaHCO_3$ with equimolar Na-gluconate. Ca^{2+}/Mg^{2+}-free Ringer was made by replacing all $CaCl_2$ and $MgCl_2$ with 4.6 mM NMDG-Cl. Na-free Ringer was made by replacing all Na-salts with NMDG. NMDG-Cl was prepared by titrating NMDG solution with HCl. NMDG-HCO_3 was prepared by equilibrating NMDG solution with 5%/10%/85% $CO_2/O_2/N_2$ gas mixture.

Table 2-1. Ringer solutions for CO_2/HCO_3 transport experiments (all values in mM).

	Control Ringer	Low Cl Ringer	Low HCO_3 Ringer	Ca^{2+} & Mg^{2+} free Ringer	Na-free Ringer
NaCl	116.5		116.5	116.5	
$NaHCO_3$	26.2	26.2	2.62	26.2	
KCl	5		5	5	5
Glucose	5	5	5	5	5
Taurine	2	2	2	2	2
$CaCl_2$	1.8		1.8		1.8
$MgCl_2$	0.5	0.5	0.5		0.5
sucrose	16	17	16	16	
Na-gluconate		116.5	23.58		
K-gluconate		5			
Ca-gluconate		5.7			
Mg-gluconate		0.36			
NMDG-Cl				4.6	116.5
NMDG-HCO_3					26.2

All Ringer solutions have pH 7.4 after equilibration with 5%/10%/85% $CO_2/O_2/N_2$ gas mixture.

In all lactate transport experiments, CO_2/HCO_3-buffered Ringer (pH 7.4 with 5% CO_2) has the following ionic composition (Table 2-2) (in mM): 133.7 Na^+, 116.1 Cl^-, 26.2 HCO_3^-, 5 K^+, 0.5 Mg^{2+}, 1.8 Ca^{2+}, 2 Taurine, 5 Glucose. Lactate Ringer was prepared by adding 20 mM Na-lactate, and replacing 20 mM of NaCl with NMDG-Cl.

Table 2-2. Ringer solutions for lactate transport experiments (all values in mM).

	Control Ringer	Control Ringer w/ lactate	Na-free Ringer	Na-free Ringer w/ lactate
NaCl	106.5	86.5		
$NaHCO_3$	26.2	26.2		
KCl	5	5	5	5
Glucose	5	5	5	5
Taurine	2	2	2	2
$CaCl_2$	1.8	1.8	1.8	1.8
$MgCl_2$	0.5	0.5	0.5	0.5
Na-lactate		20		
sucrose	35	2	33	
NMDG-Cl		20	106.5	106.5
NMDG-HCO_3			26.2	26.2
NMDG-Lactate				20

All Ringer solutions have pH 7.4 after equilibration with 5%/10%/85% $CO_2/O_2/N_2$ gas mixture.

The CO_2/HCO_3-free Ringer (HEPES buffered; Table 2-3) has the same ionic composition as CO_2/HCO_3 Ringer except: (1) all HCO_3 was replaced with gluconate; (2) 7 mM HEPES acid was added to the CO_2/HCO_3-free Ringer and titrated with NMDG to reach pH 7.4 (at 36.9 ^oC). Cl-free Ringer solution contains $CaSO_4$ instead of $CaCl_2$; mercury sulfate electrodes (sat. K_2SO_4; Koslow, NJ) were used instead of calomel electrodes. Since Cl-free Ringer was made by replacing all Cl with gluconate (138.7 mM), 5.9 mM $CaSO_4$ and 0.85 mM Mg-gluconate was added to this Ringer to compensate for Ca^{2+} and Mg^{2+} chelation by gluconate. Na-free Ringer containing lactate was prepared by adding NMDG-lactate, which was made by titrating NMDG solution with lactic acid.

Table 2-3. CO_2/HCO_3-free Ringer Solutions for lactate transport experiments (all values in mM).

	CO_2/HCO_3 free Ringer	CO_2/HCO_3 free Ringer w/ lactate	Cl & CO_2/HCO_3 free Ringer	Cl & CO_2/HCO_3 free Ringer w/ lactate	Na & CO_2/HCO_3 free Ringer	Na & CO_2/HCO_3 free Ringer w/ lactate
NaCl	106.5	106.5				
KCl	5	5			5	5
Glucose	5	5	5	5	5	5
Taurine	2	2	2	2	2	2
$CaCl_2$	1.8	1.8			1.8	1.8
$MgCl_2$	0.5	0.5			0.5	0.5
Na-lactate				20		
HEPES	7	7	7	7	7	7
NMDG	5	5	5	5	5	5
sucrose	25	24	25	22	64	30
Na-gluconate	26.2	6.2	132.7	112.7		
K-gluconate			5	5		
Mg-gluconate			0.85	0.79		
Ca-sulfate			5.9	5.3		
NMDG-Cl					107.5	107.5
NMDG-Lactate						20

All Ringer solutions should have pH 7.4 ± 0.1, add more or less NMDG to obtain pH 7.4.

Dorzolamide hydrochloride was purchased from U.S. Pharmacopeia (MD, Rockville). DIDS (4,4′-diisothiocyanostilbene-2,2′-disulfonic acid) and Nigericin were purchased from Calbiochem (CA, La Jolla). pCMBS (p-chloromercuribenzenesulfonic acid) was purchased from Toronto Research Chemicals (Ontario, Canada). Benzolamide was a kind gift from Dr. Erik Swenson of the University of Washington (WA, Seattle). All other chemicals were purchased from Sigma-Aldrich Co. (MO, St Louis).

In all physiological experiments, intracellular pH, TEP, and R_T were recorded simultaneously. The hfRPE produces a response (i.e., pH_i, TEP, or R_T changes) when Ringer solution with a special composition (e.g., low HCO_3 Ringer, or 20 mM lactate Ringer) was perfused into the apical or basal baths. For every experiment, two initial

control responses (2 min per pulse) were obtained to assure consistency and reversibility of the control responses. Next, the hfRPE was exposed to drug/condition for 4-5 minutes (or until the resting pH and TEP stabilizes) before another response was obtained (in the continued presence of the drug/condition). After washing out the drug or returning to control condition, a control response was obtained to assess the reversibility of the drug/condition's effect on the transporter activity corresponding to the control pulses.

Table 2-4. List of compounds.

Compound	Conc. (μM)	Effects
Acetazolamide	100	Membrane permeable CA inhibitor (non-specific)
Amiloride	1000	Inhibits Na^+/H^+ exchanger
Ba^{2+}	2000	Inhibits K^+-channels
BAPTA-AM	20	Membrane permeable Ca^{2+} chelator
Benzolamide	10	Membrane impermeable CA inhibitor (non-specific)
Bumetanide	100	Inhibits $Na^+/K^+/2Cl^-$ co-transporter
CFTRinh-172	10	Inhibits CFTR Cl-channel
DIDS	500	Inhibits anion channels and transporters
Dorzolamide	250	Membrane permeable CA inhibitor (non-specific)
Ethoxyzolamide	10	Membrane permeable CA inhibitor (non-specific)
Forskolin	40	Elevates cAMP to activate CFTR Cl-channel
Ionomycin	10	Ca^{2+}-ionophore for $[Ca^{2+}]_i$ calibration
Niflumic acid	100	Inhibits MCT1 and Ca^{2+}-dependent Cl-channels
Nigericin	20	H^+/K^+ exchanger (ionophore) for pH_i calibration
Ouabain	100	Inhibits $3Na^+/2K^+$ ATPase
pCMBS	50	Inhibits MCT1
probenecid	500	Inhibits organic anion transporter
Zn^{2+}	200	Inhibits ClC-2 Cl-channel and Na^+/H^+ exchanger

CHAPTER 3: CO_2-induced Ion and Fluid Transport in RPE

Section 3.1 – Introduction

The retinal pigment epithelium (RPE) is a polarized monolayer of cells that is part of the blood-retina barrier in the back of the vertebrate eye. This epithelium separates the choroidal blood supply from the extracellular or subretinal space (SRS) that surrounds the retinal photoreceptors. By transporting ions and fluid from the SRS to the choroid (Hughes et al., 1998; Maminishkis et al., 2002), the RPE plays a critical role in maintaining the volume and chemical composition of the SRS. Large amounts of CO_2 and H_2O are deposited into the SRS due to the high metabolic activity of the photoreceptors (Wangsa-Wirawan & Linsenmeier, 2003). The choroid's high blood circulation, ≈ 1200 mL/min/100 g (Alm & Bill, 1987) and its proximity to the photoreceptor inner segments makes the choroid a very effective sink for the removal of these metabolites. Failure of the RPE to remove CO_2 would result in SRS acidosis detrimental to retinal function (Sillman et al., 1972; Meyertholen et al., 1986; Takahashi et al., 1993). In addition, abnormal accumulation of fluid in the SRS can cause retinal detachment and degeneration (Fisher et al., 2005).

In vivo studies of retinal metabolism show that SRS CO_2 level increases following the transition from light to dark (Wangsa-Wirawan & Linsenmeier, 2003). Since CO_2 is normally highly membrane permeable, the delivery of CO_2 from the SRS into the choroid was assumed to be achieved via passive diffusion. We show that the higher apical to basolateral membrane surface area results in a 10-fold higher CO_2 diffusion rate across the apical membrane than across the basolateral membrane. The relatively lower CO_2-

permeability at the basolateral membrane allows it to act as a bottleneck for CO_2 diffusion, thus trapping CO_2 within the cell. This accumulation of CO_2 in the cell causes the subsequent hydration of CO_2 into HCO_3 by the catalytic activity of CA II. This in turn stimulates HCO_3-efflux at the basolateral membrane. Therefore, the increase in SRS CO_2 level increases net $NaHCO_3$ absorption, which in turn drives solute-linked fluid transport across the RPE. In the transition from light to dark, the RPE can respond to the increased metabolic load by increasing the clearance of CO_2/HCO_3 and fluid from the SRS. This would help protect and maintain the health and integrity of the retina/RPE complex by preventing acidosis in the subretinal space and an abnormal separation of retina and RPE.

Section 3.2 – CO_2 permeability at the apical and basolateral membranes

The study began with the unusual observation that in hfRPE, perfusing 13% or 1% CO_2 equilibrated Ringer to the apical membrane produced significantly larger pH_i responses than at the basolateral membrane (Fig. 3-1).

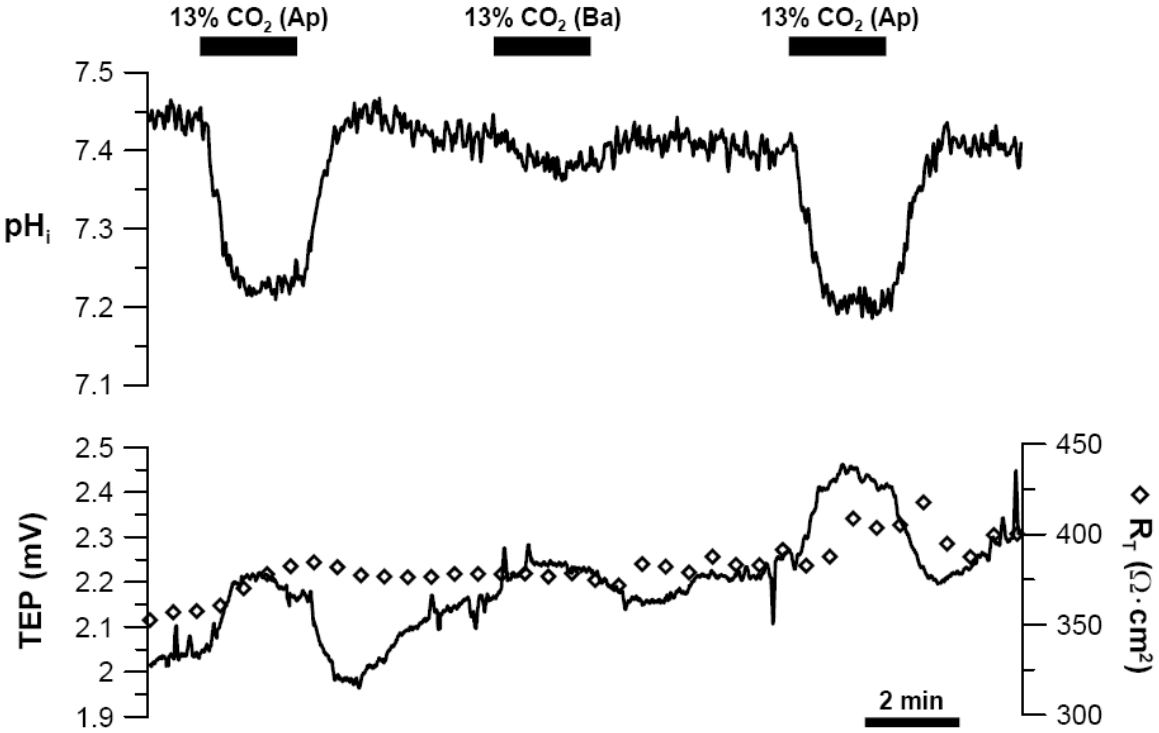

Fig. 3-1: 13% Apical or basal CO_2 induced pH_i, TEP, and R_T responses.

Fig. 3-1 shows that increasing CO_2 from 5% to 13% in the apical or basal baths acidified the hfRPE by ≈ 0.25 and ≈ 0.04, respectively. Data from 13 experiments shows that 13% apical CO_2 decreased pH_i by 0.23 ± 0.03, from 7.37 ± 0.05 to 7.14 ± 0.06; in contrast, the 13% basal bath CO_2 induced acidification (ΔpH_i = 0.03 ± 0.01) was almost 8-fold smaller. Similarly in Fig. 3-2, decreasing CO_2 from 5% to 1% in the apical or basal baths alkalinized the hfRPE by ≈ 0.35 and ≈ 0.03, respectively.

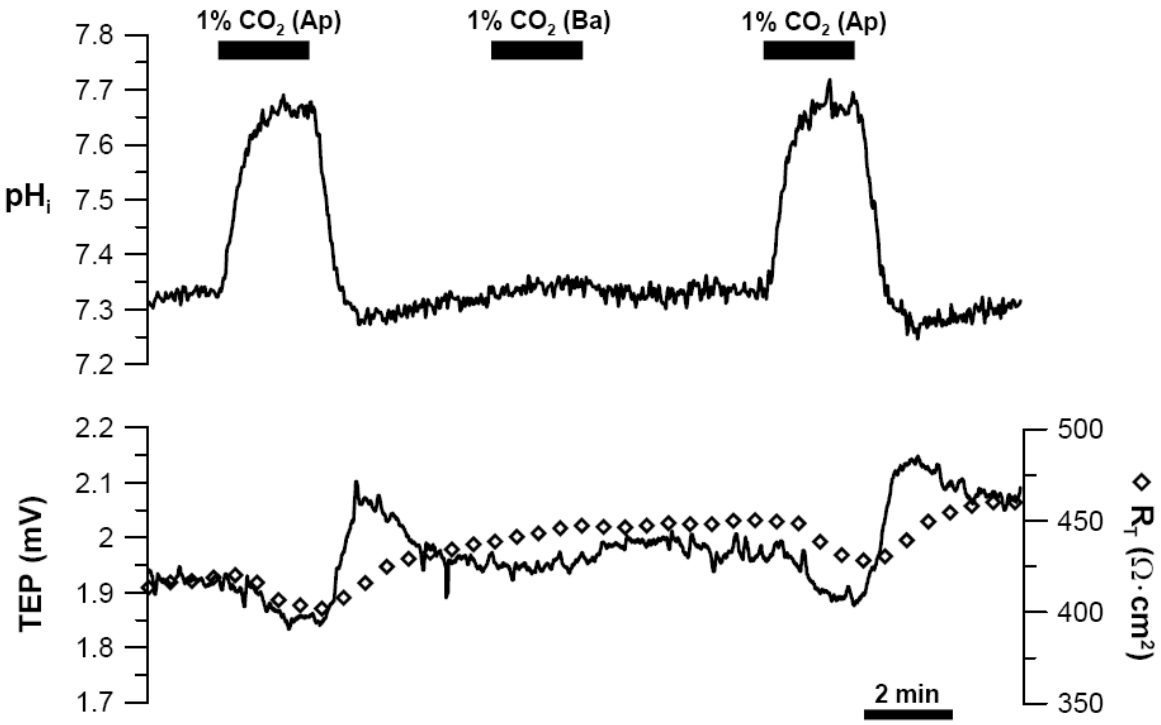

Fig. 3-2: 1% Apical or basal CO_2 induced pH_i, TEP, and R_T responses.

In four experiments, decreasing apical or basal bath CO_2 from 5% to 1% alkalinized the cell by 0.41 ± 0.05 and 0.03 ± 0.03, respectively. The CO_2-induced changes in TEP and R_T were relatively small and not statistically significant. In freshly isolated native hfRPE preparations, 13% apical CO_2 also caused significantly larger acidification (ΔpH_i = 0.29 ± 0.04) than 13% basal CO_2 (ΔpH_i = 0.03 ± 0.02; n = 4; $p < 0.05$). This difference in the apical/basolateral CO_2-induced pH_i response is even more pronounced in bovine RPE-choroid preparations: no pH_i response to 13% basal CO_2 was observed, but a significant acidification was produced by 13% apical CO_2 (ΔpH_i = 0.39 ± 0.09; n = 6). In addition, significant differences between the 13% apical and basal bath induced pH_i responses were also observed in native fetal human RPE-choroid preparations.

Apical membrane processes increase the effective apical surface area of native frog RPE-choroid by ≈ 30-fold relative to the basolateral surface area (Miller & Steinberg, 1977). Electron micrographs of hfRPE provide evidence for similar structures in hfRPE (Maminishkis et al., 2006) and supports the notion of a relatively larger apical surface area. This difference suggests a possible basis for the ≈ 8-fold difference in the ΔpH_i produced by altering CO_2 (from 5 to 13%) in the apical versus basal bath. We can also determine the relative CO_2-permeability of the apical vs. the basolateral membrane by using the total buffering capacity of the cell (sections 2.3 & 3.11). With this method, we calculated that the RPE apical membrane has a 10-fold higher CO_2 permeability than the basolateral membrane.

hfRPE monolayers grown on transwell filters lack Bruch's membrane and a thick choroidal vasculature – it is flimsy and is easily damaged/stretched by the pressures exerted by the constant apical and basal perfusion of Ringer solution. Therefore, a mesh (250 μm thick) is placed under the basolateral surface of the hfRPE monolayer for structural support (Fig. 3-3). However, CO_2-diffusion into the cell from the basal bath may be hindered by the mesh and by the transwell filter itself. To eliminate the mesh as a possible diffusion barrier, we show that the 13% basal bath CO_2 produced the same ΔpH_i with or without the mesh. To test if the transwell filter is a diffusion barrier, the hfRPE monolayer was uniformly damaged by mounting its apical surface facing the mesh (Fig. 3-3).

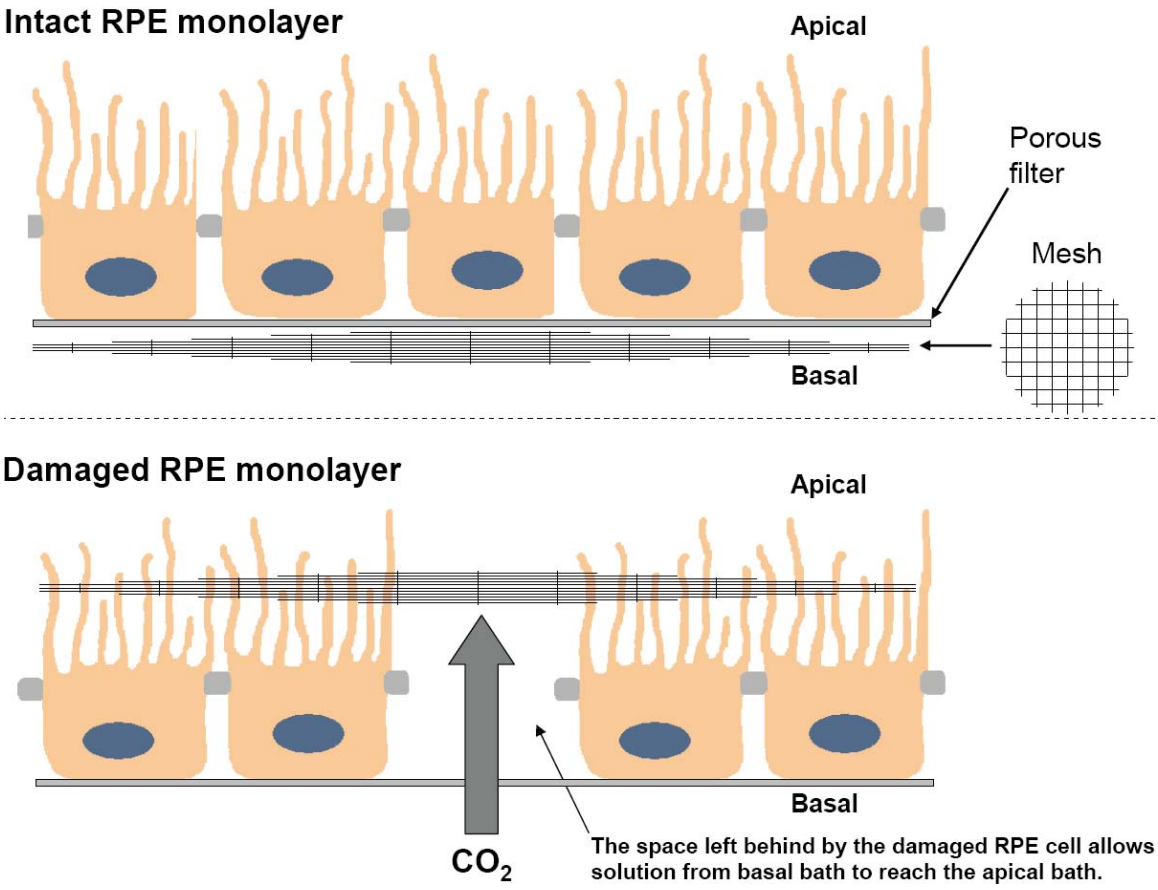

Fig. 3-3: RPE monolayer damage by plastic mesh. Upper panel – intact RPE monolayer with proper mesh position. Lower panel – RPE monolayers are damaged by mounting the mesh on top of the RPE apical membrane.

This configuration allows CO_2 from the basal bath to diffuse through the intact filter to reach the apical membrane surface by diffusing through the empty spaces (where the RPE were damaged). If the filter was a significant barrier to CO_2, the difference between 13% apical and basal CO_2-induced ΔpH_i in the damaged hfRPE would be similar to that in an intact hfRPE (≈ 8-fold).

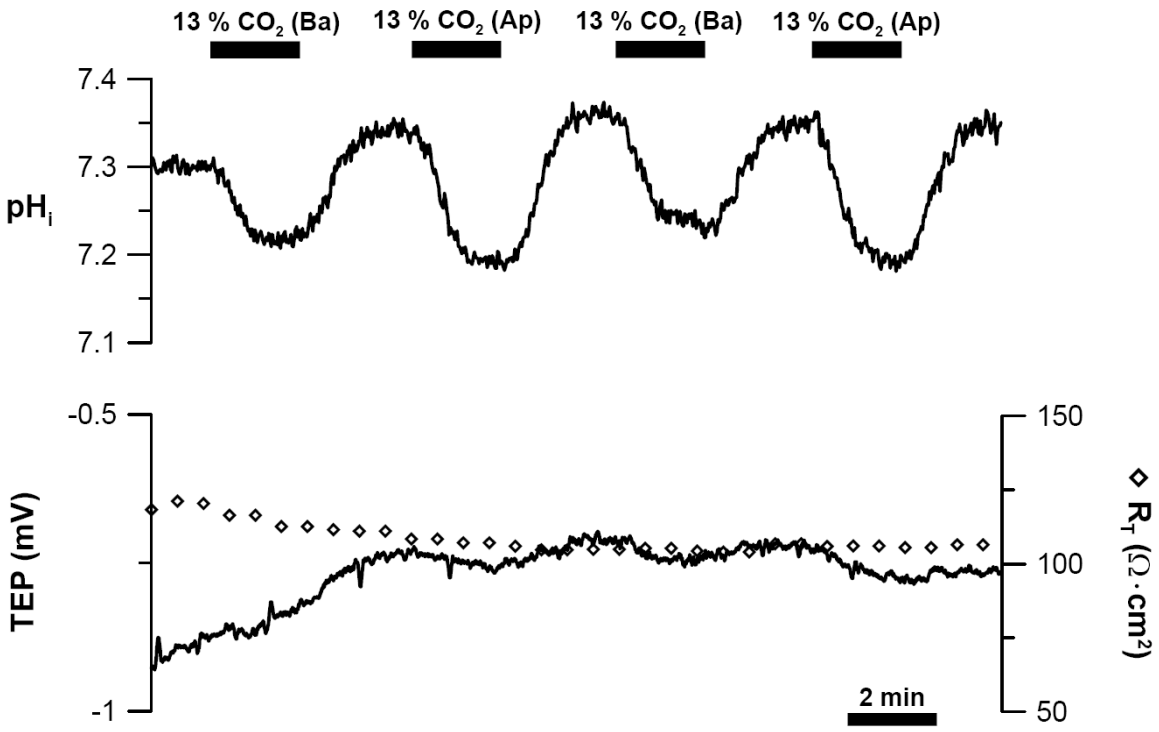

Fig. 3-4: 13% Apical or basal CO_2 induced pH_i, TEP, and R_T responses in damaged RPE monolayer.

However as shown in Fig. 3-4, 13% basal CO_2 caused a significantly larger acidification in the damaged hfRPE monolayer compared to intact hfRPE (compare with Fig. 3-1). In five damaged RPE monolayers tested, the difference in CO_2-induced ΔpH_i was ≈ 2.5-fold and the calculated relative CO_2 permeability was 3.0 ± 1.5. This indicates that the filter did limit CO_2-diffusion rate, but that alone cannot account for the large difference in relative difference in CO_2-permeability of the apical and basolateral membranes of intact hfRPE monolayers. From this observation, we infer that the basolateral membrane is relatively less permeable to CO_2 than the apical membrane.

There are two interpretations for this observed difference in CO_2 permeability: (1) apical CO_2-permeability is higher because of its relatively larger total surface area; (2) the chemical and physical composition of basolateral membrane is a CO_2-barrier that completely blocks CO_2 diffusion, similar to the apical membranes of gastric or colonic epithelia (Waisbren *et al.*, 1994; Endeward & Gros, 2005). We can eliminate the latter possibility with the following experiment: the basal bath CO_2 was increased from 5 to 13% when we stop apical perfusion (Fig. 3-5). Stopping apical perfusion eliminates the convective flow at the apical bath, thus increasing the thickness of the unstirred layer at the apical membrane surface and reduces CO_2 diffusion out of the apical membrane. If the basolateral membrane does maintain a CO_2-barrier, then reducing the rate of CO_2 diffusion would not affect the 13% basal CO_2 induced pH_i-response.

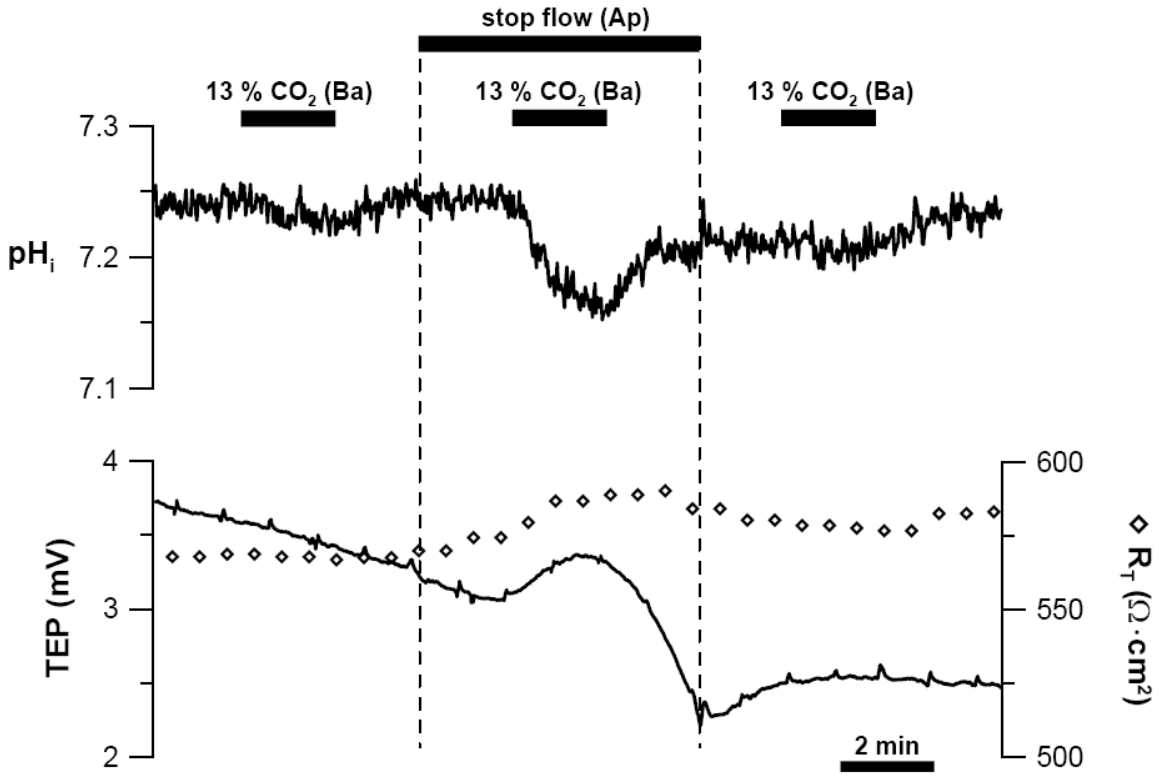

Fig. 3-5: 13% basal CO_2 induced pH_i, TEP, and R_T responses in the absence apical perfusion.

However when apical perfusion was stopped, the 13% basal CO_2-induced ΔpH_i was ≈ 3-fold greater than with continuous perfusion ($p < 0.05$; $n = 4$). This observation indicates that more of the CO_2 that diffuses into the basolateral membrane accumulates within the cytosol to cause the larger acidification mainly due to a reduced CO_2-efflux from the apical membrane. From this result, we infer that the basolateral membrane is CO_2 permeable and that the relatively higher apical membrane CO_2 permeability is probably due to its larger surface area.

The tight junction prevents the free flow of ions, large molecules (e.g., proteins or glucose), and water across the epithelium. Since CO_2 is a gas and is a small molecule, it may readily cross the tight junctions. If true, CO_2 may diffuse from the basal bath, across the tight junction into the apical bath, where it enters the cell from the apical membrane. To test this possibility, tight junctions were disrupted by removing all Ca^{2+} and Mg^{2+} from both solution baths for 15 minutes before adding 13% CO_2 Ringer to the basal bath (Fig. 3-6). This maneuver disrupts tight junctions by dissociating the link between tight junction proteins (claudins and occludin) and the intracellular adaptor proteins (e.g., ZO-1, -2, -3) (Brown & Davis, 2002; Rothen-Rutishauser *et al.*, 2002). Since $R_T \approx$ tight junction resistance (R_S) in cultured hfRPE, the observation that $[Ca^{2+}]_o$ and $[Mg^{2+}]_o$ removal decreases R_T ($-17 \pm 7\ \Omega \cdot cm^2 \cdot min^{-1}$; $n = 5$) indicates disruption of tight junctions. When control Ringer was returned to both solution baths, R_T slowly recovered at a rate of $12 \pm 4\ \Omega \cdot cm^2 \cdot min^{-1}$. However, the 13% basal CO_2-induced acidification was identical to control even in the absence of extracellular Ca^{2+} ($p > 0.05$; $n = 5$), suggesting that the basolateral membrane is the main pathway for CO_2-entry from the basal bath.

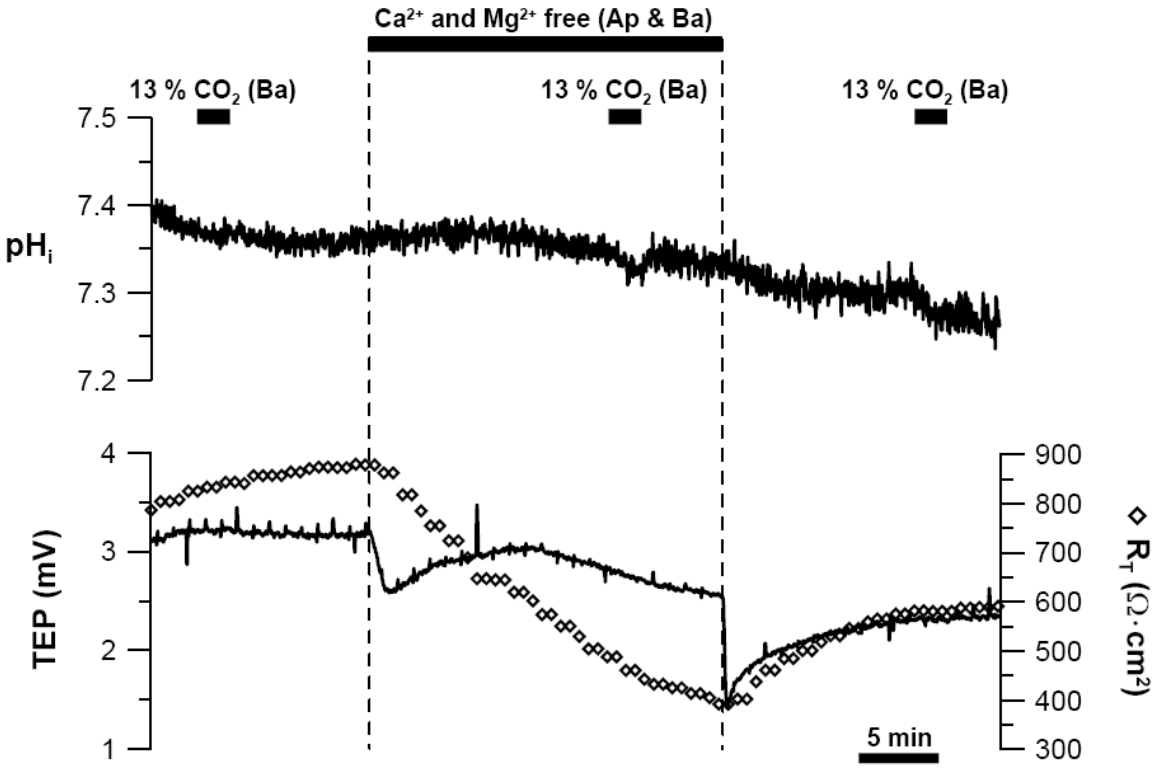

Fig. 3-6: 13% basal CO_2 induced pH_i, TEP, and R_T responses in the absence of Ca^{2+} and Mg^{2+} in both apical and basal baths.

Another possible CO_2-transport mechanism arises from the ability of aquaporin 1 (AQP1) to function as a CO_2 channel (Cooper & Boron, 1998; Endeward *et al.*, 2006). In cultured hfRPE cells, AQP1 mRNA is highly expressed in human RPE (Wang and Miller, ARVO 2007, #6034). In addition, AQP1 was also detected specifically at the apical membrane (data not shown), corroborating an earlier study on rat RPE (Stamer et al., 2003). However, pCMBS (1 mM; non-specific AQP1 inhibitor) did not block or inhibit 13% apical CO_2 induced acidification (n = 3), inconsistent with the AQP1 hypothesis.

This asymmetry in apical and basolateral membrane CO_2-permeability has a very unique function. This feature allows the RPE to "trap" CO_2 within the cell. Accumulation of CO_2 in the cytosol favors CO_2 conversion into HCO_3 by the catalytic activity of cytosolic carbonic anhydrase II (CA II). CA II-mediated formation of HCO_3 in the cell stimulates HCO_3-efflux from the basolateral membrane via HCO_3-transporters. However, besides simple diffusion, CO_2 can also be transported across the apical membrane in its hydrated form, HCO_3, via transporters. In this regard, there is strong electrophysiological evidence for an electrogenic $Na/2HCO_3$ co-transporter at the apical membrane of frog and bovine RPE (Hughes et al., 1989; Kenyon et al., 1997). In addition, this $Na/2HCO_3$ co-transporter (NBC1) has been immunolocalized to the apical membrane of rat RPE (Bok et al., 2001). Since CO_2 is an acid, and HCO_3 is a base, it is possible that CO_2-entry into the cell is balanced by concomitant HCO_3-entry at the apical membrane, thus maintaining pH_i homeostasis of the RPE. This notion is further discussed in the next section.

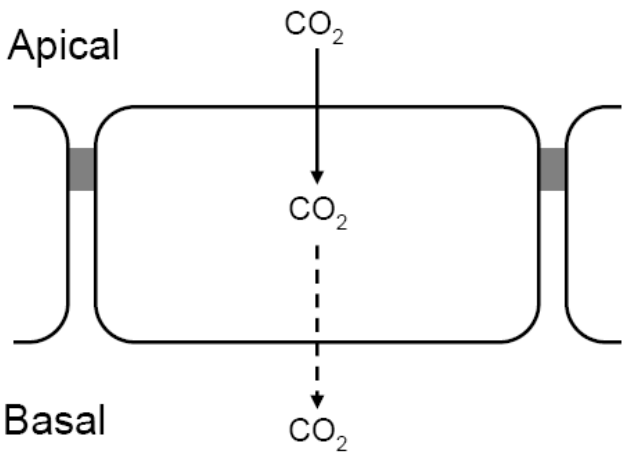

Section 3.1 conclusion: RPE apical membrane is more CO_2-permeable than its basolateral membrane

Supporting experimental observations	Interpretation	Fig.
13% apical CO_2 causes 10-fold larger acidification than 13% basal CO_2	Apical membrane is more CO_2-permeable than basolateral membrane	3-1
1% apical CO_2 causes 10-fold larger acidification than 1% basal CO_2	Apical membrane is more CO_2-permeable than basolateral membrane	3-2
Damaging RPE monolayer decreases 13% apical CO_2-induced acidification	The polycarbonate porous membrane does not limit CO_2-diffusion	3-4
Damaging RPE monolayer increases 13% basal CO_2-induced acidification	The polycarbonate porous membrane does not limit CO_2-diffusion	3-4
Stopping apical flow increases 13% basal CO_2-induced acidification	Apical membrane is more CO_2-permeable than basolateral membrane	3-5
Mounting RPE monolayer upside-down did not affect 13% CO_2-induced responses	Differences apical/basal bath perfusion rate did not affect CO_2-permeability	N/A

Section 3.3 – HCO_3 transport at the apical membrane

To test the activity of apical NBC1 in cultured hfRPE, we added DIDS (NBC1 inhibitor) to the apical bath and compared the resultant pH_i and TEP responses in control Ringer (26.2 mM HCO_3) vs. low HCO_3 Ringer (2.62 mM HCO_3) in the apical bath (Fig. 3-7).

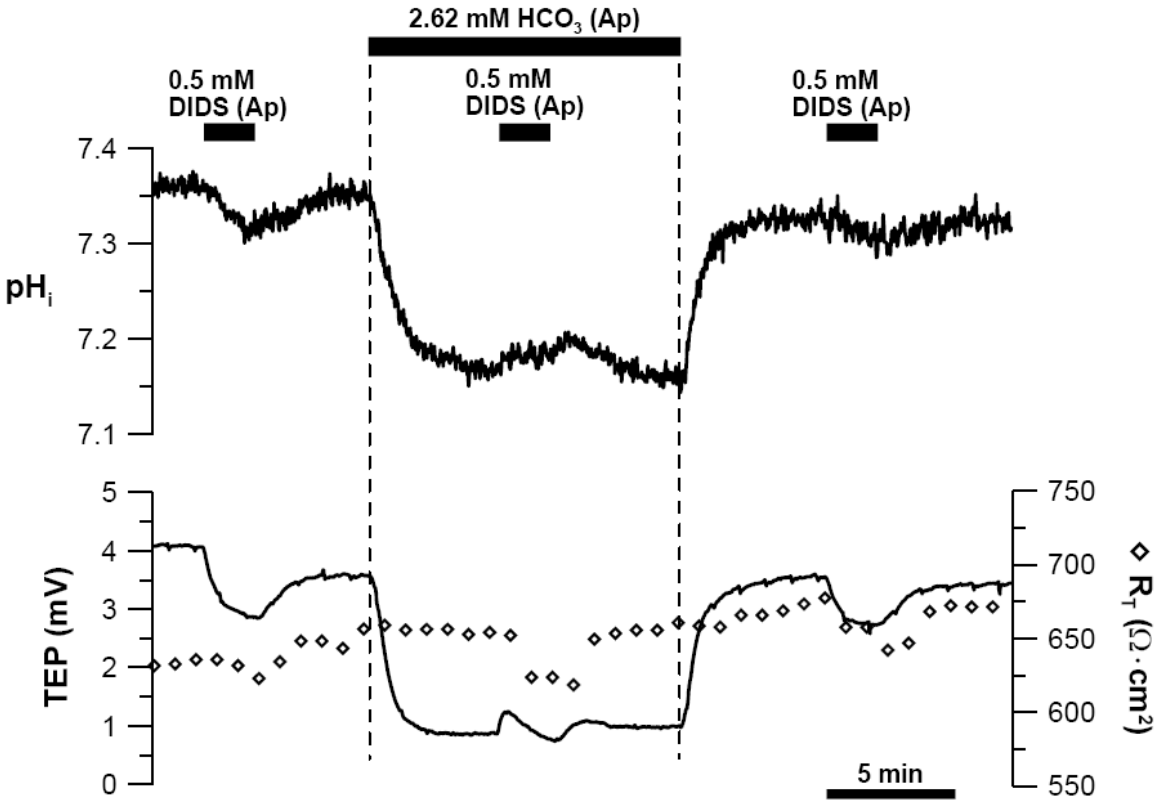

Fig. 3-7: Apical DIDS induced pH_i, TEP, and R_T responses in the presence of low [HCO_3] Ringer (2.62 mM) in the apical bath.

NBC1, like any transporter, is driven by the concentration gradient of its substrate (i.e., Na and HCO_3). Normally, the large inward Na-gradient drives $Na/2HCO_3$ transport into the cell. Data from six experiments showed that in control Ringer, apical DIDS acidified the cell by 0.05 ± 0.02 and decreased TEP by 1.59 ± 0.63 mV. When [HCO_3] in the apical bath was reduced 10-fold (from 26.2 mM to 2.62 mM), the resultant HCO_3-

gradient reverses NBC1 to transport $NaHCO_3$ out of the cell. In this condition, we found that adding DIDS to the apical bath alkalinized the cell by 0.04 ± 0.01 and transiently increased TEP by 0.30 ± 0.15 mV. These apical DIDS-induced pH_i and TEP responses are consistent with the inhibition of an electrogenic HCO_3-dependent mechanism in the forward or reverse direction.

Reducing apical bath [HCO_3] decreased pH_i and TEP – these responses reflect a change in $Na/2HCO_3$-transport activity and we can use this maneuver to further study NBC1 mediated HCO_3-transport. To test this possibility, we decreased apical bath [HCO_3] 10-fold and compared the resultant pH_i and TEP responses in the presence or absence of apical DIDS (Fig. 3-8).

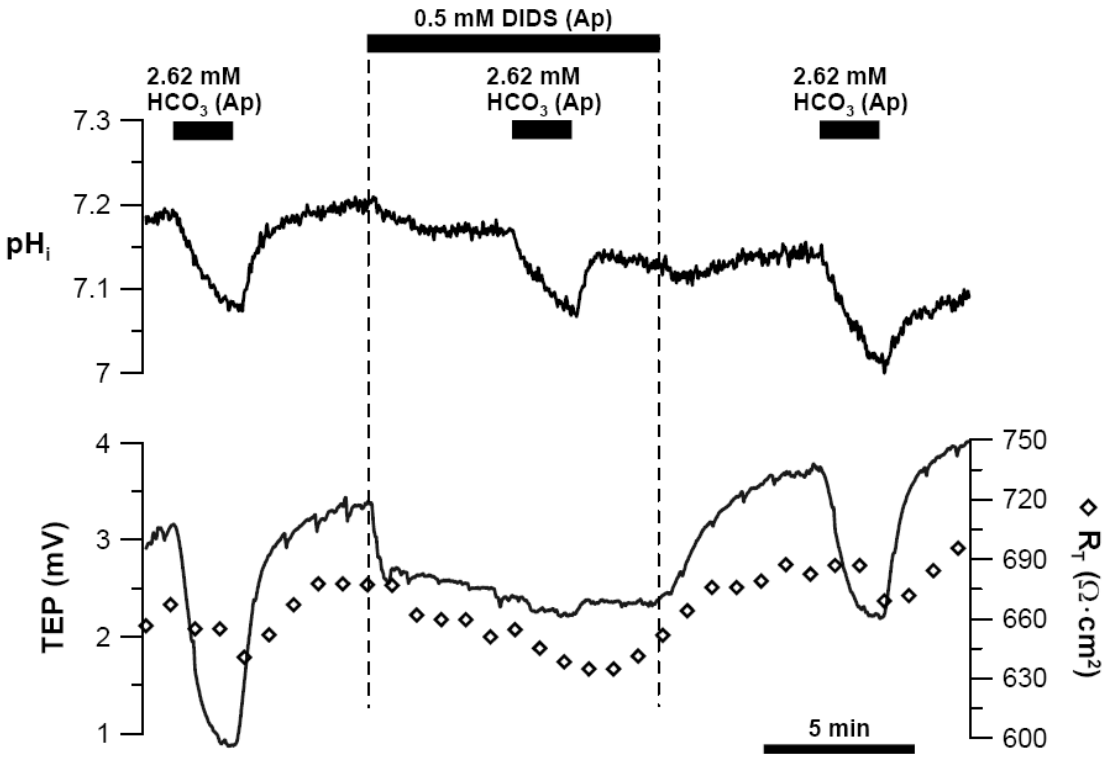

Fig. 3-8: Apical bath Δ[HCO_3]-induced pH_i, TEP, and R_T responses in the presence of apical DIDS.

In three experiments, DIDS reduced the apical bath $\Delta[HCO_3]$-induced TEP response 7-fold (from $\Delta TEP = 2.1 \pm 0.2$ mV to 0.3 ± 0.2 mV; $p < 0.01$). The effect of DIDS on the TEP response was partially reversible following a five-minute washout ($\Delta TEP = 1.28 \pm 0.22$ mV). This result indicates that apical DIDS almost completely blocked the apical membrane $Na/2HCO_3$ co-transporter activity. Surprisingly, the apical bath $\Delta[HCO_3]$-induced acidification ($\Delta pH_i = 0.10 \pm 0.02$) was not significantly affected by DIDS ($\Delta pH_i = 0.09 \pm 0.01$; $n = 3$; $p > 0.05$), suggesting the presence of a DIDS-insensitive HCO_3-transporter at the apical membrane.

Besides pNBC1 (SLC4A4; GeneID: 8671), a DIDS-insensitive and electroneutral Na/HCO_3 co-transporter, NBC3/NBCn1 (SLC4A7; GeneID: 9497), is also highly expressed at the apical membrane of human RPE (Wang and Miller, ARVO 2007, #6034; Zhi et al., ARVO 2007, #2532). Our observation that apical DIDS had little effect on the apical bath $\Delta[HCO_3]$-induced acidification suggests that NBC3 is highly active in the RPE. However, this does not indicate that NBC1 has a lower activity than NBC3 because NBC1 is electrogenic, and is therefore limited by both the membrane voltage and HCO_3-gradient. In contrast, NBC3 is limited only by the HCO_3-gradient. Thus the relative activities of NBC1 and NBC3 cannot be accurately evaluated by comparing the apical bath $\Delta[HCO_3]$-induced pH_i responses in the presence vs. absence of apical DIDS.

The presence of carbonic anhydrase II (CA II) and several apical membrane-bound carbonic anhydrases (e.g., CAs IV, IX, XII, and XIV) support the notion of HCO_3-mediated CO_2 transport from the SRS into the RPE via the electrogenic $Na/nHCO_3$ co-

transporter as illustrated in Fig 2-4. According to the bicarbonate transport metabolon theory (Sterling *et al.*, 2001; Alvarez *et al.*, 2003), a membrane bound CA physically binds and interacts with HCO_3-transporters at the apical membrane (e.g., NBC1 and NBC3). If this synergistic form of HCO_3-transport exists in RPE, increasing CO_2 level at the apical surface and in the vicinity of the active site of transmembrane CAs should stimulate the conversion of CO_2 and H_2O into H^+ and HCO_3. The resultant increase in local [HCO_3] near the ion-pore of the HCO_3-transporter enhances HCO_3-entry into the cell. In the remainder of this section, we present experiments to evaluate this possibility.

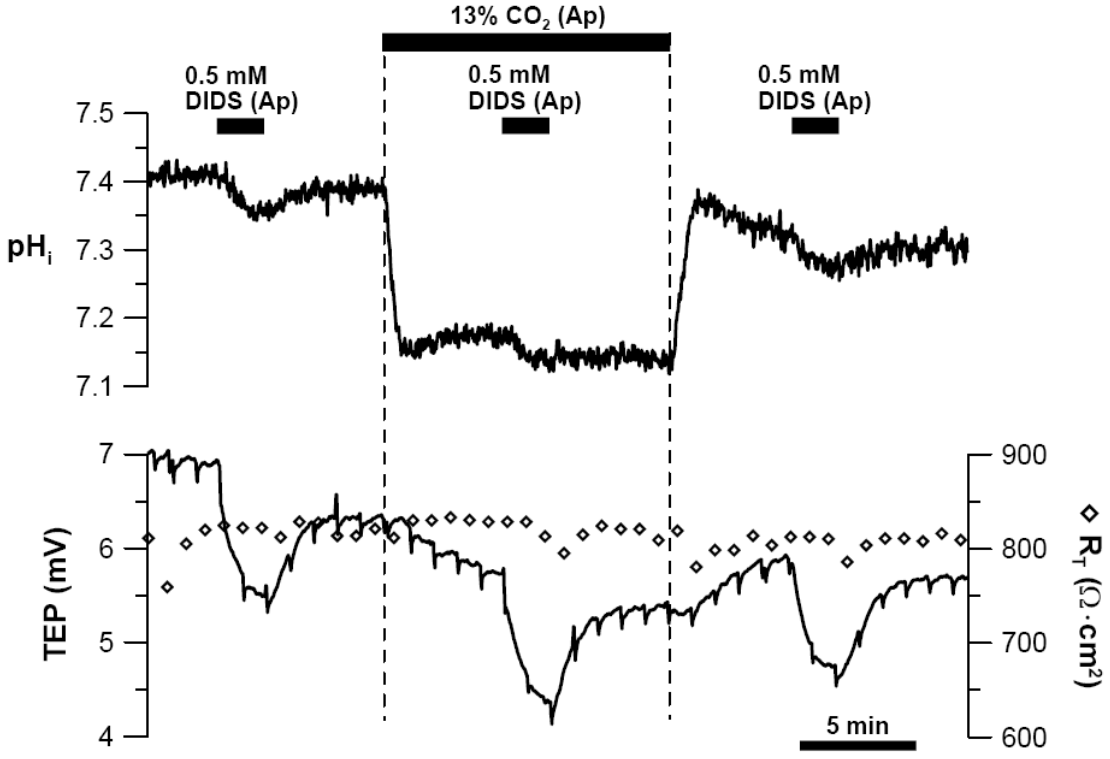

Fig. 3-9: DIDS induced pH_i, TEP, and R_T responses in the presence of 13% apical CO_2.

Our first step is to determine if increasing apical bath CO_2 stimulates HCO_3-entry into the cell via NBC1. To test this hypothesis, we compared apical DIDS (0.5 mM) induced pH_i and TEP responses in control (5% CO_2) Ringer to that in 1% or 13% CO_2 equilibrated

Ringer (Fig. 3-9). If NBC1 activity is enhanced by an increased CO_2 level in the apical bath, then DIDS-induced inhibition of NBC1 should cause larger pH_i and TEP responses in 13% apical CO_2 than in control (5% CO_2). Alternatively, if decreasing apical bath CO_2 from 5% to 1% decreased NBC1 activity, the DIDS-induced pH_i and TEP responses should be smaller in 1% apical CO_2 than in control. In four experiments, apical DIDS induced pH_i and TEP responses in control (5% CO_2) Ringer ($\Delta pH_i = 0.05 \pm 0.02$; $\Delta TEP = 1.52 \pm 0.33$ mV) were the same as that in 13% CO_2 equilibrated Ringer ($\Delta pH_i = 0.05 \pm 0.02$; $\Delta TEP = 1.57 \pm 0.67$ mV; $p > 0.05$). Similarly, the apical DIDS induced pH_i and TEP responses in control Ringer ($\Delta pH_i = 0.05 \pm 0.02$; $\Delta TEP = 1.66 \pm 0.59$ mV) were the same as that in 1% CO_2 equilibrated Ringer ($\Delta pH_i = 0.06 \pm 0.02$; $\Delta TEP = 1.31 \pm 0.78$ mV; $n = 5$; $p > 0.05$; Fig. 3-10).

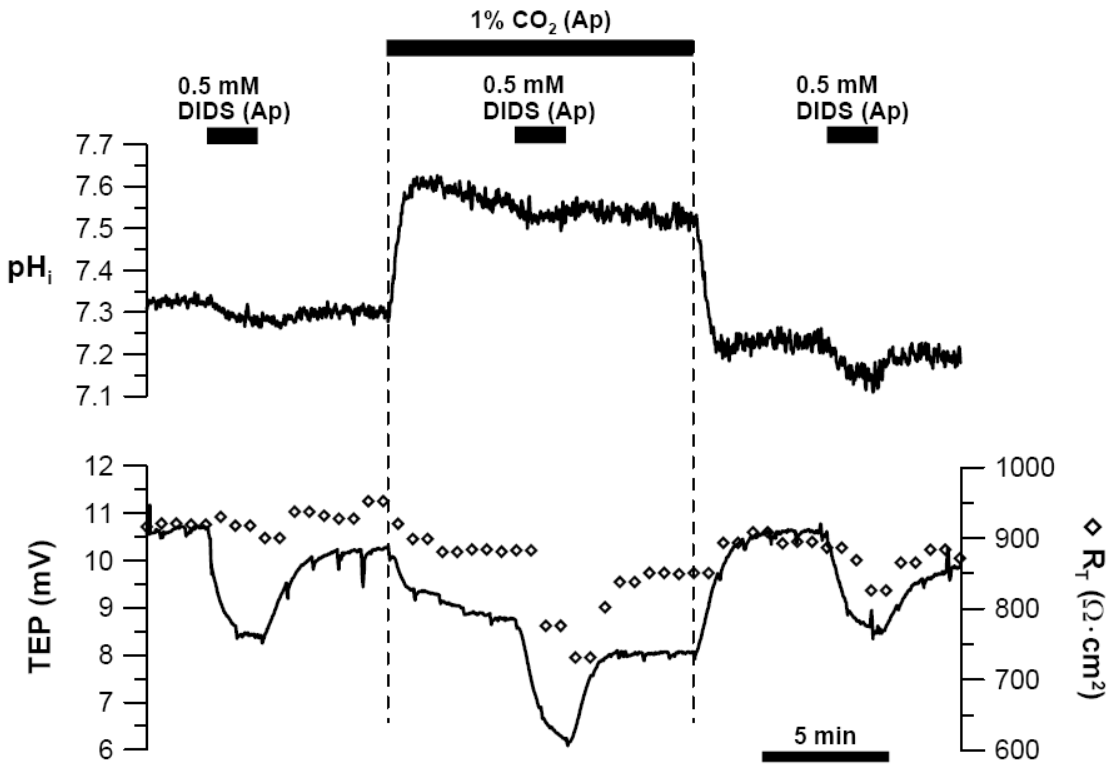

Fig. 3-10: DIDS induced pH_i, TEP, and R_T responses in the presence of 1% apical CO_2.

To further test the pH_i-sensitivity of the apical membrane $Na/2HCO_3$ co-transporter, we perfused 13% CO_2 equilibrated Ringer into the apical bath in the presence or absence of 0.5 mM apical DIDS (Fig. 3-11). If increasing apical bath CO_2 stimulates NBC1, 13% apical CO_2 should cause a larger acidification in the absence of NBC1 activity.

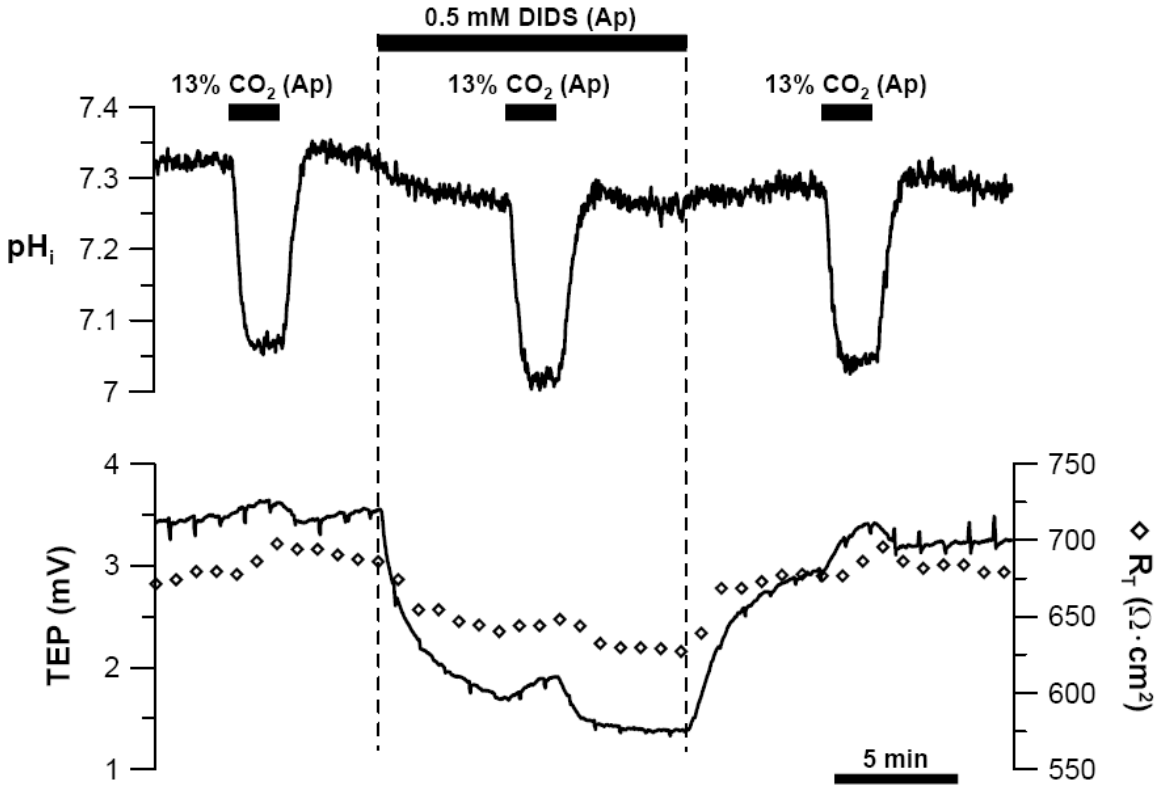

Fig. 3-11: 13% apical CO_2 induced pH_i, TEP, and R_T responses in the presence of apical DIDS.

However, in the presence of apical DIDS, the 13% CO_2-induced acidification (ΔpH_i = 0.22 ± 0.03) was the same as control (ΔpH_i = 0.22 ± 0.02; n = 4; p > 0.05). Taken together, these observations (Fig. 3-9, -10, -11) lead to the conclusion that $Na/2HCO_3$ co-transport activity is unaffected by apical bath CO_2. This is probably due to the high CO_2-permeability of the apical membrane; CO_2/HCO_3 equilibration across the apical

membrane is achieved very quickly, which prevented the formation of a HCO_3-gradient needed to increase the rate of $NaHCO_3$ transport via NBC1.

According to Fig. 1-4, HCO_3 that enters the RPE via NBC1 can be converted by CA II into CO_2 and H_2O in the cytosol. By effectively removing HCO_3 (by converting it to CO_2) near NBC1's ion-pore in the cytosol, CA II facilitates apical $Na/2HCO_3$ co-transport activity by maintaining a high local $[HCO_3]$ gradient across the transporter. We test this notion by decreasing apical bath $[HCO_3]$ (10-fold) and comparing the resultant pH_i and TEP responses in the presence of 250 μM apical dorzolamide (DZA; CA II inhibitor) to that in control (Fig. 3-12).

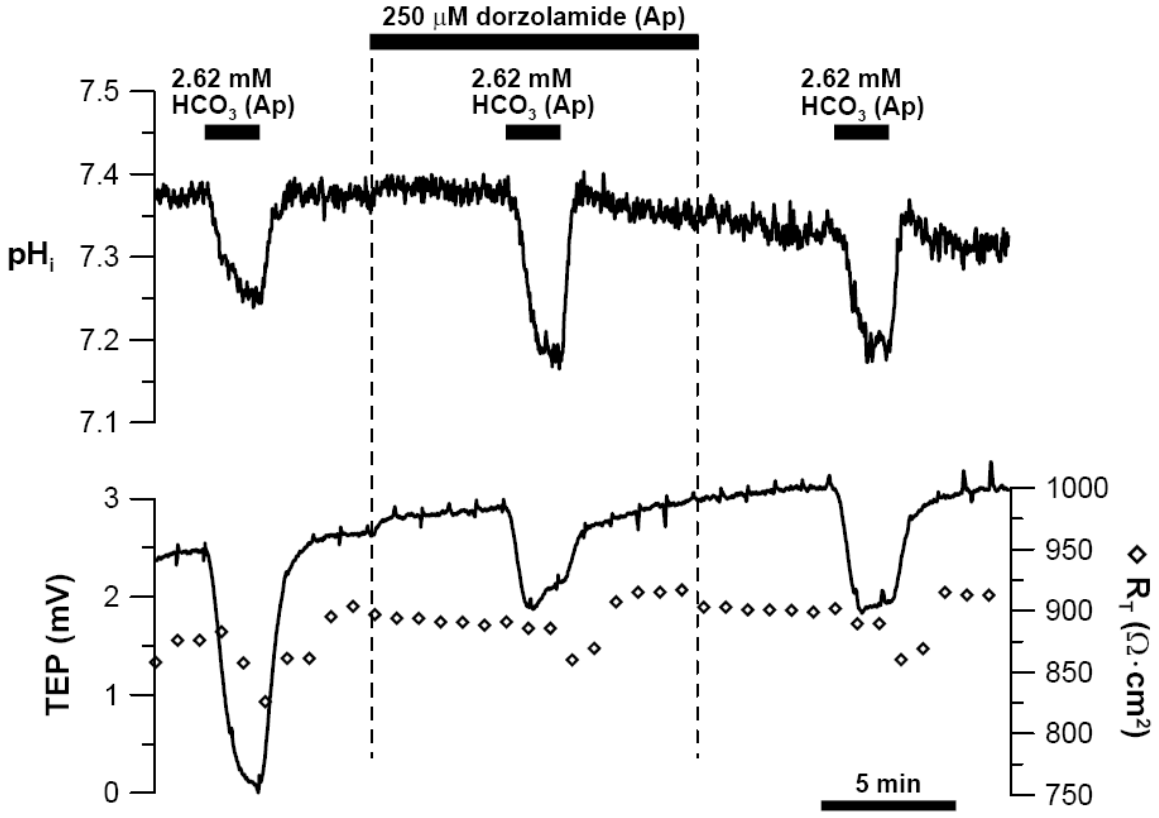

Fig. 3-12: Apical bath $\Delta[HCO_3]$-induced pH_i, TEP, and R_T responses in the presence of apical dorzolamide.

In five experiments, DZA decreased apical bath $\Delta[HCO_3]$-induced TEP response by 60% (from 2.25 ± 0.81 to 0.89 ± 0.29 mV; $p < 0.01$) and increased the pH_i response from 0.11 ± 0.01 to 0.19 ± 0.01 ($p < 0.01$) – the effect of DZA on these responses were partially reversible following washout ($\Delta TEP = 1.27 \pm 0.46$ mV; $\Delta pH_i = 0.17 \pm 0.02$). The reduced apical bath $\Delta[HCO_3]$-induced TEP response in the presence of DZA indicates inhibition of apical $Na/2HCO_3$ co-transport activity. On the other hand, the apical bath $\Delta[HCO_3]$-induced acidification was larger in the presence of DZA because CA II-inhibition reduces intracellular CO_2/HCO_3 buffering capacity, which compromises the ability of the RPE to buffer the acidification caused by HCO_3-efflux from the apical membrane. This experiment indicates that NBC1 activity is dependent on CA II activity.

In summary, increasing apical bath CO_2 did not stimulate $NaHCO_3$ transport via NBC1. This result may seem counter intuitive in the context of the HCO_3-transport metabolon (see Fig. 1-9), but it can be understood by taking into account the higher apical membrane CO_2 permeability than the basolateral membrane; 13% CO_2 in the apical bath equilibrates very quickly in the cytosol. The lower CO_2 permeability of the basolateral membrane causes CO_2 to accumulate in the cytosol, thus allowing CO_2 level in the cytosol to approximately equal that in the apical bath. Without a large CO_2 gradient across the apical membrane, little or no CO_2 is converted into HCO_3 for NBC1-mediated HCO_3-transport. In contrast, 13% apical CO_2 generates a large CO_2 gradient across the basolateral membrane, which should drive carbonic anhydrase-mediated conversion of CO_2 to HCO_3 for HCO_3-transport across the basolateral membrane (see next section).

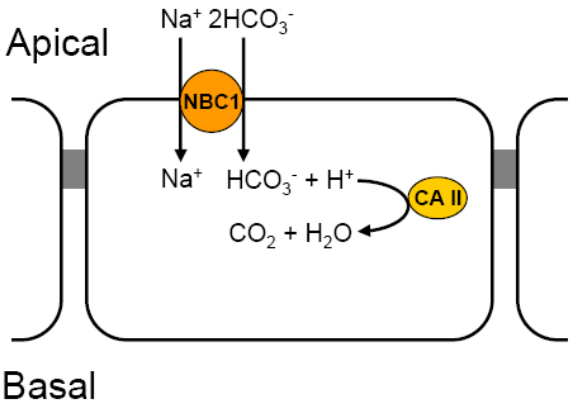

Section 3.2 conclusions: HCO_3 is transported across the apical membrane via the electrogenic and DIDS-sensitive Na/2HCO_3 co-transporter (NBC1)
NBC1 activity is unaffected by CO_2-gradient (13% apical CO_2)
NBC1 activity is dependent on carbonic anhydrase II activity

Supporting experimental observations	Interpretation	Fig.
Apical DIDS increased pH_i in control (26 mM HCO_3), but decreased pH_i in low HCO_3 Ringer (2.6 mM)	HCO_3 is transported across the apical membrane via HCO_3-transporter	3-7
Apical DIDS decreased TEP in control (26 mM HCO_3), but increased TEP in low HCO_3 Ringer (2.6 mM)	HCO_3 is transported across the apical membrane via an electrogenic HCO_3-transporter	3-7
Decreasing apical bath [HCO_3] decreased pH_i	HCO_3 is transported across the apical membrane via NBC1 and/or NBC3	3-8
Apical bath Δ[HCO_3]-induced acidification is unaffected by apical DIDS	HCO_3 is transported across the apical membrane via NBC3	3-8
Decreasing apical bath [HCO_3] decreased TEP	HCO_3 is transported across the apical membrane via an electrogenic HCO_3-transporter	3-8
Apical bath Δ[HCO_3]-induced TEP response is blocked by apical DIDS	HCO_3 is transported across the apical membrane via NBC1	3-8
Apical DIDS-induced pH_i and TEP responses were the same in 5%, 1% or 13% apical CO_2	CO_2-gradient or cell acidification did not affect NBC1 activity	3-9 & 3-10
13% apical CO_2-induced pH_i response were unaffected by apical DIDS	CO_2-gradient or cell acidification did not affect NBC1 activity	3-11
Apical bath Δ[HCO_3]-induced TEP response was reduced by apical dorzolamide	NBC1 activity is dependent on cytosolic carbonic anhydrase II	3-12

Section 3.4 – HCO_3-transport at RPE basolateral membrane

In frog RPE, a DIDS-sensitive Cl/HCO_3 exchanger was found at the basolateral membrane (Lin & Miller, 1994). The activity of this Cl/HCO_3 exchanger is pH_i dependent; it was inhibited by acid and activated by base. Normally, the Cl/HCO_3 exchanger uses the Cl-gradient (inward) to drive HCO_3 out of the cell. We can evaluate basolateral membrane Cl/HCO_3 exchanger activity in hfRPE by reducing basal bath [Cl] (from 126 mM to 1 mM). This creates a large outward Cl gradient across the basolateral membrane that drives HCO_3 into the cell to cause an alkalinization ($\Delta pH_i = 0.22$; Fig. 3-13). In three experiments this alkalinization ($\Delta pH_i = 0.18 \pm 0.05$) was abolished by 0.5 mM basal DIDS ($\Delta pH_i = 0.02 \pm 0.01$; $n = 3$; $p < 0.05$).

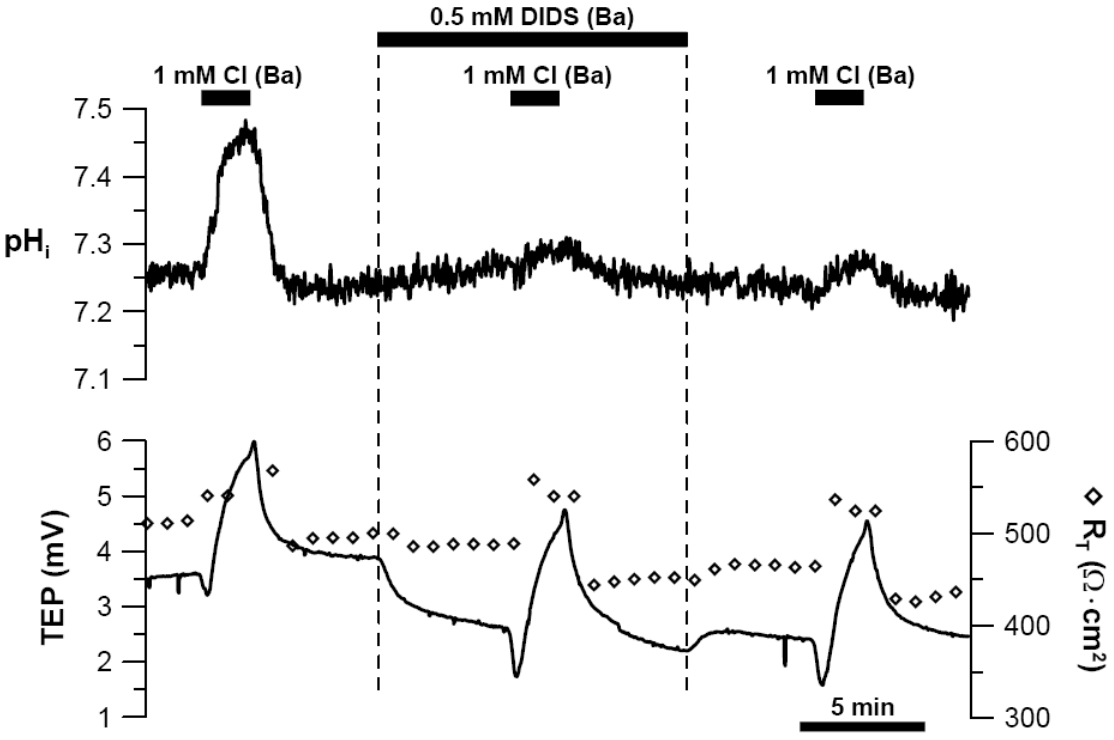

Fig. 3-13: Basal bath Δ[Cl]-induced pH_i, TEP, and R_T responses in the presence of basal DIDS.

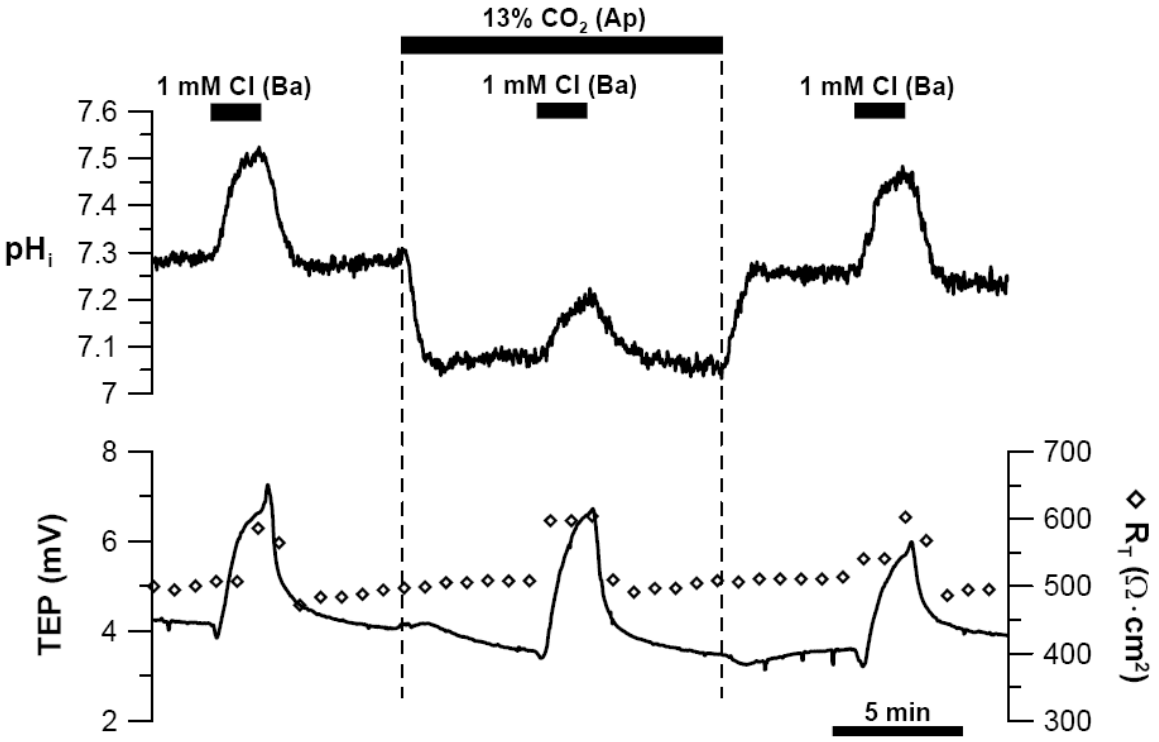

Fig. 3-14: Basal bath Δ[Cl]-induced pH_i, TEP, and R_T responses in 13% apical CO_2.

Next, we tested the pH_i-dependence of the Cl/HCO_3 exchanger by comparing the basal bath Δ[Cl]-induced pH_i response in 5% vs. 13% apical bath CO_2 (Fig. 3-14). The steady-state pH_i in 5% and 13% apical bath CO_2 differed significantly, which required us to use the total buffering capacity of the hfRPE to calculate equivalent H^+-fluxes. In the presence of 13% CO_2 equilibrated Ringer in the apical bath, the basal bath Δ[Cl]-induced change in H^+-flux was 2.3 ± 1.0 $mM \cdot min^{-1}$, ≈ 4-fold smaller than the H^+-flux in 5% CO_2 (9.0 ± 4.5 $mM \cdot min^{-1}$; n = 7; $p < 0.01$); this effect was fully reversible. Fig. 3-15 shows a parallel experiment in which basal bath [Cl] was reduced in the presence of 1% CO_2 equilibrated Ringer in the apical bath.

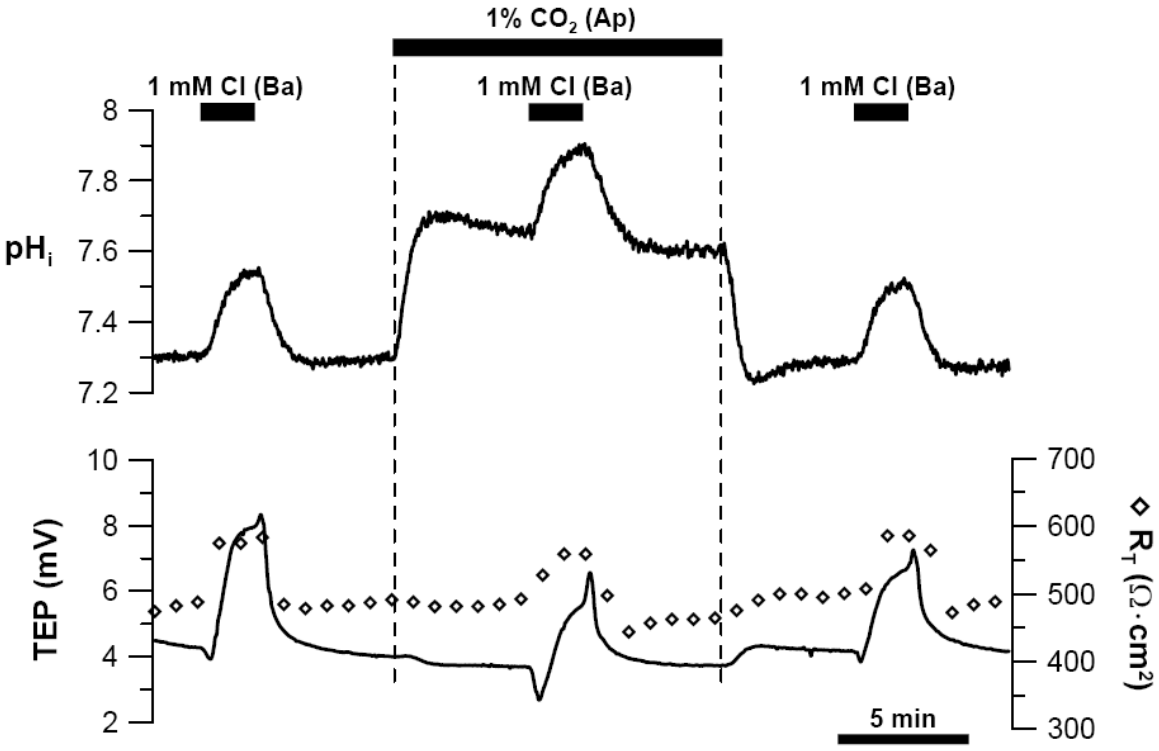

Fig. 3-15: Basal bath Δ[Cl]-induced pH_i, TEP, and R_T responses in 1% apical CO_2.

In 1% apical bath CO_2, the basal bath Δ[Cl]-induced proton flux was 27.4 ± 10.8 $mM \cdot min^{-1}$, or ≈ 5-fold larger than the flux in 5% CO_2 (5.9 ± 6.5 $mM \cdot min^{-1}$; n = 5; p = 0.01). These experiments indicate that the DIDS-sensitive basolateral membrane Cl/HCO_3 exchanger in hfRPE is pH_i-dependent. From our laboratory's Affymetrix data, AE2 (SLC4A2; GeneID: 6522) is the only AE isoform detected in cultured fetal human RPE and in native adult and fetal human RPE. Since AE2 is pH-sensitive (Kurschat et al., 2006; Stewart et al., 2007), it is possibly the isoform located at the basolateral membrane of hfRPE.

In the retina, the transition from light to dark is followed by increased metabolism and CO_2 and water release into the subretinal space. In section 2 of this chapter, we

hypothesized that the relatively higher apical vs. basolateral membrane CO_2-permeability could produce a large CO_2-gradient across the basolateral membrane *in vivo*. With the help of carbonic anhydrase activity, this CO_2-gradient can drive HCO_3 out of the basolateral membrane via HCO_3-transporters. Although the Cl/HCO_3 exchanger (AE2) is a HCO_3-transporter, our experiments (Fig. 3-13) show that AE2 is inhibited by 13% apical CO_2. To facilitate an increased HCO_3-efflux from the basolateral membrane, the RPE requires an alternate HCO_3-efflux pathway. In this regard, evidence of an electrogenic $Na/nHCO_3$ co-transporter at the basolateral membrane has been reported in bovine RPE (Kenyon *et al.*, 1997). This transporter may work in parallel with AE2 to mediate HCO_3-efflux at the basolateral membrane.

To test the basolateral membrane $Na/nHCO_3$ co-transporter activity in hfRPE, we reduced basal bath $[HCO_3]$ by 10-fold to induce a large $[HCO_3]$-gradient across the basolateral membrane. This maneuver causes HCO_3 to leave the cell via both AE2 and the $Na/nHCO_3$ co-transporter, resulting in intracellular acidification. Since this $Na/nHCO_3$ co-transporter is an electrogenic mechanism, HCO_3-efflux via this transporter will depolarize the basolateral membrane, which increases TEP. In contrast, AE2 is electroneutral (no transfer of net ionic charges across the membrane) and therefore could not have contributed to the TEP response; the basal bath $\Delta[HCO_3]_o$ induced TEP response originates solely from $Na/nHCO_3$ co-transport activity. In confluent monolayers of hfRPE, reducing basal bath $[HCO_3]$ 10-fold (5% CO_2) acidified the cells by 0.20 ± 0.05 with an equivalent H^+-flux of 6.2 ± 1.5 $mM \cdot min^{-1}$ ($n = 45$), and increased TEP by 1.18 ± 0.60 mV ($n = 53$).

Table 3-1. Summary of basal bath Δ[HCO_3]-induced pH_i responses.

inhibitor/condition[a]		2.62 mM basal bath [HCO_3]-induced pH_i response[b]					
Apical	**Basal**	**Data**	**Control**	**w/ inhibitor**	**Recovery**	**p[c]**	**n**
	DIDS	**ΔpH_i**	-0.20 ± 0.04	-0.09 ± 0.05	-0.12 ± 0.03	S	5
		H^+-flux	-6.5 ± 1.2	-3.6 ± 2.7	-4.3 ± 1.3	S	
Na-free	**Na-free**	**ΔpH_i**	-0.21 ± 0.04	-0.08 ± 0.01	-0.14 ± 0.02	S	3
		H^+-flux	-7.2 ± 1.7	-2.8 ± 0.7	-4.9 ± 0.8	S	
amiloride		**ΔpH_i**	-0.22 ± 0.03	-0.28 ± 0.05	-0.21 ± 0.04	S	5
		H^+-flux	-7.1 ± 1.3	-8.3 ± 1.6	-5.7 ± 1.4	S	
bumetanide		**ΔpH_i**	-0.20 ± 0.03	-0.21 ± 0.03	-0.22 ± 0.03	NS	4
		H^+-flux	-6.9 ± 1.8	-6.8 ± 0.9	-7.6 ± 1.6	NS	
ouabain		**ΔpH_i**	-0.18 ± 0.02	-0.20 ± 0.02	-0.23 ± 0.03	NS	3
		H^+-flux	-5.1 ± 2.1	-5.4 ± 3.2	-5.7 ± 2.7	NS	
DIDS		**ΔpH_i**	-0.19 ± 0.03	-0.23 ± 0.03	-0.21 ± 0.01	S	7
		H^+-flux	-5.0 ± 1.1	-6.0 ± 1.1	-5.3 ± 0.9	S	
	DZA	**ΔpH_i**	-0.17 ± 0.01	-0.18 ± 0.03	-0.18 ± 0.02	NS	4
		H^+-flux	-5.2 ± 0.3	-5.1 ± 0.7	-5.6 ± 0.4	NS	
13% CO_2		**ΔpH_i**	-0.21 ± 0.05	-0.20 ± 0.03	-0.24 ± 0.04	NS	9
		H^+-flux	-6.0 ± 1.3	-6.1 ± 2.3	-6.5 ± 1.4	NS	
1% CO_2		**ΔpH_i**	-0.24 ± 0.08	-0.20 ± 0.06	-0.20 ± 0.06	NS	5
		H^+-flux	-7.2 ± 1.8	-10.7 ± 1.9	-6.0 ± 1.3	S	

a. Blank cells indicate that control Ringer was perfused into the corresponding bath.

b. H^+-flux has units of $mM \cdot min^{-1}$ and all values are reported as mean ± SD.

c. Student's t-test for statistical significance between basal bath Δ[HCO_3]-induced pH_i response in control vs. in the presence of inhibitor/condition. "S" indicates statistical significance ($p < 0.05$), "NS" indicates statistical insignificance ($p > 0.05$).

Table 3-2. Summary of basal bath Δ[HCO_3]-induced TEP responses.

inhibitor/condition[a]		2.62 mM basal bath [HCO_3]-induced TEP response (mV)[b]				
Apical	**Basal**	**Control**	**w/ inhibitor**	**Recovery**	**p[c]**	**n**
	DIDS	1.41 ± 0.69	0.42 ± 0.29	0.56 ± 0.25	S	5
Na-free	**Na-free**	1.01 ± 0.21	0.04 ± 0.07	0.79 ± 0.38	S	3
amiloride		1.28 ± 0.58	1.24 ± 0.50	1.23 ± 0.40	NS	5
bumetanide		0.89 ± 0.28	0.80 ± 0.18	0.97 ± 0.29	NS	6
ouabain		1.26 ± 0.59	1.17 ± 0.49	1.19 ± 0.51	NS	5
DIDS		0.86 ± 0.16	0.49 ± 0.07	0.63 ± 0.15	S	6
	DZA	1.44 ± 0.80	0.98 ± 0.50	1.06 ± 0.55	S	9
13% CO_2		1.11 ± 0.67	1.35 ± 0.78	1.07 ± 0.67	S	9
1% CO_2		1.26 ± 0.74	0.37 ± 0.32	0.99 ± 0.59	S	5

a. Blank cells indicate that control Ringer was perfused into the corresponding bath.

b. All ΔTEP values are reported as mean ± SD.

c. Student's t-test for statistical significance between basal bath Δ[HCO_3]-induced TEP response in control vs. in the presence of inhibitor/condition. "S" indicates statistical significance ($p < 0.05$), "NS" indicates statistical insignificance ($p > 0.05$).

Electrogenic members of the NBC family of Na/HCO_3 transporters (e.g., NBC1 and NBC4) are DIDS sensitive. To ensure that the basal bath $\Delta[HCO_3]$-induced pH_i and TEP responses are mediated by a $Na/nHCO_3$ co-transporter, we compared these pH_i and TEP responses in the presence vs. absence of 0.5 mM DIDS in the basal bath (Fig. 3-16).

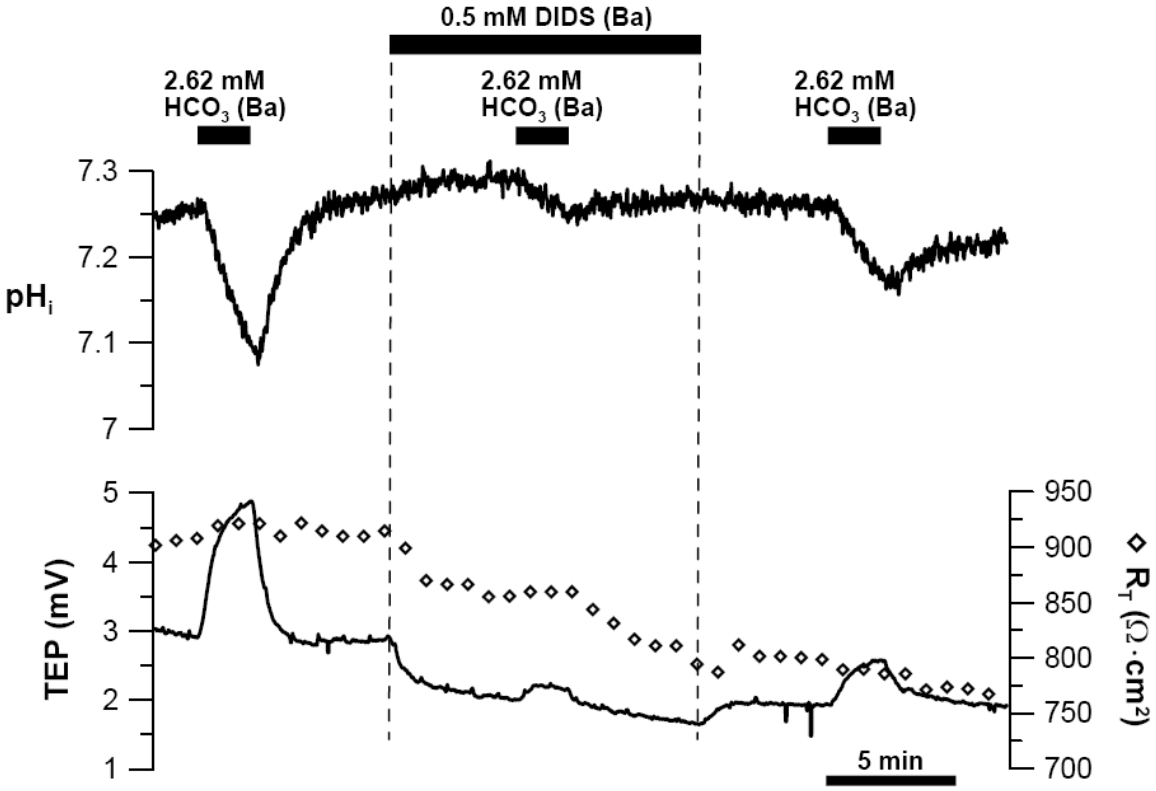

Fig. 3-16: Basal bath $\Delta[HCO_3]$-induced pH_i, TEP, and R_T responses in the presence of basal DIDS.

In five experiments, basal DIDS reduced the basal bath $\Delta[HCO_3]$-induced acidification by ≈ 50% (Table 3-1), and reduced the TEP response by ≈ 70% (Table 3-2). The inhibitory effect of DIDS on the pH_i and TEP responses was irreversible (5 min washout). The significant inhibition of the basal bath $\Delta[HCO_3]$-induced acidification by basal DIDS indicates that HCO_3-transporters at the basolateral membrane are DIDS-

sensitive. Since TEP respond only to electrogenic processes, the significant inhibition of the TEP response by basal DIDS indicates a reduction in Na/nHCO_3 co-transport activity.

Since the Na/nHCO_3 co-transporter is a Na-dependent mechanism, the removal of Na from both apical and basal baths should eliminate its activity. Therefore, we reduced basal bath [HCO_3] and measure the resultant pH_i and TEP responses in the presence or absence of Na (Fig. 3-17).

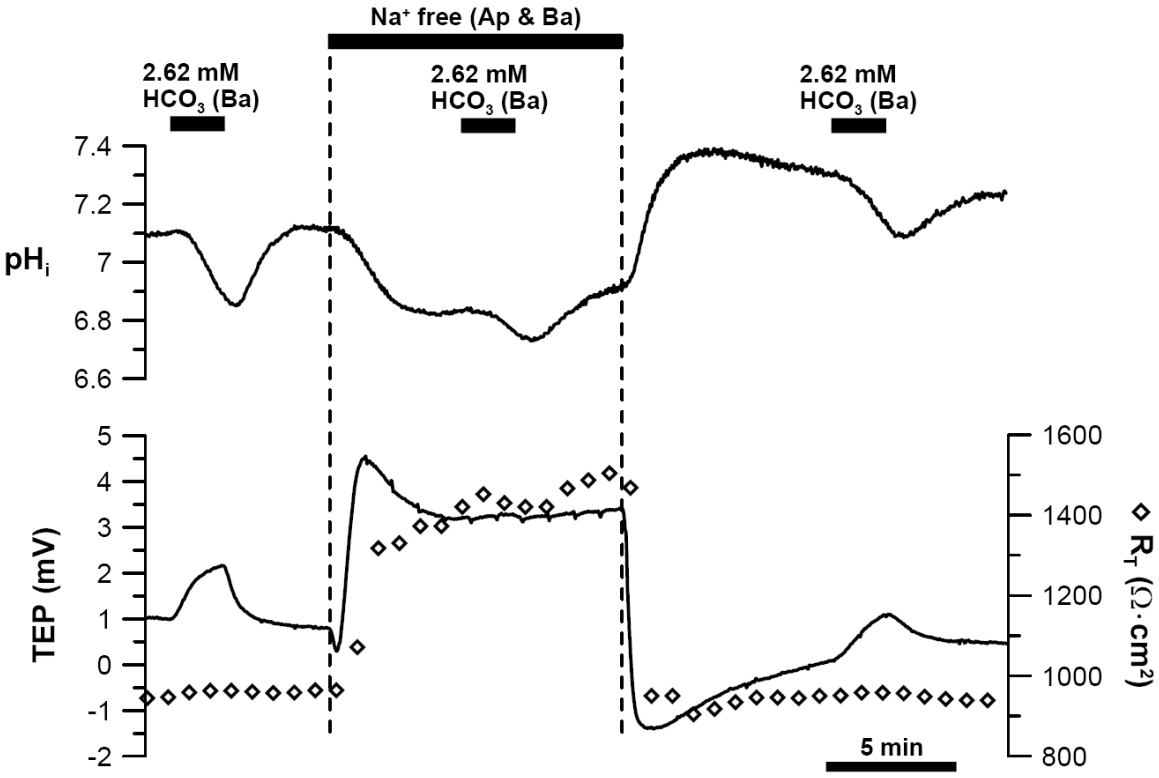

Fig. 3-17: Basal bath Δ[HCO_3]-induced pH_i, TEP, and R_T responses in the absence of Na^+.

When Na is removed from both apical and basal baths, the cell acidified by ~ 0.3 pH-units. This observation is consistent with HCO_3-efflux from both the apical and basolateral membranes via Na-linked HCO_3 transporters. In three experiments, Na-removal reduced the basal bath Δ[HCO_3]-induced acidification by more than 2-fold

compared to control (Table 3-1). In addition, the basal bath $\Delta[HCO_3]$-induced TEP response was essentially abolished in the absence of Na, and this effect was reversible (Table 3-2). These experiments indicate that although reducing basal bath $[HCO_3]$ causes HCO_3-efflux via both AE2 and $Na/nHCO_3$ co-transporter, the TEP response corresponds specifically to $Na/nHCO_3$ co-transporter activity due to its electrogenicity and Na-dependence. This allows one to distinguish the activity of the $Na/nHCO_3$ co-transporter from that of AE2.

Affymetrix data on human RPE (native adult and fetal RPE, and cultured fetal RPE) (Wang and Miller, ARVO 2007, #6034) show high mRNA expression levels for NBC1 (SLC4A4; GeneID: 8671) and NBC4/NBCe2 (SLC4A5; GeneID: 57835), both of which are candidates for the identity of the basolateral membrane $Na/nHCO_3$ co-transporter in human RPE. Although this co-transporter's identity is unknown, both NBC1 and NBC4 have been shown to transport $Na:HCO_3$ with a stoichiometry of 1:2 (Hughes *et al.*, 1989; Gross *et al.*, 2001; Virkki *et al.*, 2002), suggesting inward Na/HCO_3 co-transport from the basolateral membrane. However, NBC4 transports $Na:HCO_3$ with a 1:3 stoichiometry at the apical membrane of the choroid plexus epithelium (Millar & Brown, 2008). Since both the RPE and the choroid plexus epithelium derives from the neural ectoderm and share many similarities in HCO_3-transport mechanisms (Brown et al., 2004; Praetorius, 2007), it is possible that the RPE expresses NBC4 at the basolateral membrane and transports $Na/nHCO_3$ with a 1:3 $Na:HCO_3$ stoichiometry. In addition, our calculation of the reversal potential of the $Na/nHCO_3$ co-transporter indicate that a 1:3 stoichiometry is

required for Na/nHCO_3 transport out of the cell; this calculation is based on our estimation of resting $[Na]_i$ and pH_i in control Ringer with the following equation:

$$E_{NBC} = \frac{2.3RT}{F(n-1)} \log\left(\frac{[Na^+]_{in}}{[Na^+]_{out}}\right)\left(\frac{[HCO_3^-]_{in}}{[HCO_3^-]_{out}}\right)^n$$, where $[Na^+]_{in}$ = 15.7 mM, $[Na^+]_{out}$ = 143.7 mM, $[HCO_3^-]_{in}$ = 27.9 mM, $[HCO_3^-]_{out}$ = 26.2 mM. *n* is the stoichiometry of the Na/nHCO_3 co-transporter. For a Na:HCO_3 transport stoichiometry of 1:2 and 1:3, we calculated the reversal potential of the Na/nHCO_3 co-transporter NBC (E_{NBC}) to be -55.7 and -27 mV respectively. To transport Na/nHCO_3 out of the cell against the strong inward Na-gradient in control conditions, E_{NBC} must be more depolarized than V_B (-49.8 ± 3.7 mV; Maminishkis et al, 2006) and this condition is achieved for a Na:HCO_3 transport stoichiometry of 1:3. The isoform of this basolateral membrane NBC has not been determined.

When apical bath CO_2 is increased, CO_2 diffuses into the cell and accumulates within the cytosol, which shifts the CO_2/HCO_3 equilibrium towards the formation of HCO_3 and H^+ (catalyzed by carbonic anhydrase II). In this section, we showed that 13% apical CO_2 acidified the cell and inhibited the Cl/HCO_3 exchanger (AE2) at the basolateral membrane, indicating that AE2 cannot serve as the main HCO_3-efflux pathway when apical bath CO_2 increases. However, we also confirmed the presence and activity of an alternate HCO_3-efflux pathway at the basolateral membrane – Na/nHCO_3 co-transporter (NBC). In the next section, we investigate if increasing apical bath CO_2 can stimulate this Na/nHCO_3 co-transporter.

Section 3.5 – Basolateral membrane NBC: dependence on CO_2 and HCO_3

Carbonic anhydrase II (CA II) catalyzes the conversion of CO_2 into HCO_3, which is subsequently transported out of the basolateral membrane via the Na/nHCO_3 co-transporter (NBC). Since optimal HCO_3-transport requires a steady supply of HCO_3, inhibition of CA II by dorzolamide (DZA) should reduce Na/nHCO_3 co-transport across the basolateral membrane. This notion was tested by reducing basal bath [HCO_3] 10-fold in the presence of DZA (250 μM) in the basal bath (Fig. 3-18).

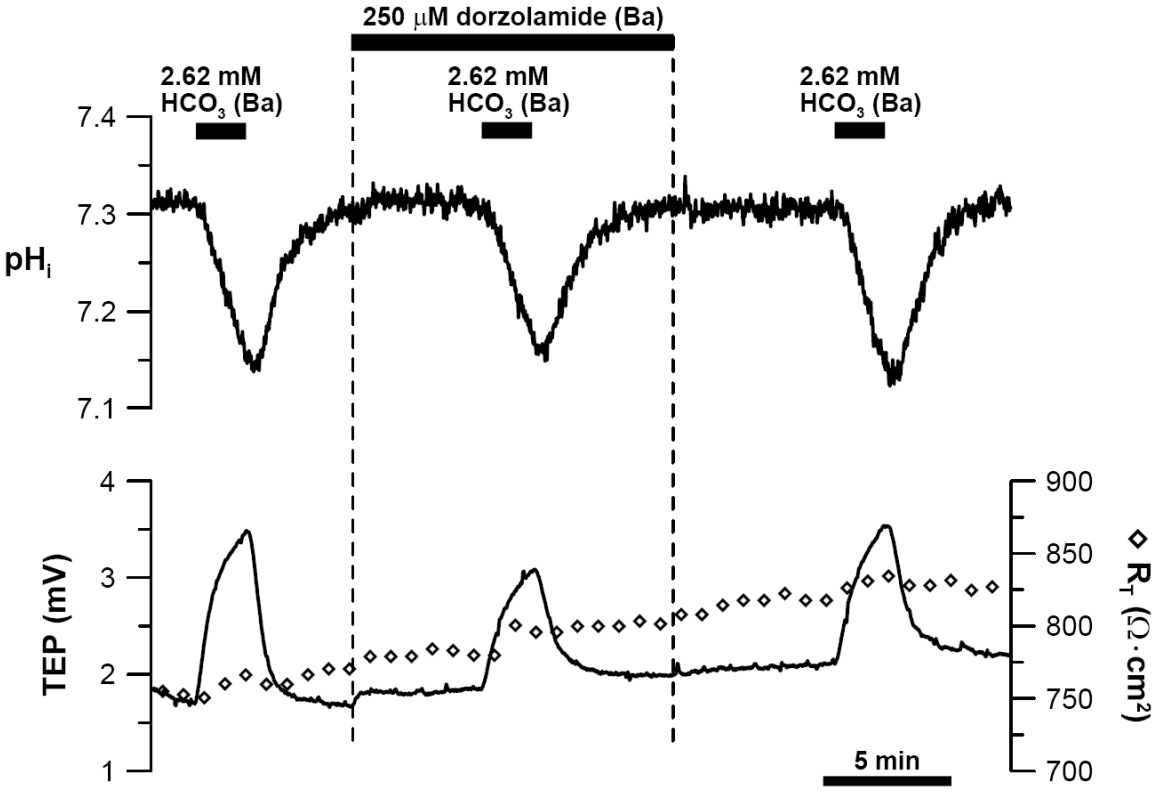

Fig. 3-18: Basal bath Δ[HCO_3]-induced pH_i, TEP, and R_T responses in the presence of dorzolamide in the basal bath.

In a total of nine experiments, DZA reduced the basal bath Δ[HCO_3]-induced TEP response by ≈ 30% (Table 3-2) suggesting that CA II-inhibition reduces basolateral

membrane NBC activity. In contrast, DZA did not affect the basal bath $\Delta[HCO_3]$-induced acidification (Table 3-1). This lack of effect probably occurred because the DZA-induced reduction in basolateral membrane HCO_3 efflux is counteracted by a concomitant reduction in intracellular CO_2/HCO_3 buffering capacity.

A 13% CO_2-load applied to the apical membrane should increase basolateral membrane NBC activity by shifting intracellular CO_2/HCO_3 equilibrium towards the formation of HCO_3 (facilitated by CA II activity). To test this hypothesis, we made a 10-fold reduction in basal bath $[HCO_3]$ (from 26.2 mM to 2.62 mM) and compared the resultant pH_i and TEP responses in 5% vs. 13% apical bath CO_2 (Fig. 3-19).

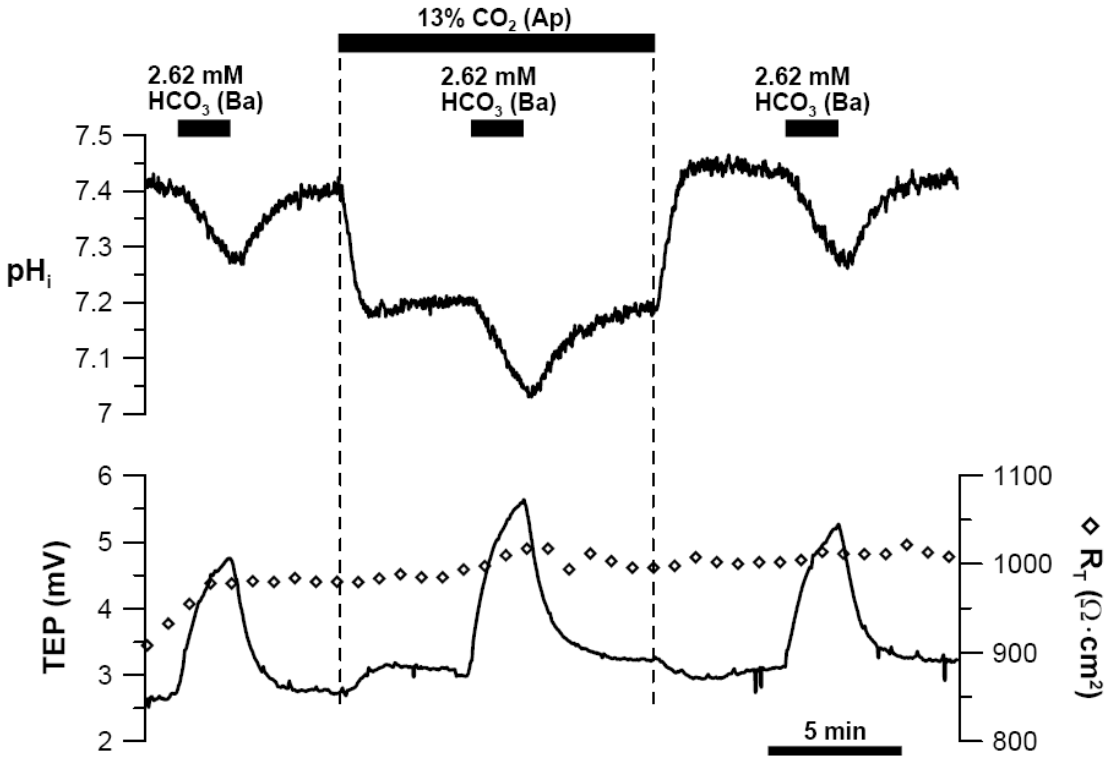

Fig. 3-19: Basal bath $\Delta[HCO_3]$-induced pH_i, TEP, and R_T responses with 13% apical CO_2.

With 13% CO_2 in the apical bath, decreasing basal bath [HCO_3] induced a TEP response that was ≈ 20% larger than control (Table 3-2). However, there was no change in basal bath Δ[HCO_3]-induced pH_i response (ΔpH_i and H^+-flux) in the presence of 5% or 13% apical bath CO_2 (Table 3-1). Presumably, 13% apical CO_2 did not significantly alter H^+-flux caused by basal bath Δ[HCO_3] because the CO_2-induced increase in HCO_3-efflux via the Na/nHCO_3 co-transporter was offset by concomitant inhibition of the pH_i-sensitive Cl/HCO_3 exchanger, thus producing no observable change in net H^+-flux. In similar experiments, we reduced basal bath [HCO_3] in 1% apical bath CO_2 (Fig. 3-20).

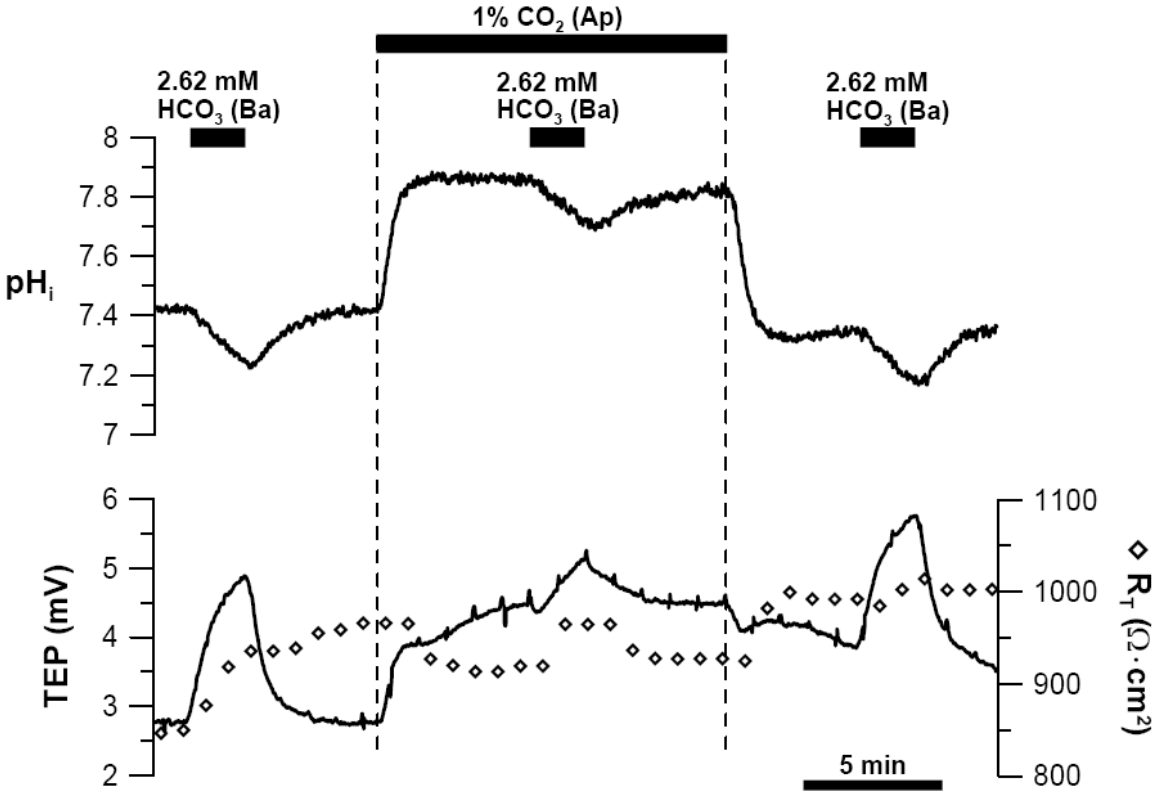

Fig. 3-20: Basal bath Δ[HCO_3]-induced pH_i, TEP, and R_T responses with 1% apical CO_2.

This maneuver should reduce free-HCO_3 in the cell and subsequently decrease basolateral membrane NBC activity. In 1% apical CO_2, the basal bath Δ[HCO_3]-induced

TEP response was more than 5-fold smaller than in 5% apical CO_2 (Table 3-2). This result indicates that intracellular CO_2 is a significant source of HCO_3-supply for the basolateral membrane NBC. 1% apical CO_2 increased the basal bath $\Delta[HCO_3]$-induced equivalent H^+-flux from 7.2 ± 1.8 to 10.7 ± 1.9 $mM \cdot min^{-1}$ (n = 5; p = 0.04). The H^+-flux in the presence of 1% apical bath CO_2 was larger probably because the resultant alkalinization activated the Cl/HCO_3 exchanger more than the reduction in $Na/nHCO_3$ co-transport activity.

By showing that 13% and 1% apical CO_2 increased and decreased the basal bath $\Delta[HCO_3]$-induced TEP response respectively, we confirmed our hypothesis that an increase in apical bath CO_2 stimulates HCO_3 efflux from the basolateral membrane via the basolateral membrane NBC. As shown in Fig. 3-18, this process is facilitated by cytosolic CA II activity. Since 13% apical CO_2 stimulates $NaHCO_3$ efflux from the basolateral membrane, we should observe a decrease in intracellular [Na]. In addition, since Na is a substrate of the basolateral membrane NBC, we expect its activity to depend on one or more Na-transport mechanism as its main source of Na. These mechanisms are explored in the next few sections.

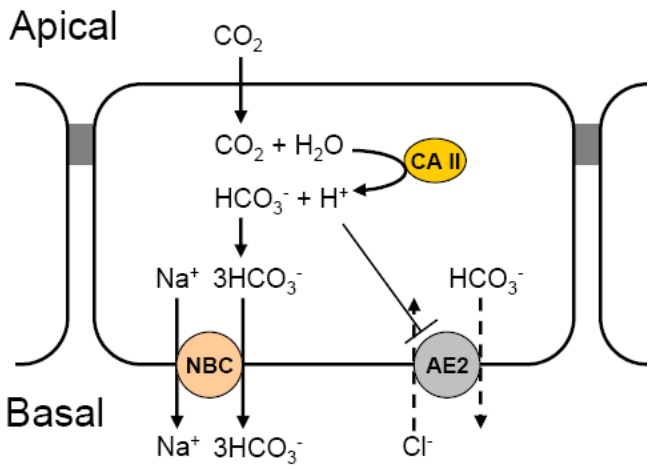

Sections 3.3 & 3.4 conclusions: Basolateral membrane HCO_3-transport is mediated by a Cl/HCO_3 exchanger (AE2) and an electrogenic $Na/nHCO_3$ co-transporter (NBC)
HCO_3-transport via basolateral membrane NBC is dependent on carbonic anhydrase II activity
Increasing apical bath CO_2 stimulates HCO_3-transport via basolateral membrane NBC

Supporting experimental observations	Interpretation	Fig.
Decreasing basal bath [Cl] increased pH_i, and this alkalinization is blocked by basal DIDS	HCO_3 is transported across the basolateral membrane via AE2	3-13
Basal bath Δ[Cl] induced alkalinization is inhibited and activated in 13% and 1% apical CO_2, respectively	AE2-mediated HCO_3-transport is pH_i-dependent	3-14 & 3-15
Decreasing basal bath [HCO_3] decreased pH_i, and this acidification is reduced by basal DIDS	HCO_3 is transported at the basolateral membrane via both AE2 and NBC	3-16
Decreasing basal bath [HCO_3] increased TEP, and this response is blocked by basal DIDS	Electrogenic HCO_3-transport at the basolateral membrane is DIDS-sensitive	3-16
Decreasing basal bath [HCO_3] decreased pH_i, and this acidification is reduced in the absence of Na^+	HCO_3 is transported at the basolateral membrane via both AE2 and NBC	3-17
Decreasing basal bath [HCO_3] increased TEP, and this response is abolished by Na^+-removal	Electrogenic HCO_3-transport at the basolateral membrane is Na-dependent	3-17
Basal bath Δ[HCO_3]-induced TEP response is reduced by basal dorzolamide	HCO_3-transport via basolateral membrane NBC is dependent on CA II activity	3-18
Basal bath Δ[HCO_3]-induced TEP response is increased in 13% apical CO_2	Increasing apical bath CO_2 stimulates basolateral membrane NBC	3-19
Basal bath Δ[HCO_3]-induced TEP response is decreased in 1% apical CO_2	Decreasing apical bath CO_2 stimulates basolateral membrane NBC	3-20

Section 3.6 – CO_2 and Na-transport

We showed that 13% apical CO_2 increased the basal bath $\Delta[HCO_3]$-induced TEP response (Fig. 3-19), suggesting that 13% apical CO_2 activates the basolateral membrane $Na/nHCO_3$ co-transporter, which should decrease $[Na]_i$. To test this notion, we observed the change in intracellular [Na] (with Na-sensitive dye) when apical bath CO_2 was increased from 5% to 13% (Fig. 3-21). Surprisingly, 13% apical CO_2 increased $[Na]_i$ from 15.7 ± 3.3 to 24.0 ± 5.3 mM (n = 6; $p < 0.05$).

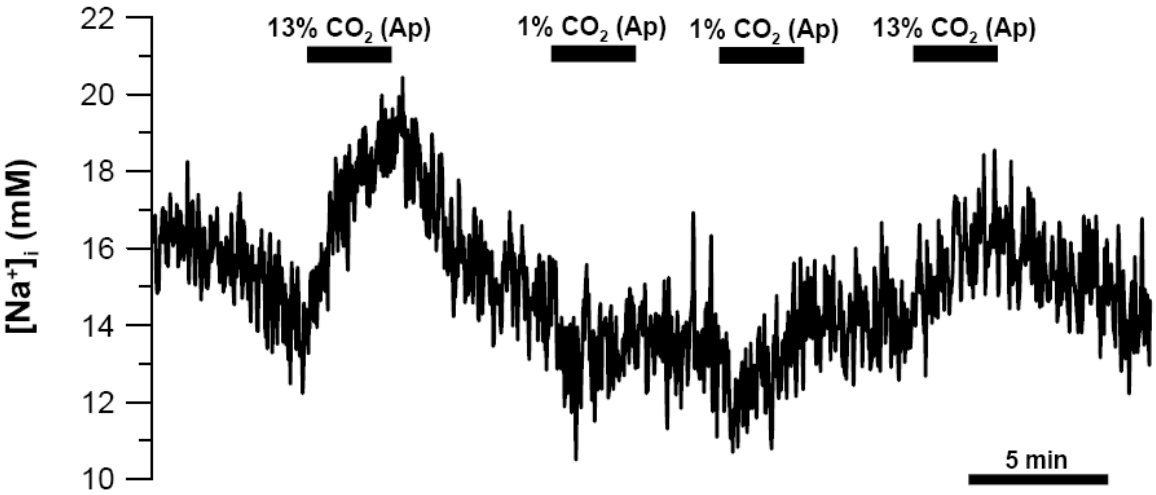

Fig. 3-21: 13% apical or basal CO_2 induced $[Na]_i$ responses.

This suggests that one or more Na-entry pathways at the apical membrane are affected by 13% apical CO_2 to produce the observed increase in $[Na]_i$. Early studies showed that the Na/H exchanger can be activated by intracellular acidification (Aronson et al., 1982; Dunham et al., 2004). Therefore it is possible that 13% apical CO_2 induced acidification stimulated NHE activity, which drives Na into the cell – this may explain the 13% apical CO_2 induced increase in $[Na]_i$. To test whether 13% apical CO_2-induced acidification activated NHE, we compared the effect of 1 mM amiloride (NHE inhibitor) on the

steady-state pH_i of the RPE in control Ringer (5% CO_2) to that in 13% CO_2 equilibrated Ringer (Fig. 3-22). If 13% apical CO_2 stimulated NHE activity, its inhibition by amiloride should cause a large acidification. However in three experiments, adding 1 mM amiloride into the apical bath did not cause any change in steady-state pH_i in either 5% or 13% apical bath CO_2.

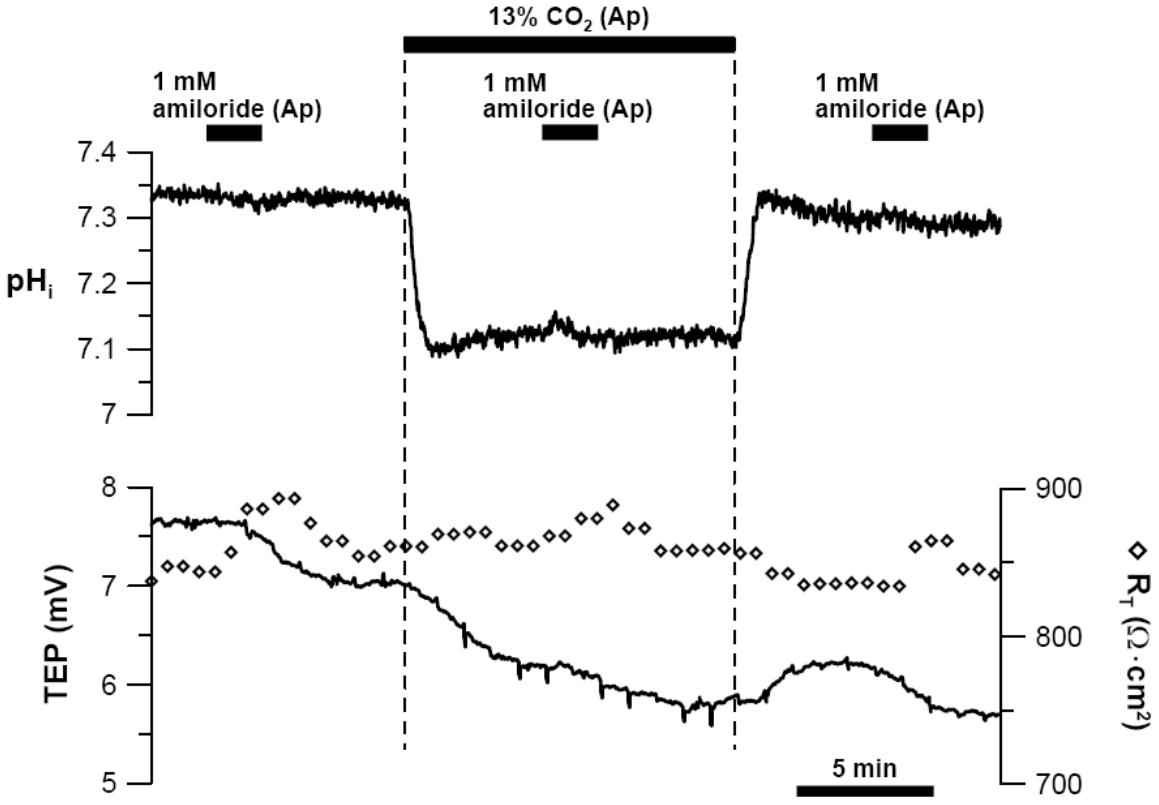

Fig. 3-22: Apical amiloride-induced pH_i, TEP, and R_T responses with 13% apical CO_2.

As an additional test, we compared the magnitude of the 13% apical CO_2-induced acidification in the presence or absence of 1 mM amiloride in the apical bath (Fig. 3-23). If NHE activity (H^+-efflux) helps buffer the 13% CO_2 induced acidification, this acidification should be significantly larger in the presence of apical amiloride.

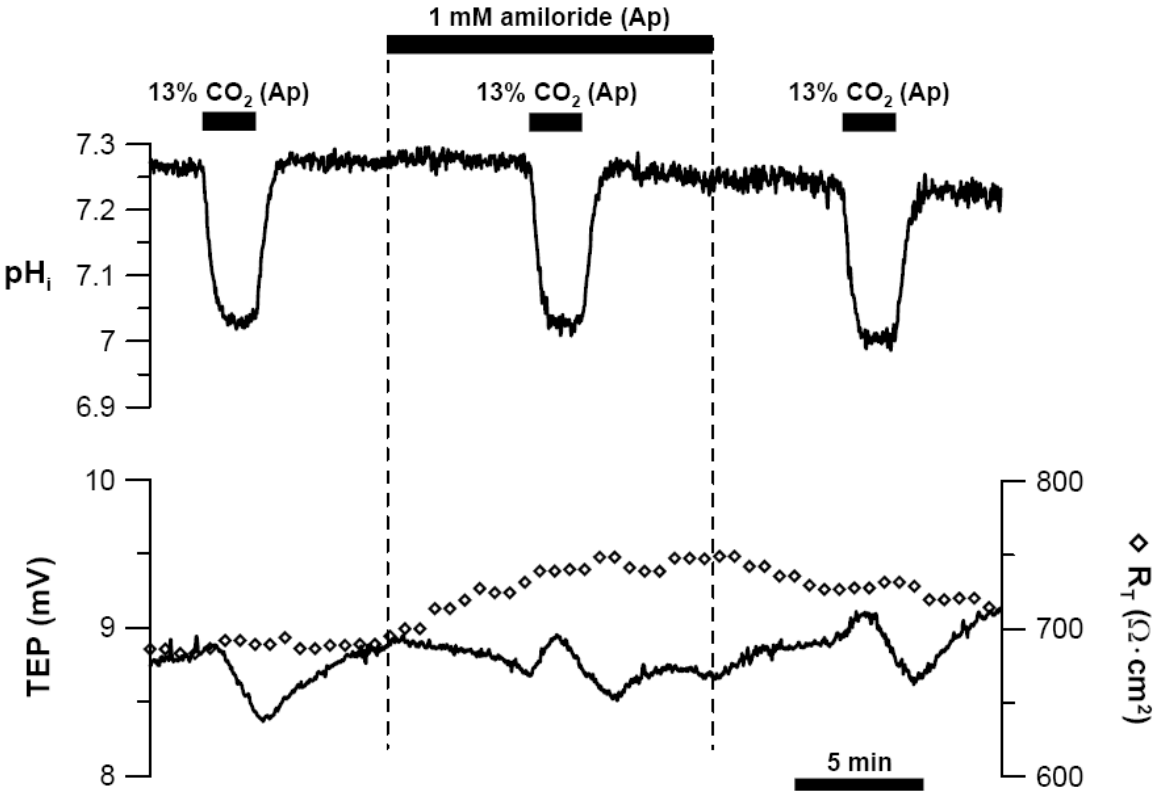

Fig. 3-23: 13% apical CO_2-induced pH_i, TEP, and R_T responses in the presence of apical amiloride.

In four experiments, amiloride did not affect the 13% apical CO_2-induced acidification ($\Delta pH_i = 0.23 \pm 0.01$) compared to control ($\Delta pH_i = 0.22 \pm 0.02$; $p > 0.05$). These experiments indicate that 13% apical CO_2-induced acidification did not activate NHE, therefore it could not have contributed to the CO_2-induced $[Na]_i$ increase. This lack of participation might have occurred for three reasons: (1) the 13% CO_2-induced acidification was too small; (2) there was no change in the proton-gradient across the Na/H exchanger; (3) the 13% CO_2 equilibrated Ringer is acidic relative to control (pH 7.09 vs. 7.5) and the low extracellular pH may have inhibited the Na/H exchanger (Aronson et al., 1983). We ruled out the first possibility with a 10 mM NH_4 pre-pulse

that caused only ≈ 0.1 decrease in pH_i (n = 4) but still showed the characteristic Na/H exchanger mediated pH_i recovery; in comparison, 13% apical CO_2 acidified the cell by more than 0.2 pH-units. In addition, we showed that reducing basal bath [HCO_3] acidified the cell by only ≈ 0.2 but was able to activate the Na/H exchanger. Na/2HCO_3 entry via NBC1 was eliminated as a possible cause of the 13% apical CO_2-induced $[Na]_i$-increase because: (1) the apical DIDS induced pH_i and TEP responses were the same in 5% or 13% apical bath CO_2 (Fig. 3-9); (2) the magnitude of the 13% apical CO_2-induced pH_i response was unaltered in the presence of apical DIDS (Fig. 3-11).

In alveolar epithelium, 3Na/2K ATPase activity is reduced by CO_2-induced acidification (Briva et al., 2007), suggesting the possibility of a similar effect in RPE. In frog RPE, 13% CO_2-induced acidification activated the Na/K/2Cl co-transporter (NKCC1) due to a reduction in $[Cl]_i$ that follows the inhibition of the basolateral membrane Cl/HCO_3 exchanger (Edelman et al., 1994). Both the 13% apical CO_2-induced inhibition of the 3Na/2K ATPase and activation of the Na/K/2Cl co-transporter can increase $[Na]_i$. The increased $[Na]_i$ should facilitate $NaHCO_3$ transport via the basolateral membrane NBC. However, NBC only requires one Na^+ ion for every three HCO_3^- ion transported, thus Na may not be the limiting substrate for this Na/3HCO_3 co-transporter.

Section 3.7 – Basolateral membrane NBC: dependence on Na or HCO_3 as substrate

Since $[Na]_i$ is low (15 mM) compared to $[Na]_o$ (≈ 140 mM), we expected Na-linked transporters at the apical membrane (Fig. 1-3) to provide substrate that would help drive the outward transport of $Na/nHCO_3$ at the basolateral membrane. There are four major Na-linked transporters at the apical membrane: (1) Na/H exchanger (NHE); (2) Na/K/2Cl co-transporter (NKCC1); (3) 3Na/2K ATPase (ATP); (4) $Na/2HCO_3$ co-transporter (NBC1). If NHE (Na^+ in; H^+ out) provides the main source of $[Na]_i$ for basolateral membrane $Na/nHCO_3$ transport out of the cell, inhibition of NHE with amiloride should reduce basolateral membrane $Na/nHCO_3$ activity.

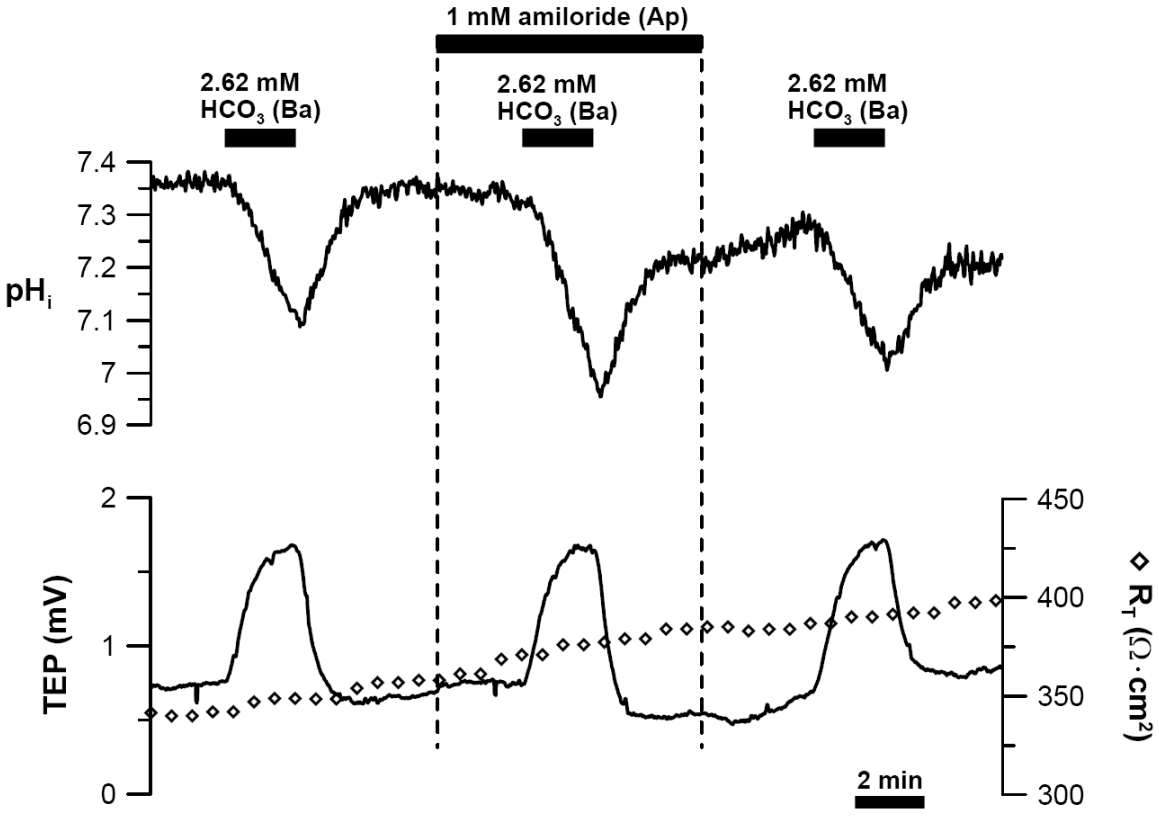

Fig. 3-24: Basal bath $\Delta[HCO_3]$-induced pH_i, TEP, and R_T responses in the presence of apical amiloride.

To test this notion, we reduced basal bath [HCO_3] (10-fold) and observed the resultant pH_i and TEP responses in the presence or absence of 1 mM apical amiloride (Fig. 3-24). In five experiments, amiloride did not affect basal bath Δ[HCO_3]-induced TEP response (Table 3-2), indicating that the apical membrane Na/H exchanger does not provide substrate for basolateral Na/nHCO_3 co-transport activity. On the other hand, the basal bath Δ[HCO_3]-induced acidification and H^+-flux was larger in the presence of apical amiloride compared to control (Table 3-1). This observation indicates that the Na/H exchanger normally acts to buffer cell acidification produced by HCO_3-efflux from the basolateral membrane.

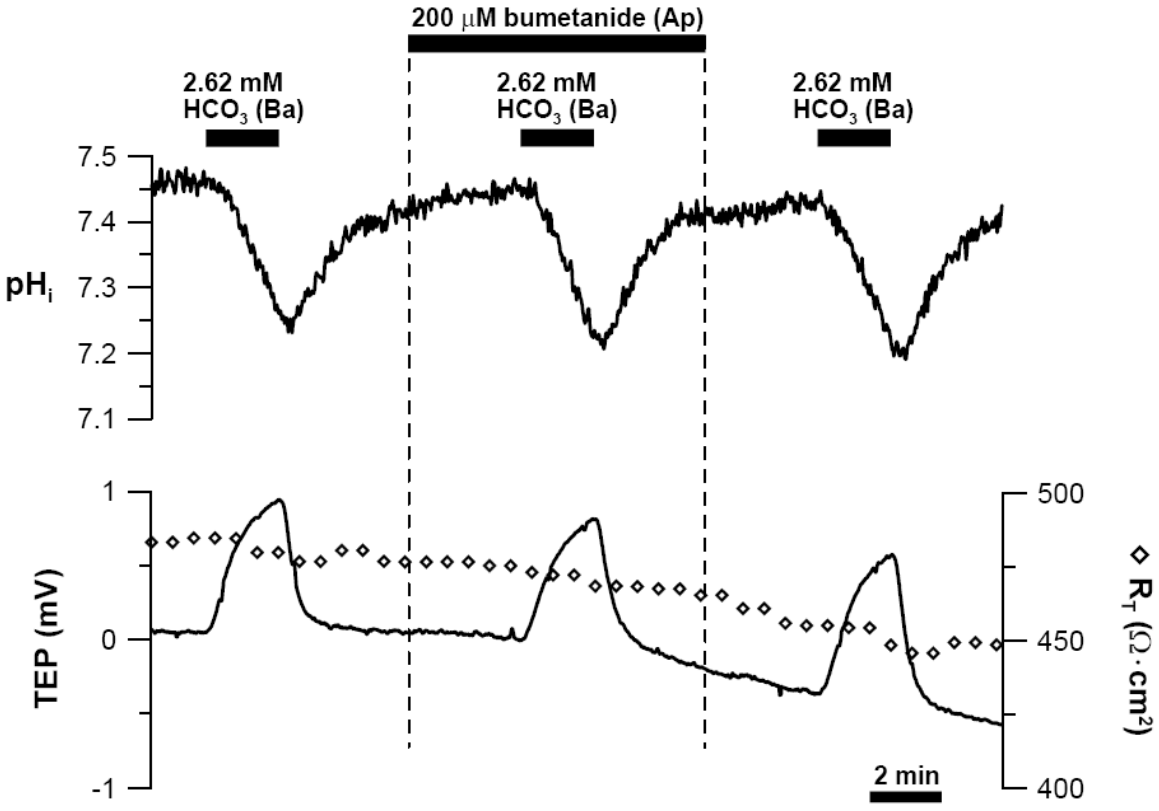

Fig. 3-25: Basal bath Δ[HCO_3]-induced pH_i, TEP, and R_T responses in the presence apical bumetanide.

Next, we test if Na-entry via NKCC1 facilitates basolateral Na/nHCO_3 co-transport activity (Fig. 3-25). We inhibited NKCC1 with 200 μM apical bumetanide, which did not affect the basal bath Δ[HCO_3]-induced pH_i (ΔpH_i and H^+-flux) and TEP responses (Tables 3-1 & 3-2). This lack of effect suggests that Na-entry via the NKCC1 does not contribute significantly to basolateral Na/nHCO_3 co-transport activity. We also evaluated the effect of Na-extrusion by the apical membrane 3Na/2K ATPase on the activity of the basolateral membrane Na/nHCO_3 co-transporter (Fig. 3-26).

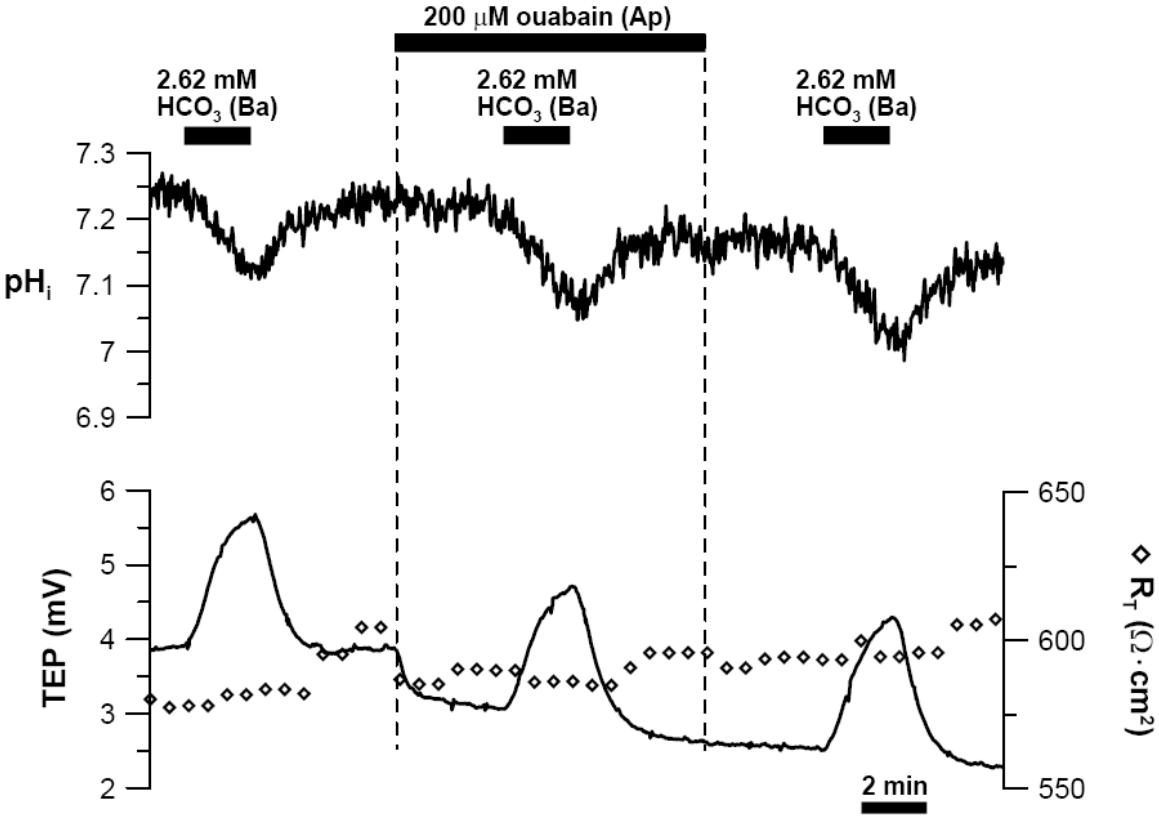

Fig. 3-26: Basal bath Δ[HCO_3]-induced pH_i, TEP, and R_T responses in the presence apical ouabain.

Unlike NHE, NKCC1, or NBC1, the 3Na/2K ATPase transports three Na^+ ions out of the cell in exchange for two K^+ ions. Thus its inhibition by ouabain should increase $[Na]_i$,

which may stimulate basolateral Na/nHCO_3 co-transport activity. Adding 200 μM ouabain into the apical bath caused an acute TEP-decrease (ΔTEP = 0.55 ± 0.47 mV; n = 5), as expected from inhibition of the 3Na/2K ATPase. However, apical ouabain did not affect the basal bath Δ[HCO_3]-induced pH_i (ΔpH_i and H^+-flux) and TEP responses (Tables 3-1 & 3-2), indicating that Na-extrusion by the 3Na/2K ATPase does not reduce or limit basolateral Na/nHCO_3 co-transport activity.

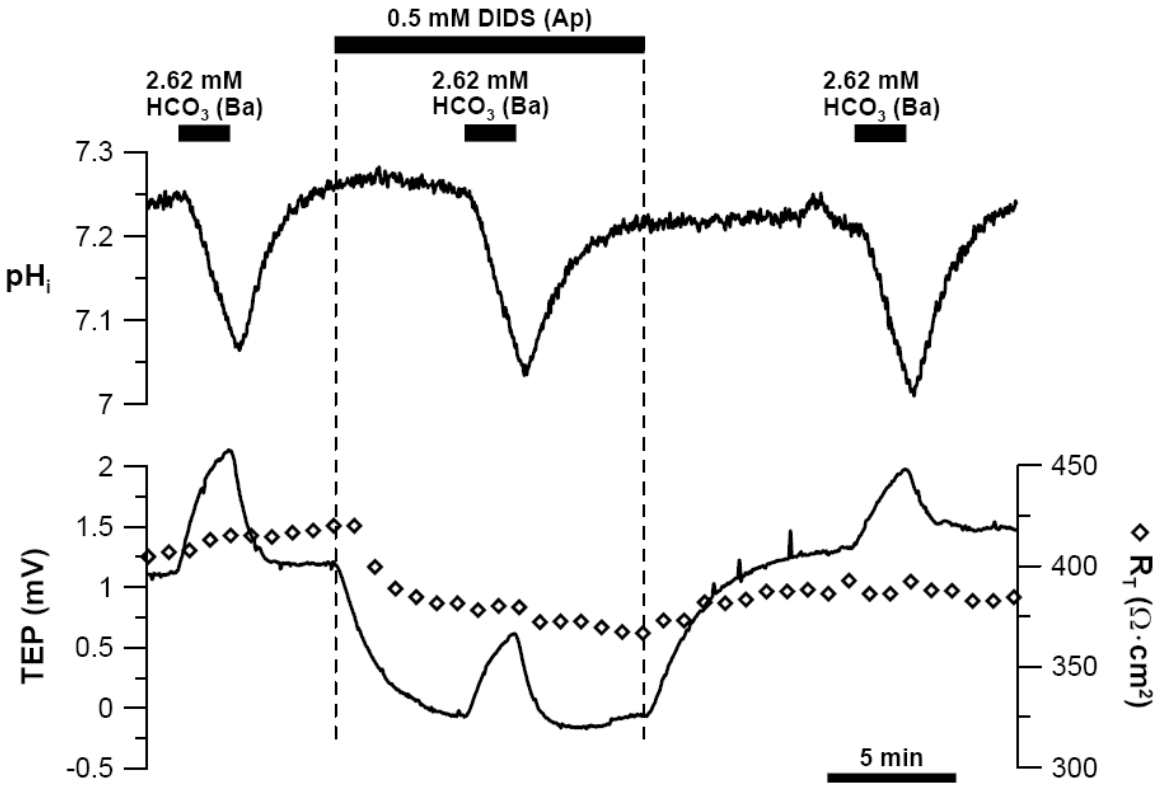

Fig. 3-27: Basal bath Δ[HCO_3]-induced pH_i, TEP, and R_T responses in the presence apical DIDS.

The basolateral membrane Na/nHCO_3 co-transporter may be dependent on Na and HCO_3 entry from the apical membrane via the electrogenic Na/2HCO_3 co-transporter (NBC1). Therefore, we tested the coupling between the apical and basolateral membrane Na/HCO_3 co-transporters by decreasing basal bath [HCO_3] (10-fold) in the presence of 0.5 mM

apical DIDS (Fig. 3-27). In seven experiments, the basal bath $\Delta[HCO_3]$-induced TEP response decreased from 0.86 ± 0.17 to 0.49 ± 0.06 mV ($p < 0.05$) in the presence of apical DIDS, suggesting that inhibiting apical HCO_3-entry via the $Na/2HCO_3$ co-transporter reduces the HCO_3-supply that drives basolateral $Na/nHCO_3$ co-transport. However, apical DIDS increased the basal bath $\Delta[HCO_3]$-induced acidification and H^+-flux by ≈ 20% (Table 3-1). This observation suggests that normally, apical HCO_3-entry via the $Na/2HCO_3$ co-transporter is a buffer that counteracts the acidification caused by HCO_3-efflux from the basolateral membrane.

From these experiments, we conclude that HCO_3 (not Na) is the limiting substrate for the basolateral membrane $Na/nHCO_3$ co-transporter. This is supported by the following evidence: (1) reducing basal bath $[HCO_3]$ 10-fold caused a TEP response that was reduced in the presence of apical DIDS, suggesting that inhibiting NBC1 reduced basolateral $Na/nHCO_3$ co-transport activity; (2) the basal bath $\Delta[HCO_3]$-induced TEP response was reduced in the presence of basal DZA, suggesting that CA-inhibition reduces basolateral $Na/nHCO_3$ co-transport. DZA reduces HCO_3-transport in two ways: first, DZA slows CA-mediated hydration of CO_2 to HCO_3; second, DZA inhibits the apical membrane $Na/2HCO_3$ co-transporter, as evidenced by the reduction of apical bath $\Delta[HCO_3]$-induced TEP response in the presence of apical DZA; (3) the basal bath $\Delta[HCO_3]$-induced TEP response was increased in 13% apical bath CO_2 and decreased in 1% apical bath CO_2. This suggests that apical CO_2-entry and its subsequent conversion into HCO_3 is an important source of HCO_3-substrate for basolateral $Na/nHCO_3$ co-transport activity.

In addition to showing that the basolateral membrane Na/nHCO_3 co-transporter is dependent on apical HCO_3-supply, we also eliminated Na as a limiting substrate for basolateral Na/nHCO_3 co-transport by examining three Na-transport proteins at the apical membrane of the RPE (Hughes et al., 1998): (1) amiloride-sensitive Na/H exchanger (NHE); (2) bumetanide-sensitive Na/K/2Cl co-transporter (NKCC1); (3) ouabain-sensitive 3Na/2K ATPase (ATP). In hfRPE, the presence of amiloride, bumetanide, or ouabain in the apical bath had no effect on the basal bath $\Delta[HCO_3]$-induced TEP responses, suggesting that these Na-transport mechanisms are not linked to basolateral Na/nHCO_3 co-transport activity. Taken together, our data indicate that the basolateral membrane Na/nHCO_3 co-transporter is mainly driven by HCO_3 supplied by NBC1 mediated Na/2HCO_3 entry and CA II-mediated hydrolysis of CO_2 to HCO_3.

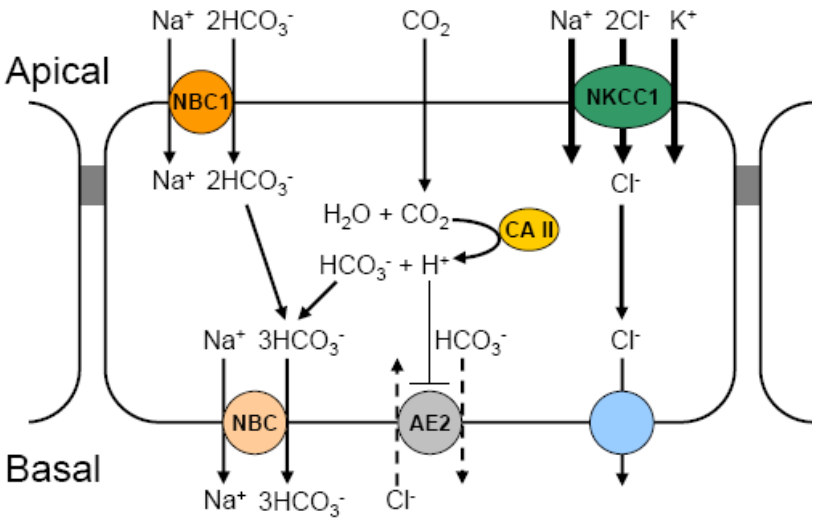

Sections 3.5 & 3.6 conclusions: Increasing apical CO_2 increases intracellular Na^+

HCO_3-transport via basolateral membrane NBC is dependent on HCO_3-transport via NBC1

Supporting experimental observations	Interpretation	Fig.
13% apical CO_2 increases [Na^+]	Increasing apical bath CO_2 activates Na^+-dependent mechanisms at the apical membrane	3-21
Apical amiloride did not affect steady-state pH_i at 5% or 13% apical CO_2	Increasing apical bath CO_2 did not activate NHE-mediated Na/H exchange	3-22
Apical amiloride did not affect 13% apical CO_2 induced acidification	Increasing apical bath CO_2 did not activate NHE-mediated Na/H exchange	3-23
Basal bath $\Delta[HCO_3]$-induced TEP response is unaffected by apical amiloride	Electrogenic HCO_3-transport at the basolateral membrane is DIDS-sensitive	3-24
Basal bath $\Delta[HCO_3]$-induced TEP response is unaffected by apical bumetanide	HCO_3 is transported at the basolateral membrane via both AE2 and NBC	3-25
Basal bath $\Delta[HCO_3]$-induced TEP response is unaffected by apical ouabain	Electrogenic HCO_3-transport at the basolateral membrane is Na-dependent	3-26
Basal bath $\Delta[HCO_3]$-induced TEP response is reduced by apical DIDS	HCO_3-transport via basolateral membrane NBC is dependent on NBC1 activity	3-27

Section 3.8 – CO_2 induced fluid transport in hfRPE

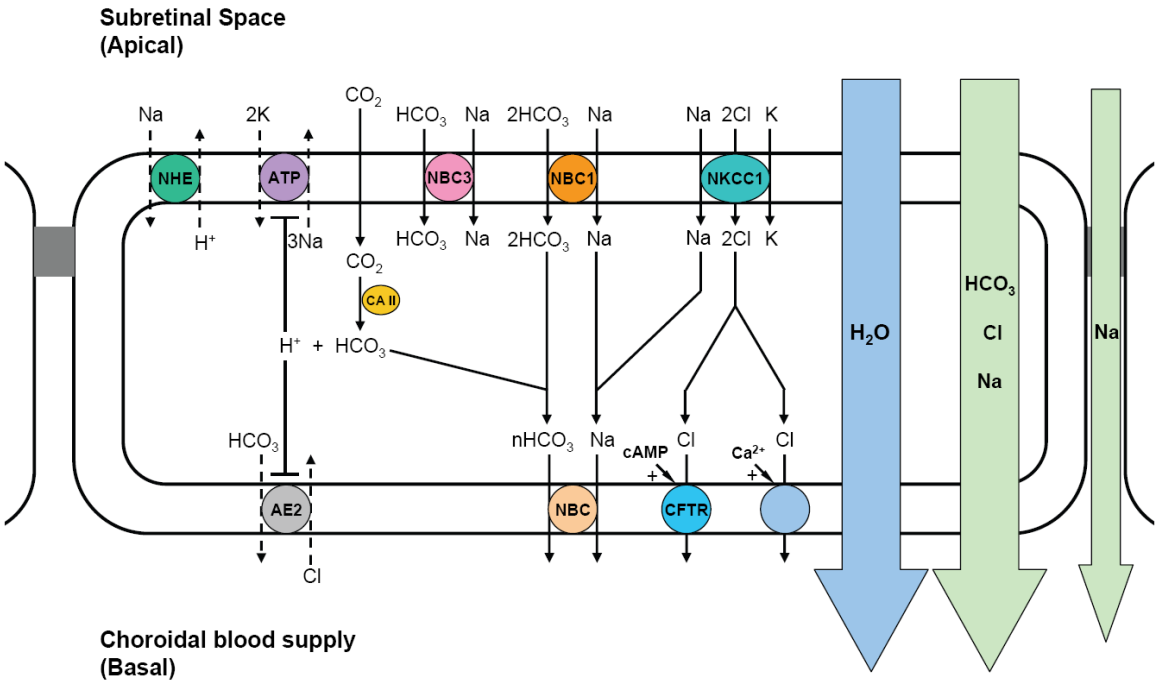

Fig. 3-28: CO_2 induced ion and fluid transport in human retinal pigment epithelium. CO_2 enters the RPE at its apical membrane by diffusion, or it may be transported in the form of HCO_3 via NBC1 and NBC3. CO_2 exits RPE basolateral membrane as HCO_3, mainly via basolateral membrane NBC – this process is facilitated by carbonic anhydrase II (CA II) activity.

The model in Fig. 3-28 predicts that 13% apical CO_2 would increase net Na, Cl, and HCO_3 absorption, producing an increase in steady-state fluid-absorption (J_V) across the RPE. In four experiments, increasing CO_2 from 5% to 13% in both solution baths increased J_V by more than 2-fold (from 2.8 ± 1.6 to 6.7 ± 2.3 $\mu l \cdot cm^{-2} \cdot hr^{-1}$; n = 5; $p < 0.05$). In another set of experiments, decreasing CO_2 from 5% to 1% in both solution baths decreased steady-state fluid absorption by ≈ 60% (from 8.8 ± 3.9 to 3.4 ± 1.1 $\mu l \cdot cm^{-2} \cdot hr^{-1}$; n = 4; $p < 0.05$).

In bovine RPE, net active Cl absorption is mediated by the Na/K/2Cl co-transporter at the apical membrane (Edelman et al., 1994) and by Ca^{2+}-activated and cAMP/PKA-dependent CFTR Cl channels at the basolateral membrane (Joseph & Miller, 1991; Bialek *et al.*, 1995; Hughes *et al.*, 1998). Evidence for the expression and basolateral membrane localization of CFTR in hfRPE has been presented (Blaug et al., 2003). The 13% apical CO_2-induced activation of the Na/K/2Cl co-transporter and inhibition of the Cl/HCO_3 exchanger would both increase net Cl absorption across the RPE.

HCO_3 transport also plays a significant role in RPE fluid transport. We tested the role of the apical membrane $Na/2HCO_3$ co-transporter in fluid transport by adding 0.5 mM DIDS into the apical bath and measuring the resultant change in steady-state fluid absorption rate (J_V). In four experiments, 0.5 mM apical DIDS decreased J_V by more than 50% (from 16.7 ± 4.8 to 7.7 ± 3.7 $\mu l \cdot cm^{-2} \cdot hr^{-1}$; $p < 0.05$), suggesting that HCO_3-transport via NBC1 mediates a major component of fluid absorption across the RPE apical membrane. The presence of NBC3 at the apical membrane suggests that it also contributes to HCO_3-mediated fluid transport. At the basolateral membrane, HCO_3 transporters, and several Cl-channels are DIDS-sensitive. Not surprisingly, the addition of 0.5 mM DIDS to the basal bath decreased J_V from 20.3 ± 8.2 to 11.2 ± 6.0 $\mu l \cdot cm^{-2} \cdot hr^{-1}$ ($n = 9$; $p < 0.05$). In addition, dorzolamide or acetazolamide decreases steady-state fluid absorption across hfRPE *in vitro* (Zhi et al., ARVO 2007, #2532). These observations are corroborated in the present experiments by the DZA-induced inhibition of NBC1 the apical membrane and the $Na/nHCO_3$ co-transporter at the basolateral membrane.

Interestingly, animal models showed that systemically administered acetazolamide increases fluid absorption across the RPE (Wolfensberger, 1999). Furthermore, clinical studies showed that acetazolamide reduces macular edema in some patients with retinitis pigmentosa and uveitis (Cox *et al.*, 1988; Fishman *et al.*, 1989). It has been proposed that acetazolamide increases RPE fluid absorption *in vivo* by affecting membrane-bound carbonic anhydrases at the basolateral membrane (Wolfensberger, 1999), but there is no known membrane-bound CAs at the basolateral membrane of native RPE (Zhi et al., ARVO 2007, #2532). In addition, acetazolamide readily permeates RPE basolateral membrane, which would reduce fluid absorption by inhibiting cytosolic CA II, as observed *in vitro* (Zhi et al., ARVO 2007, #2532). More recently, Xu and colleagues show that acetazolamide induces hypoxia-inducible factor 1 alpha (HIF-1α) expression in rat cerebral cortex (Xu *et al.*, 2009). This finding suggest the possibility that chronic exposure of RPE cells to acetazolamide may exert its therapeutic effects against macular edema via HIF-1α-mediated regulation of proteins involved in fluid transport. Therefore, the key to understanding why acetazolamide has opposite effects on RPE fluid transport *in vitro* vs. *in vivo* may lie in the difference between acute and chronic effects of acetazolamide on RPE physiology.

Section 3.9 – HCO_3-mediated ion and fluid transport in the choroid plexus epithelium—a comparison with retinal pigment epithelium

Both the RPE and the choroid plexus epithelium (CPE) develop from neural ectoderm, therefore it is not surprising to find many similarities in the solute transport mechanisms of these two epithelia (Hughes et al., 1998; Brown et al., 2004; Praetorius, 2007). As demonstrated in this study, HCO_3-transport mediates net solute and fluid absorption in human RPE. This is supported by experiments where acetazolamide or dorzolamide reduced steady-state fluid absorption by ≈ 50% in hfRPE cultures (Zhi et al., ARVO 2007, #2532). Similarly in the CPE, HCO_3-transport is an important mediator of CSF-production (Saito & Wright, 1983, 1984); CSF-secretion is inhibited by basal DIDS (Deng & Johanson, 1989). In addition, acetazolamide reduces CSF-secretion by ≈ 40% (Vogh et al., 1987). Acetazolamide is used to prevent cerebral edema at high altitudes (Wright et al., 2008) and to reduce CSF-pressure in children with hydrocephalus (Cowan & Whitelaw, 1991). The inhibitory effect of acetazolamide on CSF-secretion led to the notion that CO_2-entry into the CPE from the blood-plasma and the subsequent hydration of CO_2 into HCO_3 stimulates $NaHCO_3$-secretion across the apical membrane. This conclusion is supported by experiments in cat CPE, where ≈ 40% of Na-secretion is attributed to CA II-mediated HCO_3 formation from CO_2 (Vogh & Maren, 1975). Perhaps not surprising, this mechanism of CO_2-driven HCO_3 transport is also found in the RPE.

Despite many similarities, the RPE normally absorbs Na (Cl + HCO_3) and fluid, while the CPE secretes Na (Cl + HCO_3) and fluid which helps form cerebrospinal fluid (CSF). As in the RPE, the CPE expresses Na/HCO_3 co-transporters at both the apical and

basolateral membranes. However, the most striking difference is that both NBC1/NBCe1 and NBC3/NBCn1 in the RPE are expressed at the apical membrane (Zhi et al., ARVO 2007, #2532), whereas in the CPE, these two transporters are expressed at the basolateral membrane (Brown et al., 2004; Praetorius, 2007). This difference suggests that NBC4, which is found at the apical membrane of the CPE (Millar & Brown, 2008), may be the unidentified Na/nHCO_3 co-transporter at the basolateral membrane of the RPE. We hypothesize that the difference in the membrane location of these HCO_3 transporters (i.e., NBC1, NBC3, and NBC4) in the RPE and CPE is the basis for their difference in HCO_3 and fluid transport direction.

If the CO_2-permeability difference of the apical and basolateral membranes of the RPE also manifests in the CPE, what is its functional significance? In the central nervous system, metabolic CO_2 produced by the brain is released into the CSF, and is subsequently neutralized by HCO_3 secreted from the CPE. We hypothesize that the CPE has a relatively lower CO_2 permeability at the apical membrane than at the basolateral membrane, and this property would promote CA II-mediated HCO_3 secretion across the apical membrane. This possibility remains to be evaluated.

Section 3.10 – Physiological implications

Upon dark adaptation, oxygen consumption in the retina increases (Kimble *et al.*, 1980; Medrano & Fox, 1995; Cringle *et al.*, 2002; Yu & Cringle, 2002), thus generating and depositing more CO_2 and H_2O into the SRS. Both CO_2 and H_2O generation can be estimated from the rate of oxygen consumption measured *in situ* in cat and non-human primate eyes (Wangsa-Wirawan & Linsenmeier, 2003). Our calculations (section 3-11) provide an estimate of CO_2 production in adult human photoreceptors of ≈ 0.29 and 0.54 $mmol \cdot hr^{-1}$ in light and dark respectively. Considering that SRS [CO_2] is ≈ 2 mM, impaired CO_2-transport across the RPE could cause significant SRS or RPE acidification resulting in photoreceptor or RPE cell death. In addition, oxidative phosphorylation in the adult retina produces water at a rate of ≈ 0.5 $\mu l \cdot cm^{-2} \cdot hr^{-1}$ in light and 0.9 $\mu l \cdot cm^{-2} \cdot hr^{-1}$ in dark adapted eyes. Since glycolysis in the retina accounts for ≈ 95% of its total glucose consumption (Winkler et al., 2008), the combined retinal water production by aerobic respiration and glycolysis is calculated to be 3.6 and 6.5 $\mu l \cdot cm^{-2} \cdot hr^{-1}$ in the light and dark respectively. The CO_2 induced changes in ion-transport in the RPE is one of many events that follows the transition from light to dark *in vivo*, others include: (1) an increase in SRS [K^+] from ≈ 3 to 5 mM; (2) the decrease in SRS [Ca^{2+}]; (3) the decrease in SRS pH (Steinberg et al., 1983; Borgula et al., 1989; Livsey et al., 1990; Yamamoto et al., 1992; Gallemore et al., 1994). Dark-adaptation decreases SRS volume in situ (Li et al., 1994a; Li et al., 1994b). In addition, in a rat model of retinal re-attachment (Maminishkis et al., 2002), fluid clearance from the SRS was faster in the dark-adapted eye (Maminishkis A., personal communication), suggesting that steady-state fluid-absorption across the RPE is higher in the dark.

In the dark adapted eye, the high oxidative metabolism in the inner segments of the photoreceptors generates CO_2 and H_2O that are deposited into the SRS. The RPE utilizes the limited CO_2-diffusion at the basolateral membrane to drive Na, Cl, and HCO_3 transport across the RPE, which increases solute-driven fluid-transport – this mechanism not only prevents CO_2 accumulation in the SRS, but also removes water from the vicinity of the photoreceptors. This helps maintain the proper anatomic relationship between the photoreceptors and the RPE apical membrane, thus avoiding retinal-detachment and photoreceptor degeneration (Stone et al., 1999; Wickham et al., 2006; Nakazawa et al., 2007).

Section 3.11 – Appendix

Relative CO_2 membrane permeability

$$\frac{d[CO_2]}{dt} = D \cdot \left(CO_{2,in} - CO_{2,out}\right)$$

Differentiating the CO_2/HCO_3 equilibrium constant,

$$\frac{d[CO_2]}{dt} = \frac{[HCO_3^-]}{K_a} \cdot \frac{d[H^+]}{dt}$$

Combining the above equations give,

$$\frac{[HCO_3^-]_{in}}{K_a} \cdot \frac{d[H^+]_{Ap}}{dt} = D_{Ap} \cdot \left(CO_{2,in} - CO_{2,out}\right)$$

$$\frac{[HCO_3^-]_{in}}{K_a} \cdot \frac{d[H^+]_{Ba}}{dt} = D_{Ba} \cdot \left(CO_{2,in} - CO_{2,out}\right)$$

The relative permeability (P) of CO_2 at the apical vs. the basolateral membrane is,

$$P = \frac{D_{Apical}}{D_{Basal}} = \frac{d[H^+]_{Ap}}{dt} \div \frac{d[H^+]_{Ba}}{dt}$$

Where D is the diffusion coefficient and $\frac{d[H^+]_{Ap}}{dt}$ and $\frac{d[H^+]_{Ba}}{dt}$ are the H^+-fluxes caused by perfusing 13% CO_2 equilibrated Ringer to the apical and basal bath respectively. The H^+-fluxes were obtained by multiplying the 13% CO_2 induced dpH_i/dt with the total buffering capacity of the hfRPE. Based on these considerations, the relative permeability of apical vs. basolateral membrane of hfRPE to CO_2 is 9.9 ± 4.4 (n = 7).

Retinal water production by aerobic respiration

In the dark, outer retina O_2 consumption (Wangsa-Wirawan & Linsenmeier, 2003) is: 4.2 ± 0.5 ml $O_2 \cdot 100g^{-1}$ min^{-1}

In the light, outer retina O_2 consumption (Wangsa-Wirawan & Linsenmeier, 2003) is: 2.3 ± 0.6 ml $O_2 \cdot 100g^{-1}$ min^{-1}

Wet weight of human retina (Bhosale & Bernstein, 2005) is: 5.44 g

Oxygen consumption in the dark (density of oxygen at 36.9 ^oC is 0.039 mmol/ml):

$$0.042\,ml\,O_2 \cdot g^{-1} min^{-1} \times 60\,min \cdot hr^{-1} \times 5.44\,g \times 0.0393\,mM \cdot ml^{-1} = 0.54\,mmol\,O_2 \cdot hr^{-1}$$

Oxygen consumption in the light:

$$0.023\,ml\,O_2 \cdot g^{-1} min^{-1} \times 60\,min \cdot hr^{-1} \times 5.44\,g \times 0.0393\,mM \cdot ml^{-1} = 0.29\,mmol\,O_2 \cdot hr^{-1}$$

In aerobic respiration, one molecule of water is generated for every molecule of oxygen consumed. Therefore, water generated in the dark is:

$$0.54\,mmol\,O_2 \cdot hr^{-1} \times 18\,mg \cdot mmol^{-1} \times 1\,\mu l \cdot mg^{-1} = 9.72\,\mu l\,H_2O \cdot hr^{-1}$$

Water generated in the light is:

$$0.29\,mmol\,H_2O \cdot hr^{-1} \times 18\,mg \cdot mmol^{-1} \times 1\,\mu l \cdot mg^{-1} = 5.22\,\mu l\,H_2O \cdot hr^{-1}$$

Assuming that the entire retina surface is 10.94 cm^2 (http://webvision.med.utah.edu/), the total rate of fluid generated by the retina through aerobic respiration:

In the dark: $\frac{9.72\,\mu l\,H_2O / hr}{10.94\,cm^2} = 0.89\,\mu l\ H_2O \cdot cm^{-2} \cdot hr^{-1}$

In the light: $\frac{5.31\,\mu l\,H_2O / hr}{10.94\,cm^2} = 0.48\,\mu l\ H_2O \cdot cm^{-2} \cdot hr^{-1}$

Total retinal water production in the light and dark

For every glucose molecule that undergoes aerobic respiration, six molecules of CO_2 are produced. Therefore, glucose consumption by aerobic respiration in the dark is:

$$0.54\ mmol \cdot hr^{-1} \times \frac{1\, glu\cos e}{6\, CO_2} = 0.09\, mmol \cdot hr^{-1}$$

Glucose consumption by aerobic respiration in the light is:

$$0.29\ mmol \cdot hr^{-1} \times \frac{1\, glu\cos e}{6\, CO_2} = 0.05\, mmol \cdot hr^{-1}$$

Assuming that glycolysis in the retina accounts for 95% of glucose consumption in the dark (Winkler et al., 2008), the rate of water generation by glycolysis in the dark is:

$$0.09\, mmol \cdot hr^{-1} \times \frac{95}{5} \times \frac{2\, H_2O}{1\, glu\cos e} \times \frac{18\, \mu l}{1\, mmol} \times \frac{1}{10.94\, cm^2} = 5.6\, \mu l \cdot cm^{-2} \cdot hr^{-1}$$

The rate of water generation by glycolysis in the light is:

$$0.05\, mmol \cdot hr^{-1} \times \frac{95}{5} \times \frac{2\, H_2O}{1\, glu\cos e} \times \frac{18\, \mu l}{1\, mmol} \times \frac{1}{10.94\, cm^2} = 3.1\, \mu l \cdot cm^{-2} \cdot hr^{-1}$$

Total water produced by aerobic respiration and glycolysis in dark:

$= 0.89 + 5.6 = 6.5\ \mu l \cdot cm^{-2} \cdot hr^{-1}$

Total water produced by aerobic respiration and glycolysis in light:

$= 0.48 + 3.1 = 3.6\ \mu l \cdot cm^{-2} \cdot hr^{-1}$

J_V of human RPE *in vivo* has been estimated using B-scan ultrasonography to be ≈ 11 $\mu l \cdot cm^{-2} \cdot hr^{-1}$ (Chihara & Nao-i, 1985), comparable to our *in vitro* measurements (Fig. 13).

CO_2 production in the light and dark

CO_2 production = O_2 consumption. CO_2 production in dark: 4.2 ± 0.5 ml $CO_2 \cdot 100g^{-1}$ min^{-1}, and in light: 2.3 ± 0.6 ml $O_2 \cdot 100g^{-1}$ min^{-1}. Therefore, CO_2 production increases by 1.4 – 2.6 fold after transitioning from light to dark. This increase in CO_2 production translates to an increase in SRS CO_2 concentration, from 5% to 10 ± 3%.

CHAPTER 4: Lactate Induced Ion Transport Mechanisms in RPE

Section 4.1 – Introduction

Photoreceptor metabolism is higher in the dark than in light (Yamamoto *et al.*, 1992; Wang *et al.*, 1997a; Wang *et al.*, 1997b; Padnick-Silver & Linsenmeier, 2002; Winkler *et al.*, 2008) and it is estimated that ATP consumption by rod photoreceptor is ≈ 4-fold higher in the dark (Okawa *et al.*, 2008). The high ATP production is needed to drive the Na/K ATPase and Ca^{2+} ATPase at the photoreceptor inner segments, to maintain the "dark current" that circulates between the photoreceptor inner and outer segments (Ames *et al.*, 1992; Krizaj & Copenhagen, 1998; Okawa *et al.*, 2008). Therefore in the dark, oxidative metabolism at the photoreceptor inner segments increases, thus reducing the local oxygen levels (Wangsa-Wirawan & Linsenmeier, 2003) and increasing the need for glycolysis-derived ATP. More than 80% of all glucose consumed by photoreceptors is converted to lactic acid (Wang *et al.*, 1997a; Wang *et al.*, 1997b; Winkler *et al.*, 2008) indicating that the retina is highly dependent on glycolysis as a source of ATP, even in the presence of oxygen (Winkler *et al.*, 2000; Padnick-Silver & Linsenmeier, 2002; Winkler *et al.*, 2004). This finding is consistent with the high lactate concentration (4 - 13 mM) in the subretinal space (SRS) compared to that in blood (≈ 1 mM) (Adler & Southwick, 1992). Although lactate released by Müller cells in darkness can be used as an energy source for photoreceptor activity (Poitry-Yamate *et al.*, 1995; Poitry *et al.*, 2000), this mechanism is controversial (Winkler *et al.*, 2004). Regardless of the source, more lactic acid are generated in the dark and released from the retina into the SRS.

The choroidal circulation (see chapter 1) is the main pathway for the removal of photoreceptor-generated lactic acid (and CO_2) from the SRS. This process is mediated by the RPE, which expresses proton-coupled lactate (H^+/Lac^-) transporters of the MCT family at its apical (MCT1) and basolateral membranes (MCT3) (Kenyon *et al.*, 1994; la Cour *et al.*, 1994; Lin *et al.*, 1994; Zeuthen *et al.*, 1996; Philp *et al.*, 1998; Hamann *et al.*, 2003; Philp *et al.*, 2003a; Philp *et al.*, 2003b; Majumdar *et al.*, 2005). MCT lactate-transporters are electroneutral, but early *in vitro* experiments in bovine RPE showed that adding lactate to the apical bath alters RPE membrane voltage, suggesting involvement of electrogenic mechanisms (Kenyon *et al.*, 1994). In this study, we investigate these lactate-activated mechanisms. We demonstrate that apical lactate entry stimulates KCl-efflux via a Ba^{2+}-sensitive K-channel at the apical membrane and ClC-2 Cl-channel at the basolateral membrane. These channels may be activated by lactate-induced cell-swelling (Zeuthen *et al.*, 1996; Hamann *et al.*, 2003), but we show that activation of these two channels is caused by cell acidification. Lactate-induced KCl-efflux decreases RPE cell volume and prevent swell-induced osmotic stress. In addition, lactate-induced activation of apical membrane K-channel may be an important mechanism that regulates SRS K-homeostasis, which is critical for photoreceptor/RPE interactions in light-dark transitions.

All experiments presented in this chapter are performed in CO_2/HCO_3-free condition because the lactate-induced responses are more pronounced and can be easily measured. Although this eliminates interactions between lactate and HCO_3 transport mechanisms, the main features of lactate-induced pH_i, TEP, and R_T responses were preserved (Fig. 5-1). Interactions between lactate and HCO_3-transporters are explored in chapter 5.

Section 4.2 – MCT localization in cultured hfRPE

Studies in mouse and human RPE showed MCT1 and MCT3 localization at the apical and basolateral membranes, respectively (Philp *et al.*, 1998; Philp *et al.*, 2003b). First, we confirm the localization of these MCTs in hfRPE cultures since this model will be used for all physiological experiments. Western blots showed that MCT1, MCT3, and MCT4 and their accessory protein (CD147) are expressed in cultured hfRPE cells (Fig. 4-1A). Immunofluorescence imaging shows that MCT1 is localized at the apical membrane, whereas both MCT3 and MCT4 are localized to the basolateral membrane (Fig. 4-1B). CD147 was detected in both apical and basolateral membranes; CD147 labeling of the basolateral membrane is weak probably due to epitope masking by MCT 3 or 4. CD147 (or basigin) is an accessory protein that associates with MCTs to regulate their membrane targeting and localization – its detection indicates proper distribution of MCTs in cultured hfRPE.

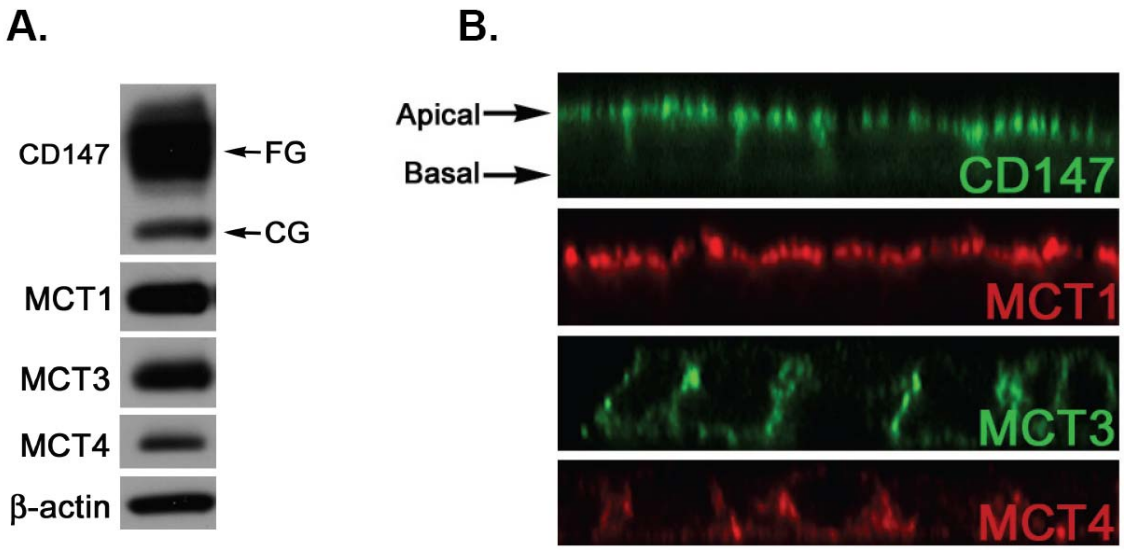

Fig. 4-1: Expression and localization of CD147 and MCTs in cultured hfRPE monolayer. (A) Western blot (CG – core-glycosylated, 29.2 kD; FG – fully-glycosylated, 59 kD); (B) immunolabeling.

MCT4 is normally absent in native RPE, but it is expressed in cultured RPE (e.g., ARPE-19) (Philp *et al.*, 2003b). MCT4 is expressed in highly glycolytic cells (Dimmer *et al.*, 2000). Studies in renal cells show that MCT4 expression is upregulated in hypoxia (low O_2) via hypoxia-inducible factor 1-alpha (HIF-1α) (Ullah *et al.*, 2006). HIF-1α controls expression of many genes involved in glycolysis, such as lactate dehydrogenase A (LDHA) and pyruvate dehydrogenase kinase 1 (PDK1) (Gleadle & Ratcliffe, 1998; Semenza, 2003). When cells are placed in culture, they abandon oxidative metabolism and depend on glycolysis as the main source of energy (Gstraunthaler *et al.*, 1999). This is because O_2 supply from the environment to the confluent hfRPE is limited by a large diffusion layer (4.4 mm of stagnant media), thus causing hypoxia (Pettersen *et al.*, 2005). Based upon these studies, we infer that cultured RPE cells express high levels of MCT4 due to hypoxia-induced activation of HIF-1α.

MCT3 (Km $\approx$ 6 mM (Grollman *et al.*, 2000)) has significantly higher affinity for L-lactate than MCT4 (Km $\approx$ 30 mM (Philp *et al.*, 1998)). A simple calculation with Michaelis-Menten kinetics show that MCT3 transports lactate at a rate $\approx$ 2 – 4 folds faster than MCT4 (assuming $[Lactate]_i$ in RPE ranges between 2 and 20 mM). Does this mean that MCT3 (rather than MCT4) is the major H/Lac co-transporter at the basolateral membrane? Not necessarily. Although MCT3 transports lactate faster than MCT4, MCT4 may be expressed at a much higher levels than MCT3, thus compensating for its lower lactate binding affinity. Therefore, at least in cultured hfRPE, MCT4 can contribute significantly to lactate-transport.

Section 4.3 – Lactate induced pH_i responses in RPE

Lactate transport at the apical membrane can be studied by imposing a lactate gradient across the apical membrane. This maneuver drives lactic acid into the RPE via MCT1, thus causing intracellular acidification. In this study, we stimulate MCT1 by perfusing 20 mM lactate Ringer into the apical bath and MCT1 activity is reflected by the subsequent changes in pH_i, TEP, and R_T. As shown in Fig. 4-2, apical lactate produced a pH_i response with two successive phases: a fast acidification (R1) followed by a slow alkalinization (R2). In the absence of CO_2/HCO_3, we took the intrinsic buffering capacity of the cell (β_i) into account to determine the rate of H^+-entry ($\Delta pH_i/\Delta t \times \beta_i$).

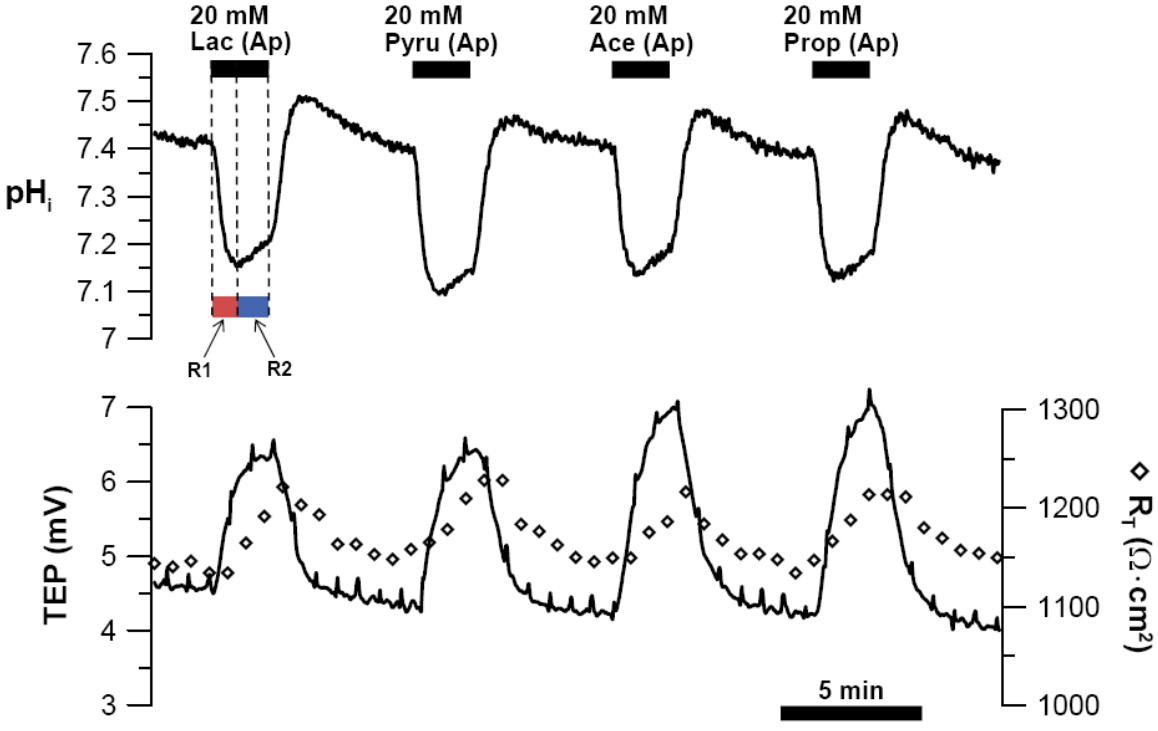

Fig. 4-2: Apical monocarboxylate (i.e., lactate, pyruvate, acetate, or propionate) induced pH_i, TEP, and R_T responses.

During R1, the hfRPE acidified at a rate of -6.32 ± 1.46 mM·min^{-1} and R2 has a rate of 0.71 ± 0.31 mM·min^{-1} (n = 65). Concomitantly, apical lactate also increased TEP and R_T by 1.39 ± 0.60 mV and 52 ± 21 Ω·cm^2 (n = 87), respectively. The pH_i responses are presented in H^+-flux, which is determined by taking into account the intrinsic buffering capacity of the RPE. To make sure that these responses are down-stream effects of H^+-coupled monocarboxylate transporter (MCT1) activity, we compared the pH_i, TEP, and R_T responses induced by apical addition of various monocarboxylates (20 mM of lactate, pyruvate, acetate, or propionate) (Fig. 4-2). Adding various monocarboxylates (i.e., pyruvate, acetate, or propionate) to the apical bath produced similar but generally larger pH_i, TEP, and R_T responses compared to that caused by lactate (Table 4-1), suggesting that MCT1 has lower affinity for lactate than for other monocarboxylates. Based on R1 values, MCT1 substrate specificity in hfRPE (lactate = acetate < pyruvate = propionate) resembles MCT1 in Ehrlich Lettré tumor cells (Jackson & Halestrap, 1996). Some discrepancies can be expected due to H^+-coupled monocarboxylate transport at the basolateral membrane via MCT3, which also exhibits substrate preference.

Table 4-1. monocarboxylate-induced pH_i, TEP, and R_T responses.

	lactate	pyruvate	acetate	propionate
R1 (mM·min^{-1})[a]	-6.17 ± 0.93	-8.28 ± 1.85	-7.15 ± 1.20	-8.48 ± 2.51
R2 (mM·min^{-1})	0.71 ± 0.12	0.87 ± 0.27	0.85 ± 0.23	0.93 ± 0.19
ΔTEP (mV)	1.75 ± 0.45	1.99 ± 0.46	2.60 ± 0.52	2.70 ± 0.52
ΔR_T (Ω·cm^2)	81 ± 15	77 ± 10	66 ± 12	75 ± 12

a. values are presented as mean ± SD from five tissues.

To test the activity of MCT1, we measured lactate-induced pH_i, TEP, and R_T responses in the presence of MCT1 inhibitors. In the first experiment, we perfused lactate Ringer to

the apical bath in the presence or absence 50 μM apical pCMBS (p-chloromercuribenzenesulfonic acid; MCT1 inhibitor) (Fig. 4-3).

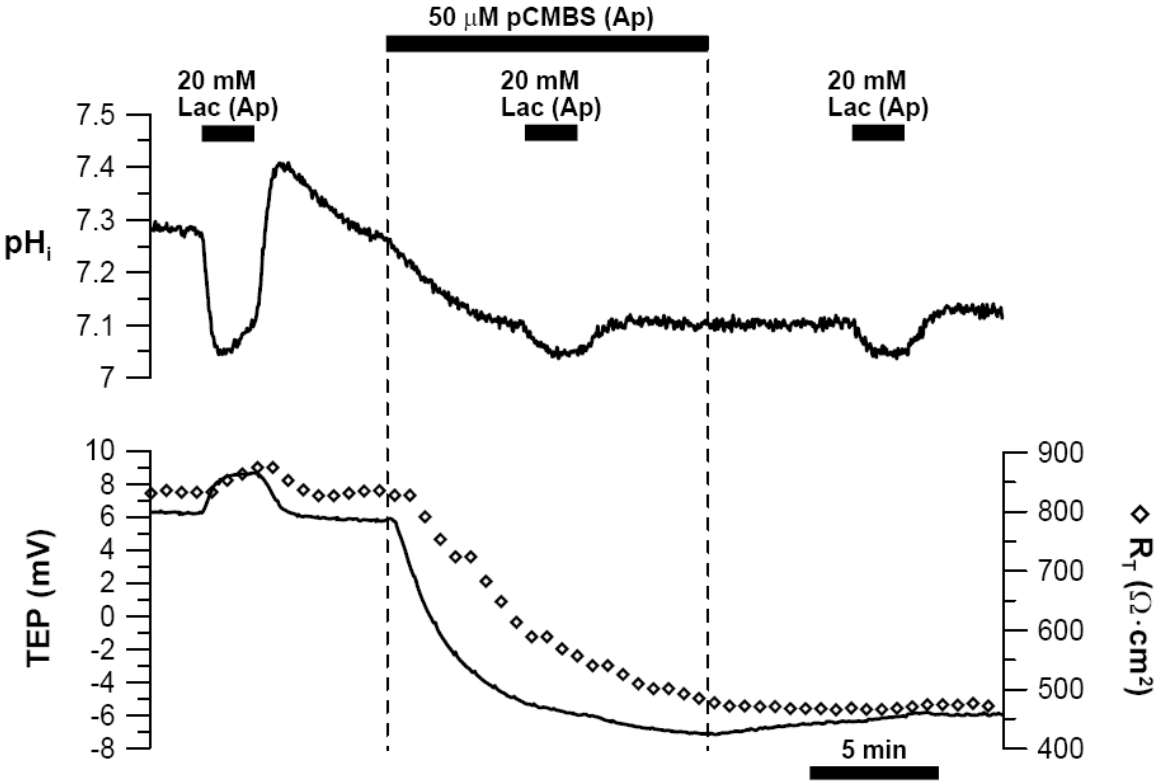

Fig. 4-3: Apical lactate induced pH_i, TEP, and R_T responses in the presence of apical pCMBS.

Adding pCMBS (50 μM) into the apical bath acidified the cells and significantly decreased steady-state TEP and R_T (ΔpH_i = -0.15 ± 0.01; ΔTEP = -11.99 ± 0.87 mV; ΔR_T = -305 ± 87 Ω·cm^2; n = 4). In four experiments, pCMBS almost completely blocked the apical lactate-induced pH_i, TEP, and R_T responses (Table 4-2) – the effects of pCMBS on the pH_i, TEP, and R_T responses were irreversible even after 5 min washout.

Table 4-2. Apical lactate-induced pH_i, TEP, and R_T responses.

inhibitor/condition[a]		Apical lactate-induced pH_i, TEP, and R_T responses[b]					
Apical	**Basal**		**Control**	**w/ inhibitor**	**Recovery**	**p[c]**	**n**
pCMBS		**R1**	-8.19 ± 0.94	-1.03 ± 0.09	-1.51 ± 0.20	S	4
		R2	1.09 ± 0.06	0.13 ± 0.08	-0.06 ± 0.08	S	
		ΔTEP	1.99 ± 0.31	0.04 ± 0.08	0.24 ± 0.29	S	
		ΔR_T	27 ± 13	0	0	S	
Niflumic acid		**R1**	-5.93 ± 1.29	-3.22 ± 0.79	-6.24 ± 0.89	S	7
		R2	0.78 ± 0.25	0.49 ± 0.23	0.77 ± 0.26	S	
		ΔTEP	1.58 ± 0.73	1.08 ± 0.52	1.47 ± 0.79	S	
		ΔR_T	48 ± 12	38 ± 13	36 ± 11	NS	
Amiloride		**R1**	-5.02 ± 1.22	-7.03 ± 2.71	-4.86 ± 1.16	S	6
		R2	0.78 ± 0.32	0	0.60 ± 0.29	S	
		ΔTEP	1.48 ± 0.79	1.39 ± 0.84	1.47 ± 1.01	NS	
		ΔR_T	43 ± 16	38 ± 15	37 ± 18	NS	
Na-free	**Na-free**	**R1**	-7.36 ± 1.47	-14.2 ± 2.53	-7.33 ± 4.31	S	3
		R2	1.34 ± 0.24	0	1.17 ± 0.32	S	
		ΔTEP	1.86 ± 0.32	1.15 ± 0.16	2.06 ± 0.24	S	
		ΔR_T	42 ± 3	48 ± 22	46 ± 9	NS	

a. Blank cells indicate that control Ringer was perfused into the corresponding bath.

b. H^+-flux in R1 and R2 has units of $mM \cdot min^{-1}$, ΔTEP has units of mV, ΔR_T has units of $\Omega \cdot cm^2$, and all values are reported as mean ± SD.

c. Student's t-test for statistical significance between apical lactate-induced response in control vs. in the presence of inhibitor. "S" indicates statistical significance ($p < 0.05$), "NS" indicates statistical insignificance ($p > 0.05$).

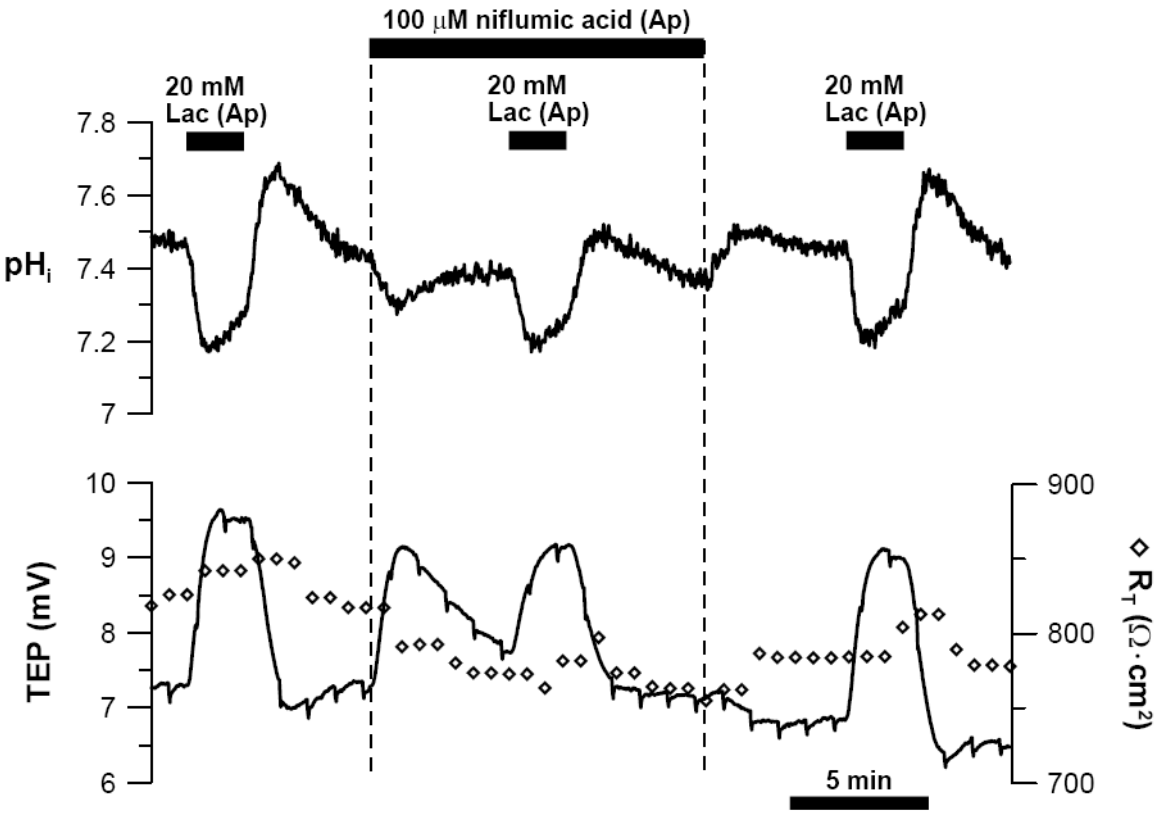

Fig. 4-4: Apical lactate induced pH_i, TEP, and R_T responses in the presence of apical niflumic acid.

In a similar experiment, we tested the effect of another MCT1 inhibitor, niflumic acid (apical bath; 100 μM), on the apical lactate-induced pH_i and TEP responses (Fig. 4-4). Adding niflumic acid to the apical bath acidified the cells, increased steady-state TEP, and decreased R_T (ΔpH_i = -0.12 ± 0.03; ΔTEP = 1.17 ± 0.74 mV; ΔR_T = -38 ± 13 $\Omega \cdot cm^2$; n = 7). In the presence of niflumic acid, apical lactate-induced R1 and R2 of the pH_i response were significantly reduced (Table 4-2). In addition, the lactate-induced TEP response was reduced by ≈ 30% (Table 4-2). In contrast, the effect of niflumic acid on lactate-induced R_T response was statistically insignificant (Table 4-2).

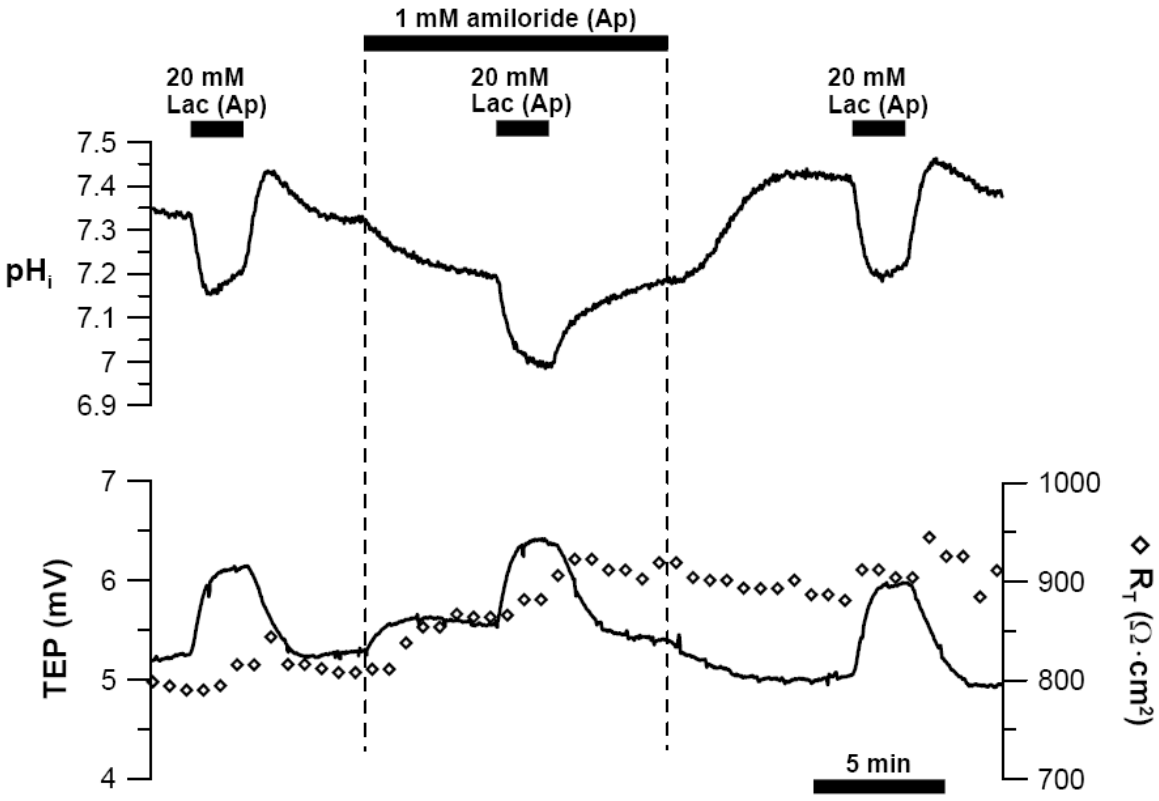

Fig. 4-5: Apical lactate induced pH_i, TEP, and R_T responses in the presence of apical amiloride.

In RPE, a Na/H exchanger (NHE) is expressed at the apical membrane and is stimulated by cell acidification (Lin *et al.*, 1992; Kenyon *et al.*, 1997). Therefore, R2 of the pH_i response observed in Fig. 4-2, -3, -4 may reflect lactate-induced NHE activation. To test this possibility, we compared lactate induced pH_i, TEP, and R_T responses in the presence of apical amiloride (1 mM; NHE inhibitor) (Fig. 4-5). In these experiments, adding amiloride *per se* acidified the cells, and increased steady-state TEP and R_T (ΔpH_i = -0.13 ± 0.02; ΔTEP = 0.28 ± 0.09 mV; ΔR_T = 63 ± 41 $\Omega \cdot cm^2$). In contrast, amiloride did not affect steady-state pH_i in the presence of CO_2/HCO_3 (Fig. 3-22), indicating that NHE is more active in the absence of CO_2/HCO_3 buffering. Apical lactate acidified the cell with the same magnitude in the presence or absence of amiloride, but when intrinsic buffering

capacity was taken into account, R1 of the lactate-induced pH_i response is significantly larger compared to control (Table 4-2), suggesting that apical lactate activated NHE during R1. In addition, the R2 recovery phase is completely abolished by apical amiloride (Table 4-2), but the TEP and R_T responses were unchanged.

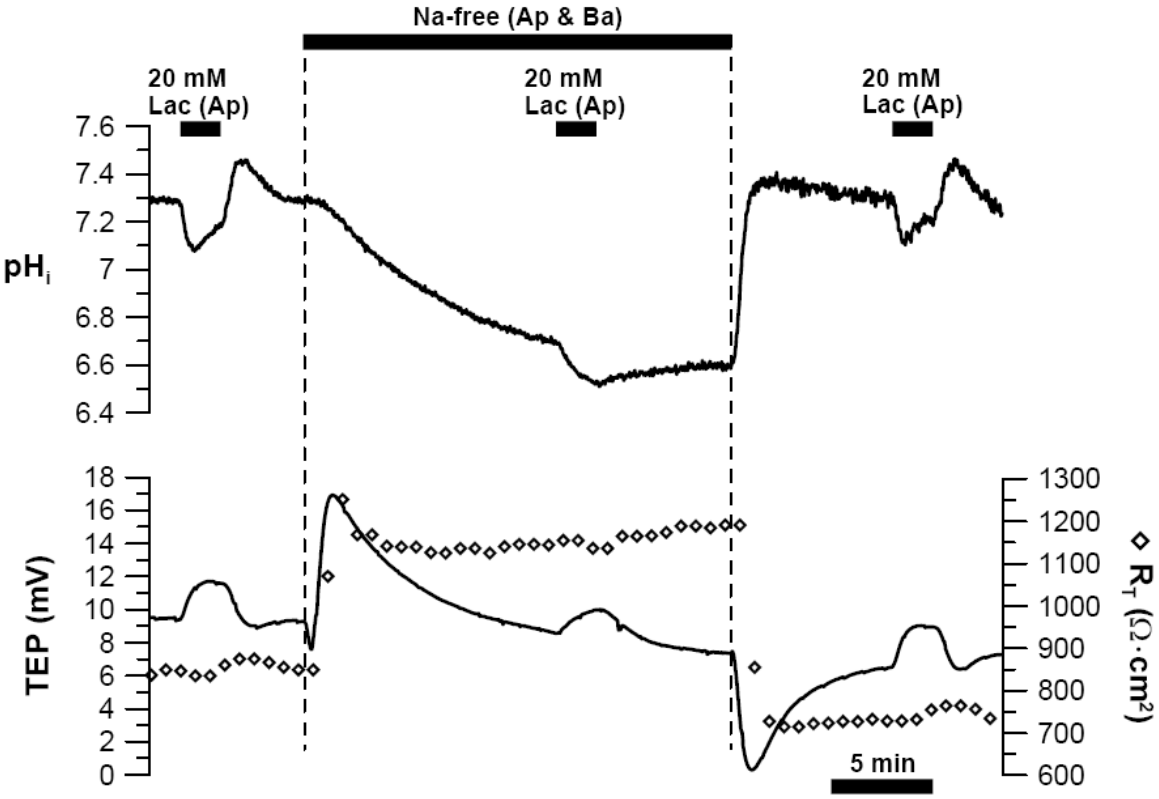

Fig. 4-6: Apical lactate induced pH_i, TEP, and R_T responses in the absence of Na.

Since NHE (Na/H exchanger) is a Na-linked transporter, we can eliminate its activity by removing all Na from both apical and basal baths. Consistent with this notion, R2 was completely blocked by 1 mM apical amiloride (Fig. 4-6). Removing Na decreased steady-state pH_i and TEP, and increased R_T (ΔpH_i = -0.77 ± 0.06; ΔTEP = -2.82 ± 1.39 mV; ΔR_T = 412 ± 88 $\Omega \cdot cm^2$). Although NHE normally exchanges H^+ for Na-entry, $[Na]_o$ removal generates a large outward Na-gradient that reverses NHE activity to transport H^+

into the cell and cause cell acidification. As shown in Fig. 4-6, apical lactate-induced acidification in the absence of Na ($\Delta pH_i = -0.14 \pm 0.02$) was smaller compared to control ($\Delta pH_i = -0.22 \pm 0.01$; $p < 0.05$). However when buffering capacity is taken into account, R1 was ≈ two-folds larger in the absence of Na compared to control (Table 4-2). In addition, R2 of the pH_i response was absent in Na-free condition. These observations suggest that apical lactate activated NHE during R1 and R2.

In this section, we showed that apical lactate-induced pH_i response is a two-phased process composed of a fast intracellular acidification (R1) followed by a slow alkalinization (R2). R1 reflects H/Lac entry via MCT1 because it can be inhibited by niflumic acid and pCMBS, both are potent MCT1 inhibitors (Jackson & Halestrap, 1996; Morris & Felmlee, 2008). R2 reflects NHE activity because it can be eliminated by apical amiloride (1 mM) or by Na-removal from both apical and basal baths. As shown in Figs. 4-3 and 4-4, lactate-induced acidification is required for the concomitant TEP and R_T responses, indicating that these responses originate from the activation of secondary mechanisms downstream of H/Lac entry. In the next section, we study the mechanisms underlying these TEP and R_T responses.

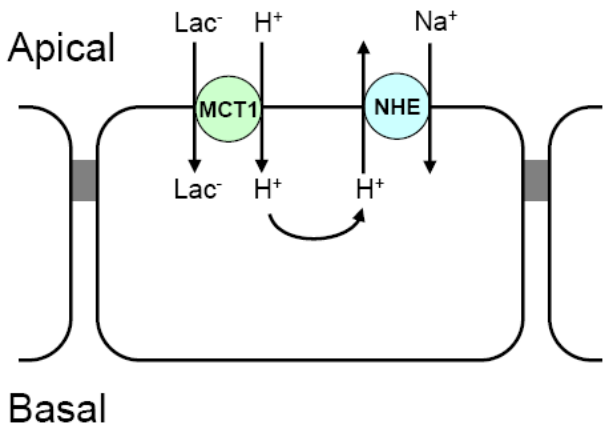

Sections 4.1 & 4.2 conclusions: MCT1 mediates H/Lac co-transport across the apical membrane of RPE
H/Lac entry via MCT1 activates NHE

Supporting experimental observations	Interpretation	Fig.
MCT1 is immunolabeled to the apical membrane	MCT1 is localized to the apical membrane	4-1B
MCT3 and MCT4 are immunolabeled to the basolateral membrane	MCT3 and MCT4 are localized to the basolateral membrane	4-1B
Western blots detected MCT1, MCT3, and MCT4 proteins in RPE lysates	MCT1, MCT3, and MCT4 proteins are expressed in RPE	4-1A
Apical lactate caused pH_i response with acidification (R1) and alkalinization (R2)	Lactate entered the cell via MCT1 to generate R1	4-2
R1 is blocked by pCMBS (MCT1 inhibitor)	Lactate entered the cell via MCT1 to generate R1	4-3
R1 is inhibited by niflumic acid (MCT1 inhibitor)	Lactate entered the cell via MCT1 to generate R1	4-4
R1 is increased by amiloride	Apical lactate activates NHE during R1	4-5
R2 is blocked by amiloride	Apical lactate activates NHE during R2	4-5
R1 is increased in the absence of Na^+	Apical lactate activates NHE during R1	4-6
R2 is increased in the absence of Na^+	Apical lactate activates NHE during R2	4-6

Section 4.4 – Lactate-induced TEP and R_T responses: involvement of Cl channels

Adding lactate to the apical bath increases TEP by ≈ 1.5 mV. This increase in TEP can originate from V_A hyperpolarization, V_B depolarization, or both. The latter case may be caused by the activation of a Cl channel at the basolateral membrane, leading to basolateral Cl-efflux and the subsequent V_B depolarization. If true, removing all Cl in both solution baths should eliminate this TEP response (Fig. 4-7). However, this maneuver cannot be performed with calomel electrodes ($HgCl_2$) because these electrodes use Cl as the conductive ion; absence of Cl would prevent the electrode from providing a reliable measurement of TEP and R_T. Therefore, we replaced the calomel electrodes with $HgSO_4$ electrodes (filled with sat. K_2SO_4). In this experiment, control and lactate Ringer solutions contains $CaSO_4$ (instead of $CaCl_2$) to provide SO_4^{2-} as conductive ion.

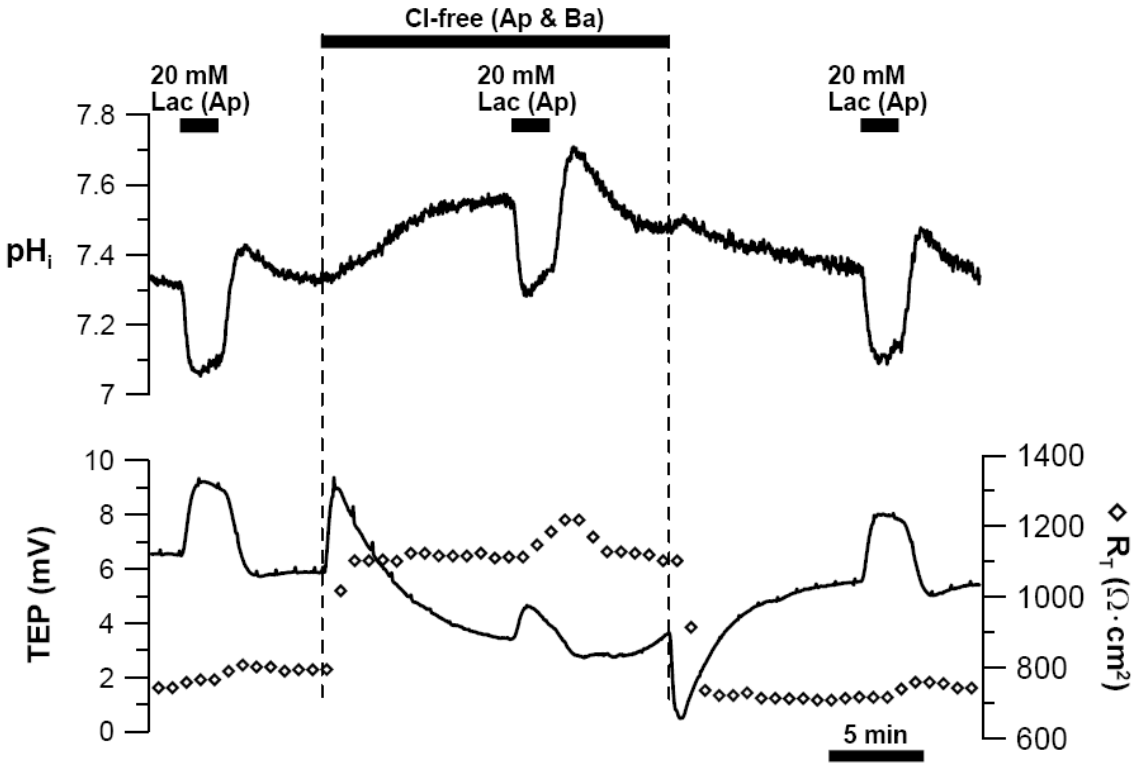

Fig. 4-7: Apical lactate induced pH_i, TEP, and R_T responses in the absence of Cl.

Table 4-3. Apical lactate-induced pH_i, TEP, and R_T responses.

inhibitor/condition[a]		Apical lactate-induced pH_i, TEP, and R_T responses[b]					
Apical	**Basal**		**Control**	**w/ inhibitor**	**Recovery**	**p[c]**	**n**
Cl-free	**Cl-free**	**R1**	-6.04 ± 1.31	-5.34 ± 0.67	-6.17 ± 0.98	NS	5
		R2	0.63 ± 0.34	0.59 ± 0.09	0.61 ± 0.04	NS	
		ΔTEP	1.72 ± 0.73	0.61 ± 0.36	1.47 ± 1.24	S	
		ΔR_T	38 ± 19	90 ± 48	32 ± 12	S	
Bume-tanide		**R1**	-5.96 ± 1.42	-5.77 ± 0.85	-5.51 ± 0.71	NS	6
		R2	0.46 ± 0.28	0.68 ± 0.18	0.37 ± 0.20	S	
		ΔTEP	1.05 ± 0.46	0.71 ± 0.28	1.05 ± 0.51	S	
		ΔR_T	57 ± 17	56 ± 20	51 ± 18	NS	
	$CFTR_{inh}$-172	**R1**	-6.98 ± 1.41	-6.78 ± 1.59	-8.33 ± 3.13	NS	5
		R2	0.95 ± 0.14	0.95 ± 0.22	1.10 ± 0.34	NS	
		ΔTEP	2.10 ± 0.78	2.06 ± 0.67	2.10 ± 0.65	NS	
		ΔR_T	54 ± 20	53 ± 17	53 ± 12	NS	
	Forskolin	**R1**	-7.18 ± 0.69	-7.98 ± 1.37	-8.26 ± 1.49	NS	3
		R2	0.28 ± 0.06	0.27 ± 0.14	0.42 ± 0.25	NS	
		ΔTEP	1.16 ± 0.27	1.20 ± 0.31	1.02 ± 0.35	NS	
		ΔR_T	64 ± 36	58 ± 38	66 ± 39	NS	

a. Blank cells indicate that control Ringer was perfused into the corresponding bath.

b. H^+-flux in R1 and R2 has units of $mM \cdot min^{-1}$, ΔTEP has units of mV, ΔR_T has units of $\Omega \cdot cm^2$, and all values are reported as mean ± SD.

c. Student's t-test for statistical significance between apical lactate-induced response in control vs. in the presence of inhibitor. "S" indicates statistical significance ($p < 0.05$), "NS" indicates statistical insignificance ($p > 0.05$).

Removing Cl from both apical and basal baths increased steady-state pH_i and R_T (ΔpH_i = 0.18 ± 0.08; ΔR_T = 285 ± 74 $\Omega \cdot cm^2$; n = 5). In five experiments, both R1 and R2 of the apical lactate-induced pH_i responses were the same in the presence or absence of Cl, indicating that this maneuver did not impede apical H/Lac entry. However, the apical lactate-induced TEP-response was reduced by ≈ 3-fold in the absence of Cl (Table 4-3). In addition, apical lactate-induced R_T response was more than two-fold larger (Table 4-3). Both observations suggest that lactate stimulates Cl-dependent mechanisms. However, Cl-removal did not completely eliminate the TEP response, suggesting involvement of other Cl-independent mechanisms.

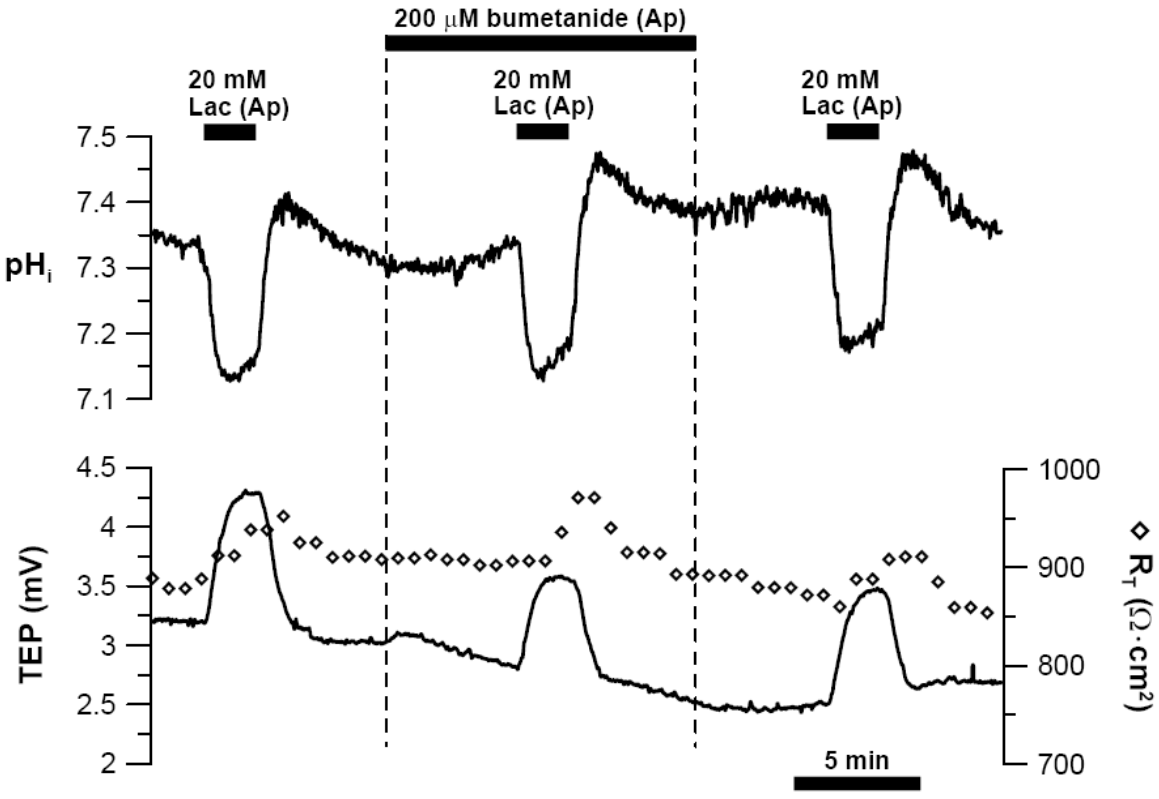

Fig. 4-8: Apical lactate induced pH_i, TEP, and R_T responses in the presence of apical bumetanide.

In RPE, CFTR and Ca^{2+}-dependent Cl-channels are major Cl-conductances at the basolateral membrane (Blaug *et al.*, 2003; Li *et al.*, 2009), and their activities are sustained by apical Cl-entry via NKCC1 at the apical membrane (see Fig. 1-8). Therefore, apical bumetanide (NKCC1 inhibitor) should reduce lactate-induced TEP response (Fig. 4-8). Consistent with this notion, the TEP response was reduced by ≈ 30% in the presence of bumetanide compared to control (Table 4-3). Bumetanide had no effect on R1, but R2 was larger in the presence of bumetanide compared to control (Table 4-3), possibly due to bumetanide-induced decrease in $[Na]_i$ which facilitates NHE activity.

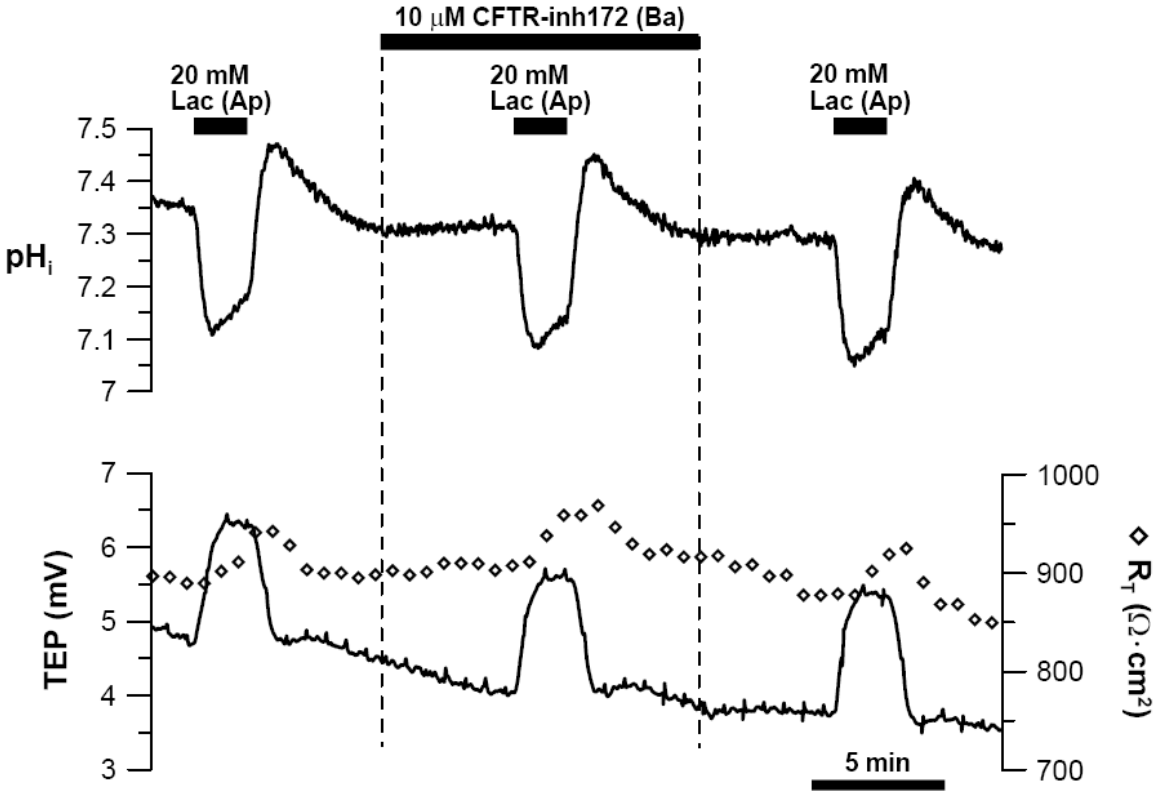

Fig. 4-9: Apical lactate induced pH_i, TEP, and R_T responses in the presence of basal CFTRinh-172.

To identify the lactate-activated basolateral membrane Cl-conductance, we determined lactate-induced responses in the presence of CFTRinh-172, a specific CFTR-inhibitor (Ma *et al.*, 2002), in the basal bath (Fig. 4-9). However, apical lactate-induced pH_i, TEP, and R_T responses were unaffected by CFTRinh-172 (Table 4-3), suggesting that apical lactate did not stimulate CFTR. However, CFTRinh-172 *per se* had little effect on steady-state TEP, suggesting that CFTR may not be fully active. Therefore, we stimulated the cAMP-activated CFTR by adding 40 μM forskolin into the basal bath. Forskolin stimulates adenylyl cyclase activity which catalyzes production of cAMP from ATP. However, apical lactate-induced pH_i, TEP, and R_T responses were also unaffected by forskolin (Table 4-3). These data indicate that lactate did not activate CFTR.

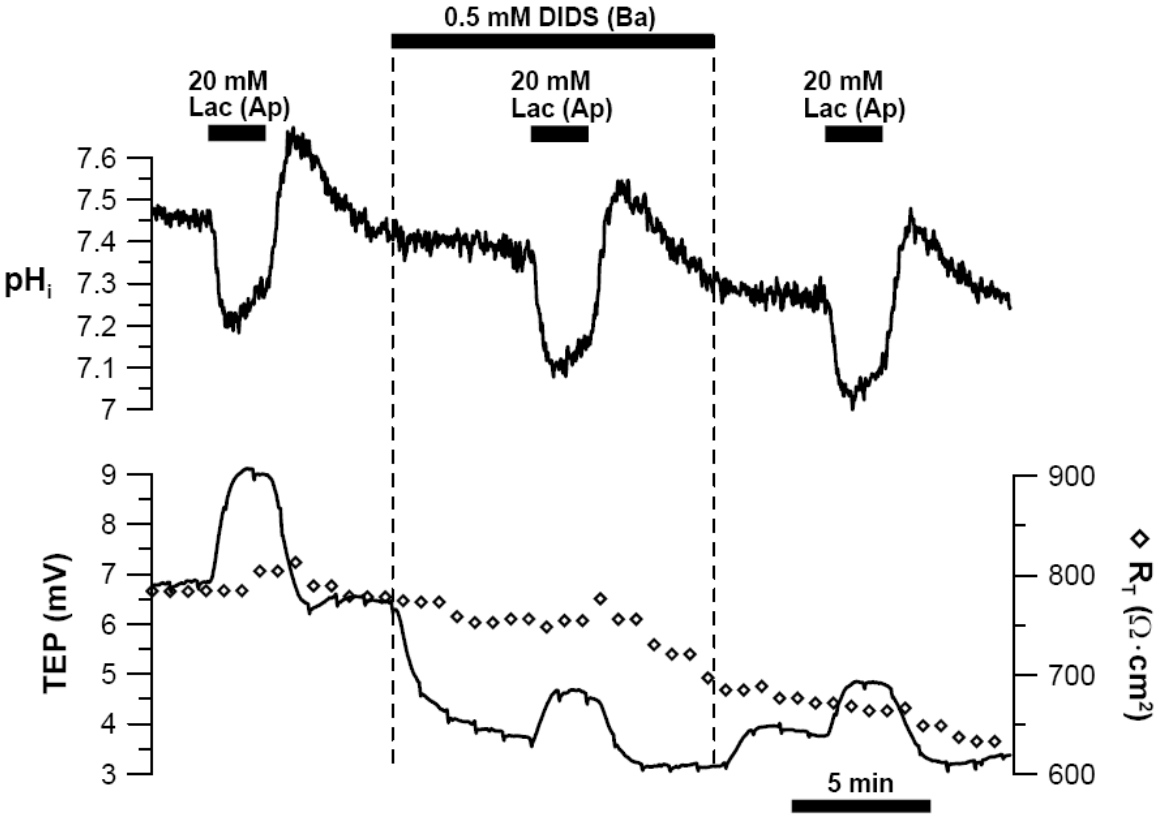

Fig. 4-10: Apical lactate induced pH_i, TEP, and R_T responses in the presence of basal DIDS.

Table 4-4. Apical lactate-induced pH_i, TEP, and R_T responses.

inhibitor/condition[a]		Apical lactate-induced pH_i, TEP, and R_T responses[b]					
Apical	**Basal**		**Control**	**w/ inhibitor**	**Recovery**	**p[c]**	**n**
	DIDS	**R1**	-5.02 ± 1.81	-6.12 ± 1.90	-7.42 ± 3.16	NS	5
		R2	0.74 ± 0.10	0.87 ± 0.24	1.00 ± 0.44	NS	
		ΔTEP	1.28 ± 0.73	0.46 ± 0.32	0.38 ± 0.39	S	
		ΔR_T	40 ± 8	35 ± 7	26 ± 5	NS	
BAPTA		**ΔTEP**	1.65 ± 0.50	1.56 ± 0.32	1.43 ± 0.51	NS	5
		ΔR_T	70 ± 17	72 ± 19	79 ± 13	NS	
	Zn^{2+}	**R1**	-6.29 ± 1.09	-7.18 ± 1.37	-11.0 ± 2.82	S	7
		R2	0.54 ± 0.20	0.18 ± 0.20	0	S	
		ΔTEP	1.14 ± 0.42	0.41 ± 0.18	0.57 ± 0.16	S	
		ΔR_T	60 ± 25	70 ± 25	47 ± 31	NS	
Zn^{2+}		**R1**	-7.25 ± 1.48	-6.68 ± 1.02	-6.44 ± 1.14	NS	4
		R2	0.54 ± 0.11	0.12 ± 0.20	0.73 ± 0.21	S	
		ΔTEP	1.23 ± 0.40	1.48 ± 0.41	1.35 ± 0.45	S	
		ΔR_T	58 ± 8	46 ± 11	42 ± 10	NS	
Ba^{2+}		**R1**	-6.65 ± 1.49	-6.76 ± 1.37	-7.35 ± 1.19	NS	5
		R2	0.54 ± 0.29	0.46 ± 0.20	0.52 ± 0.32	NS	
		ΔTEP	1.27 ± 0.30	0.73 ± 0.12	1.26 ± 0.28	S	
		ΔR_T	53 ± 25	83 ± 45	56 ± 29	S	

a. Blank cells indicate that control Ringer was perfused into the corresponding bath.

b. H^+-flux in R1 and R2 has units of $mM \cdot min^{-1}$, ΔTEP has units of mV, ΔR_T has units of $\Omega \cdot cm^2$, and all values are reported as mean ± SD.

c. Student's t-test for statistical significance between apical lactate-induced response in control vs. in the presence of inhibitor. "S" indicates statistical significance ($p < 0.05$), "NS" indicates statistical insignificance ($p > 0.05$).

Does lactate activate Ca^{2+}-activated Cl conductance? Ca^{2+}-activated Cl-channels can be blocked by DIDS, whereas CFTR is DIDS-insensitive (Bialek *et al.*, 1995; Schultz *et al.*, 1999; Quinn *et al.*, 2001). Fig. 4-10 shows that basal DIDS did not affect steady-state pH_i, but it significantly decreased TEP (2.58 ± 0.69 mV; n = 5) – consistent with inhibition of a Ca^{2+}-activated Cl conductance, but there was no significant change in pH_i or R_T. In five experiments, basal DIDS reduced the lactate-induced TEP response by 64% (Table 4-4), suggesting that lactate activated the DIDS-sensitive Ca^{2+}-dependent Cl conductance at the basolateral membrane.

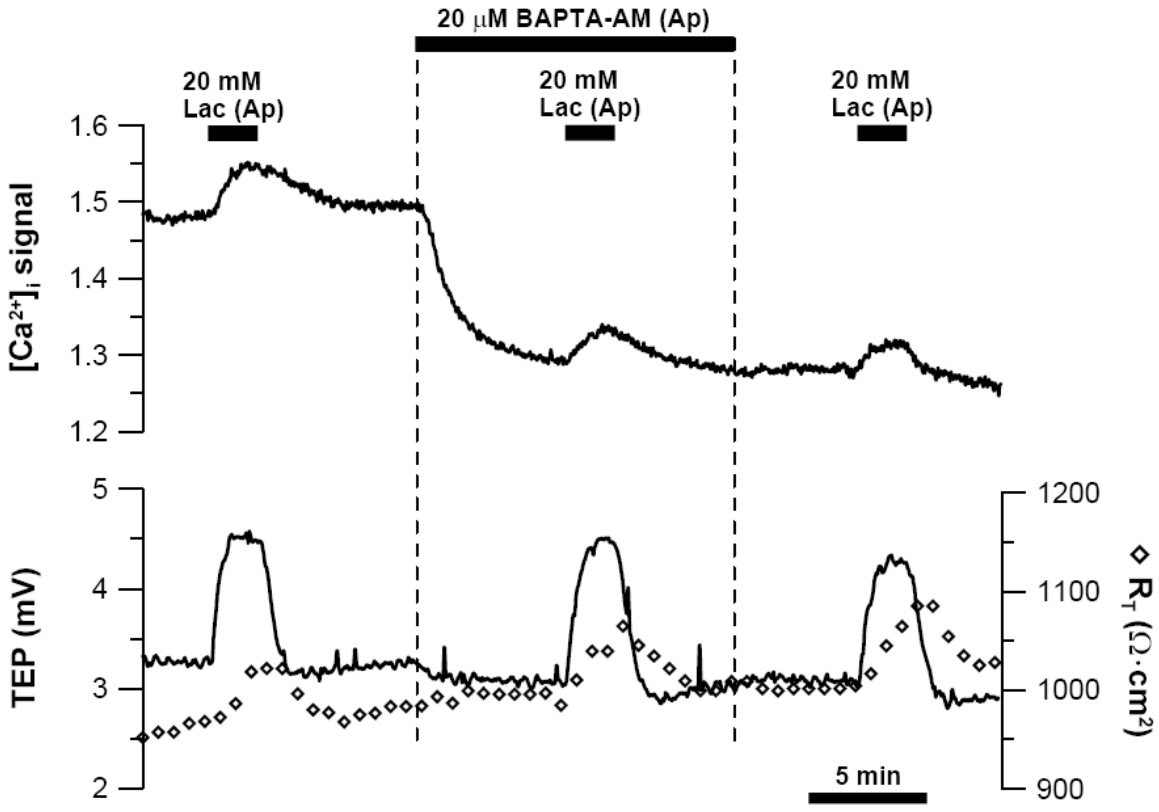

Fig. 4-11: Apical lactate induced pH_i, TEP, and R_T responses in the presence of apical BAPTA-AM.

The Ca^{2+} dependence of this Cl-channel was tested by chelating intracellular Ca^{2+} with BAPTA-AM (20 μM), which decreased $[Ca^{2+}]_i$ by 60 ± 30 nM (n = 5). However, the lactate-induced TEP and R_T responses were identical in the presence or absence of BAPTA-AM (Table 4-4), suggesting that lactate did not activate a Ca^{2+}-dependent Cl channel and that another Cl-conductance may be involved. In this context, ClC-2 is an obvious candidate because it is an almost ubiquitously expressed Cl-channel (Thiemann *et al.*, 1992) and its expression and activity in RPE has been previously demonstrated (Wills *et al.*, 2000; Weng *et al.*, 2002; Hartzell & Qu, 2003).

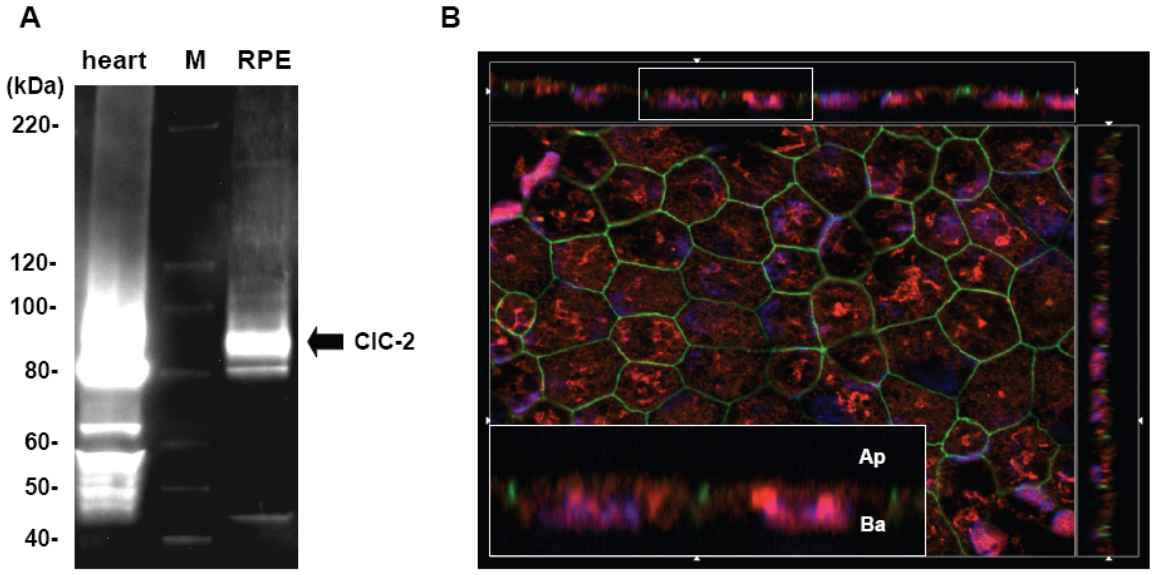

Fig. 4-12: ClC-2 Expression and Localization in RPE. (A) Western Blot analysis for ClC-2 protein expression; (B) Immunofluorescence analysis for ClC-2 protein localization.

The Western blot and immunocytochemistry data summarized in Fig. 4-12 show that ClC-2 (*CLCN2*) is highly expressed in hfRPE and localized to the basolateral membrane as well as intracellular compartments.

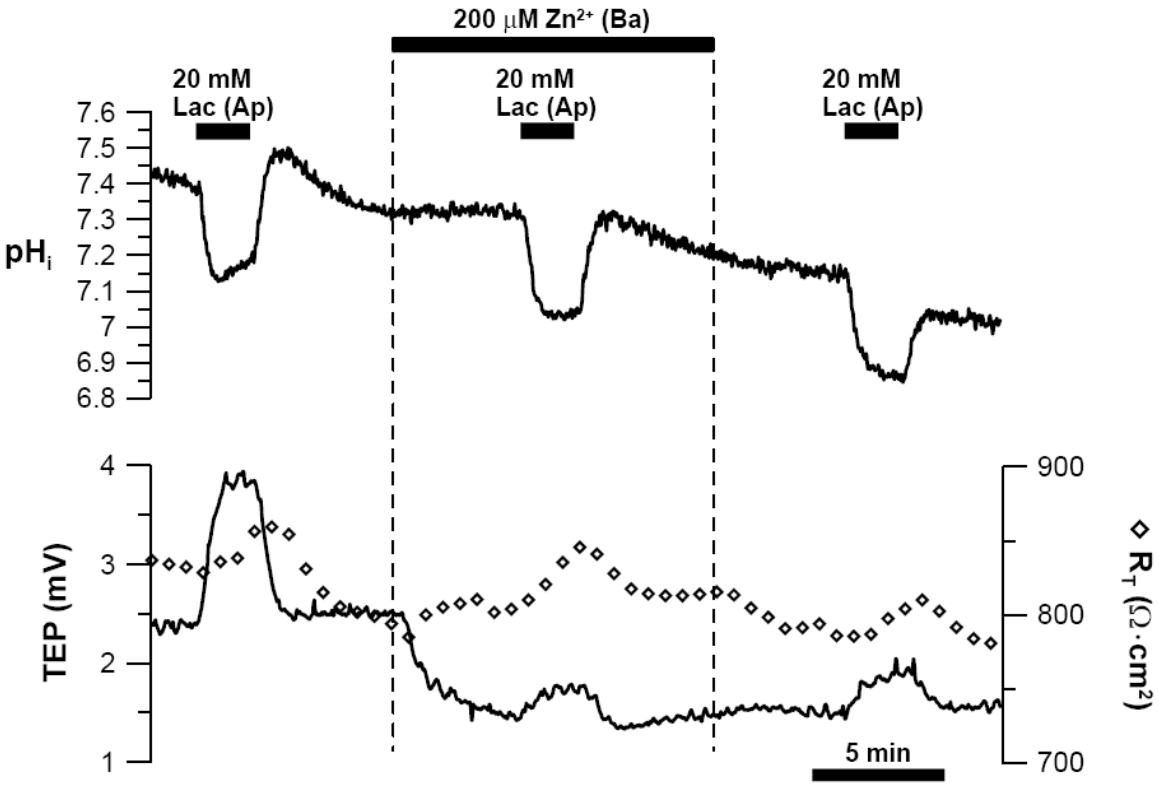

Fig. 4-13: Apical lactate-induced pH_i, TEP, and R_T responses in the presence of basal Zn^{2+}.

Since ClC-2 is inhibited by Zn^{2+} (Hartzell & Qu, 2003), we used Zn^{2+} to test ClC-2 activity (Fig. 4-13). Adding 200 μM Zn^{2+} to the basal bath did not significantly affect steady-state pH_i but it decreased TEP and increased R_T ($\Delta TEP = -1.24 \pm 0.81$ mV; $\Delta R_T = 51 \pm 25\ \Omega \cdot cm^2$; n = 15), consistent with the inhibition of a basolateral membrane Cl- current. In the presence of basal Zn^{2+}, the apical lactate-induced TEP response was reduced by 64% (Table 4-4). Although Zn^{2+} also increased the R_T response, this effect was not statistically significant (n = 10; Table 4-4). R1 of the pH_i response was unaffected by basal Zn^{2+} and R2 was gradually eliminated (Table 4-4), indicating that Zn^{2+} can enter the cell from the basal bath to reach the apical membrane, where it inhibits NHE-mediated Na/H exchange. This observation suggests that Zn^{2+} entered the cell via

Zip1 and Zip2 (Zn^{2+}-channels; (Leung *et al.*, 2008)) from the basolateral membrane. Adding 200 μM Zn^{2+} to the basal bath maximally inhibited ClC-2 because a higher Zn^{2+} concentration (500 μM) only reduced lactate-induced TEP response by 55% (ΔTEP = 1.41 ± 0.41 vs. 0.63 ± 0.33 mV; n = 6; $p < 0.05$).

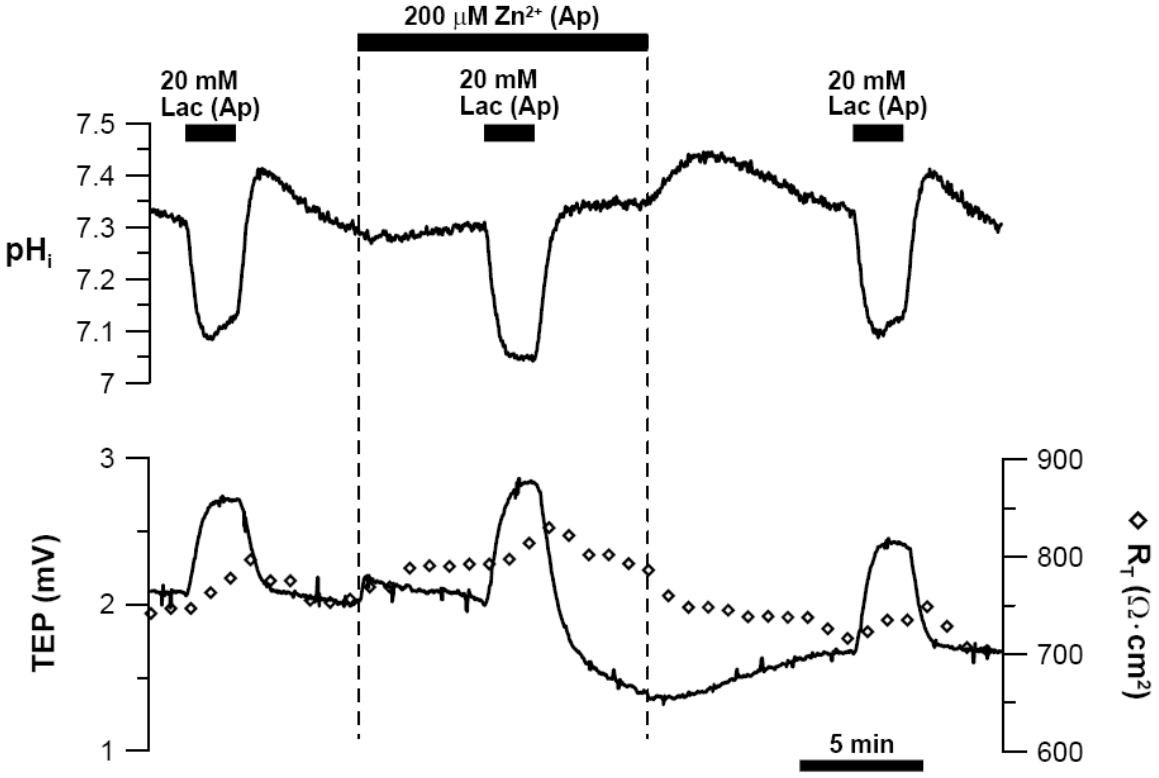

Fig. 4-14: Lactate-induced pH_i, TEP, and R_T responses in the presence of apical Zn^{2+}.

To demonstrate that basally added Zn^{2+} reduced lactate-induced TEP response by acting on basolateral membrane ClC-2, we tested the effect of apical Zn^{2+} (200 μM) on lactate-induced responses (Fig. 4-14). In four experiments, adding Zn^{2+} to the apical bath increased steady-state TEP and R_T (ΔTEP = 0.42 ± 0.26 mV; $\Delta R_T = 43 \pm 10\ \Omega \cdot cm^2$), suggesting that Zn^{2+} inhibited a channel at the apical membrane. However, the lactate-induced TEP response was larger in the presence of apical Zn^{2+} compared to control

(Table 4-4), whereas the R_T response was unaffected. Although R1 of the pH_i response was unaffected by apical Zn^{2+}, R2 of the pH_i response was significantly reduced (Table 4-4), indicating that apical Zn^{2+} inhibited NHE activity. Since apical Zn^{2+} did not reduce apical lactate-induced TEP response, this experiment confirms ClC-2 localization to the basolateral membrane.

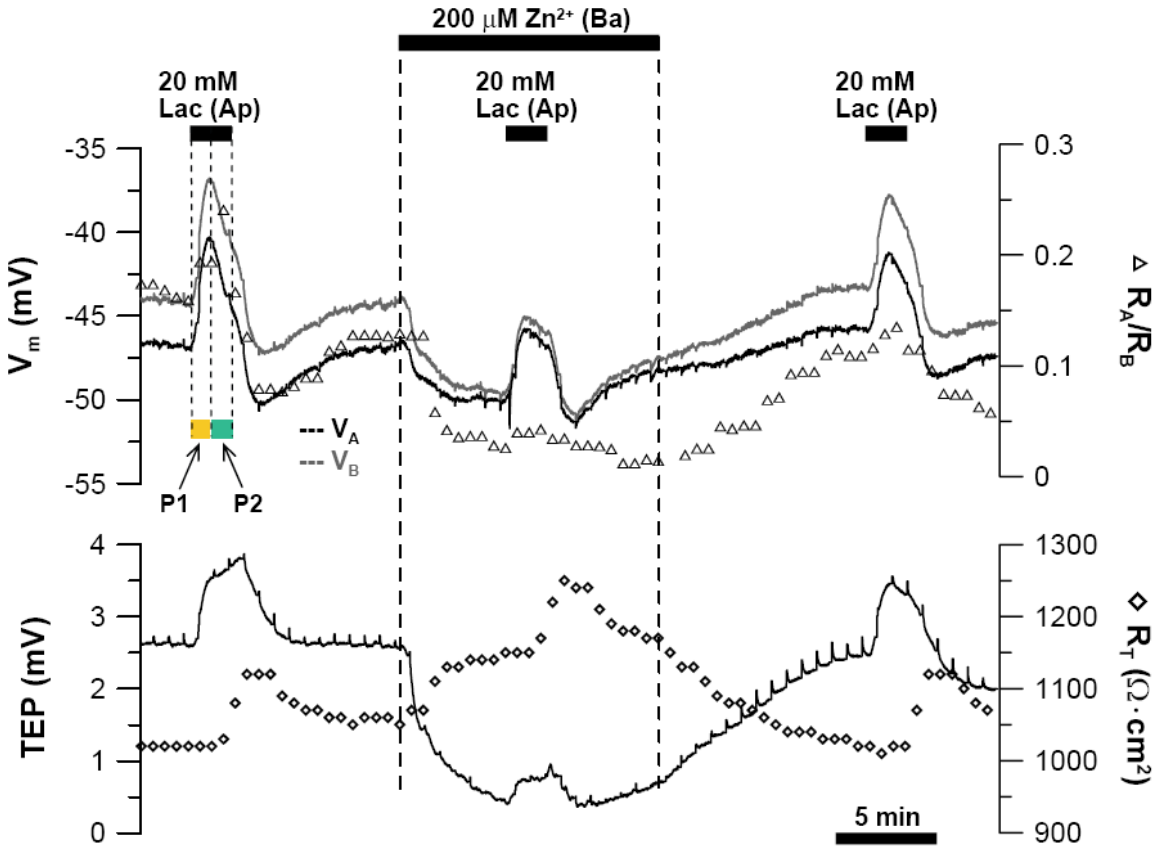

Fig. 4-15: Lactate-induced V_A, V_B, TEP, R_A/R_B, R_T responses in the presence of basal Zn^{2+}.

If lactate activated ClC-2, we should be able to detect basolateral membrane depolarization by using intracellular microelectrodes to separately measure apical and basolateral membrane voltages (V_A and V_B). Fig. 4-15 shows the apical lactate-induced changes in V_A, V_B, TEP, R_T, and R_A/R_B. Intracellular recordings show that apical lactate-

induced changes in membrane potentials (ΔV_A, ΔV_B) consist of two phases (P1 and P2). During P1, V_A and V_B rapidly depolarize with $\Delta V_B > \Delta V_A$ (TEP increase). During P2, V_A and V_B hyperpolarize relatively more slowly with $\Delta V_A > \Delta V_B$ (TEP increase). In 17 of 21 tissues tested, apical lactate increased R_A/R_B, consistent with activation of ClC-2 (which decreases R_B).

Addition of basal Zn^{2+} hyperpolarized both V_A and V_B, decreased steady-state TEP, and increased R_T (ΔV_A = -4.56 ± 3.14 mV; ΔV_B = -6.17 ± 4.23 mV; ΔTEP = -1.78 ± 1.16 mV; ΔR_T = 78 ± 34 $\Omega \cdot cm^2$; n = 5) – consistent with inhibition of ClC-2 at the basolateral membrane. In the presence of basal Zn^{2+}, the lactate-induced V_B depolarization during P1 was significantly reduced, whereas V_A depolarization in P1 was unaffected (Table 4-5), suggesting that Zn^{2+} blocked lactate-induced ClC-2 activation. In addition, both V_A and V_B hyperpolarization in P2 were significantly reduced by basal Zn^{2+}, suggesting that ClC-2 inhibition prevented activation of apical membrane K channels (see section 4.4). Furthermore, the lactate-induced increase in R_A/R_B was significantly reduced (72%) by basal Zn^{2+}, but its effect on the R_T response was statistically insignificant (Table 4-5).

Table 4-5. Apical lactate-induced V_A, V_B, TEP, and R_T responses.

inhibitor[a]		Apical lactate-induced V_A, V_B, TEP and R_T responses[b]					
Apical	Basal			Control	w/ inhibitor	p[c]	n
	Zn^{2+}	P1	ΔV_A	4.87 ± 1.40	3.90 ± 0.62	NS	5
			ΔV_B	5.54 ± 1.54	4.11 ± 0.77	S	
		P2	ΔV_A	-3.13 ± 1.27	-0.92 ± 0.55	S	
			ΔV_B	-2.89 ± 1.34	-0.79 ± 0.50	S	
			ΔTEP	0.94 ± 0.30	0.30 ± 0.18	S	
			ΔR_T	74 ± 28	80 ± 30	NS	
			$\Delta R_A/R_B$	0.06 ± 0.03	0.02 ± 0.02	S	
Ba^{2+}		P1	ΔV_A	4.81 ± 0.97	5.87 ± 1.04	S	6
			ΔV_B	5.74 ± 1.20	6.12 ± 1.07	NS	
		P2	ΔV_A	-3.08 ± 1.31	-1.68 ± 0.87	S	
			ΔV_B	-3.09 ± 1.24	-1.46 ± 0.74	S	
			ΔTEP	0.98 ± 0.44	0.48 ± 0.09	S	
			ΔR_T	60 ± 30	67 ± 31	NS	
			$\Delta R_A/R_B$	0.09 ± 0.05	-0.10 ± 0.06	S[d]	
	Ba^{2+}	P1	ΔV_A	4.49 ± 0.84	3.05 ± 0.67	S	5
			ΔV_B	5.16 ± 0.87	3.48 ± 0.75	S	
		P2	ΔV_A	-3.30 ± 0.77	-2.86 ± 1.23	NS	
			ΔV_B	-3.06 ± 0.92	-2.72 ± 1.15	NS	
			ΔTEP	0.87 ± 0.22	0.49 ± 0.08	S	
			ΔR_T	49 ± 10	39 ± 10	NS	
			$\Delta R_A/R_B$	0.08 ± 0.03	0.09 ± 0.04	NS[e]	
Ba^{2+}	Ba^{2+} Zn^{2+}	P1	ΔV_A	4.76 ± 0.63	3.41 ± 0.46	S	5
			ΔV_B	5.63 ± 0.70	3.52 ± 0.55	S	
		P2	ΔV_A	-2.95 ± 1.42	-0.81 ± 0.63	S	
			ΔV_B	-3.00 ± 1.42	-0.92 ± 0.70	S	
			ΔTEP	1.01 ± 0.34	0.10 ± 0.06	S	
			ΔR_T	49 ± 19	68 ± 18	S	
			$\Delta R_A/R_B$	0.09 ± 0.02	-0.02 ± 0.05	S[e]	

a. Blank cells indicate that control Ringer was perfused into the corresponding bath.

b. V_A, V_B, and TEP responses are presented in mV. ΔR_T has units of $\Omega \cdot cm^2$. All values are reported as mean ± SD.

c. Student's t-test for statistical significance between apical lactate-induced response in control vs. in the presence of inhibitor. "S" indicates statistical significance ($p < 0.05$), "NS" indicates statistical insignificance ($p > 0.05$).
d. Apical lactate had no effect on R_A/R_B in two of the six tissues tested, statistical analysis was performed with data from the remaining four tissues.
e. Apical lactate had no effect on R_A/R_B in one of the five tissues tested, statistical analysis was performed with data from the remaining four tissues.

In summary, we provided evidence to show that apical lactate stimulated ClC-2 at the basolateral membrane. In the first step, we show that apical lactate induced TEP response involves Cl-transport: (1) the lactate-induced TEP response was reduced in the absence of Cl (both apical and basal baths); (2) the TEP response was smaller in the presence of apical bumetanide to inhibit apical Cl-entry via Na/K/2Cl co-transporter (NKCC1); (3) the TEP response was reduced by basal DIDS. Cl-conductance at the RPE basolateral membrane is mainly comprised of cAMP-activated CFTR and Ca^{2+}-dependent Cl-channels (Hughes *et al.*, 1998). Our data suggests that lactate did not activate CFTR since lactate-induced TEP response was unaffected by either forskolin or CFTR-inh172 in the basal bath. This Cl-channel is also not Ca^{2+}-dependent because BAPTA-AM (a cell-permeable Ca^{2+}-chelator) decreased $[Ca^{2+}]_i$, but did not affect lactate-induced TEP response.

Next, we showed that lactate stimulated ClC-2 at the basolateral membrane with the following observations: (1) apical lactate-induced V_B depolarization in P1 was smaller in the presence of basal Zn^{2+}, whereas V_A depolarization remained unchanged; (2) the apical lactate-induced TEP response was reduced by basal Zn^{2+}, but not by apical Zn^{2+}. In

addition, western blots indicate that ClC-2 protein is expressed in hfRPE membrane fractions. With immunofluorescence, we also confirmed ClC-2 localization at the basolateral membrane surface of confluent cultured hfRPE monolayers, although ClC-2 was also detected in intracellular compartments. Collectively, our data confirmed the presence and activity of ClC-2 at the RPE basolateral membrane, and that this channel is activated by apical lactate. However, ClC-2 is not the only electrogenic mechanism activated by apical lactate, as evidenced by the following experiments: (1) Cl-removal (both baths) did not completely eliminate the lactate-induced TEP response; (2) neither basal DIDS nor basal Zn^{2+} (200, 500, or 1000 μM) completely eliminated this TEP response; (3) lactate induced V_A and V_B depolarization in P1 phase was not completely blocked by basal Zn^{2+}; (4) apical lactate-induced V_A and V_B hyperpolarization (in P2) but the activation of ClC-2 depolarizes V_A and V_B (in P1) – the latter observation does not reflect ClC-2 activity. The next section shows that apical lactate activates apical membrane K-channels.

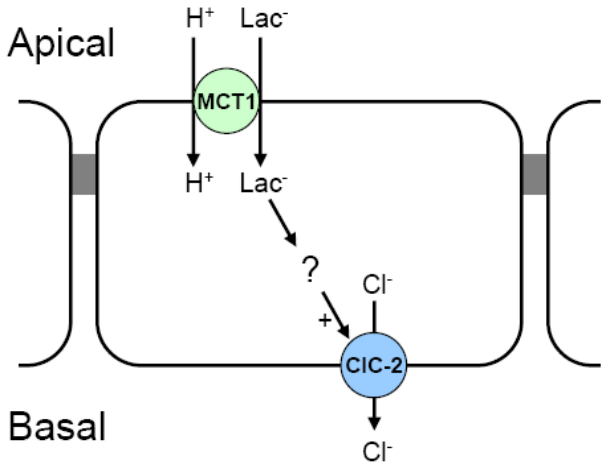

Section 4.3 conclusion: Apical lactate activates ClC-2 Cl-channel at the basolateral membrane

Supporting experimental observations	Interpretation	Fig.
Apical lactate depolarized V_B (in P1) and increased TEP	Apical lactate activates an electrogenic mechanism at the basolateral membrane	4-15
Cl-removal reduced apical lactate-induced TEP response	Apical lactate activates a Cl-dependent mechanism	4-7
CFTR-inh172 did not affect apical lactate-induced TEP response	Apical lactate did not activate CFTR	4-9
Forskolin did not affect apical lactate-induced TEP response	Apical lactate did not activate CFTR	N/A
Basal DIDS reduced apical lactate-induced TEP response	Apical lactate activated DIDS-sensitive Cl-channel at the basolateral membrane	4-10
BAPTA did not affect apical lactate-induced TEP response	Apical lactate did not activate a Ca^{2+}-dependent Cl-channel	4-11
Basal Zn^{2+} reduced apical lactate-induced TEP response	Apical lactate activates Zn^{2+}-sensitive ClC-2 at the basolateral membrane	4-13
Apical Zn^{2+} did not reduce apical lactate-induced TEP response	Effect of Zn^{2+} on ClC-2 is localized to the basolateral membrane	4-14
Apical lactate depolarized V_B (in P1), which is blocked by basal Zn^{2+}	Apical lactate activates ClC-2 (depolarizes V_B)	4-15
Apical lactate increased R_A/R_B, which is blocked by basal Zn^{2+}	Apical lactate activates ClC-2 (decrease R_B)	4-15

Section 4.5 – Lactate induced TEP and R_T responses: involvement of K channels

Given the high K-conductance at the apical membrane and that activation of this K-channel hyperpolarizes V_A and increases TEP, we sought to determine if lactate activates this channel. To this end, we compared the lactate-induced pH_i, V_A, V_B, TEP, R_T, and R_A/R_B responses in the presence or absence of 2 mM apical Ba^{2+} (K-channel inhibitor) (Fig. 4-16 and 4-17).

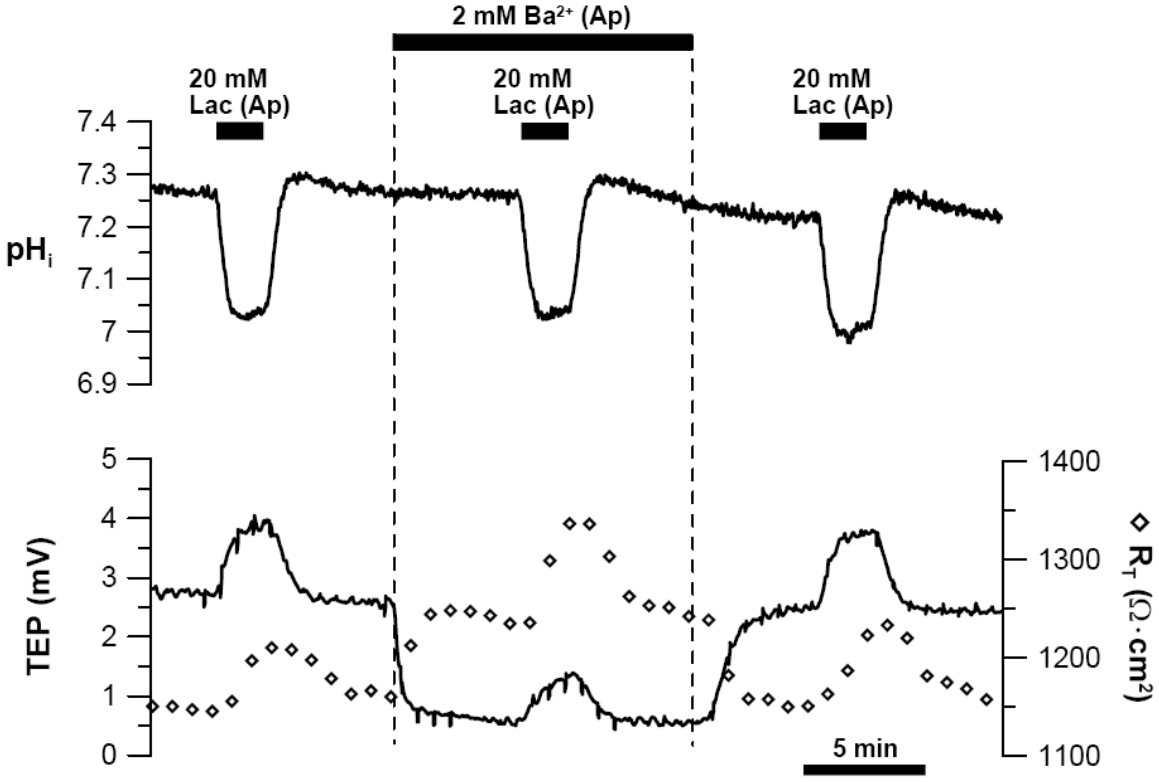

Fig. 4-16: Apical lactate induced pH_i, TEP, and R_T responses in the presence of apical Ba^{2+}.

Apical Ba^{2+} did not affect steady-state pH_i, but it significantly depolarized V_A and V_B, increased R_A/R_B, decreased TEP, and increased R_T (ΔV_A = 12.58 ± 4.39 mV; ΔV_B = 9.74 ± 3.36 mV; $\Delta R_A/R_B$ = 0.39 ± 0.18; n = 6) (ΔTEP = -3.52 ± 1.87 mV; ΔR_T = 88 ± 70 $\Omega \cdot cm^2$; n = 16) – consistent with inhibition of apical membrane K-channels.

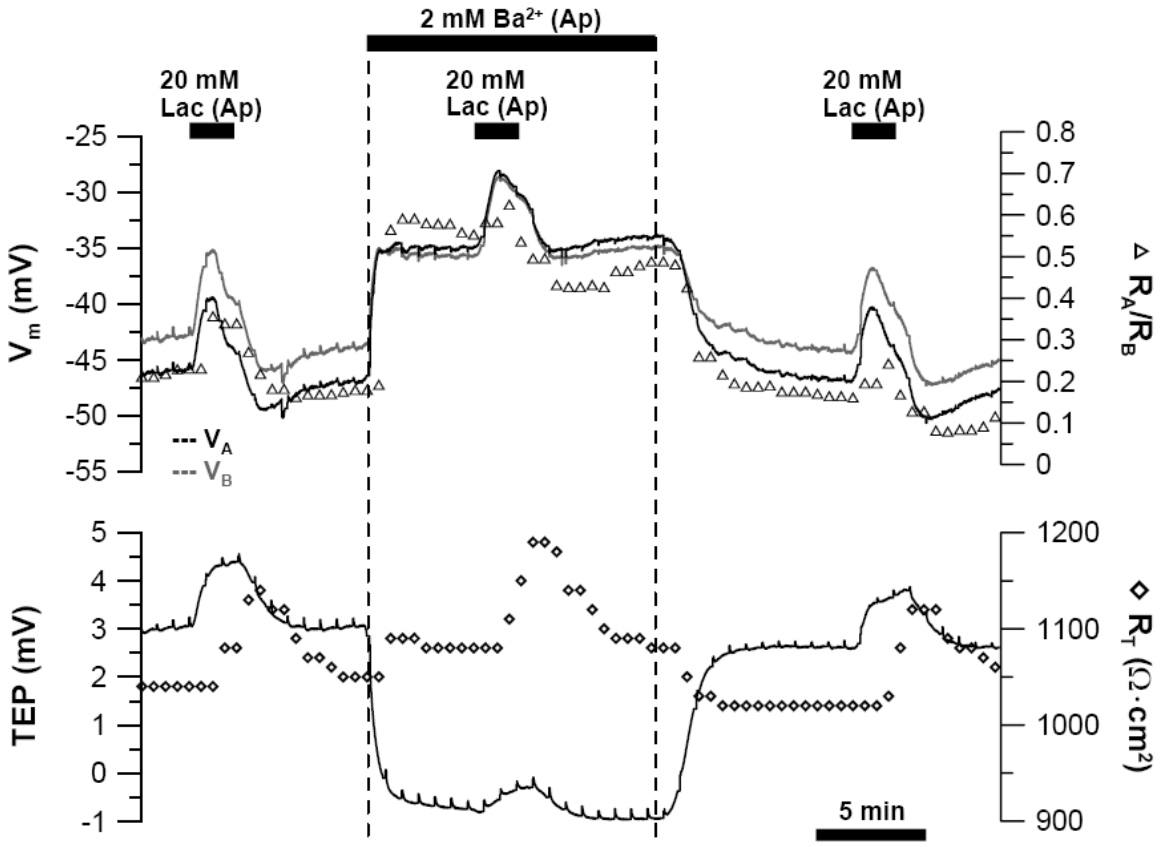

Fig. 4-17: Apical lactate induced V_A, V_B, TEP, R_A/R_B, R_T responses in the presence of apical Ba^{2+}.

In five experiments, apical lactate-induced pH_i-response (R1 & R2) was unaffected by Ba^{2+} (Table 4-4). On the other hand, lactate-induced V_A depolarization in P1 was larger in the presence of Ba^{2+}, whereas the V_B depolarization was unaffected (Table 4-5). In addition, V_A and V_B hyperpolarization in P2 were significantly reduced by apical Ba^{2+}. Further, the lactate-induced TEP response was reduced by almost 2-fold (from ΔTEP = 1.11 ± 0.39 mV to 0.59 ± 0.17 mV; n = 11; $p < 0.05$), and the R_T response was increased by ≈ 30% (from ΔR_T = 57 ± 27 to 74 ± 37 $\Omega \cdot cm^2$; n = 11; $p < 0.05$). These observations are consistent with activation of Ba^{2+}-sensitive K-channels at the apical membrane.

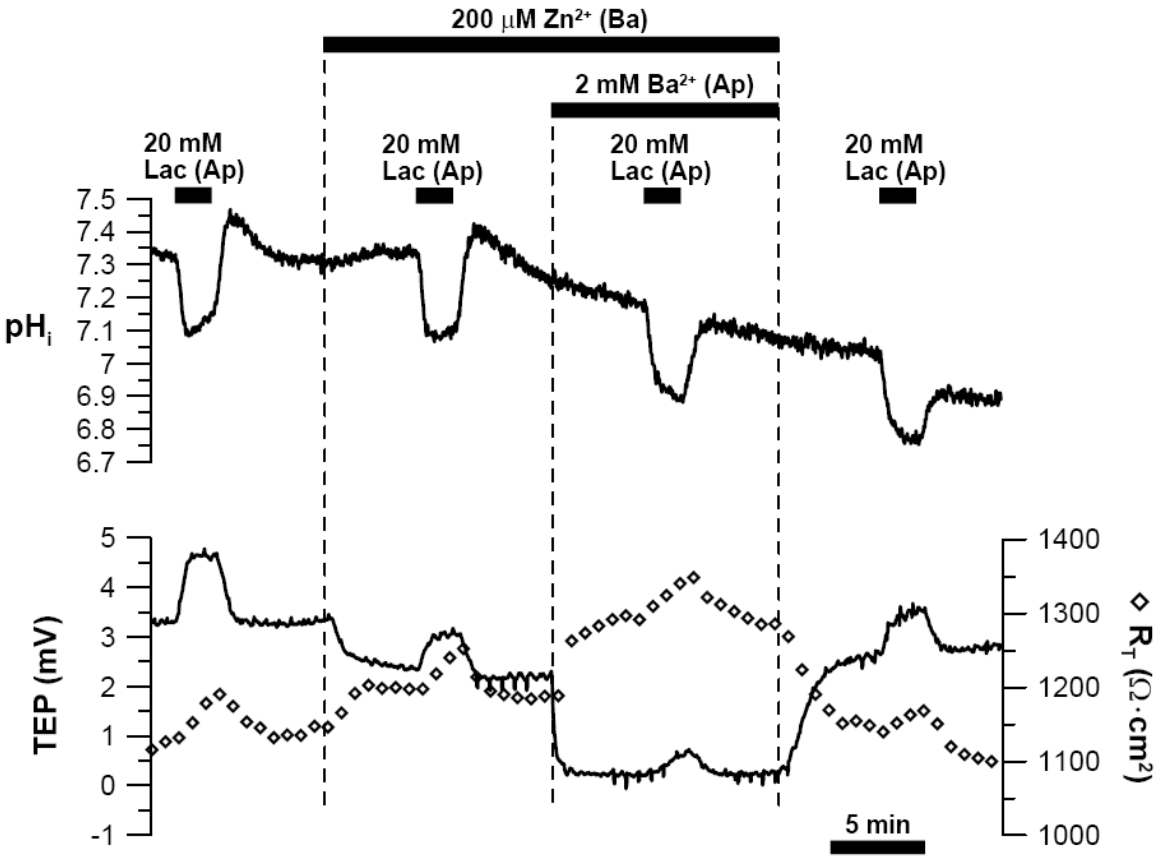

Fig. 4-18: Lactate-induced pH_i, TEP, and R_T responses in the presence of basal Zn^{2+} followed by both basal Zn^{2+} and apical Ba^{2+} simultaneously.

If apical lactate stimulated Ba^{2+}-sensitive K-channels and Zn^{2+}-sensitive ClC-2 at the apical and basolateral membrane respectively, adding apical Ba^{2+} and basal Zn^{2+} simultaneously should eliminate the lactate-induced TEP response (Fig. 4-18). In these experiments, apical lactate-induced responses were measured first in the presence of basal Zn^{2+}, followed by both apical Ba^{2+} and basal Zn^{2+}. In the presence of basal Zn^{2+}, the lactate-induced TEP response was reduced from 1.02 ± 0.33 to 0.51 ± 0.17 mV ($n = 6$; $p < 0.05$). This TEP response was further decreased from 0.51 ± 0.17 to 0.22 ± 0.13 mV ($n = 6$; $p < 0.05$) in the presence of both apical Ba^{2+} and basal Zn^{2+}. In contrast, the

effect of Ba^{2+} and Zn^{2+} on the R_T response was statistically insignificant. The incomplete inhibition of the TEP response and the lack of effect on R_T suggest the involvement of additional mechanisms – one that increases both TEP and R_T. A possible mechanism is lactate-induced inhibition of a basolateral membrane K-channel. If lactate-induced inhibition of basolateral membrane K-channel contributed to the initial V_A and V_B depolarization in P1, basal Ba^{2+} (2 mM) should reduce this response (Fig. 4-19).

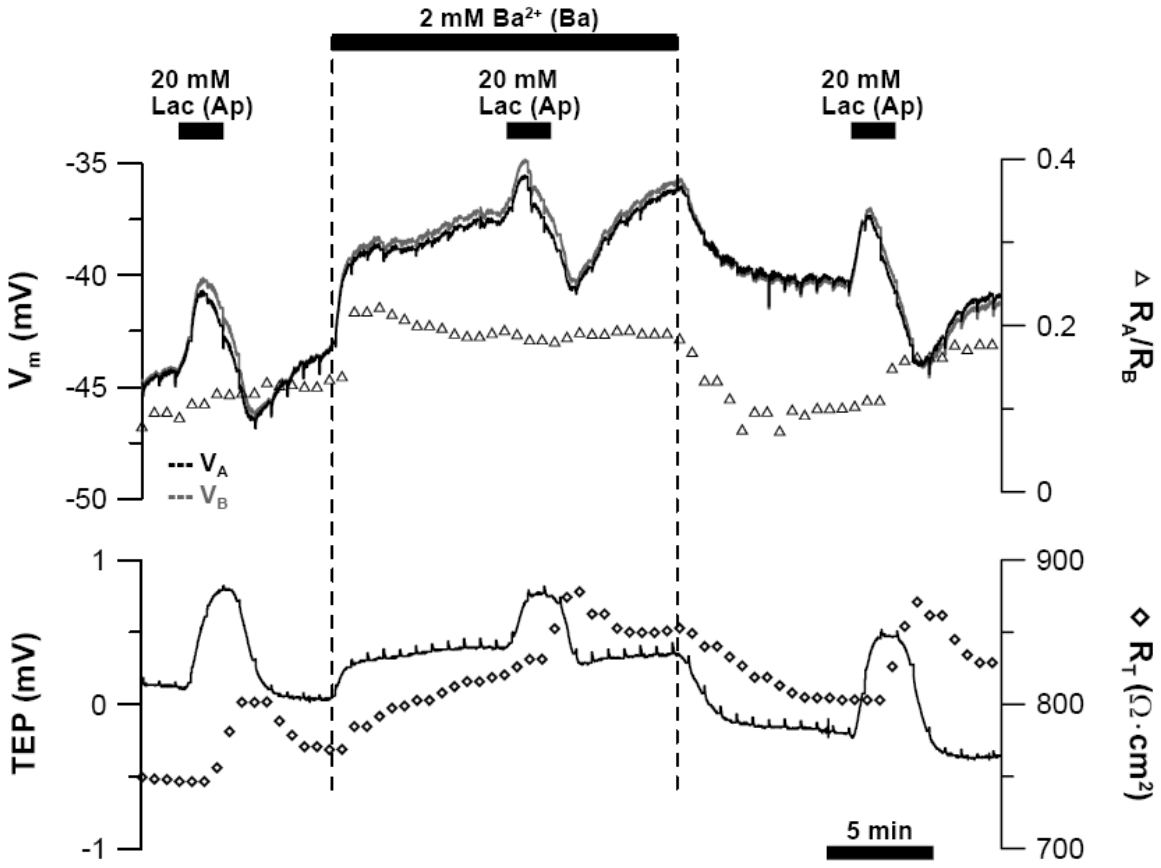

Fig. 4-19: Apical lactate induced V_A, V_B, TEP, R_A/R_B, R_T responses in the presence of basal Ba^{2+}.

Adding Ba^{2+} to the basal bath depolarized V_A and V_B ($\Delta V_A = 6.68 \pm 2.51$ mV; $\Delta V_B = 7.22 \pm 2.68$ mV), and increased both TEP and R_T ($\Delta TEP = 0.59 \pm 0.27$ mV; $\Delta R_T = 46 \pm 13\ \Omega \cdot cm^2$), consistent with inhibition of basolateral K-conductance. In five experiments,

basal Ba^{2+} (2 mM) reduced apical lactate-induced V_A and V_B depolarization in P1 by ≈ 30%, whereas V_A and V_B hyperpolarization in P2 were unaffected (Table 4-5). Furthermore, basal Ba^{2+} also reduced lactate-induced TEP and R_T responses (Table 4-5), but it did not affect lactate-induced increase in R_A/R_B. These observations suggest that apical lactate inhibited a Ba^{2+}-sensitive K-channel at the basolateral membrane. However, basal Ba^{2+} did not eliminate the lactate induced R_T response, suggesting that apical lactate increases R_T via other mechanisms. Possible lactate-activated mechanisms that can increase R_T are presented in the next section (section 4-5).

If apical lactate-induced activation of ClC-2 and apical membrane K-channel, and inhibition of basolateral membrane K-channel caused all the changes observed in V_A, V_B, TEP, and R_T, the simultaneous inhibition of all these channels should completely eliminate these responses. This notion was tested by adding 2 mM Ba^{2+} (both apical and basal baths) and 200 μM Zn^{2+} (basal bath) simultaneously (Fig. 4-20). In the presence of Ba^{2+} and Zn^{2+}, the lactate-induced TEP and R_A/R_B responses were completely eliminated, and the R_T response was increased by ≈ 40% (Table 4-5). V_A and V_B depolarization in P1 were both significantly reduced but not eliminated (Table 4-5). In addition, the V_A and V_B hyperpolarization in P2 were significantly reduced.

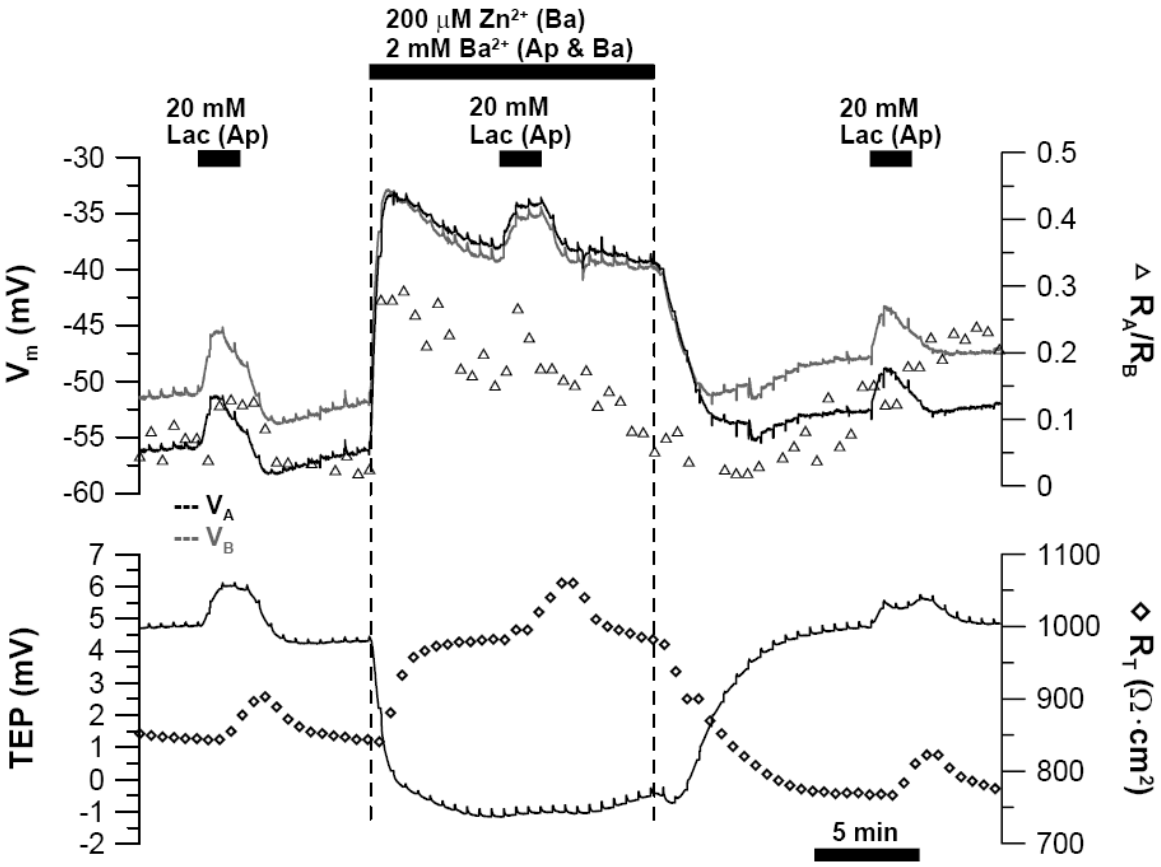

Fig. 4-20: Apical lactate induced V_A, V_B, TEP, R_A/R_B, R_T responses in the presence of both Zn^{2+} (basal bath) and Ba^{2+} (apical and basal baths).

Although the addition of Ba^{2+} and Zn^{2+} completely eliminated the lactate induced TEP response, the V_A and V_B depolarization in P1 was not completely eliminated, albeit reduced. Electrical shunting between apical and basolateral membranes cannot account for this observation (all hfRPE have $R_T > 500\ \Omega \cdot cm^2$). The equivalent increase in both V_A and V_B (without any ΔTEP) is consistent with a change in liquid junction potential at the microelectrode tip, possibly due to a decrease in $[Cl]_i$. Apical lactate can decrease $[Cl]_i$ by increasing Cl-efflux via ClC-2, and causing cell-swelling, which dilutes the cytosol. However, blocking ClC-2 with Zn^{2+} did not eliminate lactate-induced V_A and

V_B responses in P1, therefore cell-swelling probably generated the junction potential in P1.

Besides K-channels and ClC-2, other transport mechanism may be involved in lactate transport. A recent study showed that SMCT1, an electrogenic Na-linked lactate co-transporter (2:1 Na/Lac), is expressed exclusively at RPE basolateral membrane (Martin *et al.*, 2007). However, our data suggest that SMCT1 contributes little to lactate transport: (1) thermodynamics predict that the large inward Na-gradient across the basolateral membrane prevents Na/lactate efflux via SMCT1; (2) 2Na/Lac efflux from the basolateral membrane via SMCT1 should decrease TEP, but apical lactate increased TEP; (3) the lactate-induced TEP response was completely blocked by Ba^{2+} (apical and basal) and Zn^{2+} (basal) – no other mechanisms contributed to this TEP response.

In summary, based on the following evidence, we show that apical lactate stimulated apical membrane K-channels, which hyperpolarize V_A throughout P1 and P2 and increases TEP: (1) V_A depolarization in P1 was larger in the presence of apical Ba^{2+}, whereas V_B depolarization was unaffected; (2) the lactate-induced TEP response was smaller in the presence of apical Ba^{2+}; (3) the V_A and V_B hyperpolarization in P2 were reduced by apical Ba^{2+}. In addition, inhibition of either apical K-efflux (with Ba^{2+}) or basolateral Cl-efflux (via ClC-2; with Zn^{2+}) reduces the V_A and V_B hyperpolarization in P2 phase, suggesting that the activities of these two channels are electrically coupled to preserve charge neutrality. Surprisingly, apical lactate decreased R_A/R_B in the presence of apical Ba^{2+} (lactate increases R_A/R_B in control) (Table 4-5). This is unusual because if

lactate activates apical K-channel (which decreases R_A and reduces R_A/R_B), K-channel inhibition with apical Ba^{2+} should amplify the lactate-induced increase in R_A/R_B. We postulate that the large V_A and V_B depolarization caused by apical Ba^{2+} increases basolateral membrane K-channel conductance and activity (assuming outwardly rectifying channel). In its highly active state, its inhibition by lactate would cause a more pronounced increase in R_B, thus producing a significant decrease in R_A/R_B. In support of this hypothesis, this lactate-induced decrease in R_A/R_B (in the presence of apical Ba^{2+}) was eliminated by basal Ba^{2+}.

The following results support the notion that lactate inhibits a K-channel at the basolateral membrane: (1) both V_A and V_B depolarization in P1 were reduced by basal Ba^{2+}; (2) lactate-induced TEP and R_T responses were reduced by basal Ba^{2+}. However, evidence suggests that this K-channel is normally less active than apical membrane K-channel and ClC-2 because: (1) inhibition of basolateral K-channel contributes to a decrease in R_A/R_B by increasing R_B, but lactate produced a net increase in R_A/R_B; (2) lactate-induced R_A/R_B increase was unaffected by basal Ba^{2+}. The effect of basal Ba^{2+} on apical membrane K-channel and ClC-2 is minimal because basal Ba^{2+} did not affect V_A and V_B hyperpolarization in P2. Next, we show that the inhibition of all these channels (i.e., apical and basolateral membrane K-channels, and ClC-2) eliminates the lactate induced TEP response, but did not affect lactate-induced V_A and V_B depolarization. This observation suggests that lactate caused cell swelling, which is discussed further in the next section.

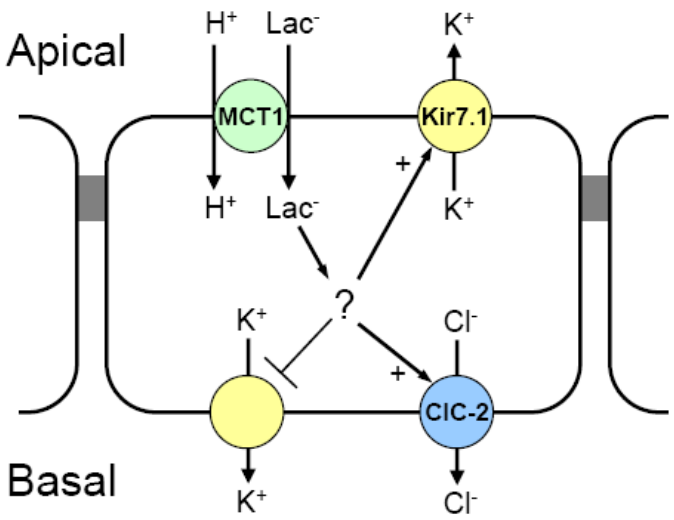

Section 4.4 conclusions: Apical lactate activates Kir 7.1 K-channel at the apical membrane
Kir 7.1 and ClC-2 activity is electrically coupled
Apical lactate inhibits a Ba^{2+}-sensitive K-channel at the basolateral membrane

Supporting experimental observations	Interpretation	Fig.
Apical lactate hyperpolarize V_A (in P2) and increased TEP	Apical lactate activates an electrogenic mechanism at the apical membrane	4-17
Apical barium reduced apical lactate induced TEP response	Apical lactate activates a Ba^{2+} sensitive K-channel at the apical membrane	4-17
Apical barium increased V_A depolarization in P1	Apical lactate activates a Ba^{2+} sensitive K-channel at the apical membrane	4-17
Apical barium reduced V_A hyperpolarization in P2	Apical lactate activates a Ba^{2+} sensitive K-channel at the apical membrane	4-17
Basal Zn^{2+} reduced V_A hyperpolarization in P2	Kir 7.1 and ClC-2 activities are electrically coupled	4-15
Basal Ba^{2+} reduced apical lactate induced TEP response	Apical lactate inhibits a Ba^{2+}-sensitive K-channel at the basolateral membrane	4-19
Basal Ba^{2+} reduced V_A and V_B depolarization (in P1)	Apical lactate inhibits a Ba^{2+}-sensitive K-channel at the basolateral membrane	4-19
Zn^{2+} and Ba^{2+} eliminated lactate-induced TEP response	Apical lactate activates Kir 7.1 and ClC-2, and inhibits a basolateral membrane K-channel	4-20

Section 4.6 – Mechanism of lactate induced ion-channel activation or inhibition

The lactate-induced changes in K-channel and ClC-2 activities may be caused by cell swelling or acidification. As previously discussed, microelectrode experiments suggest that apical lactate caused cell-swelling, which may activate these ion-channels. Mammalian cells respond to hypoosmotic challenge by activating K- and Cl- channels to drive KCl and fluid out of the cell (Nilius *et al.*, 1997; Eggermont *et al.*, 2001). The RPE expresses BK-channel (Ca^{2+}-activated K-channel) and ClC-2 (Grunder *et al.*, 1992; Furukawa *et al.*, 1998; Xiong *et al.*, 1999; Sheu *et al.*, 2004) – both are swell-activated ion-channels and may participate in regulatory volume decrease.

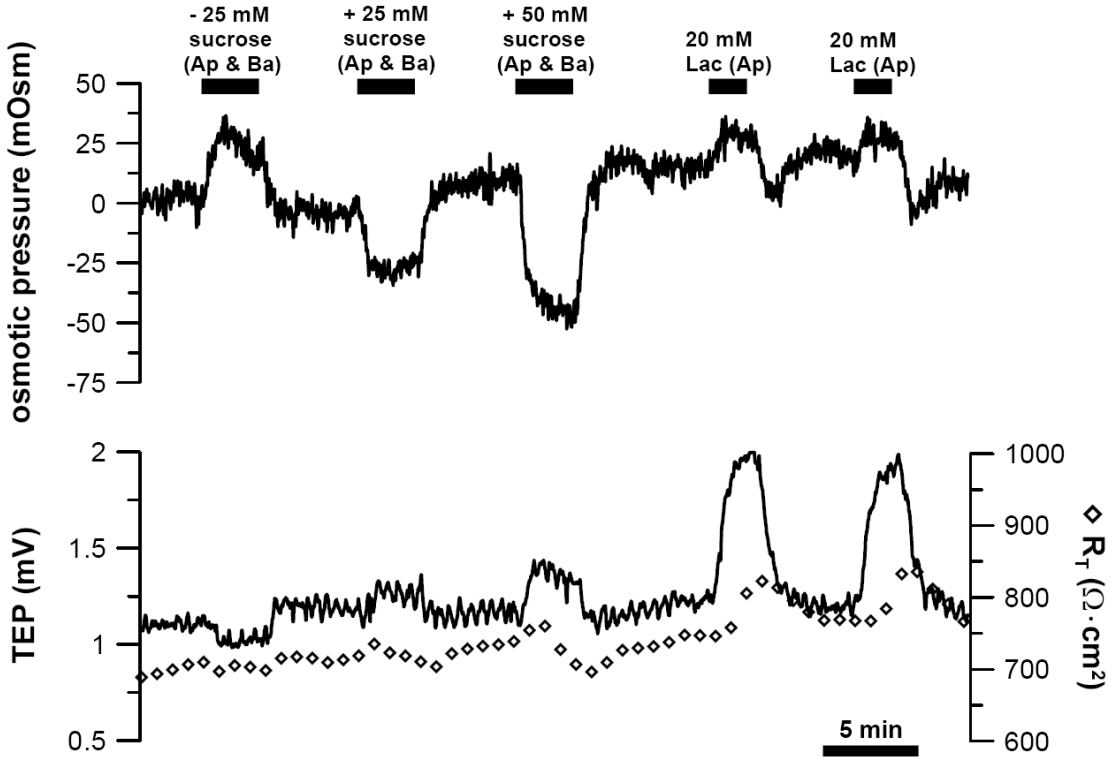

Fig. 4-21: Apical lactate vs. hyperosmotic Ringer solution induced cell-swelling.

To better quantify lactate-induced cell swelling, we used a pH_i-insensitive dye (calcein) with a three-point osmolarity calibration (with 280, 330, 355 mOsm Ringer) to show that

apical lactate caused cell-swelling equivalent to 8 ± 2 mOsm (n = 6; Fig. 4-21). If apical membrane K-channels and ClC-2 are indeed activated by cell-swelling, decreasing Ringer osmolarity (from 305 to 280 mOsm; both solution baths) should increase TEP. However, hypoosmotic Ringer decreased TEP by 0.28 ± 0.16 mV, whereas lactate increased TEP by 1.06 ± 0.34 mV (n = 6). Furthermore, hypo-osmotic Ringer did not affect R_T. These observations suggest that cell-swelling did not activate apical K-channel or basolateral K-channel and ClC-2.

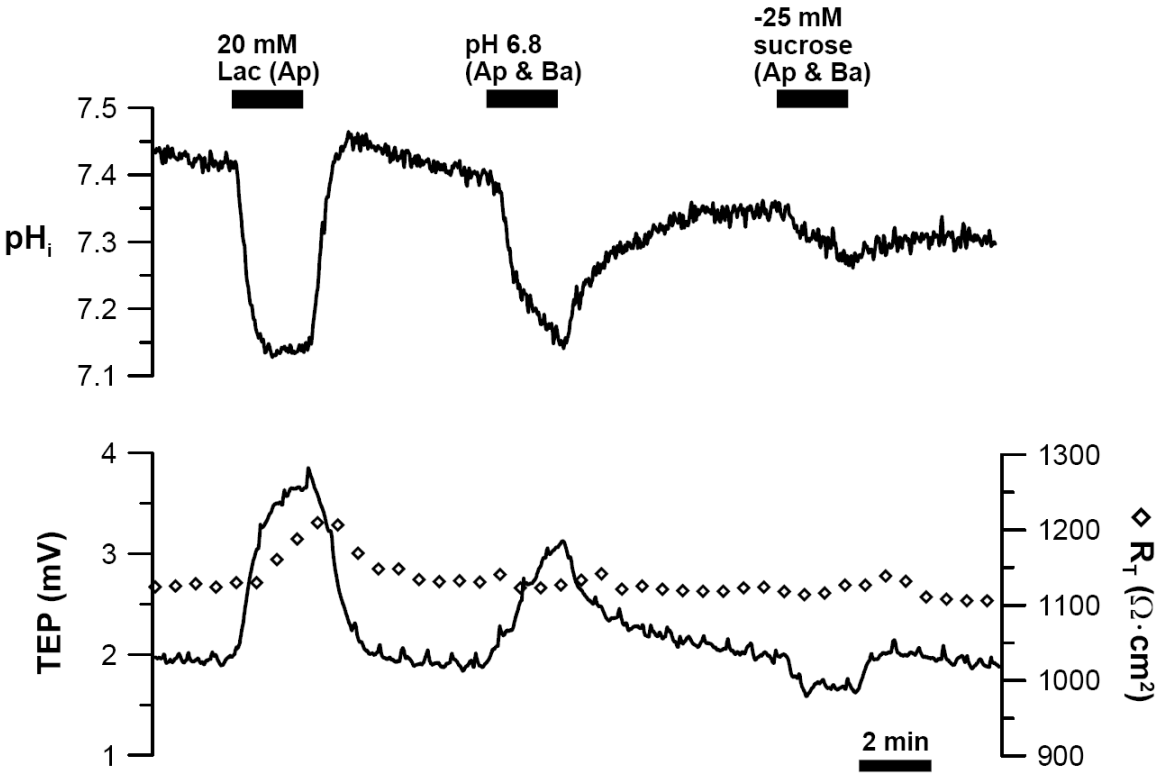

Fig. 4-22: Lactate, low pH (6.8), and hypotonic induced pH_i, TEP, and R_T responses.

Alternatively, apical lactate may stimulate these K-channels and ClC-2 by causing cell acidification. Kir 7.1 K-channels are highly expressed in RPE apical membrane and is activated by mild intracellular acidification (Yuan *et al.*, 2003; Hughes & Swaminathan,

2008). In addition, ClC-2 is stimulated by acidic conditions (Jordt & Jentsch, 1997; Hartzell & Qu, 2003). Consistent with this notion, we show that acidifying the cell by reducing bath pH (pH 6.8; both solution baths) produced a TEP response (0.83 ± 0.45 mV) with a magnitude comparable to that caused by 20 mM apical lactate (ΔTEP = 1.20 ± 0.52 mV; n = 5; $p < 0.05$) (Fig. 4-22). However unlike lactate, low pH Ringer had no effect on R_T. If cell acidification stimulated ClC-2 activity, we should be able to block low pH Ringer-induced TEP response with basal Zn^{2+} (200 μM) (Fig. 4-23).

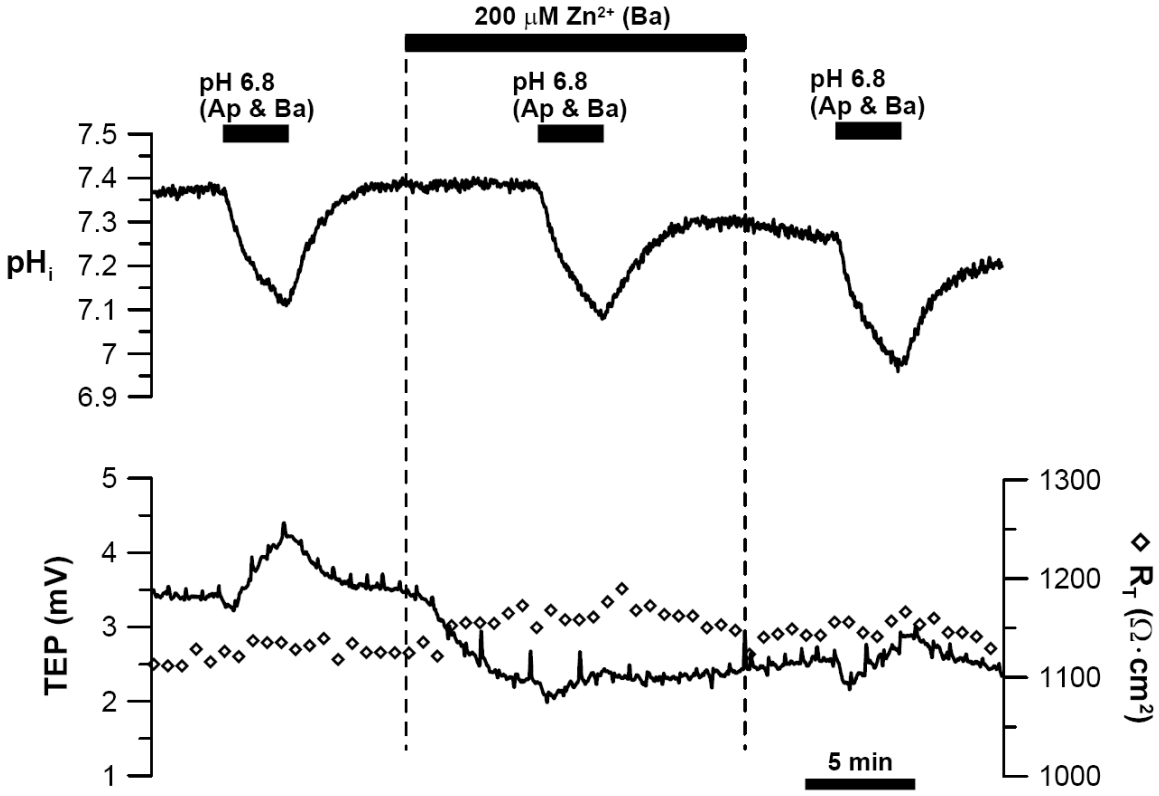

Fig. 4-23: pH 6.8 Ringer induced pH_i, TEP, and R_T responses in the presence of basal Zn^{2+}.

Consistent with our hypothesis, Zn^{2+} reduced the low pH-induced TEP response by more than 2-fold (from ΔTEP = 1.04 ± 0.47 to 0.35 ± 0.13 mV; n = 5; $p < 0.05$) – this effect was irreversible. Although low pH Ringer induced acidification was unaffected by basal

Zn^{2+}, upon returning to control Ringer (switched from low pH Ringer), cell pH_i was unable to return to baseline – consistent with the irreversible inhibitory effect of Zn^{2+} on NHE. Since apical membrane K-channels are electrically coupled to ClC-2 activity, we tested if lactate-induced cell acidification activated apical membrane K-channels. Low pH Ringer (both solution baths) induced pH_i, TEP, and R_T responses were measured in the presence or absence of 2 mM apical Ba^{2+} (Fig. 4-24).

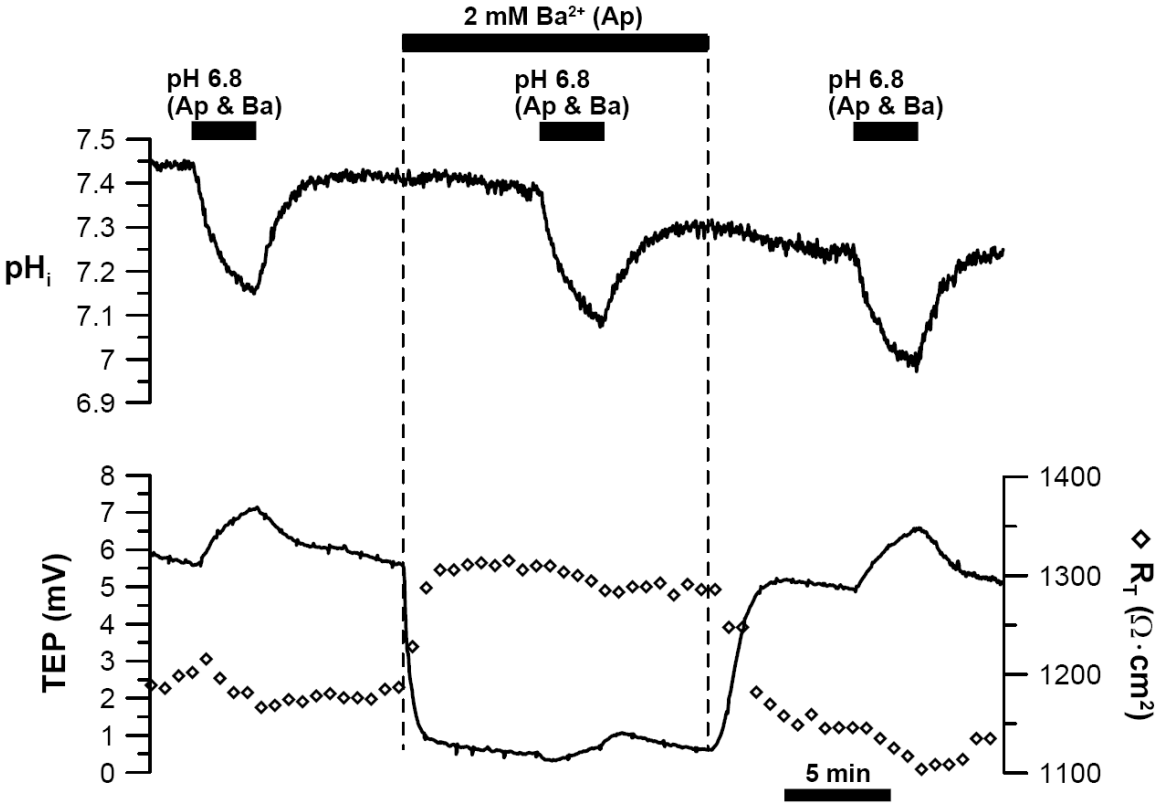

Fig. 4-24: pH 6.8 Ringer induced pH_i, TEP, and R_T responses in the presence of apical Ba^{2+}.

Interestingly in the presence of apical Ba^{2+}, low pH Ringer <u>decreased</u> TEP (ΔTEP = -0.31 ± 0.12 mV), whereas in absence of Ba^{2+}, low pH Ringer <u>increased</u> TEP (ΔTEP = 0.80 ± 0.42 mV; $n = 5$; $p < 0.05$). The low pH Ringer induced pH_i response was unaffected by

apical Ba^{2+}, however upon returning to control Ringer, the recovery to baseline pH_i was slower compared to control.

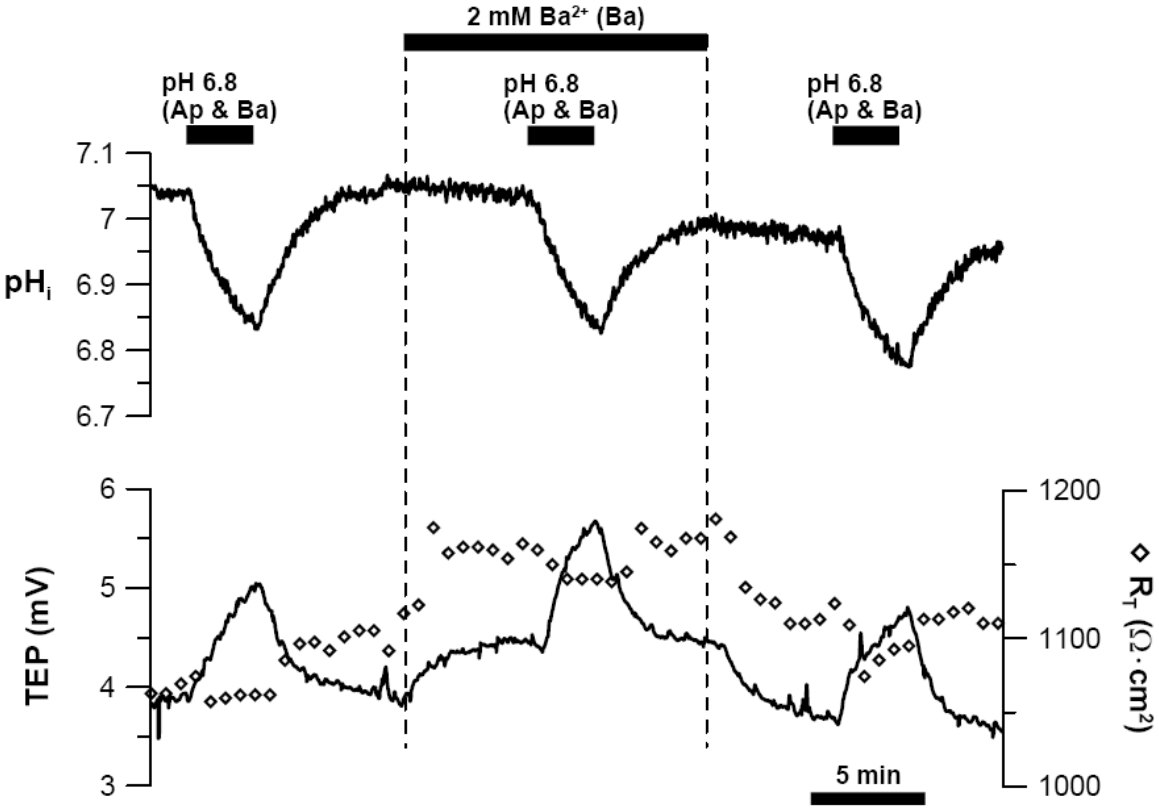

Fig. 4-25: pH 6.8 Ringer induced pH_i, TEP, and R_T responses in the presence of basal Ba^{2+}.

Finally, we test the pH_i-sensitivity of the basolateral membrane K-channel; low pH Ringer was perfused to both apical and basal baths in the presence or absence of 2 mM basal Ba^{2+} (Fig. 4-25). Unexpectedly, the low pH Ringer-induced TEP response slightly increased in the presence of basal Ba^{2+} (from $\Delta TEP = 1.14 \pm 0.37$ to 1.45 ± 0.40 mV; $n = 5$; $p < 0.05$). This experiment indicates that cell acidification did not inhibit basolateral membrane K-channels.

Collectively, our data indicates that cell acidification activates apical membrane K-channels and basolateral membrane ClC-2, but does not inhibit basolateral membrane K-channel (Fig. 4-26). This is also consistent with the notion that lactate-induced inhibition of basolateral membrane K-channel is not as significant as its activation of apical membrane K-channel and ClC-2. The observations that either basal Zn^{2+} or apical Ba^{2+} can almost completely block the low pH Ringer-induced TEP response corroborate our conclusion in section 4.4 that KCl-efflux via these two channels are electrically coupled. The apical lactate-stimulated apical membrane K-channel is most likely Kir 7.1 because (1) it is activated by intracellular acidification with maximal activity at pH 7.1 (Yuan *et al.*, 2003) and (2) it is the major K-conductance at the apical membrane of the RPE (Shimura *et al.*, 2001; Yang *et al.*, 2003; Yang *et al.*, 2008b).

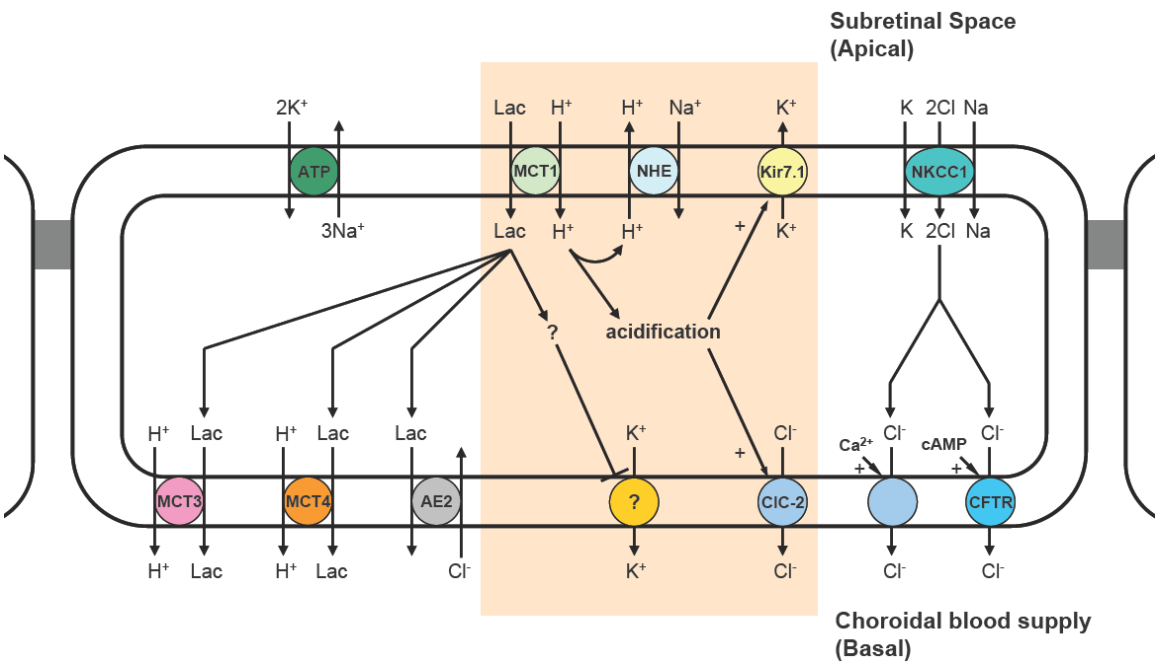

Fig. 4-26: Lactate-induced ion transport mechanisms in RPE. Lactate entry via MCT1 activates NHE and Kir 7.1 at the apical membrane, and ClC-2 at the basolateral membrane. Lactate inhibits a basolateral membrane K-channel via an unknown mechanism.

Although apical lactate inhibited a basolateral membrane K-channel, this channel is not pH_i-sensitive because basal Ba^{2+} had no effect on low pH Ringer-induced TEP response. Furthermore, low pH Ringer did not appreciably increase R_T. We also show that this K-channel is not Ca^{2+}-dependent: BAPTA-AM (intracellular Ca^{2+} chelator) had no effect on lactate-induced TEP and R_T responses. Collectively, our data indicates that lactate activates a Ba^{2+}-sensitive, pH-insensitive, and outwardly rectifying K-channel at the basolateral membrane, whose activity has been demonstrated in RPE cells (Strauss *et al.*, 1993; Hughes *et al.*, 1995; Strauss *et al.*, 2002).

Apical lactate caused a large increase in R_T and is consistent with inhibition of basolateral membrane K-channel, but this R_T response was only modestly reduced by basal Ba^{2+}. In addition, this R_T response is time-delayed relative to V_A, V_B, and TEP responses – R_T began to increase at the start of P2. However, lactate-induced inhibition of basolateral membrane K-channel occurs in P1, suggesting that other mechanisms caused this R_T response. Although apical lactate caused cell swelling and intracellular acidification, neither hypo-osmotic challenge nor extracellular acidification affected R_T. One possibility is that lactate increases R_T by increasing tight junction resistance, perhaps by interacting with tight junction proteins or its adaptors. Alternatively, carboxylates may be the main effector of the R_T response since other monocarboxylates (e.g., pyruvate, acetate, and propionate) also increased R_T.

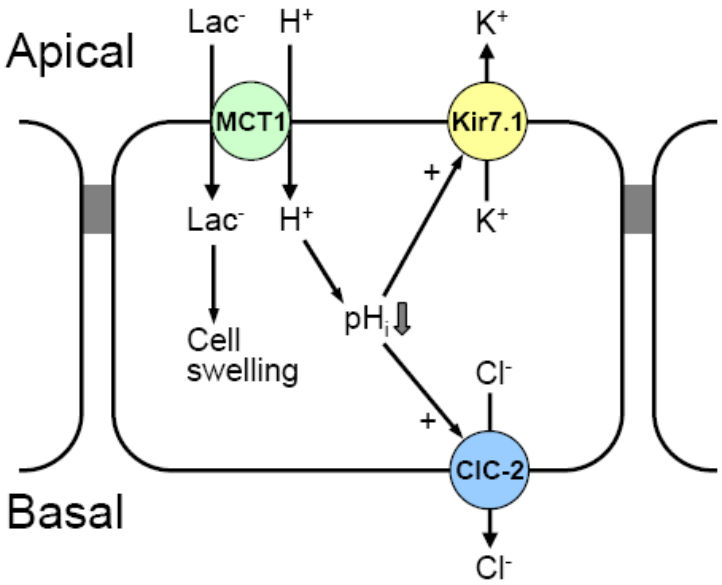

Section 4.5 conclusions: Apical lactate causes cell swelling
Intracellular acidification activates Kir 7.1 and ClC-2

Supporting experimental observations	Interpretation	Fig.
Zn^{2+} and Ba^{2+} did not eliminate lactate-induced V_A and V_B depolarization (in P1)	Lactate causes microelectrode junction potential, indicating cell-swelling	4-20
Hypo-osmotic solution and lactate alters calcein fluorescence signals in the same direction	Lactate causes cell swelling	4-21
Hypo-osmotic solution causes cell-swelling but decreased TEP (lactate increased TEP)	Cell swelling did not activate Kir 7.1 or ClC-2	4-21
Low pH (6.8) Ringer increases TEP	Cell acidification activates electrogenic mechanisms	4-22
Basal Zn^{2+} blocks low pH (6.8) Ringer-induced TEP response	Cell acidification activates ClC-2	4-23
Apical Ba^{2+} blocks low pH (6.8) Ringer-induced TEP response	Cell acidification activates Kir 7.1	4-24
Basal Ba^{2+} did not affect low pH (6.8) Ringer-induced TEP response	Cell acidification did not inhibit basolateral membrane K-channel	4-25

Section 4.7 – Lactate, HCO_3, and fluid transport in RPE

In addition to lactate-induced activation of KCl transport, the CO_2/HCO_3 buffering system in the RPE helps regulate cell volume and pH_i (Kenyon *et al.*, 1997). Early studies show that MCT1 interacts with HCO_3-transporters (Becker *et al.*, 2004) and carbonic anhydrases (CAs) (Wetzel *et al.*, 2001; Becker *et al.*, 2005). Preliminary data shows that the apical membrane $Na/2HCO_3$ co-transporter (NBC1) and HCO_3-buffering by CAs facilitates lactate-transport across RPE (Adijanto et al, ARVO 2009). The interactions between MCT1, NBCs, and CAs in RPE are currently being studied.

In RPE, the activity of the apical membrane Na/K ATPase increases in the dark (Griff *et al.*, 1985) due to a higher SRS $[K^+]$ level (≈ 5 mM) in the dark than in light (≈ 2 mM). A high SRS $[K^+]$ in the dark is due to: (1) active K-channel activity at photoreceptor inner segments (Gallemore *et al.*, 1998); (2) CO_2-driven fluid transport across the RPE dehydrates the SRS, thus increasing SRS $[K^+]$ (see Chapter 3); (3) lactate-induced increase in Kir 7.1 conductance at the apical membrane increases SRS $[K^+]$. By increasing SRS $[K^+]$ and Na/K ATPase activity, lactate enhances CO_2/HCO_3 transport in two ways: (1) Na/K ATPase activity maintains a favorable Na^+-gradient that facilitates NBC1-mediated HCO_3-transport across the apical membrane (Adijanto *et al.*, 2009); (2) increased Kir 7.1 and Na/K ATPase activity increases TEP, which facilitates paracellular Na-absorption – Na acts as the counter-ion for transcellular HCO_3-transport.

Since lactate is transported across the RPE in addition to facilitating HCO_3-transport, the addition of lactate to the apical bath should increase steady-state fluid transport across the

tissue. Assuming that all lactate produced by photoreceptors (0.137 μmol/min; (Wang *et al.*, 1997b)) is transported across the RPE, we calculated that lactate-absorption should be accompanied by ≈ 2.5 $\mu L/cm^2 \cdot hr$ of fluid across the tissue to maintain osmotic balance. However, adding lactate to the apical bath did not affect steady-state fluid absorption in any RPE preparations tested (e.g., bovine, frog, human, and cultured hfRPE) (data not shown), suggesting that apical lactate may counteract the osmotic effects of its absorption by activating solute-secreting mechanisms.

The RPE maintains pH homeostasis in the SRS by transporting photoreceptor generated CO_2 and lactate to the choroidal blood supply. In the dark adapted eye, photoreceptors produce large amounts of CO_2 and lactate, which are released into the SRS – accumulation of these metabolic by-products in RPE causes cell swelling and osmotic stress. In this study, we demonstrate how the RPE decreases cell volume to mitigate this osmotic stress, by using lactate to activate KCl efflux via Kir 7.1 and ClC-2 at the apical and basolateral membranes respectively. In addition, lactate-induced ClC-2 activation may help regulate ion-transport at the paracellular pathway. In support of this notion, mice lacking ClC-2 expression exhibit reduced TEP and has a smaller short-circuit current across the RPE (Bosl *et al.*, 2001). These mice also develop early onset retinal degeneration. Therefore, lactate-induced activation of Kir 7.1 and ClC-2 may help prevent osmotic stress-induced RPE damage, thus maintaining photoreceptor health and integrity.

CHAPTER 5: Lactate and CO_2/HCO_3 Transport in RPE

Section 5.1 – Introduction

The concept of acid-base coupled H_2CO_3-transport via MCT1 and NBC1 has been demonstrated in Xenopus oocytes (Becker *et al.*, 2004; Becker & Deitmer, 2004). The localization and activity of MCT1, NBC1, and NBC3 at the RPE apical membrane (Hughes *et al.*, 1989; Bok *et al.*, 2001; Philp *et al.*, 2003b; Adijanto *et al.*, 2009) suggests that these transporters may be acid-base coupled, and are therefore functionally dependent on each other. In this model, HCO_3 transport via NBC1 buffers protons entering the cell via MCT1, thus maintaining a favorable H^+-gradient across the cell that increases lactate transport (see Fig. 1-6). Furthermore, carbonic anhydrases (CAs) catalyze the hydration/dehydration reaction between CO_2 and HCO_3^-, which has been shown to enhance the activity of MCT1 (Wetzel *et al.*, 2001; Becker *et al.*, 2005; Svichar *et al.*, 2006) and NBCs (Alvarez *et al.*, 2003; Loiselle *et al.*, 2004; McMurtrie *et al.*, 2004; Pushkin *et al.*, 2004). Since membrane bound CA (CA XIV) is localized at the RPE apical membrane (Nagelhus *et al.*, 2005), it may functionally interact with MCT1 and NBC1 to enhance both lactate and HCO_3 transport into the cell at the apical membrane.

In chapter 4, we show that lactate stimulates several ion transport mechanisms in RPE (Fig. 4-26). Conducting these experiments in CO_2/HCO_3-free (HEPES buffered) conditions simplifies the lactate transport system, but this maneuver eliminates potential MCT1 interactions with HCO_3-dependent mechanisms such as the electrogenic $Na/2HCO_3$ co-transporter (NBC1) (Becker *et al.*, 2004), the electroneutral Na/HCO_3 co-

transporter (NBC3), and carbonic anhydrases (Wetzel *et al.*, 2001; Becker *et al.*, 2005). In addition to K and Cl channel mediated volume regulation (see Chapter 4), the CO_2/HCO_3 buffering system in the RPE helps regulate cell volume and pH_i (Kenyon *et al.*, 1997).

In this chapter, we investigate interactions between MCT1 and NBCs, and test the role of CAs in a "lactate-bicarbonate-transport metabolon". We show that MCT1-mediated H/Lac co-transport enhances HCO_3-transport via NBC1 and NBC3 at the apical membrane. We also show that H^+-buffering by these HCO_3-transporters and carbonic anhydrases facilitates lactate-transport across RPE. Interactions between NBC1, NBC3, MCT1, and CAs are synergistic, thus maximizing lactate, HCO_3, and fluid transport across the apical membrane. In the next section, we demonstrate that lactate is transported across the basolateral membrane mainly by AE2, with some contribution from MCT3 & MCT4.

Section 5.2 – Lactate and HCO_3 transport at the RPE apical membrane

As demonstrated in chapter 4, lactate transport across the apical membrane is mediated by MCT1. To study the interactions between lactate and HCO_3 transport mechanisms in RPE, we compared the effect of iso-osmotic addition of 20 mM lactate (pH 7.4) into the apical bath in the presence vs. absence of CO_2/HCO_3 (Fig. 5-1).

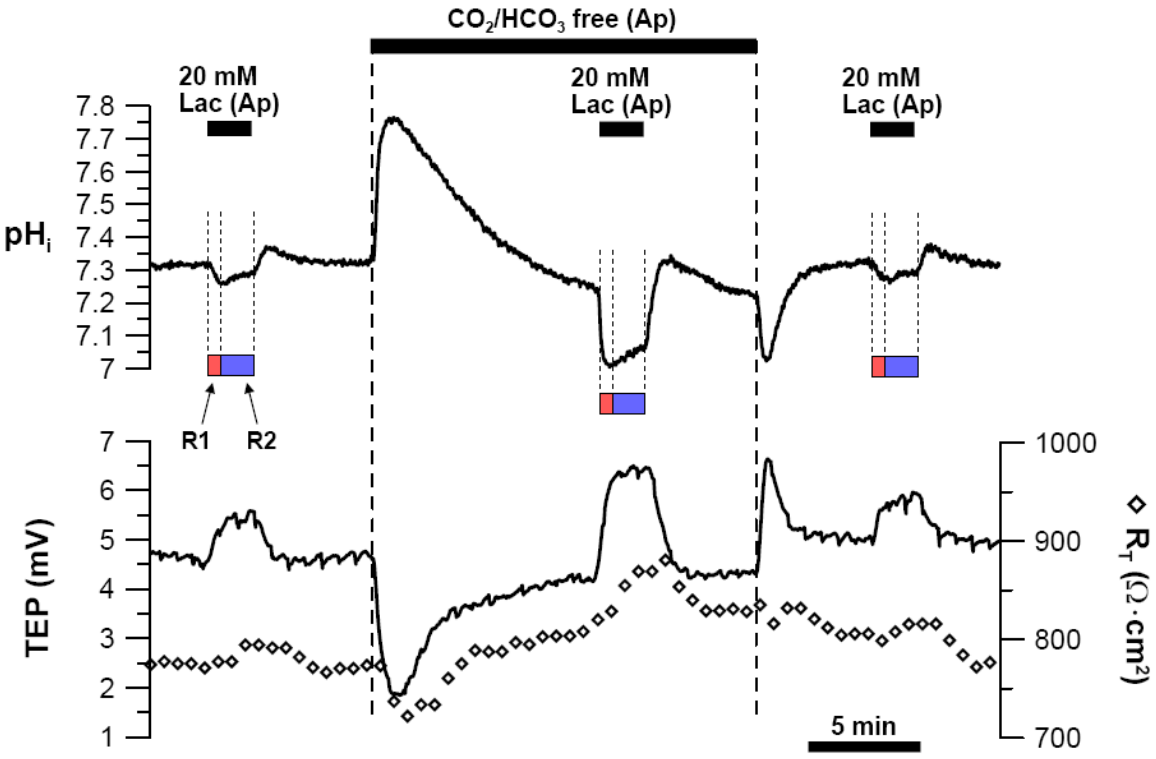

Fig. 5-1: Apical lactate induced pH_i, TEP, and R_T responses in the presence vs. absence of CO_2/HCO_3. Red box – R1 phase; blue box – R2 phase.

In either case, apical lactate produced a pH_i response with two phases (Fig. 5-1): a fast acidification (R1) followed by a slow alkalinization (R2). R1 reflects H^+-coupled lactate entry via MCT1 (Figs. 4-3 and 4-4) and R2 reflects the activity of H^+-buffering mechanisms such as the Na/H exchanger (Fig. 4-5). R1 in the presence of CO_2/HCO_3 was ≈ 2-fold larger than in the absence of CO_2/HCO_3 (-12.80 ± 4.33 vs. -6.32 ± 1.46

$mM \cdot min^{-1}$; $p < 0.01$; $n = 59$), whereas R2 was ≈ 20% larger in the presence vs. absence of CO_2/HCO_3 (0.86 ± 0.35 vs. 0.71 ± 0.31 $mM \cdot min^{-1}$; $p < 0.01$; $n = 59$) – both observations are consistent with the notion that HCO_3-transport mechanisms are activated to help buffer H^+-coupled lactate-entry via MCT1. Furthermore, lactate-induced TEP and R_T responses were respectively ≈ 30% and 40% larger in the absence of CO_2/HCO_3 (ΔTEP = 1.39 ± 0.60 vs. 0.98 ± 0.41 mV; ΔR_T = 52 ± 21 vs. 31 ± 14 $\Omega \cdot cm^2$; $p < 0.01$; $n = 59$), suggesting that lactate activated HCO_3-independent electrogenic mechanisms. This is consistent with our earlier finding: in the absence of CO_2/HCO_3, lactate activates apical membrane Kir 7.1 K-channels and basolateral membrane ClC-2 Cl-channel (sections 4.4 & 4.5) by causing cell acidification (section 4.6; Fig. 4-26).

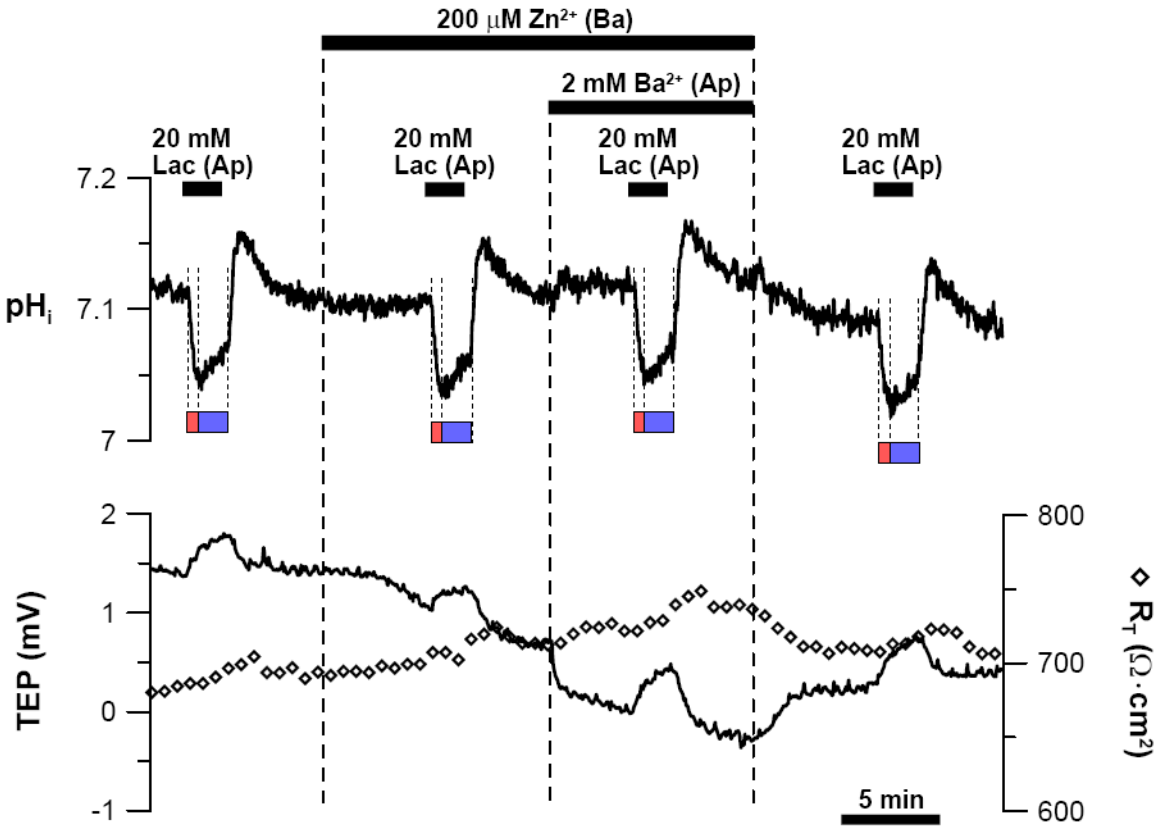

Fig. 5-2: (In CO_2/HCO_3 Ringer) Apical lactate-induced pH_i, TEP, and R_T responses in the presence of Zn^{2+} (basal) and Ba^{2+} (apical).

To test if lactate activates Kir 7.1 and ClC-2 in the presence of CO_2/HCO_3, we measured lactate-induced TEP response in the presence of Zn^{2+} (basal) and Ba^{2+} (apical) (Fig. 5-2). Surprisingly, Zn^{2+} and Ba^{2+} did not reduce lactate-induced TEP response in the presence of CO_2/HCO_3 ($\Delta TEP = 0.39 \pm 0.13$ vs. 0.54 ± 0.19; $p > 0.05$; $n = 3$). This observation suggests that lactate activated a HCO_3-dependent electrogenic mechanism that increases TEP. A possible candidate is the DIDS-sensitive and electrogenic $Na/2HCO_3$ co-transporter (NBC1) at the RPE apical membrane (Figs. 1-8 & 5-5).

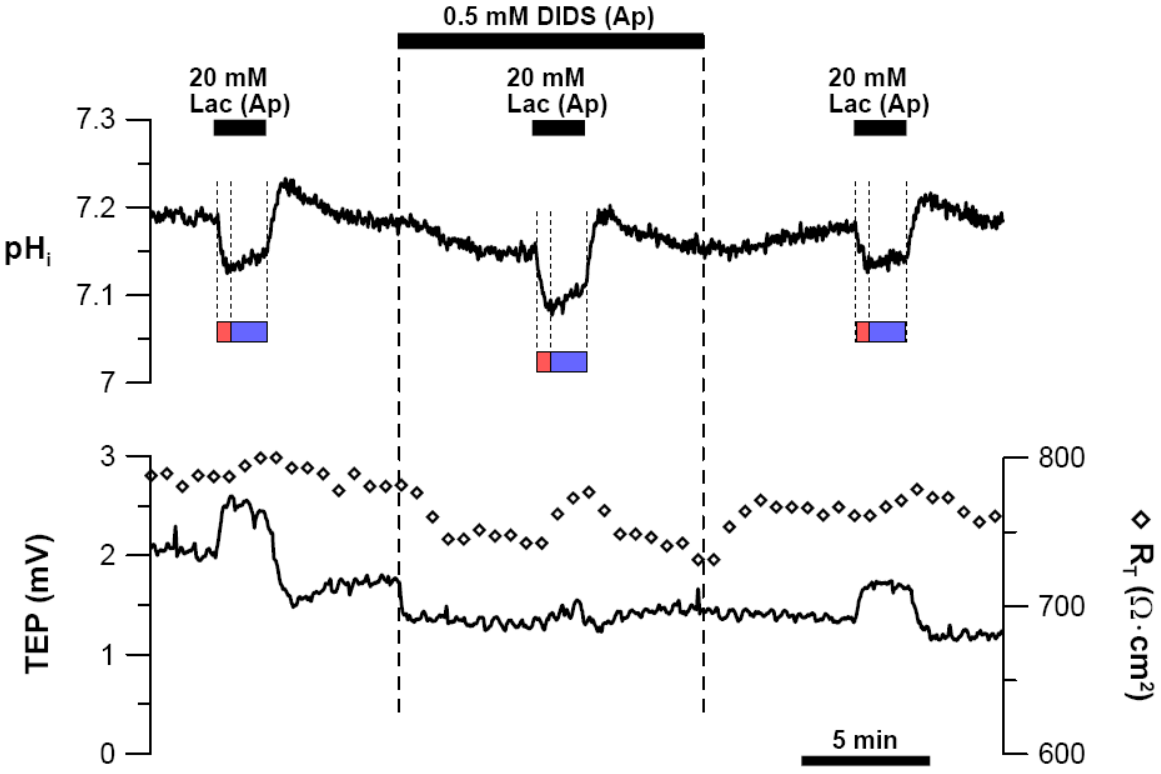

Fig. 5-3: (In CO_2/HCO_3 Ringer) Apical lactate-induced pH_i, TEP, and R_T responses in the presence of apical DIDS.

To test if lactate activates NBC1, we added 0.5 mM DIDS into the apical bath (Fig. 5-3) and found that the lactate-induced TEP response was significantly reduced from 0.82 ±

0.44 to 0.36 ± 0.33 mV (n = 12) and that the R_T response was increased by almost 2-fold (from 27 ± 14 to 50 ± 20 $\Omega \cdot cm^2$; n = 12; $p < 0.05$). These observations suggest that NBC1-mediated HCO_3 transport helps buffer H^+-entry into the cell via MCT1. Interestingly, R2 of the pH_i response was 36% larger in the presence of DIDS compared to control (R2 = 0.92 ± 0.52 vs. 0.68 ± 0.37 $mM \cdot min^{-1}$; $p < 0.05$; n = 12), suggesting that other H^+-buffering mechanisms (e.g., NHE) helped compensate for the loss of NBC1 activity.

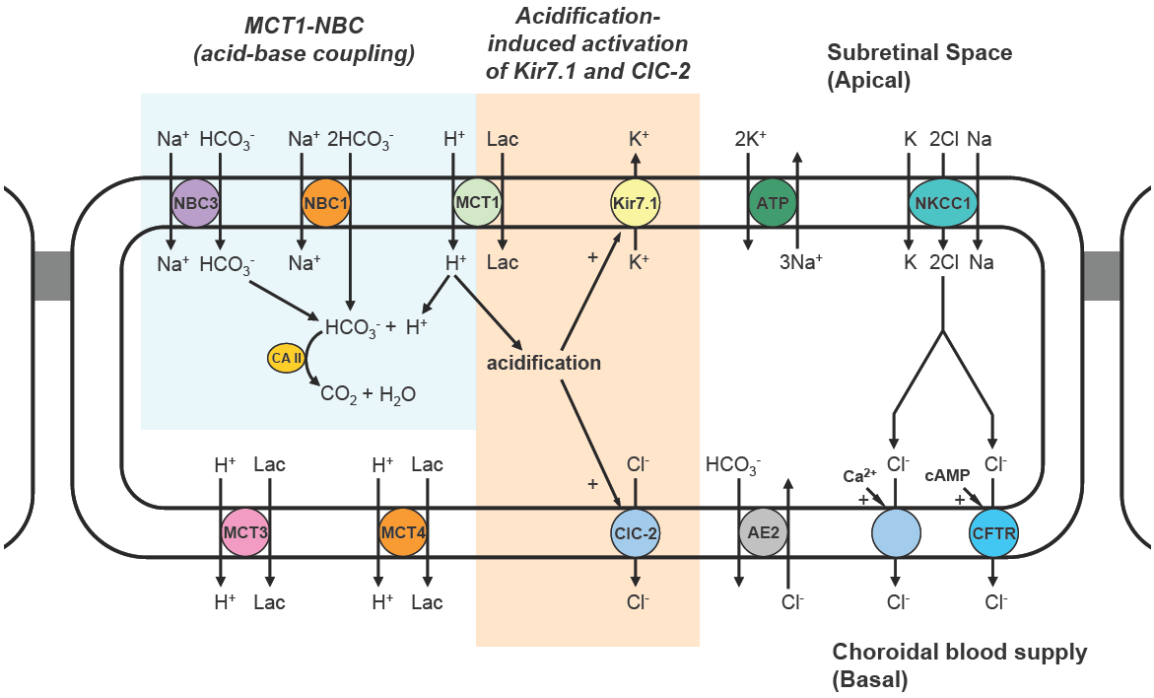

Fig. 5-4: Lactate induced ion-transport mechanisms in RPE (in the presence of CO_2/HCO_3): Lactate activates NBC1 and NBC3 (blue box), and Kir 7.1 and ClC-2 (orange box).

These experiments suggest that apical lactate can increase TEP by activating two separate mechanisms (Fig. 5-4): (1) lactate-transport via MCT1 drives apical Na/2HCO_3 co-transport into the cell via NBC1; (2) lactate-entry into the cell activates apical membrane

K-channel (Kir7.1) and basolateral membrane Cl-channel (ClC-2), and inhibits basolateral membrane K-channel (Figs. 4-20 & 4-26).

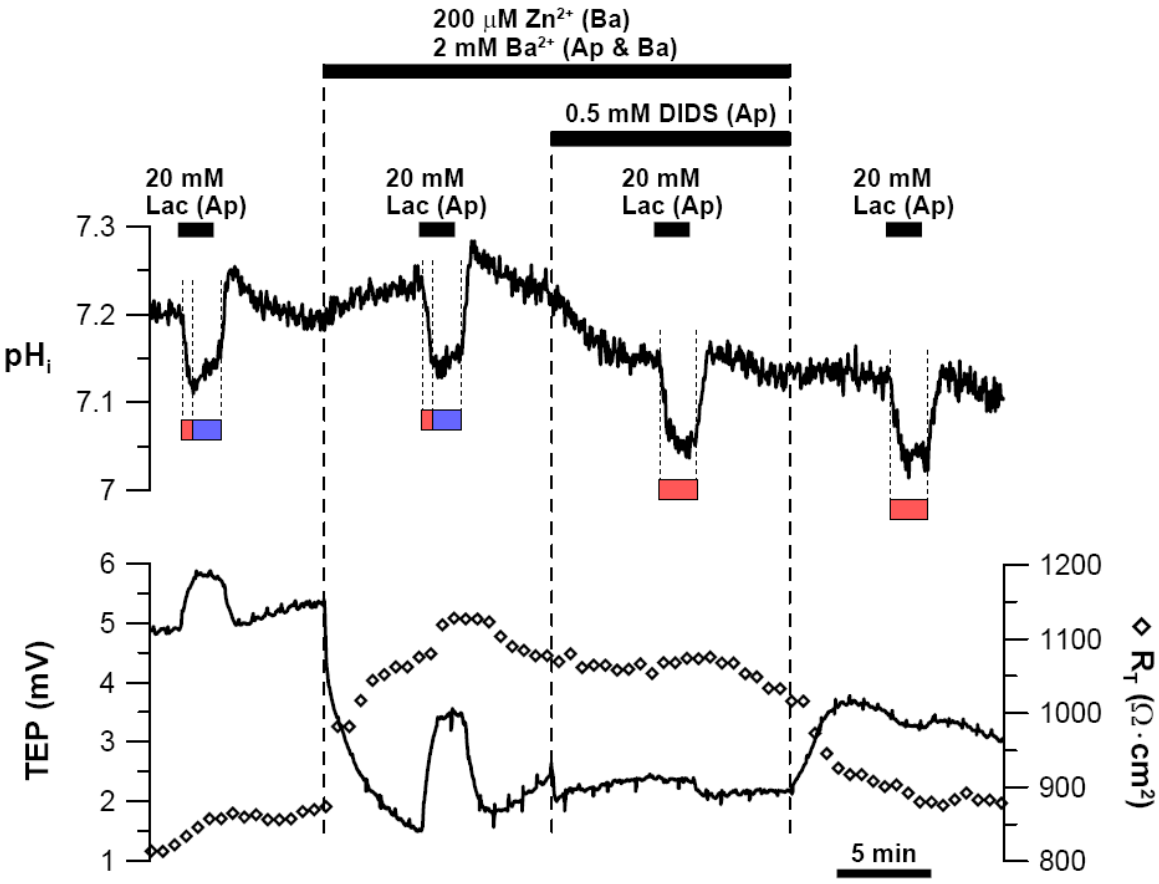

Fig. 5-5: (In CO_2/HCO_3 Ringer) Apical lactate induced pH_i, TEP, and R_T responses in the presence of Zn^{2+} (basal) and Ba^{2+} (apical & basal), then apical DIDS.

However, as shown in Fig 5-2 and 5-5, apical lactate-induced TEP response (ΔTEP = 1.36 ± 0.41 mV) was not blocked by the simultaneous addition of Ba^{2+} (apical & basal) and Zn^{2+} (basal) (ΔTEP = 1.68 ± 0.74 mV; $p > 0.05$); in some cases, the TEP response was larger in the presence of Ba^{2+} and Zn^{2+} (3 of 6 tissues). This observation does not necessarily imply that lactate does not activate K-channels and ClC-2 (in the presence of

CO_2/HCO_3) because the Ba^{2+}-induced V_A depolarization may create an electrical gradient that promotes NBC1 activity. We verified this hypothesis by showing that subsequent addition of DIDS to the apical bath (still in the presence of Ba^{2+} and Zn^{2+}) completely eliminated the lactate-induced TEP response ($p < 0.05$; Fig 5-5).

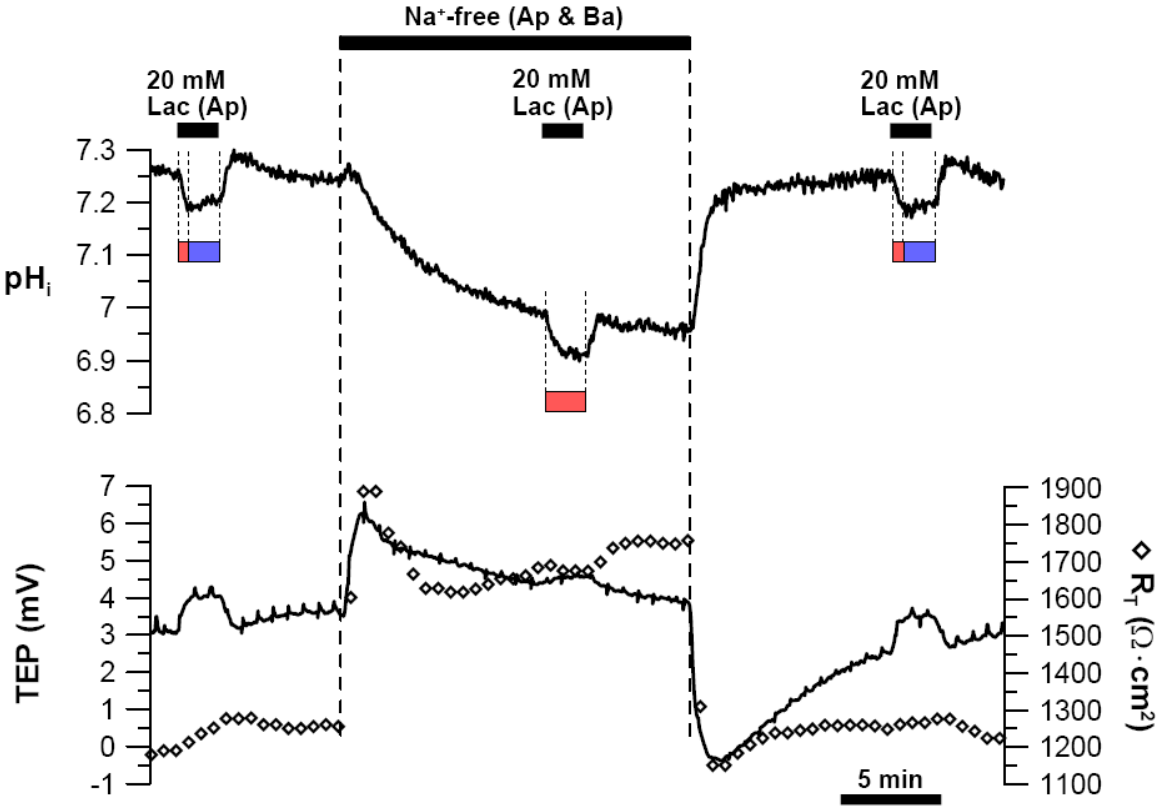

Fig. 5-6: (In CO_2/HCO_3 Ringer) Apical lactate induced pH_i, TEP, and R_T responses in the absence of Na^+ (apical & basal).

Since NBC1 is Na-linked, Na-removal from both bathing solutions should block lactate-induced TEP response (Fig. 5-6). In seven experiments, apical lactate-induced TEP response was essentially abolished upon Na-removal from both apical and basal baths. Furthermore, R2 was completely eliminated, which corroborates the notion that Na-coupled HCO_3-transporter mediates H^+-buffering in RPE. However, NBC1 is not the

only Na-linked pH_i-regulatory mechanism in RPE: other mechanisms include NBC3 (Na/HCO_3 co-transporter) and NHE (Na/H exchanger) (see Fig. 1-8).

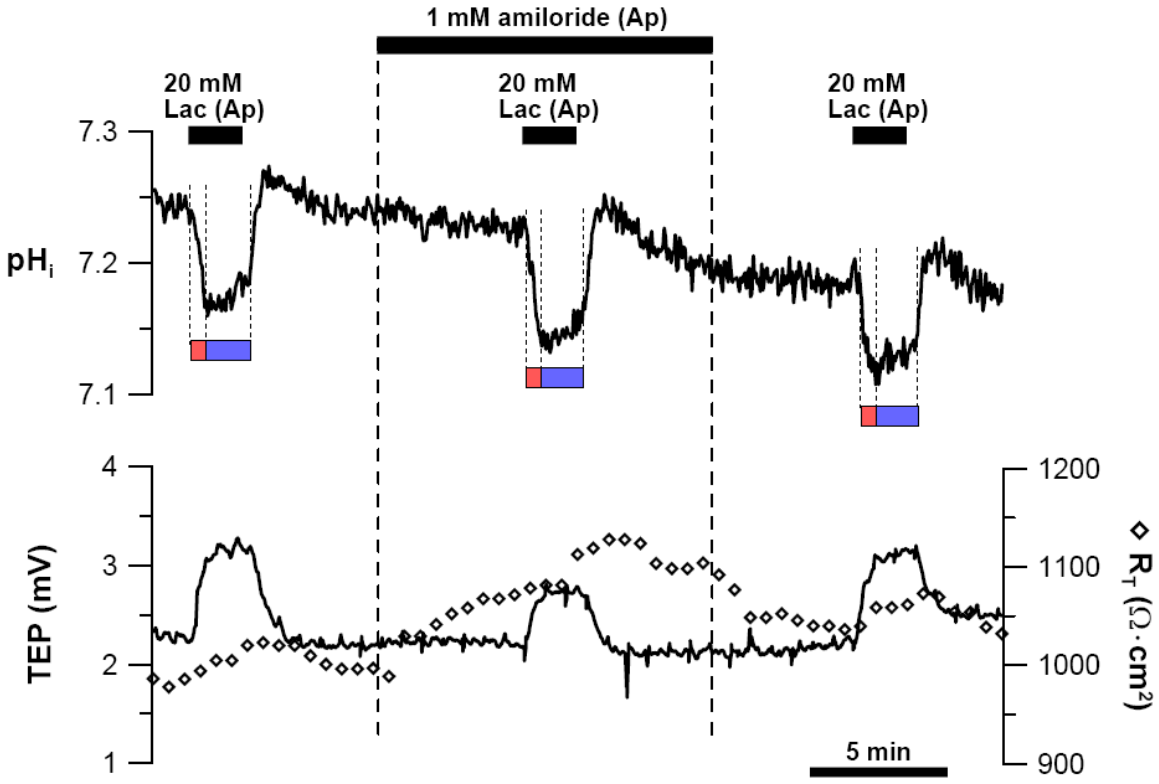

Fig. 5-7: (In CO_2/HCO_3 Ringer) Apical lactate induced pH_i, TEP, and R_T responses in presence of apical amiloride. Red box – R1 phase; blue box – R2 phase.

In chapter 4 (section 4.3), we showed that apical lactate activates the Na/H exchanger (NHE) at RPE apical membrane. NHE activity is reflected by R2 of the lactate-induced pH_i response, which is blocked by amiloride (Fig. 4-5). However in the presence of CO_2/HCO_3, amiloride reduced R2 by only 50% (R2 from 0.77 ± 0.13 to 0.38 ± 0.22 $mM \cdot min^{-1}$; $p = 0.046$; $n = 5$; Fig. 5-7) – it did not eliminate R2. In addition, amiloride had no effect on R1 ($p > 0.05$), suggesting that additional pH-regulatory mechanisms (i.e., HCO_3-transporters, possibly NBC1) are actively participating in H^+-buffering. To

test this notion, we simultaneously inhibit NHE and NBC1 with Zn^{2+} and DIDS, respectively (Fig. 5-8). Amiloride and Zn^{2+} are both NHE inhibitors, and Zn^{2+} was used in this experiment because amiloride reacts covalently with DIDS to form a light-yellow precipitate (data not shown).

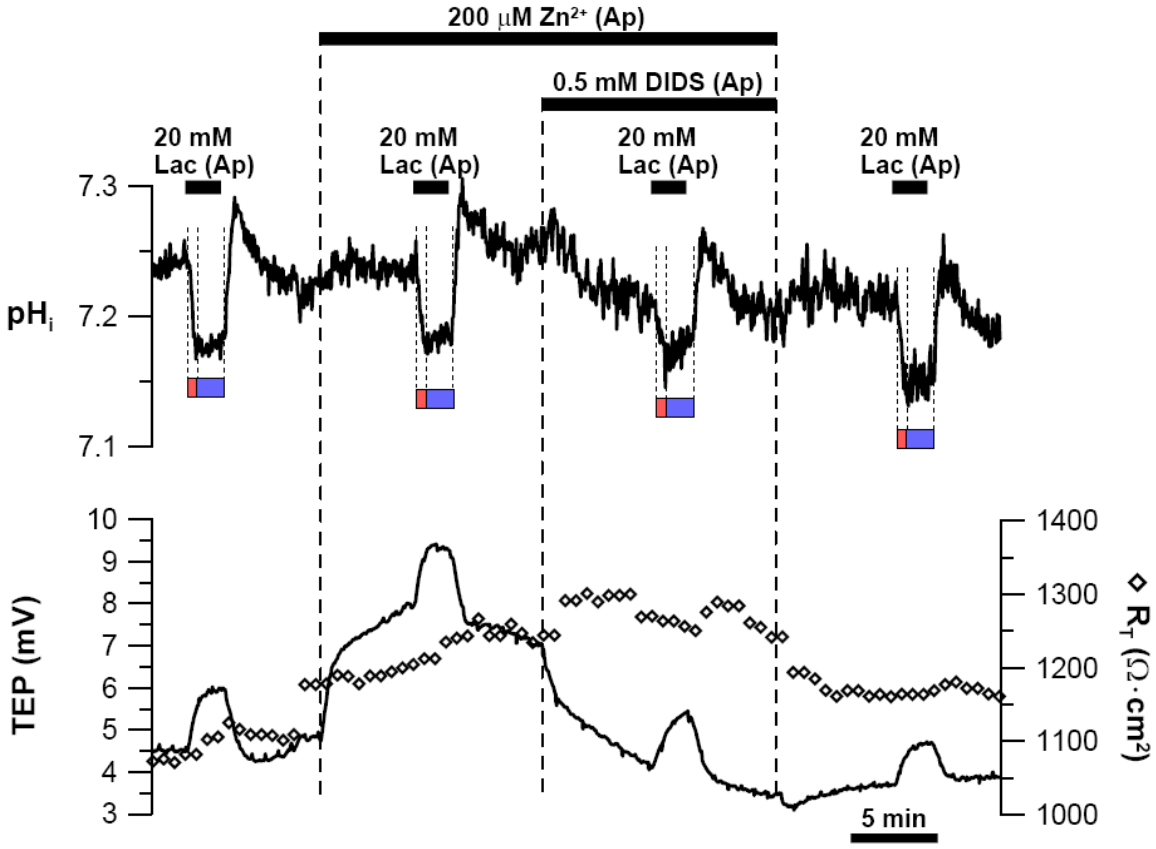

Fig. 5-8: (In CO_2/HCO_3 Ringer) Apical lactate induced pH_i, TEP, and R_T responses in presence of apical Zn^{2+}. Red box – R1 phase; blue box – R2 phase.

Like amiloride, apical Zn^{2+} *per se* had little effect on R2 ($p > 0.05$; $n = 5$). In addition, the presence of both Zn^{2+} and DIDS in the apical bath to block both NBC1 and NHE had little effect on R2 ($p > 0.05$; $n = 3$; Fig. 5-7), suggesting that the DIDS-insensitive Na/HCO_3 co-transporter (NBC3) may be actively transporting HCO_3 into the cell. To test this notion, we inhibit HCO_3-transporters (NBC1 and NBC3) by using

ethoxyzolamide (EZA; 10 μM), a membrane-permeable CA-inhibitor, to non-selectively block all cytosolic and membrane bound CAs (Fig. 5-9).

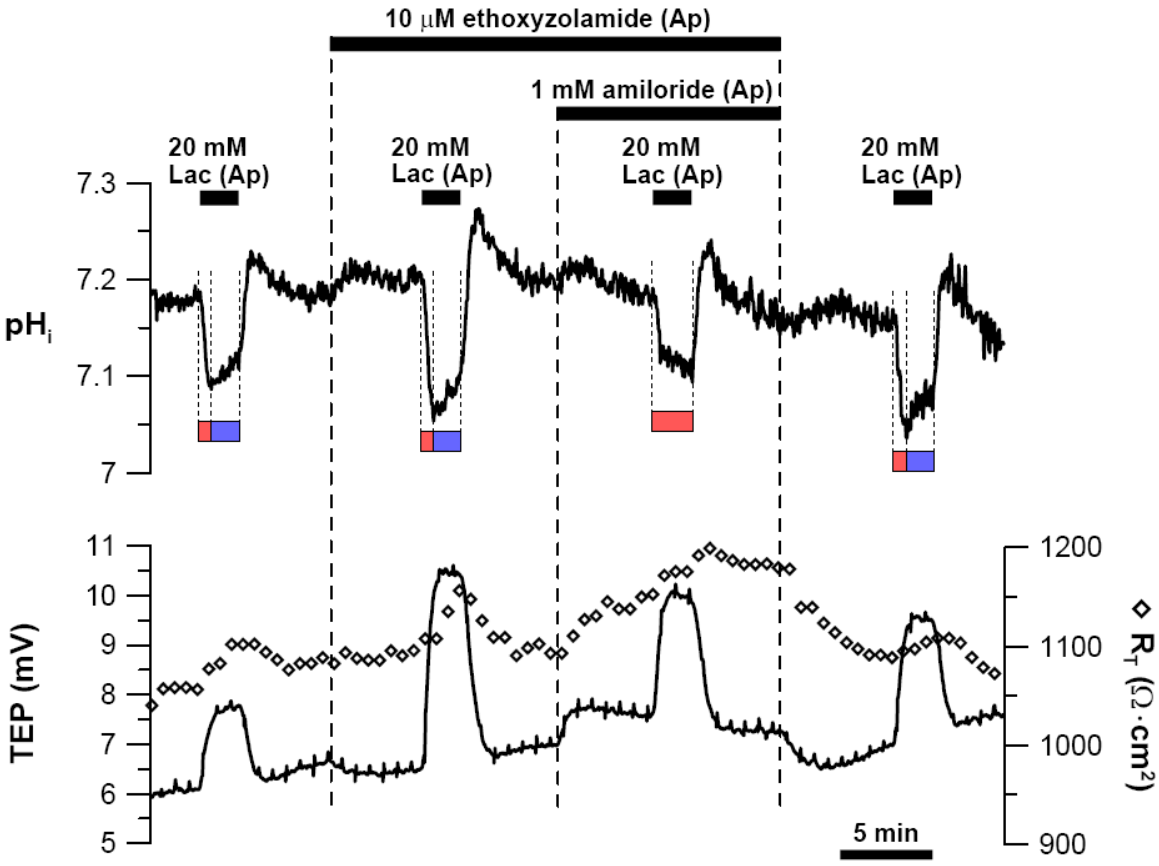

Fig. 5-9: (In CO_2/HCO_3 Ringer) Apical lactate induced pH_i, TEP, and R_T responses in presence of ethoxyzolamide (EZA) followed by amiloride in the apical bath. Red box – R1 phase; blue box – R2 phase.

In the presence of EZA in the apical bath, lactate caused larger pH_i (R1 & R2), TEP, and R_T responses compared to control ($p < 0.05$; $n = 4$). Although EZA increased R2 (from 1.03 ± 0.35 to 1.59 ± 0.58 mM·min^{-1}), subsequent addition of amiloride further reduced and eliminated R2 (from 1.59 ± 0.58 to 0.13 ± 0.51 mM·min^{-1}; $p < 0.05$; $n = 4$) – indicating that apical lactate activates NBC1, NBC3, and NHE at the apical membrane.

Although lactate-induced TEP response is larger in the presence of EZA (ΔTEP = 3.39 ± 1.22 vs. 1.60 ± 0.55 mV; $p < 0.05$; n = 4), this observation does not indicate increased NBC1 activity – the elimination of R2 by EZA and amiloride demonstrates that EZA inhibits NBC1. To verify this hypothesis, we compared lactate-induced TEP response in the presence of apical DIDS vs. in the presence of both DIDS and EZA (Fig 5-10).

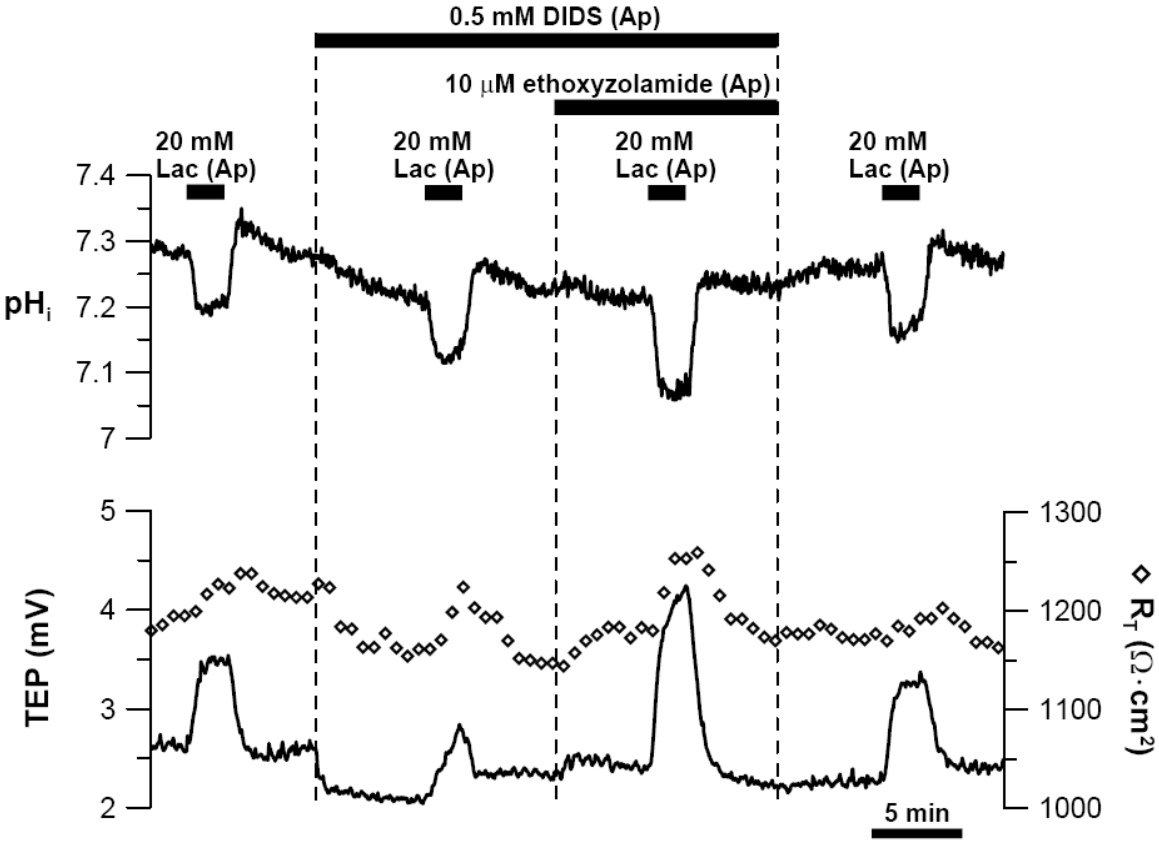

Fig. 5-10: (In CO_2/HCO_3 Ringer) Apical lactate induced pH_i, TEP, and R_T responses in presence of apical DIDS followed by apical ethoxyzolamide (EZA).

In six experiments, EZA increased lactate-induced TEP response even in the presence of apical DIDS (ΔTEP from 0.96 ± 0.86 to 1.62 ± 0.62 mV; $p < 0.05$), suggesting that EZA enhanced lactate-induced activation of HCO_3-independent mechanisms. Since lactate stimulates Kir7.1 and ClC-2 via cell acidification, EZA may enhance lactate-induced

activation of these channels by amplifying lactate-induced cell acidification (EZA decreases intracellular buffering capacity). Consistent with this notion, in the presence of apical EZA, apical lactate-induced TEP response was reduced by Ba^{2+} (apical & basal baths) and Zn^{2+} (basal bath) (from 2.32 ± 0.58 to 1.60 ± 0.56 mV; n = 4; $p < 0.05$) (Fig 5-11). The R2 phase of the pH_i response was completely eliminated in the presence of EZA and Zn^{2+} ($p < 0.05$). This observation corroborates our earlier conclusion that (in the presence of CO_2/HCO_3) apical lactate stimulates NBC1, NBC3, and NHE at the apical membrane.

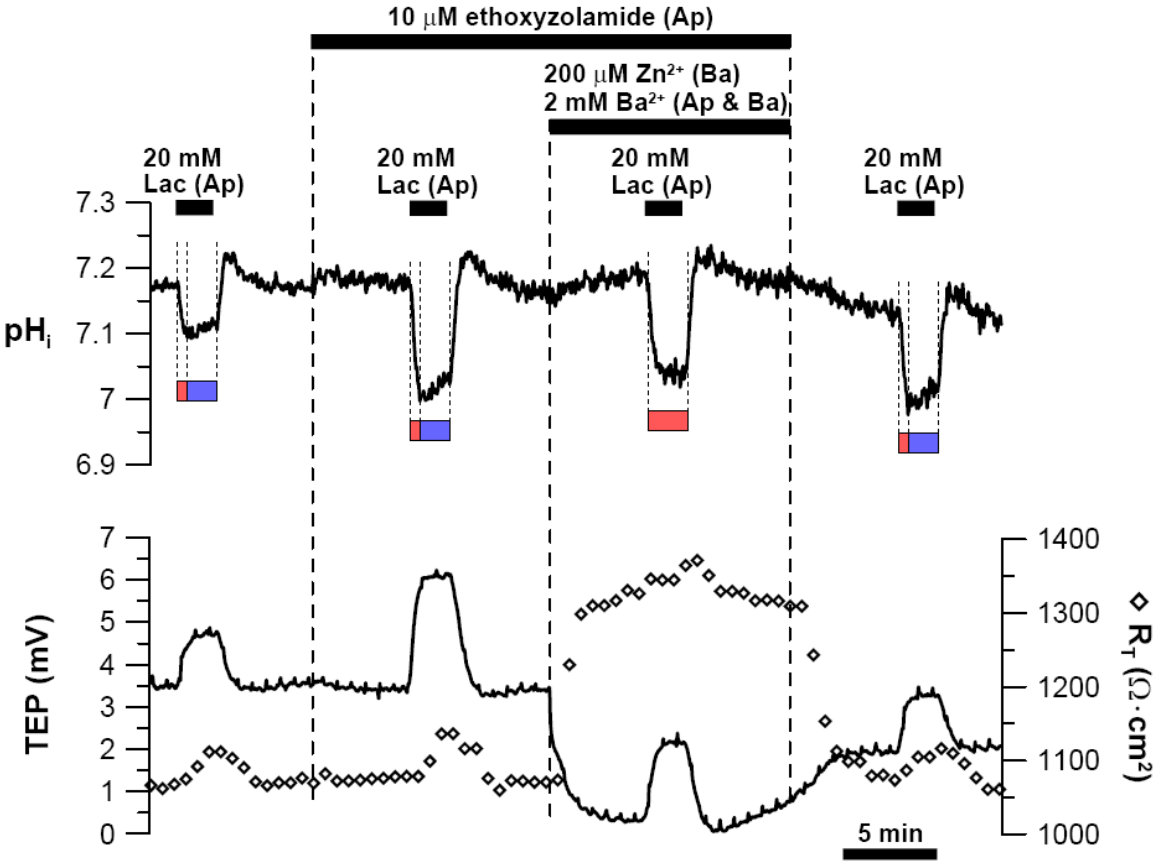

Fig. 5-11: (In CO_2/HCO_3 Ringer) Apical lactate induced pH_i, TEP, and R_T responses in presence of apical ethoxyzolamide (EZA) followed by Zn^{2+} (basal) and Ba^{2+} (apical & basal). Red box – R1 phase; blue box – R2 phase.

Collectively, our data show that indiscriminate inhibition of all CAs in the RPE reduces NBC1 and NBC3 activity. However, how much does membrane-bound CAs contribute to NBC-mediated HCO_3-transport compared to cytosolic CAs? To answer this question, we added membrane-impermeable CA-inhibitor, benzolamide (BZA; 10 μM), to the apical bath (Fig. 5-12).

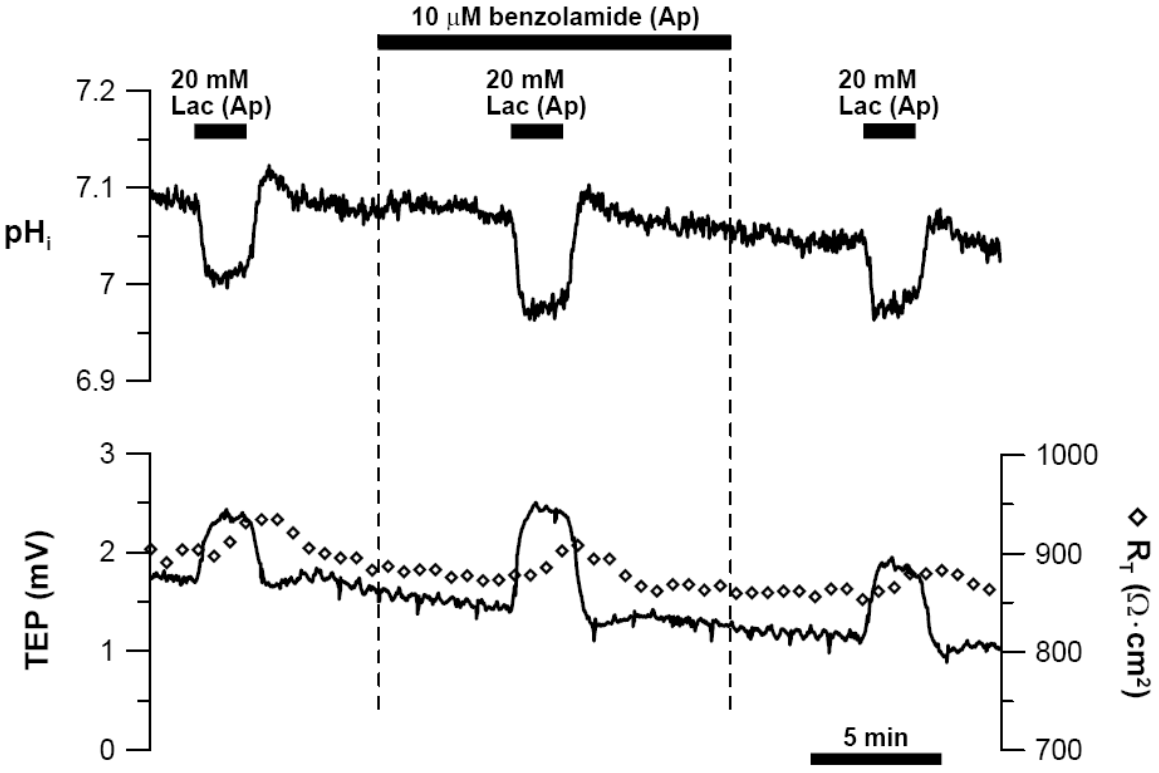

Fig. 5-12: (In CO_2/HCO_3 Ringer) Apical lactate induced pH_i, TEP, and R_T responses in the presence of apical benzolamide (BZA).

In seven experiments, apical lactate induced R1 and TEP responses were ≈ 40% and ≈ 30% larger compared to control, respectively ($p < 0.05$). However, unlike EZA, BZA had little effect on lactate-induced pH_i or R_T responses. Further, the simultaneous addition of BZA and amiloride to the apical bath did not reduce R2 of the lactate-induced

pH_i response. These experiments suggest that cytosolic CAs play a more prominent role in facilitating HCO_3-transporter activity than membrane-bound CAs.

Based on the experiments presented in this section, we showed that MCT1 is acid-base coupled with NBC1: (1) in the absence of CO_2/HCO_3, both R1 and R2 were smaller than in the presence of CO_2/HCO_3, suggesting that HCO_3-transport helps buffer H^+-coupled lactate-entry via MCT1; (2) Na-removal from both solution baths eliminates NBC1, NBC3, and NHE activities, thus blocking both R2 and TEP response; (3) apical lactate-induced TEP response was significantly reduced by apical DIDS; (4) this TEP response was completely blocked by the simultaneous addition of Zn^{2+} (basal), Ba^{2+} (apical & basal), and apical DIDS; (5) EZA or amiloride *per se* modestly reduced R2, but R2 is completely eliminated by the simultaneous addition of EZA and amiloride. At steady-state, lactate that enters the cell from the apical membrane must exit the basolateral membrane; this process is discussed in the following section.

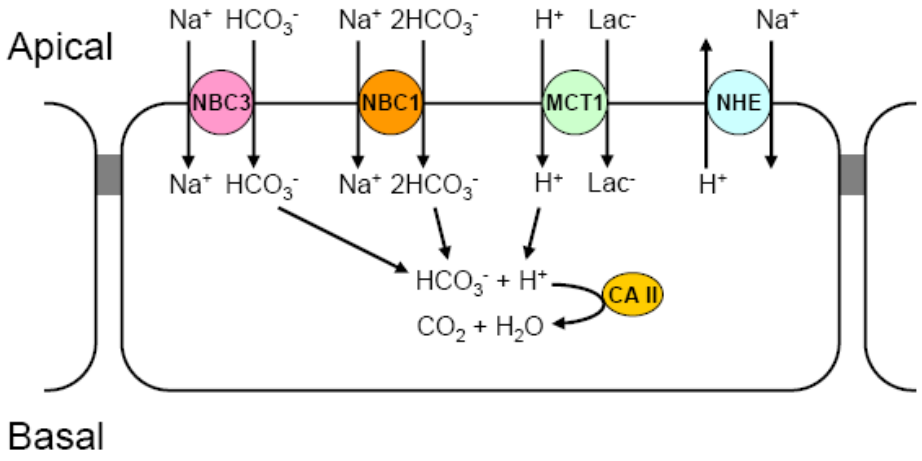

Section 5.1 conclusions: Apical H/Lac entry via MCT1 activates NHE, NBC1, and NBC3 to regulate pH_i

H/Lac transport via MCT1 drives NBC1 and NBC3 activity with the help of CAs

Supporting experimental observations	Interpretation	Fig.
R2 was present in the presence or absence of CO_2/HCO_3	Lactate activates NHE	5-1
R2 was larger in the presence vs. in the absence of CO_2/HCO_3	Lactate activates HCO_3-transporter to buffer pH_i	5-1
Na-removal from both solution baths eliminates R2	Lactate activates Na-dependent pH_i-regulatory mechanisms	5-6
Blocking NHE with amiloride decreased R2	Lactate activates NBC1 and/or NBC3	5-7
Blocking NHE with apical Zn^{2+} per did not affect R2	Lactate activates NBC1 and/or NBC3	5-8
Blocking NBC1 with apical DIDS did not decrease R2	Lactate activates NBC3 and/or NHE	5-3
Adding both apical Zn^{2+} and DIDS did not affect R2	Lactate activates NBC3	5-8
Inhibiting CAs with EZA (inhibits HCO_3-transporters) decreased R2	Lactate activates NBC1 and NBC3	5-9
Inhibiting CAs and NHE with EZA and amiloride eliminated R2	Lactate activates NBC1, NBC3, and NHE	5-9
Na-removal from both solution baths eliminates TEP response	TEP response is mediated by a Na-dependent mechanism	5-6
Apical lactate-induced TEP response was reduced by apical DIDS	Part of this TEP response reflects NBC1 activity	5-3

Section 5.3 – Lactate and HCO_3 transport at the RPE basolateral membrane

As discussed in section 1.5, lactate transport across the RPE is mediated by MCT1 at the apical membrane, and MCT3, MCT4, and AE2 at the basolateral membrane (see Fig. 1-10). At the basolateral membrane, AE2 can facilitate lactate transport in two ways (Fig. 5-13): First, HCO_3-transport via AE2 can participate in acid-base coupling with MCT3 and MCT4 (H/Lac transport) (Fig. 5-13; yellow box). Alternatively, AE2 can mediate Cl/Lac exchange to directly transport lactate out of the cell (Fig. 5-13; blue box).

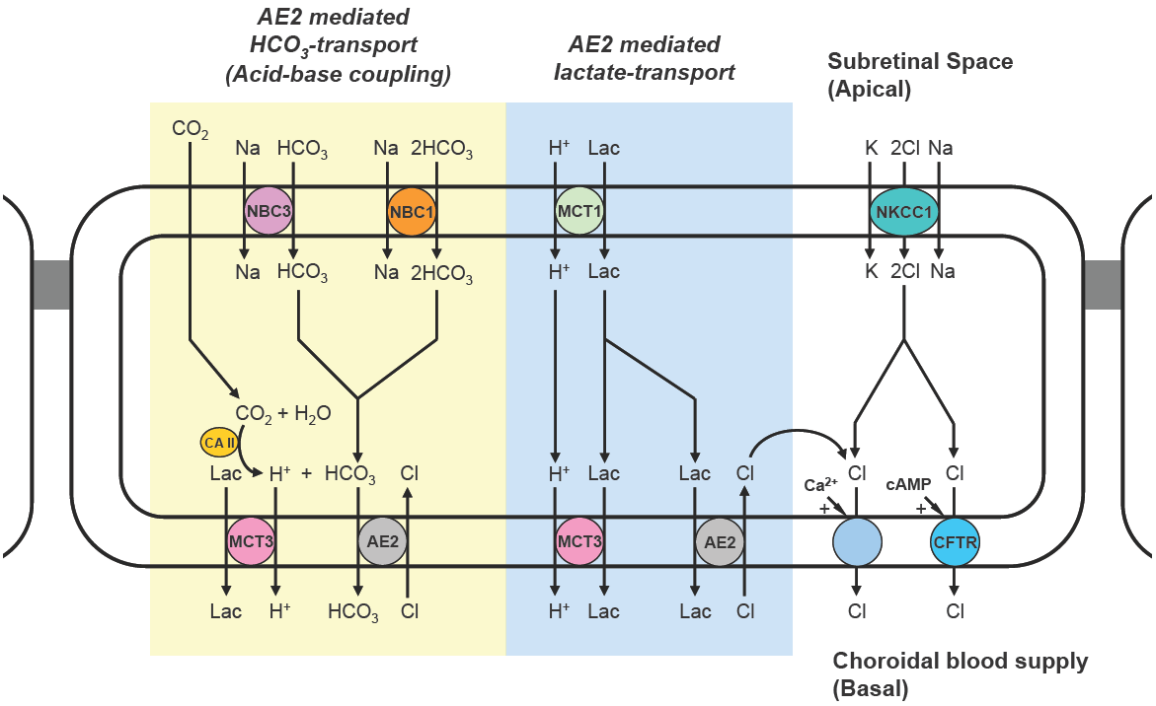

Fig. 5-13: Lactate and HCO_3 transport via AE2 at RPE basolateral membrane. Yellow box highlights acid-base coupling between MCT3 and AE2 as mediated by carbonic anhydrase II (CA II). Blue box highlights direct AE2-mediated lactate transport.

To study AE2-mediated lactate and HCO_3 transport, we added lactate to the basal bath – lactate entry into the cell via MCT3 or MCT4 should cause cell acidification, whereas lactate transport via AE2 should not affect pH_i. However, as shown in Fig. 5-14, adding

lactate to the basal bath caused cell alkalinization and decreased steady-state TEP and R_T ($\Delta pH_i = 0.04 \pm 0.01$, n = 11; $\Delta TEP = -0.38 \pm 0.18$ mV, n = 13). The R_T response however, was small and insignificant. Since AE2 can be blocked by DIDS (Fig. 3-13), we added DIDS to the basal bath and showed that DIDS completely eliminated basal lactate-induced alkalinization ($p < 0.05$; n = 6).

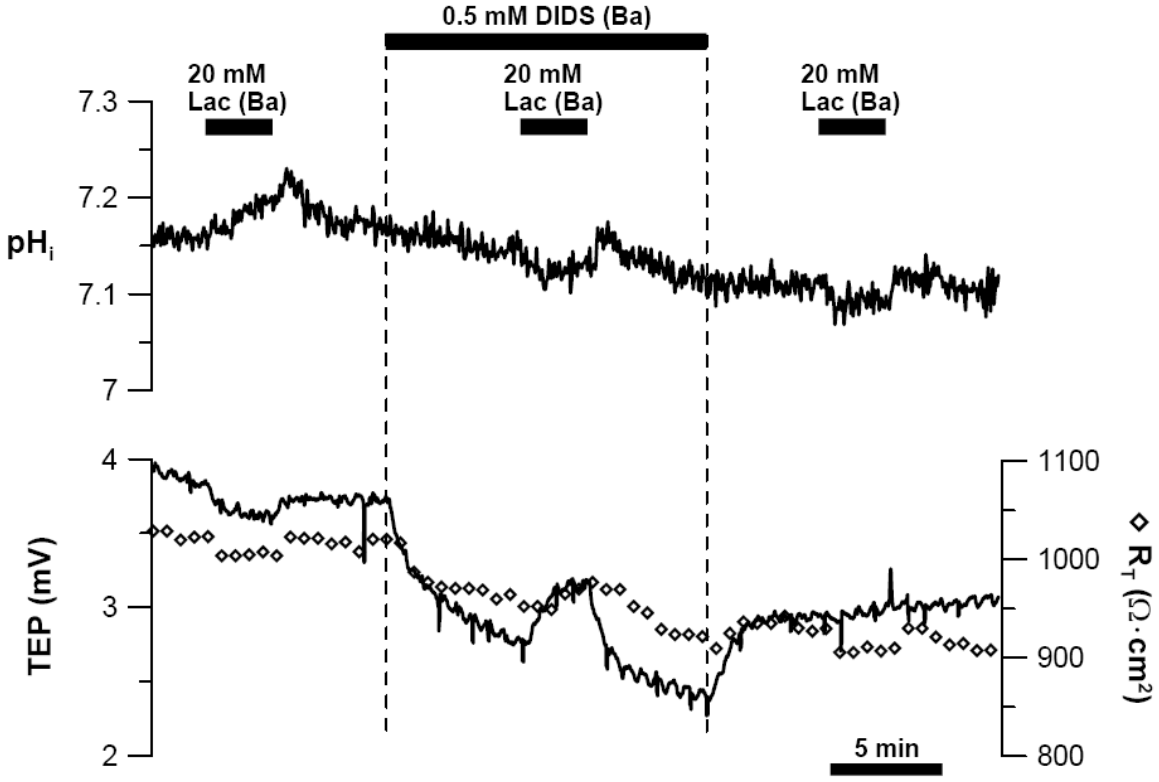

Fig. 5-14: (In CO_2/HCO_3 Ringer) Basal lactate-induced pH_i, TEP, and R_T responses in the presence of basal DIDS.

AE2-mediated lactate-transport does not directly cause cell alkalinization, thus suggesting involvement of other pH-dependent mechanisms. In this regard, we eliminated HCO_3-transport mechanisms by showing that in the absence of CO_2/HCO_3 (HEPES buffered) adding lactate into the basal bath caused cell alkalinization, and this

alkalinization was significantly reduced by basal DIDS (from $\Delta pH_i = 0.13 \pm 0.01$ to 0.05 ± 0.01; $n = 4$; $p < 0.01$; Fig. 5-15).

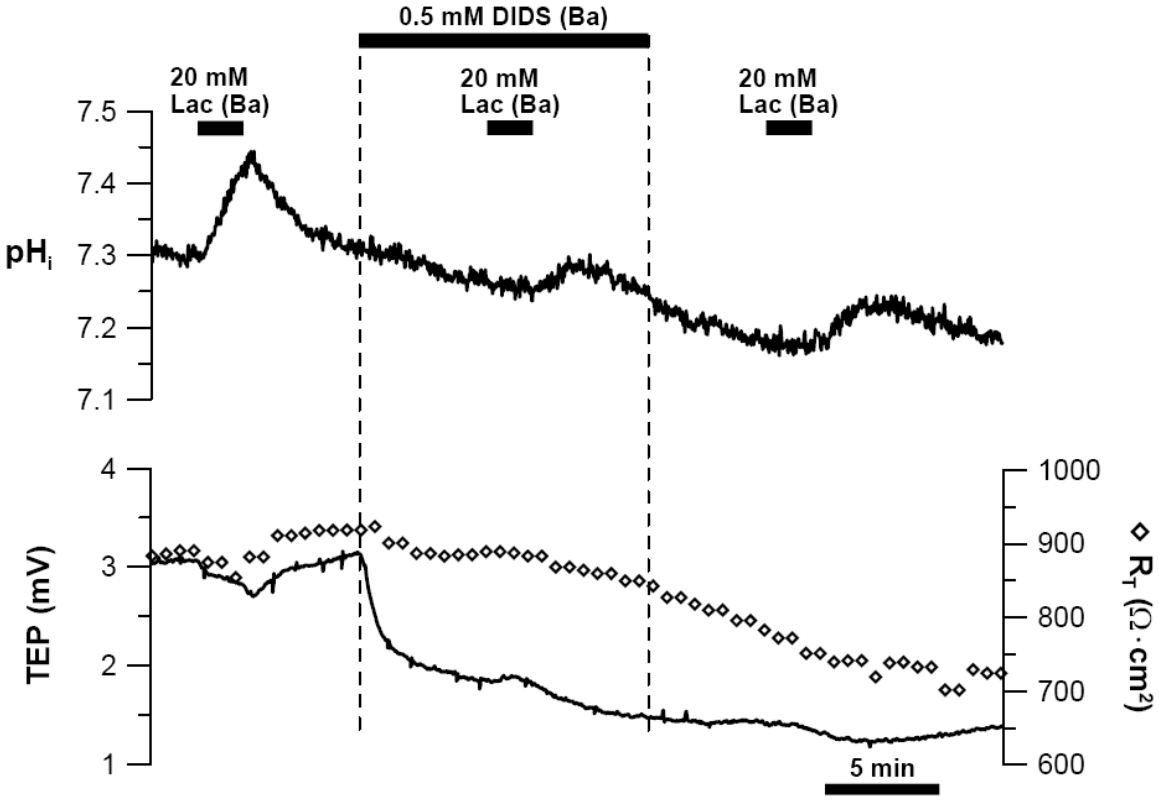

Fig. 5-15: (CO_2/HCO_3-free Ringer) Basal lactate-induced pH_i, TEP, and R_T responses in the presence of basal DIDS.

We showed that basal lactate-induced alkalinization is DIDS-sensitive and HCO_3-independent, but lactate entry into the cell via AE2 should not alter pH_i, thus suggesting the involvement of a secondary mechanism. It is possible that lactate entering the cell via AE2 is transported out of the cell at the apical membrane via MCT1 (Fig. 5-18), thus causing cell alkalinization. We confirmed this possibility by showing that basal lactate-induced alkalinization (in control; $\Delta pH_i = 0.03 \pm 0.01$) was converted into cell

acidification (ΔpH_i = -0.03 ± 0.01) in the presence of 100 μM niflumic acid (MCT1-inhibitor; see Fig. 4-4) (Fig. 5-16).

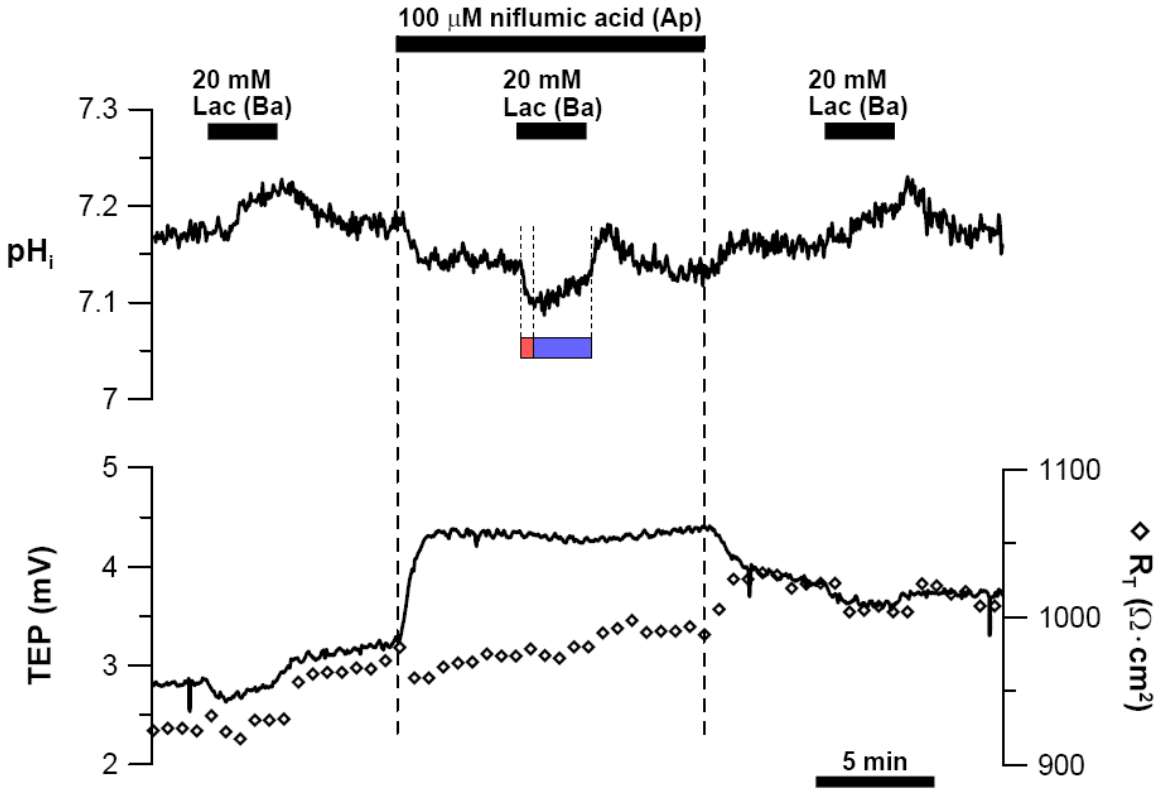

Fig. 5-16: (In CO_2/HCO_3 Ringer) Basal lactate-induced pH_i, TEP, and R_T responses in the presence of apical niflumic acid.

The basal lactate-induced pH_i response (in the presence of niflumic acid) exhibits R1 and R2 phases (see section 4.3 and Fig. 4-2) similar to that caused by apical lactate. Hence, R1 is probably caused by H/Lac entry into the cell via MCT3 and MCT4, whereas R2 reflects activation of pH_i-regulatory mechanisms at the apical membrane (i.e., NHE, NBC1, and NBC3) and/or at the basolateral membrane (i.e., NBC). In the absence of CO_2/HCO_3 (HEPES-buffered), niflumic acid also converted the basal lactate-induced alkalinization into a pH_i response with distinct R1 and R2 phases (n = 5; Fig. 5-17). In

this case, R1 reflects MCT3 and MCT4 activity, and R2 can only be attributed to NHE activity.

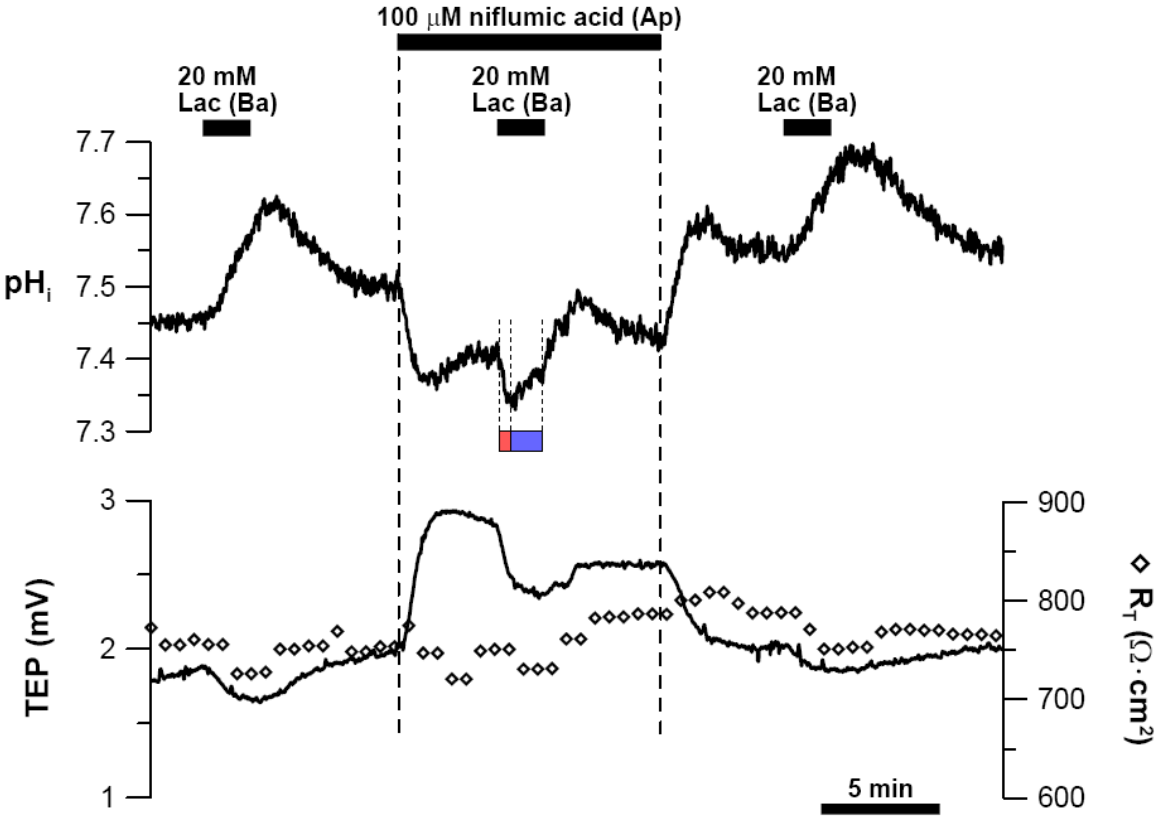

Fig. 5-17: (CO_2/HCO_3-free Ringer) Basal lactate-induced pH_i, TEP, and R_T responses in the presence of apical niflumic acid.

Although MCT3, MCT4, and AE2 are all electroneutral processes, the data summarized in Figs 5-14 to -17 shows that adding lactate to the basal bath decreased TEP. This TEP response originates from basolateral membrane hyperpolarization (Kenyon *et al.*, 1994), and this electrical response may derive from two possible mechanisms (see Fig. 5-18): (1) basal lactate entry via AE2 decreases $[Cl]_i$, which reduces Cl-channel activity, and (2) basal lactate entry via MCT3 drives electrogenic $Na/nHCO_3$ co-transport into the cell via basolateral membrane NBC (acid-base coupling). Our data corroborated the former

mechanism since the inhibition of basal lactate-induced TEP response by basal DIDS (CO_2/HCO_3-free; Fig. 5-15) or niflumic acid (which inhibits Ca^{2+}-dependent Cl-channels (Hartzell *et al.*, 2005); Fig. 5-16) is both consistent with involvement of Cl-channels.

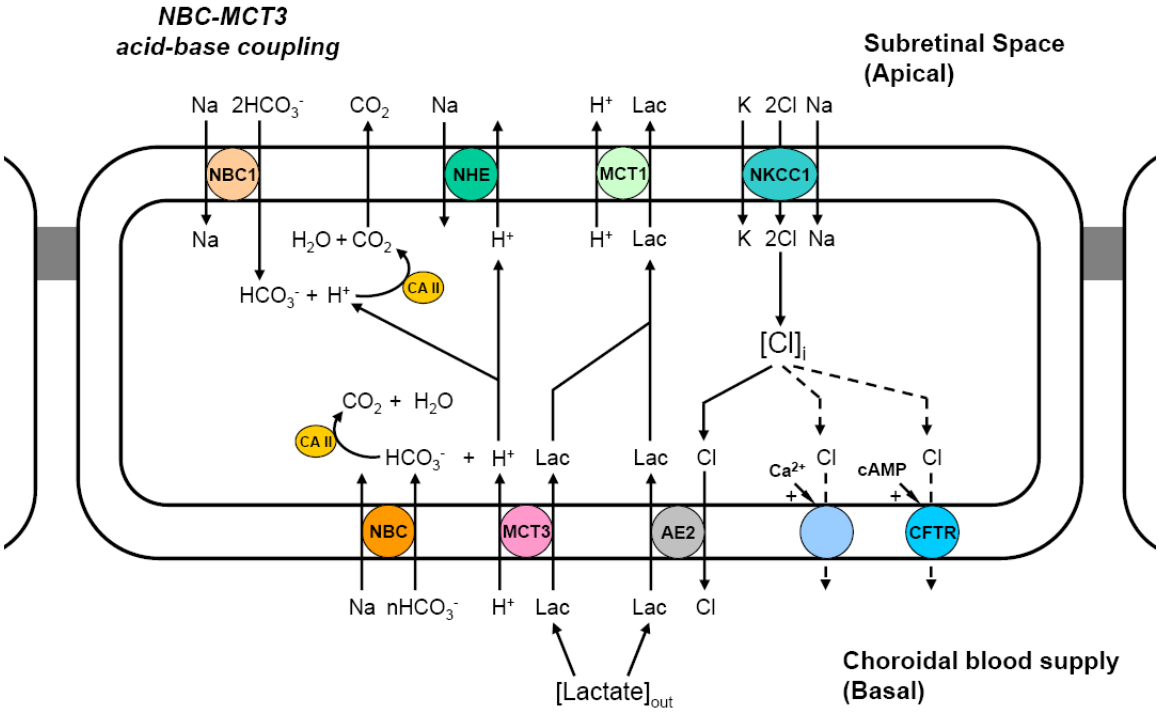

Fig. 5-18: Basal lactate-induced ion transport in RPE. At the basolateral membrane, MCT3, MCT4, and AE2 transports lactate into the cell. Lactate is subsequently transported out of the cell via MCT1 at the apical membrane. Lactate entry into the cell via AE2 reduces $[Cl]_i$, which reduces Cl-channel activity. The basolateral membrane NBC may be acid-base coupled to MCT3 activity, and this interaction may be facilitated by carbonic anhydrase II. At the apical membrane, NBC1 and NHE activity buffers protons entering the cell via MCT3.

Interestingly, Fig. 5-14 shows that basal lactate increased TEP (by 0.21 ± 0.12 mV) in the presence of basal DIDS (in CO_2/HCO_3 Ringer) – this did not occur in the absence of CO_2/HCO_3 (HEPES buffered; Fig. 5-15), thus suggesting the involvement of a HCO_3-transport mechanism. In this context, activation of NBC1 would hyperpolarize V_A and

increase TEP (see Fig. 5-18). This observation suggests that basal lactate activates NBC1, but its electrical activity is normally masked by concomitant changes in Cl- channel activity (hyperpolarize V_B; decrease TEP). There may be functional interaction between MCT3 (and MCT4) and basolateral membrane NBC, but evidence to support this notion is lacking – this is caused by experimental difficulties due to the lack of specific NBC inhibitors (DIDS will block NBC, AE2, ClC-2 channel, and Ca^{2+}-activated Cl-channel at the basolateral membrane).

In summary, we demonstrate that functional interaction between NBC1, MCT1, and CAs enhances lactate, HCO_3, and fluid transport at the RPE apical membrane. At the basolateral membrane, AE2 mediates the major component of lactate transport (compared to MCT3 & MCT4). AE2-mediated lactate-efflux from the basolateral membrane drives Cl into the cell, which is subsequently recycled back out of the cell mainly via Ca^{2+}-activated Cl-channels (perhaps with minor contributions from CFTR) – this mechanism helps drive fluid across the basolateral membrane. We show how the RPE protects itself from acidosis and osmotic stress imposed by photoreceptor generated metabolic acids in light or in the dark. We also demonstrate how the RPE uses lactate-transport mechanisms and its interactions with pH_i and volume regulating mechanisms to maintain ion, volume, and pH homeostasis in the SRS, thus preserving the health and integrity of the neural retina.

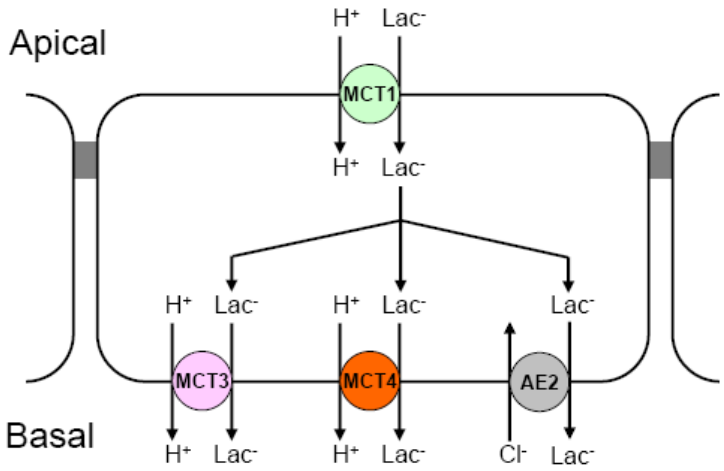

Section 5.2 Conclusion: Cl/Lac exchange via AE2 is the major lactate transport mechanism at the basolateral membrane

Supporting experimental observations	Interpretation	Fig.
Adding lactate into the basal bath caused alkalinization	Lactate entry from the basolateral membrane exits apical membrane via MCT1	5-14 to 5-17
Basal lactate caused acidification in the presence of apical niflumic acid	Lactate entry from the basolateral membrane exits apical membrane via MCT1	5-16 & 5-17
Basal lactate caused acidification in the presence of apical niflumic acid	MCT3 and MCT4 mediates lactate transport at the basolateral membrane	5-16 & 5-17
Basal DIDS blocked the basal lactate-induced alkalinization	AE2 mediates lactate transport at the basolateral membrane	5-14 & 5-15
Adding lactate into the basal bath decreased TEP	Basal lactate activated an electrogenic mechanism	5-14 to 5-17
Basal DIDS blocked the basal lactate-induced TEP decrease	Lactate transport via AE2 drives Cl-recycling by a DIDS-sensitive Cl-channel	5-14 & 5-15
Apical niflumic acid blocked the basal lactate-induced TEP decrease	Lactate transport via AE2 drives Cl-recycling by Ca^{2+}-dependent Cl-channel	5-16

CHAPTER 6: Conclusion and Future Work

Section 6.1 – Conclusion

The photoreceptors in the distal retina convert light quanta into electrical signals that are transduced through 2nd order neurons (bipolar cells, horizontal cells, amacrine cells, ganglion cells) and transmitted via the optic nerve to the brain. Although the RPE is not directly involved in this process, its close anatomical relationship to the photoreceptors is fundamentally important for maintaining photoreceptor health and photoexcitability. Vision is an energy (ATP) expensive process. Our photoreceptors expend large amounts of glucose, which is completely oxidized into CO_2 and H_2O (oxidative metabolism), or converted into lactic acid (glycolysis). Despite the extremely high choroidal blood flow, oxygen supply to the photoreceptors is limited; only ≈ 50% of all ATP used by the photoreceptors derive from oxidative metabolism. Therefore, large amounts of CO_2, lactic acid, and H_2O are released into the SRS, and their release almost doubles in the dark (see section 3-11). The accumulation of these metabolic waste products in the SRS would quickly destroy the photoreceptors, but the RPE protects the photoreceptors by transporting these metabolic waste products to the choroid.

Our *in vitro* experiments were designed to study CO_2 and lactate-transport mechanisms separately, but *in vivo* these mechanisms functionally interact with one another to enhance metabolic acid transport across the RPE. We elucidated the cellular mechanisms involved in CO_2 transport across the RPE, and showed that this process drives Na, Cl, HCO_3, and osmotically obliged water across the tissue, thus maintaining retinal adhesion to the RPE (section 3.9). We show that H^+-coupled lactate transport across the apical

membrane via MCT1 activates pH_i-regulatory mechanisms (section 5.2): (1) MCT1 activity stimulates Na/H exchanger (NHE); (2) MCT1 activity stimulates Na^+-linked HCO_3 co-transporters (NBC1 and NBC3), and this process is dependent on CA II activity. In the dark, these mechanisms help buffer both CO_2 and lactate induced cell acidification. Activation of these mechanisms increases $[Na^+]_i$, $[HCO_3^-]_i$, $[lactate]_i$, which drives isoosmotically obliged fluid across the apical membrane to cause cell swelling (section 4.6). Furthermore, the two-fold increase in CO_2 release by photoreceptors into the SRS causes its accumulation in the cell due to a ≈ 10-fold higher apical to basolateral membrane surface area (sections 3.2 & 3.11). This drives CA II-mediated CO_2 hydration into HCO_3, thus increasing $[HCO_3^-]_i$ further. Collectively, increased release of CO_2 and lactic acid by the photoreceptors causes cell swelling and osmotic stress. We show that the RPE reduces cell-swelling by activating Kir 7.1 K-channel at the apical membrane (section 4.5) and ClC-2 Cl-channel at the basolateral membrane (section 4.4). Furthermore, lactate efflux via AE2 at the basolateral membrane stimulates Ca^{2+}-activated Cl-channels (section 5.3), which drives fluid out of the basolateral membrane to help reduce RPE cell volume. KCl efflux via these channels mitigates CO_2- and lactate-induced RPE cell swelling, thus protecting the health of the RPE. We demonstrated how the RPE utilizes the changes in SRS CO_2 and lactic acid level as a signal to activate mechanisms that helps the RPE adapt to light-dark transitions in photoreceptor metabolism. Understanding these mechanisms provide us with the basis to understand the pathophysiology of disease (e.g., retinal edema and retinal detachment), which is a first step for the development of therapeutic interventions to preserve vision.

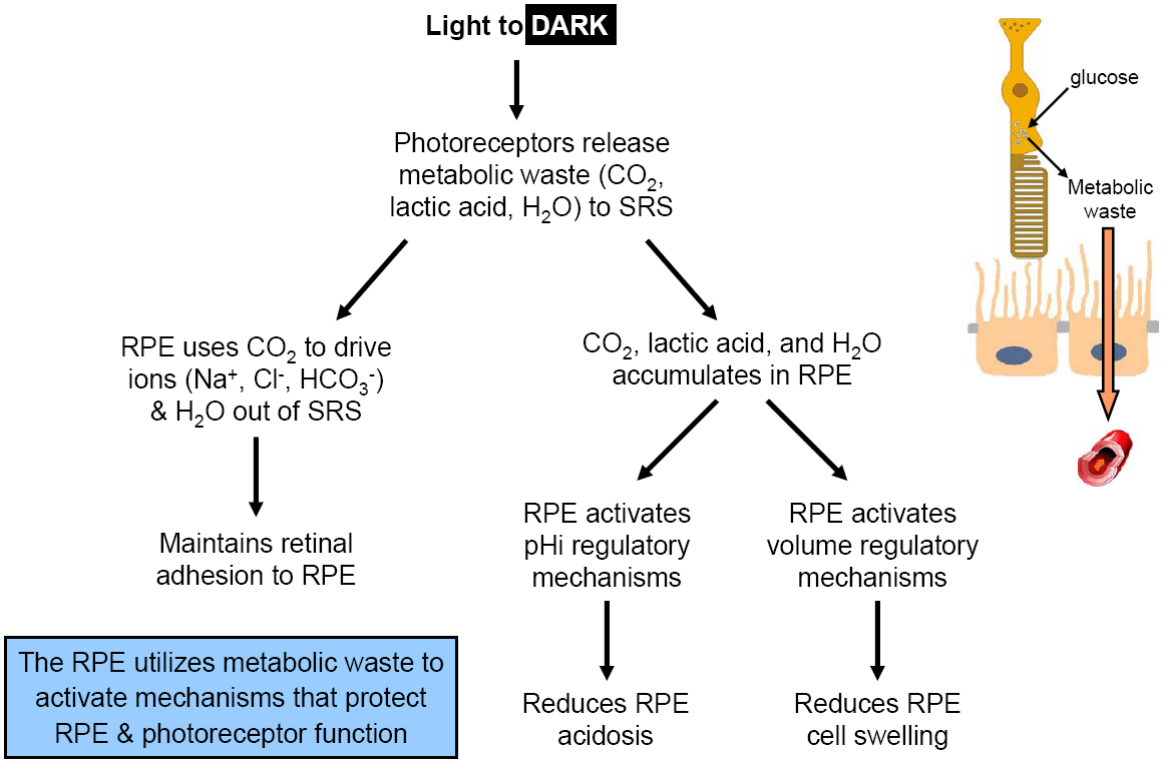

Fig. 6-1: Summary of conclusions.

Section 6.2 – RPE cell culture models for transplantation

As discussed in chapter 2 (section 2.1), the use of cell culture allows us to quickly and easily uncover physiological processes in the retinal pigment epithelium at a low cost. However, how closely does this *in vitro* culture model mimic the native tissue *in vivo*? What are the differences in gene and protein expression, and physiology of fetal and adult RPE? Microarray data show that despite many overlapping genes between these tissues, many genes that are highly expressed in native RPE are lost in culture. Furthermore, genes that are normally not expressed in native RPE are upregulated in culture. Improvement to the RPE cell culture model is a constant pursuit of the laboratory. The RPE culture model is used to study ion-transport mechanisms, map signal transduction pathways, study drug toxicity, and understand specific RPE functions. But in addition, it can also be developed for transplantation. RPE cultures that closely mimic native tissues can increase the success of transplantation in RPE-degenerative diseases such as AMD (Binder *et al.*, 2004; Binder *et al.*, 2007; da Cruz *et al.*, 2007).

To improve RPE cell culture, we find clues in the environment of the RPE *in vivo*. What are the critical factors that influence RPE growth from its interactions with the retina and choroid? How can we mimic these conditions *in vitro*? For example, adding fibroblast conditioned medium to the basal side of chick RPE has been shown to improve tight junction development and expression, which facilitates RPE polarization and maturation (Rahner *et al.*, 2004). What are the components of retinal extract used in RPE cell culture media (Hu & Bok, 2001) that enhances growth and maturation? Cultured hfRPE cells are grown in media containing 5% serum to promote cell proliferation and survival,

a condition that is not normally found *in vivo* (Maminishkis et al., 2006). To this end, RPE monolayers cultured under serum-free condition has been developed by other laboratories (Gamm *et al.*, 2008) and is better poised for transplantation purposes (serum may transfer animal pathogens to the patient) (Valtink & Engelmann, 2009). However, few experiments have been performed to study how closely this serum-free culture model mimics native RPE. Alternatively, embroyonic and induced pluripotentent stem cells (ES & iPS cells) have been coaxed to differentiate into RPE cells (Vugler *et al.*, 2008; Carr *et al.*, 2009a; Carr *et al.*, 2009b). The transplantation of these cells into the eyes of mice and rats with retinal degeneration were able to rescue visual function. Based upon these findings, one may be interested in using fibroblast cells from patients, transform them into iPS cells, and subsequently convert them into RPE cells for transplantation into the same patient. This method is highly favorable because is eliminates the problem of immune rejection. Since vectorial transport of bicarbonate, lactate, and water by the RPE is critical to RPE-photoreceptor interactions, the feasibility of these various RPE cell culture models for transplantation can be evaluated by measuring the activities of these transport mechanisms.

Section 6.3 – Lactate, retinal detachment, and proliferative vitreoretinopathy

Separation of the retina from RPE induces many changes in retina/RPE morphology and physiology (Fisher & Lewis, 2003; Leiderman & Miller, 2009; Wickham & Charteris, 2009), for example: (1) non-neuronal glia cells (i.e., astrocytes, microglia, and Müller cells) in the retina undergo morphological changes and proliferation, (2) photoreceptors begin to degenerate – they become shorter and distorted, (3) horizontal and ganglion cells undergo extensive remodeling, (4) the RPE dedifferentiates and migrates into the subretinal space and retinal layers. These changes can begin 24 hours after retinal detachment and causes irreversible vision loss after three days if not treated. Furthermore, this condition can progress into proliferative vitreoretinopathy (PVR), a disease with poor visual prognosis characterized by inflammation, proliferation, and scarring (Pastor, 1998).

In PVR, RPE undergoes epithelial-to-mesenchymal transition (EMT), in which RPE loses its epithelial markers and morphology; transforming from cobblestone-shaped cells into elongated fibroblast-like cells (Casaroli-Marano *et al.*, 1999; Saika *et al.*, 2004). EMT of RPE cells in PVR involves transforming growth factor β (TGF-β) (Parapuram *et al.*, 2009). In preliminary experiments, I excised cultured hfRPE monolayers grown on porous-filters, placed them on culture plates, and incubated them in cell culture media over 6 days (37 ^{o}C; 5% CO_2). In just three days, these RPE cells dedifferentiated into fibroblast-like cells via an EMT-like process (Fig. 6-2); they lose their pigmentation and cell-cell attachment, and undergo rapid proliferation and migration. It is likely that the hypoxic condition inherent in tissue cultures (due to large O_2 diffusion layer; see

discussion in section 4.2) activates EMT of RPE cells via hypoxia inducible factor 1 alpha (HIF-1α) (Higgins *et al.*, 2007; Higgins *et al.*, 2008; Brahimi-Horn & Pouyssegur, 2009). Although EMT of these cultured hfRPE cells are not induced by TGF-β, the downstream pathways and mechanisms activated by HIF-1α are mostly the same.

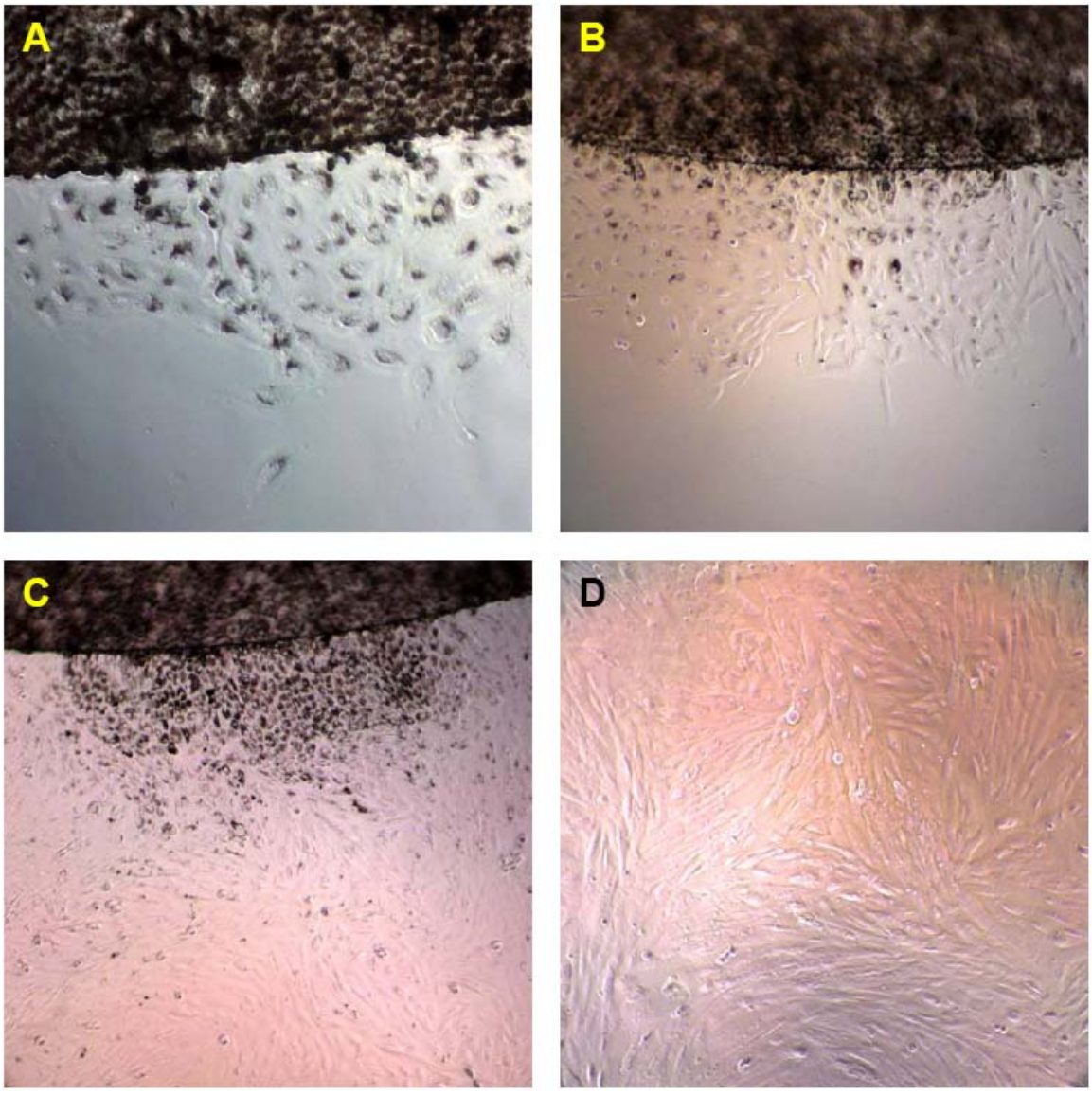

Fig. 6-2: RPE monolayers grown on porous filters undergo epithelial-to-mesenchymal transition. (A) 3 days (40x mag.), (B) 6 days (20x mag.), (C) 6 days (different sample; 20x mag.). (D) The

fibroblast-like cells were extracted and placed in a flask and grown (37 ^{o}C, 5% CO_2) for 3 days (40x mag.).

In PVR, RPE cells undergo EMT and migrate into the SRS (Wickham & Charteris, 2009). Similarly, Müller glia cells dedifferentiate and migrate into the SRS (Lewis *et al.*, 1999; Wickham & Charteris, 2009). Since cell division requires large amounts of energy, these dedifferentiated cells metabolize large amounts of glucose to produce significant amounts of CO_2 and lactic acid. This is evidenced by the lower pH of the culture media bathing dedifferentiated RPE cells (Fig. 6-2 D) vs. that bathing confluent RPE cells (data not shown) – the pH difference was determined (subjectively) by comparing the difference in media color (i.e., dedifferentiated RPE media is noticeably more yellow than RPE media). Interestingly, lactate has been shown to stabilize HIF-1α by inhibiting HIF-1α prolyl hydroxylases (Crowther *et al.*, 2001; Lu *et al.*, 2002; Lu *et al.*, 2005). Furthermore, recent studies also suggest that lactate upregulates HIF-1α in stem cells (Milovanova *et al.*, 2008; Zieker *et al.*, 2008). Since HIF-1α causes cell dedifferentiation (Jogi *et al.*, 2002; Helczynska *et al.*, 2003; Axelson *et al.*, 2005), the large amount of lactate released by dedifferentiated RPE and retinal cells into the SRS may stimulate further RPE EMT in a positive feedback loop, thus exacerbating the PVR disease process. If true, targeting lactate transport mechanisms may be a viable strategy against PVR.

Section 6.4 – NBC3 activity, interactions, and function in RPE

The RPE expresses electrogenic (NBC1) and electroneutral (NBC3) $NaHCO_3$ co-transporters (NBC1) at its apical membrane (Fig. 1-8). NBC3 is an electroneutral Na/HCO_3 co-transporter, thus its activity is not limited by the membrane voltage; it is capable of transporting large amounts of $NaHCO_3$ and may play a significant role in RPE fluid transport. The importance of NBC3 to HCO_3- and fluid- transport can be understood by comparing NBC3 localization in RPE vs. CPE (choroid plexus epithelium) (see section 3.9). NBC3 is localized to the basolateral membrane in CPE, which secretes HCO_3 and fluid. On the other hand, NBC3 is localized to the apical membrane in RPE, which absorbs HCO_3 and fluid. This difference in HCO_3 transport-direction of RPE and CPE may be in part due to their difference in NBC3 membrane localization.

Interestingly, in mice, loss of NBC3 expression leads to retinal degeneration because NBC3-mediated HCO_3-transport helps buffer photoreceptor-generated metabolic acids (Bok *et al.*, 2003). In chapter 5 (section 5.2), we demonstrated that MCT1 interacts with NBC1 to enhance both lactic acid and HCO_3 transport, and that this process depends on cytosolic CA (CA II). The same acid-base coupling mechanism between MCT1 and NBC3 may exist, which implicates NBC3 in lactate transport. However, physiological experiments to study this functional interaction were difficult to interpret and are inconclusive. This is in part due to the lack of specific (or non-specific) inhibitors against NBC3. In addition, its electroneutrality makes its activity "invisible" to detection by electrophysiological methods. In this work, all evidences for NBC3 activity in RPE are indirect (sections 3.3 & 5.2). Another way to study this transporter in RPE is via siRNA

knockdown technology, but the development of a specific siRNA against NBC3 is tedious and difficult. Alternatively, instead of working with RPE culture models, it is of considerable interest to study HCO_3 and fluid transport in the RPE and CPE of NBC3 knockout mice.

References

Abercrombie RF, Putnam RW & Roos A. (1983). The intracellular pH of frog skeletal muscle: its regulation in isotonic solutions. *The Journal of physiology* **345,** 175-187.

Adijanto J, Banzon T, Jalickee S, Wang NS & Miller SS. (2009). CO2-induced ion and fluid transport in human retinal pigment epithelium. *The Journal of general physiology* **133,** 603-622.

Adler AJ & Southwick RE. (1992). Distribution of glucose and lactate in the interphotoreceptor matrix. *Ophthalmic research* **24,** 243-252.

Alm A & Bill A. (1973). Ocular and optic nerve blood flow at normal and increased intraocular pressures in monkeys (Macaca irus): a study with radioactively labelled microspheres including flow determinations in brain and some other tissues. *Experimental eye research* **15,** 15-29.

Alm A & Bill A. (1987). Ocular Circulation. In *Adler's Physiology of the Eye, 8th ed*, ed. Moses RA & Hart WM, pp. 183-203. Mosby, St Louis, MO.

Alvarez BV, Loiselle FB, Supuran CT, Schwartz GJ & Casey JR. (2003). Direct extracellular interaction between carbonic anhydrase IV and the human NBC1 sodium/bicarbonate co-transporter. *Biochemistry* **42,** 12321-12329.

Ames A, 3rd, Li YY, Heher EC & Kimble CR. (1992). Energy metabolism of rabbit retina as related to function: high cost of Na+ transport. *J Neurosci* **12,** 840-853.

Aramant RB & Seiler MJ. (2004). Progress in retinal sheet transplantation. *Progress in retinal and eye research* **23,** 475-494.

Aronson PS, Nee J & Suhm MA. (1982). Modifier role of internal H+ in activating the Na+-H+ exchanger in renal microvillus membrane vesicles. *Nature* **299,** 161-163.

Aronson PS, Suhm MA & Nee J. (1983). Interaction of external H+ with the Na+-H+ exchanger in renal microvillus membrane vesicles. *The Journal of biological chemistry* **258,** 6767-6771.

Axelson H, Fredlund E, Ovenberger M, Landberg G & Pahlman S. (2005). Hypoxia-induced dedifferentiation of tumor cells--a mechanism behind heterogeneity and aggressiveness of solid tumors. *Seminars in cell & developmental biology* **16,** 554-563.

Baldwin KM, Hooker AM & Herrick RE. (1978). Lactate oxidative capacity in different types of muscle. *Biochemical and biophysical research communications* **83,** 151-157.

Becker HM, Broer S & Deitmer JW. (2004). Facilitated lactate transport by MCT1 when coexpressed with the sodium bicarbonate cotransporter (NBC) in Xenopus oocytes. *Biophysical journal* **86,** 235-247.

Becker HM & Deitmer JW. (2004). Voltage dependence of H+ buffering mediated by sodium bicarbonate cotransport expressed in Xenopus oocytes. *The Journal of biological chemistry* **279,** 28057-28062.

Becker HM, Hirnet D, Fecher-Trost C, Sultemeyer D & Deitmer JW. (2005). Transport activity of MCT1 expressed in Xenopus oocytes is increased by interaction with carbonic anhydrase. *The Journal of biological chemistry* **280,** 39882-39889.

Bergersen LH. (2007). Is lactate food for neurons? Comparison of monocarboxylate transporter subtypes in brain and muscle. *Neuroscience* **145,** 11-19.

Bhosale P & Bernstein PS. (2005). Quantitative measurement of 3'-oxolutein from human retina by normal-phase high-performance liquid chromatography coupled to atmospheric pressure chemical ionization mass spectrometry. *Analytical biochemistry* **345,** 296-301.

Bialek S, Joseph DP & Miller SS. (1995). The delayed basolateral membrane hyperpolarization of the bovine retinal pigment epithelium: mechanism of generation. *The Journal of physiology* **484 (Pt 1),** 53-67.

Bill A. (1975). Blood circulation and fluid dynamics in the eye. *Physiological reviews* **55,** 383-417.

Binder S, Krebs I, Hilgers RD, Abri A, Stolba U, Assadoulina A, Kellner L, Stanzel BV, Jahn C & Feichtinger H. (2004). Outcome of transplantation of autologous retinal pigment epithelium in age-related macular degeneration: a prospective trial. *Investigative ophthalmology & visual science* **45,** 4151-4160.

Binder S, Stanzel BV, Krebs I & Glittenberg C. (2007). Transplantation of the RPE in AMD. *Progress in retinal and eye research* **26,** 516-554.

Blaauwgeers HG, Holtkamp GM, Rutten H, Witmer AN, Koolwijk P, Partanen TA, Alitalo K, Kroon ME, Kijlstra A, van Hinsbergh VW & Schlingemann RO. (1999). Polarized vascular endothelial growth factor secretion by human retinal pigment epithelium and localization of vascular endothelial growth factor receptors on the inner choriocapillaris. Evidence for a trophic paracrine relation. *The American journal of pathology* **155,** 421-428.

Blaug S, Quinn R, Quong J, Jalickee S & Miller SS. (2003). Retinal pigment epithelial function: a role for CFTR? *Documenta ophthalmologica* **106,** 43-50.

Bok D, Galbraith G, Lopez I, Woodruff M, Nusinowitz S, BeltrandelRio H, Huang W, Zhao S, Geske R, Montgomery C, Van Sligtenhorst I, Friddle C, Platt K, Sparks MJ, Pushkin A, Abuladze N, Ishiyama A, Dukkipati R, Liu W & Kurtz I. (2003). Blindness and auditory impairment caused by loss of the sodium bicarbonate cotransporter NBC3. *Nature genetics* **34,** 313-319.

Bok D, Schibler MJ, Pushkin A, Sassani P, Abuladze N, Naser Z & Kurtz I. (2001). Immunolocalization of electrogenic sodium-bicarbonate cotransporters pNBC1 and kNBC1 in the rat eye. *American journal of physiology* **281,** F920-935.

Bonen A. (2001). The expression of lactate transporters (MCT1 and MCT4) in heart and muscle. *European journal of applied physiology* **86,** 6-11.

Bonen A, Heynen M & Hatta H. (2006). Distribution of monocarboxylate transporters MCT1-MCT8 in rat tissues and human skeletal muscle. *Applied physiology, nutrition, and metabolism = Physiologie appliquee, nutrition et metabolisme* **31,** 31-39.

Borgula GA, Karwoski CJ & Steinberg RH. (1989). Light-evoked changes in extracellular pH in frog retina. *Vision research* **29,** 1069-1077.

Bosl MR, Stein V, Hubner C, Zdebik AA, Jordt SE, Mukhopadhyay AK, Davidoff MS, Holstein AF & Jentsch TJ. (2001). Male germ cells and photoreceptors, both dependent on close cell-cell interactions, degenerate upon ClC-2 Cl(-) channel disruption. *The EMBO journal* **20,** 1289-1299.

Brahimi-Horn MC & Pouyssegur J. (2009). HIF at a glance. *Journal of cell science* **122,** 1055-1057.

Briva A, Vadasz I, Lecuona E, Welch LC, Chen J, Dada LA, Trejo HE, Dumasius V, Azzam ZS, Myrianthefs PM, Batlle D, Gruenbaum Y & Sznajder JI. (2007). High CO2 levels impair alveolar epithelial function independently of pH. *PLoS ONE* **2,** e1238.

Brown AM & Ransom BR. (2007). Astrocyte glycogen and brain energy metabolism. *Glia* **55,** 1263-1271.

Brown PD, Davies SL, Speake T & Millar ID. (2004). Molecular mechanisms of cerebrospinal fluid production. *Neuroscience* **129,** 957-970.

Brown RC & Davis TP. (2002). Calcium modulation of adherens and tight junction function: a potential mechanism for blood-brain barrier disruption after stroke. *Stroke; a journal of cerebral circulation* **33,** 1706-1711.

Burke JM. (2008). Epithelial phenotype and the RPE: is the answer blowing in the Wnt? *Progress in retinal and eye research* **27,** 579-595.

Carr AJ, Vugler A, Lawrence J, Chen LL, Ahmado A, Chen FK, Semo M, Gias C, da Cruz L, Moore HD, Walsh J & Coffey PJ. (2009a). Molecular characterization and functional analysis of phagocytosis by human embryonic stem cell-derived RPE cells using a novel human retinal assay. *Molecular vision* **15,** 283-295.

Carr AJ, Vugler AA, Hikita ST, Lawrence JM, Gias C, Chen LL, Buchholz DE, Ahmado A, Semo M, Smart MJ, Hasan S, da Cruz L, Johnson LV, Clegg DO & Coffey PJ. (2009b). Protective effects of human iPS-derived retinal pigment epithelium cell transplantation in the retinal dystrophic rat. *PloS one* **4,** e8152.

Casaroli-Marano RP, Pagan R & Vilaro S. (1999). Epithelial-mesenchymal transition in proliferative vitreoretinopathy: intermediate filament protein expression in retinal pigment epithelial cells. *Investigative ophthalmology & visual science* **40,** 2062-2072.

Casey JR, Sly WS, Shah GN & Alvarez BV. (2009). Bicarbonate homeostasis in excitable tissues: role of AE3 Cl-/HCO3- exchanger and carbonic anhydrase XIV interaction. *American journal of physiology* **297,** C1091-1102.

Cereijido M, Contreras RG, Shoshani L, Flores-Benitez D & Larre I. (2008). Tight junction and polarity interaction in the transporting epithelial phenotype. *Biochimica et biophysica acta* **1778,** 770-793.

Chih CP, Lipton P & Roberts EL, Jr. (2001). Do active cerebral neurons really use lactate rather than glucose? *Trends in neurosciences* **24,** 573-578.

Chihara E & Nao-i N. (1985). Resorption of subretinal fluid by transepithelial flow of the retinal pigment epithelium. *Graefe's archive for clinical and experimental ophthalmology = Albrecht von Graefes Archiv fur klinische und experimentelle Ophthalmologie* **223,** 202-204.

Chiry O, Pellerin L, Monnet-Tschudi F, Fishbein WN, Merezhinskaya N, Magistretti PJ & Clarke S. (2006). Expression of the monocarboxylate transporter MCT1 in the adult human brain cortex. *Brain research* **1070,** 65-70.

Coady MJ, Chang MH, Charron FM, Plata C, Wallendorff B, Sah JF, Markowitz SD, Romero MF & Lapointe JY. (2004). The human tumour suppressor gene SLC5A8 expresses a Na+-monocarboxylate cotransporter. *The Journal of physiology* **557,** 719-731.

Congdon N, O'Colmain B, Klaver CC, Klein R, Munoz B, Friedman DS, Kempen J, Taylor HR & Mitchell P. (2004). Causes and prevalence of visual impairment among adults in the United States. *Archives of ophthalmology* **122,** 477-485.

Cooper GJ & Boron WF. (1998). Effect of PCMBS on CO2 permeability of Xenopus oocytes expressing aquaporin 1 or its C189S mutant. *The American journal of physiology* **275,** C1481-1486.

Cowan F & Whitelaw A. (1991). Acute effects of acetazolamide on cerebral blood flow velocity and pCO2 in the newborn infant. *Acta paediatrica Scandinavica* **80,** 22-27.

Cox SN, Hay E & Bird AC. (1988). Treatment of chronic macular edema with acetazolamide. *Archives of ophthalmology* **106,** 1190-1195.

Cringle SJ, Yu DY, Yu PK & Su EN. (2002). Intraretinal oxygen consumption in the rat in vivo. *Investigative ophthalmology & visual science* **43,** 1922-1927.

Crowther M, Brown NJ, Bishop ET & Lewis CE. (2001). Microenvironmental influence on macrophage regulation of angiogenesis in wounds and malignant tumors. *Journal of leukocyte biology* **70,** 478-490.

da Cruz L, Chen FK, Ahmado A, Greenwood J & Coffey P. (2007). RPE transplantation and its role in retinal disease. *Progress in retinal and eye research* **26,** 598-635.

Daniele LL, Sauer B, Gallagher SM, Pugh EN, Jr. & Philp NJ. (2008). Altered visual function in monocarboxylate transporter 3 (Slc16a8) knockout mice. *Am J Physiol Cell Physiol* **295,** C451-457.

de Jong MC, Scheffer GL, Broxterman HJ, Hooijberg JH, Slootstra JW, Meloen RH, Kreitman RJ, Husain SR, Joshi BH, Puri RK & Scheper RJ. (2003). Multidrug-resistant tumor cells remain sensitive to a recombinant interleukin-4-Pseudomonas exotoxin, except when overexpressing the multidrug resistance protein MRP1. *Clin Cancer Res* **9,** 5009-5017.

Del Priore LV, Hornbeck R, Kaplan HJ, Jones Z, Valentino TL, Mosinger-Ogilvie J & Swinn M. (1995). Debridement of the pig retinal pigment epithelium in vivo. *Archives of ophthalmology* **113,** 939-944.

Deng QS & Johanson CE. (1989). Stilbenes inhibit exchange of chloride between blood, choroid plexus and cerebrospinal fluid. *Brain research* **501,** 183-187.

Dimmer KS, Friedrich B, Lang F, Deitmer JW & Broer S. (2000). The low-affinity monocarboxylate transporter MCT4 is adapted to the export of lactate in highly glycolytic cells. *The Biochemical journal* **350 Pt 1,** 219-227.

Dunham PB, Kelley SJ & Logue PJ. (2004). Extracellular Na+ inhibits Na+/H+ exchange: cell shrinkage reduces the inhibition. *Am J Physiol Cell Physiol* **287,** C336-344.

Economopoulou M, Hammer J, Wang FE, Fariss R, Maminishkis A & Miller SS. (2008). Expression, localization, and function of junctional adhesion molecule-C (JAM-C) in human retinal pigment epithelium. *Investigative ophthalmology & visual science*.

Edelman JL, Lin H & Miller SS. (1994). Acidification stimulates chloride and fluid absorption across frog retinal pigment epithelium. *The American journal of physiology* **266,** C946-956.

Eggermont J, Trouet D, Carton I & Nilius B. (2001). Cellular function and control of volume-regulated anion channels. *Cell biochemistry and biophysics* **35,** 263-274.

Endeward V & Gros G. (2005). Low carbon dioxide permeability of the apical epithelial membrane of guinea-pig colon. *The Journal of physiology* **567,** 253-265.

Endeward V, Musa-Aziz R, Cooper GJ, Chen LM, Pelletier MF, Virkki LV, Supuran CT, King LS, Boron WF & Gros G. (2006). Evidence that aquaporin 1 is a major pathway for CO2 transport across the human erythrocyte membrane. *Faseb J* **20,** 1974-1981.

Engelmann K & Valtink M. (2004). RPE cell cultivation. *Graefe's archive for clinical and experimental ophthalmology = Albrecht von Graefes Archiv fur klinische und experimentelle Ophthalmologie* **242,** 65-67.

Etienne-Manneville S & Hall A. (2003). Cell polarity: Par6, aPKC and cytoskeletal crosstalk. *Current opinion in cell biology* **15,** 67-72.

Feller N, Broxterman HJ, Wahrer DC & Pinedo HM. (1995). ATP-dependent efflux of calcein by the multidrug resistance protein (MRP): no inhibition by intracellular glutathione depletion. *FEBS letters* **368,** 385-388.

Fillenz M. (2005). The role of lactate in brain metabolism. *Neurochemistry international* **47,** 413-417.

Fisher SK & Lewis GP. (2003). Muller cell and neuronal remodeling in retinal detachment and reattachment and their potential consequences for visual recovery: a review and reconsideration of recent data. *Vision research* **43,** 887-897.

Fisher SK, Lewis GP, Linberg KA & Verardo MR. (2005). Cellular remodeling in mammalian retina: results from studies of experimental retinal detachment. *Progress in retinal and eye research* **24,** 395-431.

Fishman GA, Gilbert LD, Fiscella RG, Kimura AE & Jampol LM. (1989). Acetazolamide for treatment of chronic macular edema in retinitis pigmentosa. *Archives of ophthalmology* **107,** 1445-1452.

Furia TE. (1972). Sequestrants in Foods. In *CRC Handbook of Food Additives*, 2nd Edition edn, ed. Furia TE, pp. 276. CRC Press, Boca Raton.

Furukawa T, Ogura T, Katayama Y & Hiraoka M. (1998). Characteristics of rabbit ClC-2 current expressed in Xenopus oocytes and its contribution to volume regulation. *The American journal of physiology* **274,** C500-512.

Gallemore RP, Hughes BA & Miller SS. (1998). Light-induced responses of the retinal pigment epithelium. In *The retinal pigment epithelium*, ed. Marmor MF & Wolfensberger TJ, pp. 175-198. Oxford University Press, New York.

Gallemore RP, Li JD, Govardovskii VI & Steinberg RH. (1994). Calcium gradients and light-evoked calcium changes outside rods in the intact cat retina. *Visual neuroscience* **11,** 753-761.

Gamm DM, Melvan JN, Shearer RL, Pinilla I, Sabat G, Svendsen CN & Wright LS. (2008). A novel serum-free method for culturing human prenatal retinal pigment epithelial cells. *Investigative ophthalmology & visual science* **49,** 788-799.

Gladden LB. (2004). Lactate metabolism: a new paradigm for the third millennium. *The Journal of physiology* **558,** 5-30.

Gleadle JM & Ratcliffe PJ. (1998). Hypoxia and the regulation of gene expression. *Molecular medicine today* **4,** 122-129.

Griff ER, Shirao Y & Steinberg RH. (1985). Ba2+ unmasks K+ modulation of the Na+-K+ pump in the frog retinal pigment epithelium. *The Journal of general physiology* **86,** 853-876.

Grollman EF, Philp NJ, McPhie P, Ward RD & Sauer B. (2000). Determination of transport kinetics of chick MCT3 monocarboxylate transporter from retinal pigment epithelium by expression in genetically modified yeast. *Biochemistry* **39,** 9351-9357.

Gross E, Abuladze N, Pushkin A, Kurtz I & Cotton CU. (2001). The stoichiometry of the electrogenic sodium bicarbonate cotransporter pNBC1 in mouse pancreatic duct cells is 2 HCO(3)(-):1 Na(+). *The Journal of physiology* **531,** 375-382.

Grunder S, Thiemann A, Pusch M & Jentsch TJ. (1992). Regions involved in the opening of CIC-2 chloride channel by voltage and cell volume. *Nature* **360,** 759-762.

Gstraunthaler G, Seppi T & Pfaller W. (1999). Impact of culture conditions, culture media volumes, and glucose content on metabolic properties of renal epithelial cell cultures. Are renal cells in tissue culture hypoxic? *Cell Physiol Biochem* **9,** 150-172.

Gundersen D, Orlowski J & Rodriguez-Boulan E. (1991). Apical polarity of Na,K-ATPase in retinal pigment epithelium is linked to a reversal of the ankyrin-fodrin submembrane cytoskeleton. *The Journal of cell biology* **112,** 863-872.

Hamann S, Kiilgaard JF, la Cour M, Prause JU & Zeuthen T. (2003). Cotransport of H+, lactate, and H2O in porcine retinal pigment epithelial cells. *Experimental eye research* **76,** 493-504.

Hartzell C, Putzier I & Arreola J. (2005). Calcium-activated chloride channels. *Annual review of physiology* **67,** 719-758.

Hartzell HC & Qu Z. (2003). Chloride currents in acutely isolated Xenopus retinal pigment epithelial cells. *The Journal of physiology* **549,** 453-469.

Helczynska K, Kronblad A, Jogi A, Nilsson E, Beckman S, Landberg G & Pahlman S. (2003). Hypoxia promotes a dedifferentiated phenotype in ductal breast carcinoma in situ. *Cancer research* **63,** 1441-1444.

Hermansen L. (1981). Effect of metabolic changes on force generation in skeletal muscle during maximal exercise. *Ciba Foundation symposium* **82,** 75-88.

Higgins DF, Kimura K, Bernhardt WM, Shrimanker N, Akai Y, Hohenstein B, Saito Y, Johnson RS, Kretzler M, Cohen CD, Eckardt KU, Iwano M & Haase VH. (2007). Hypoxia promotes fibrogenesis in vivo via HIF-1 stimulation of epithelial-to-mesenchymal transition. *The Journal of clinical investigation* **117,** 3810-3820.

Higgins DF, Kimura K, Iwano M & Haase VH. (2008). Hypoxia-inducible factor signaling in the development of tissue fibrosis. *Cell cycle (Georgetown, Tex* **7,** 1128-1132.

Hori K, Katayama N, Kachi S, Kondo M, Kadomatsu K, Usukura J, Muramatsu T, Mori S & Miyake Y. (2000). Retinal dysfunction in basigin deficiency. *Investigative ophthalmology & visual science* **41,** 3128-3133.

Hu J & Bok D. (2001). A cell culture medium that supports the differentiation of human retinal pigment epithelium into functionally polarized monolayers. *Molecular vision* **7,** 14-19.

Hughes BA, Adorante JS, Miller SS & Lin H. (1989). Apical electrogenic NaHCO3 cotransport. A mechanism for HCO3 absorption across the retinal pigment epithelium. *The Journal of general physiology* **94,** 125-150.

Hughes BA, Gallemore RP & Miller SS. (1998). Transport mechanisms in the retinal pigment epithelium. In *The retinal pigment epithelium*, ed. Marmor MF & Wolfensberger TJ, pp. 103-134. Oxford University Press, New York.

Hughes BA, Miller SS & Machen TE. (1984). Effects of cyclic AMP on fluid absorption and ion transport across frog retinal pigment epithelium. Measurements in the open-circuit state. *The Journal of general physiology* **83,** 875-899.

Hughes BA & Swaminathan A. (2008). Modulation of the Kir7.1 potassium channel by extracellular and intracellular pH. *Am J Physiol Cell Physiol* **294,** C423-431.

Hughes BA, Takahira M & Segawa Y. (1995). An outwardly rectifying K+ current active near resting potential in human retinal pigment epithelial cells. *The American journal of physiology* **269,** C179-187.

Ishida K, Yoshimura N, Yoshida M, Honda Y, Murase K & Hayashi K. (1997). Expression of neurotrophic factors in cultured human retinal pigment epithelial cells. *Current eye research* **16,** 96-101.

Jablonski MM, Tombran-Tink J, Mrazek DA & Iannaccone A. (2000). Pigment epithelium-derived factor supports normal development of photoreceptor neurons and opsin expression after retinal pigment epithelium removal. *J Neurosci* **20,** 7149-7157.

Jackson VN & Halestrap AP. (1996). The kinetics, substrate, and inhibitor specificity of the monocarboxylate (lactate) transporter of rat liver cells determined using the fluorescent intracellular pH indicator, 2',7'-bis(carboxyethyl)-5(6)-carboxyfluorescein. *The Journal of biological chemistry* **271,** 861-868.

Jaitovich AA & Bertorello AM. (2006). Na+, K+ -ATPase: an indispensable ion pumping-signaling mechanism across mammalian cell membranes. *Seminars in nephrology* **26,** 386-392.

Jogi A, Ora I, Nilsson H, Lindeheim A, Makino Y, Poellinger L, Axelson H & Pahlman S. (2002). Hypoxia alters gene expression in human neuroblastoma cells toward an immature and neural crest-like phenotype. *Proceedings of the National Academy of Sciences of the United States of America* **99,** 7021-7026.

Jordt SE & Jentsch TJ. (1997). Molecular dissection of gating in the ClC-2 chloride channel. *The EMBO journal* **16,** 1582-1592.

Joseph DP & Miller SS. (1991). Apical and basal membrane ion transport mechanisms in bovine retinal pigment epithelium. *The Journal of physiology* **435,** 439-463.

Kennedy KM & Dewhirst MW. (2010). Tumor metabolism of lactate: the influence and therapeutic potential for MCT and CD147 regulation. *Future oncology (London, England)* **6,** 127-148.

Kenyon E, Maminishkis A, Joseph DP & Miller SS. (1997). Apical and basolateral membrane mechanisms that regulate pHi in bovine retinal pigment epithelium. *The American journal of physiology* **273,** C456-472.

Kenyon E, Yu K, La Cour M & Miller SS. (1994). Lactate transport mechanisms at apical and basolateral membranes of bovine retinal pigment epithelium. *The American journal of physiology* **267,** C1561-1573.

Kevany BM & Palczewski K. (2010). Phagocytosis of retinal rod and cone photoreceptors. *Physiology (Bethesda, Md* **25,** 8-15.

Kimble EA, Svoboda RA & Ostroy SE. (1980). Oxygen consumption and ATP changes of the vertebrate photoreceptor. *Experimental eye research* **31,** 271-288.

King GL & Suzuma K. (2000). Pigment-epithelium-derived factor--a key coordinator of retinal neuronal and vascular functions. *The New England journal of medicine* **342,** 349-351.

Kita M & Marmor MF. (1992). Retinal adhesive force in living rabbit, cat, and monkey eyes. Normative data and enhancement by mannitol and acetazolamide. *Investigative ophthalmology & visual science* **33,** 1879-1882.

Koenekoop RK. (2007). Choroideremia is caused by a defective phagocytosis by the RPE of photoreceptor disc membranes, not by an intrinsic photoreceptor defect. *Ophthalmic genetics* **28,** 185-186.

Krizaj D & Copenhagen DR. (1998). Compartmentalization of calcium extrusion mechanisms in the outer and inner segments of photoreceptors. *Neuron* **21,** 249-256.

Kurschat CE, Shmukler BE, Jiang L, Wilhelm S, Kim EH, Chernova MN, Kinne RK, Stewart AK & Alper SL. (2006). Alkaline-shifted pHo sensitivity of AE2c1-mediated anion exchange reveals novel regulatory determinants in the AE2 N-terminal cytoplasmic domain. *The Journal of biological chemistry* **281,** 1885-1896.

la Cour M, Lin H, Kenyon E & Miller SS. (1994). Lactate transport in freshly isolated human fetal retinal pigment epithelium. *Investigative ophthalmology & visual science* **35,** 434-442.

Lamb TD & Pugh EN, Jr. (2004). Dark adaptation and the retinoid cycle of vision. *Progress in retinal and eye research* **23,** 307-380.

Leiderman YI & Miller JW. (2009). Proliferative vitreoretinopathy: pathobiology and therapeutic targets. *Seminars in ophthalmology* **24,** 62-69.

Leung KW, Liu M, Xu X, Seiler MJ, Barnstable CJ & Tombran-Tink J. (2008). Expression of ZnT and ZIP zinc transporters in the human RPE and their regulation by neurotrophic factors. *Investigative ophthalmology & visual science* **49,** 1221-1231.

Lewis G, Mervin K, Valter K, Maslim J, Kappel PJ, Stone J & Fisher S. (1999). Limiting the proliferation and reactivity of retinal Muller cells during experimental retinal detachment: the value of oxygen supplementation. *American journal of ophthalmology* **128,** 165-172.

Li JD, Gallemore RP, Dmitriev A & Steinberg RH. (1994a). Light-dependent hydration of the space surrounding photoreceptors in chick retina. *Investigative ophthalmology & visual science* **35,** 2700-2711.

Li JD, Govardovskii VI & Steinberg RH. (1994b). Light-dependent hydration of the space surrounding photoreceptors in the cat retina. *Visual neuroscience* **11,** 743-752.

Li R, Maminishkis A, Banzon T, Wan Q, Jalickee S, Chen S & Miller SS. (2009). IFN{gamma} Regulates Retinal Pigment Epithelial Fluid Transport. *Am J Physiol Cell Physiol*.

Li R, Maminishkis A, Wang FE & Miller SS. (2007). PDGF-C and -D induced proliferation/migration of human RPE is abolished by inflammatory cytokines. *Investigative ophthalmology & visual science* **48,** 5722-5732.

Liebman PA, Mueller P & Pugh EN, Jr. (1984). Protons suppress the dark current of frog retinal rods. *The Journal of physiology* **347,** 85-110.

Lin H, Kenyon E & Miller SS. (1992). Na-dependent pHi regulatory mechanisms in native human retinal pigment epithelium. *Investigative ophthalmology & visual science* **33,** 3528-3538.

Lin H, la Cour M, Andersen MV & Miller SS. (1994). Proton-lactate cotransport in the apical membrane of frog retinal pigment epithelium. *Experimental eye research* **59,** 679-688.

Lin H & Miller SS. (1994). pHi-dependent Cl-HCO3 exchange at the basolateral membrane of frog retinal pigment epithelium. *The American journal of physiology* **266,** C935-945.

Linsenmeier RA. (1986). Effects of light and darkness on oxygen distribution and consumption in the cat retina. *The Journal of general physiology* **88,** 521-542.

Litchfield TM, Whiteley SJ & Lund RD. (1997). Transplantation of retinal pigment epithelial, photoreceptor and other cells as treatment for retinal degeneration. *Experimental eye research* **64,** 655-666.

Livsey CT, Huang B, Xu J & Karwoski CJ. (1990). Light-evoked changes in extracellular calcium concentration in frog retina. *Vision research* **30,** 853-861.

Loiselle FB, Morgan PE, Alvarez BV & Casey JR. (2004). Regulation of the human NBC3 Na+/HCO3- cotransporter by carbonic anhydrase II and PKA. *Am J Physiol Cell Physiol* **286,** C1423-1433.

Lu H, Dalgard CL, Mohyeldin A, McFate T, Tait AS & Verma A. (2005). Reversible inactivation of HIF-1 prolyl hydroxylases allows cell metabolism to control basal HIF-1. *The Journal of biological chemistry* **280,** 41928-41939.

Lu H, Forbes RA & Verma A. (2002). Hypoxia-inducible factor 1 activation by aerobic glycolysis implicates the Warburg effect in carcinogenesis. *The Journal of biological chemistry* **277,** 23111-23115.

Ma T, Thiagarajah JR, Yang H, Sonawane ND, Folli C, Galietta LJ & Verkman AS. (2002). Thiazolidinone CFTR inhibitor identified by high-throughput screening blocks cholera toxin-induced intestinal fluid secretion. *The Journal of clinical investigation* **110,** 1651-1658.

MacDonald C. (1994). Primary culture and the establishment of cell lines. In *Basic Cell Culture: A Practical Approach* ed. Davis JM, pp. 149-180. IRL Press, Oxford.

Magistretti PJ. (2006). Neuron-glia metabolic coupling and plasticity. *The Journal of experimental biology* **209,** 2304-2311.

Majumdar S, Gunda S, Pal D & Mitra AK. (2005). Functional activity of a monocarboxylate transporter, MCT1, in the human retinal pigmented epithelium cell line, ARPE-19. *Molecular pharmaceutics* **2,** 109-117.

Maminishkis A, Chen S, Jalickee S, Banzon T, Shi G, Wang FE, Ehalt T, Hammer JA & Miller SS. (2006). Confluent monolayers of cultured human fetal retinal pigment epithelium exhibit morphology and physiology of native tissue. *Investigative ophthalmology & visual science* **47,** 3612-3624.

Maminishkis A, Jalickee S, Blaug SA, Rymer J, Yerxa BR, Peterson WM & Miller SS. (2002). The P2Y(2) receptor agonist INS37217 stimulates RPE fluid transport in vitro and retinal reattachment in rat. *Investigative ophthalmology & visual science* **43,** 3555-3566.

Marneros AG, Fan J, Yokoyama Y, Gerber HP, Ferrara N, Crouch RK & Olsen BR. (2005). Vascular endothelial growth factor expression in the retinal pigment

epithelium is essential for choriocapillaris development and visual function. *The American journal of pathology* **167,** 1451-1459.

Martin PM, Dun Y, Mysona B, Ananth S, Roon P, Smith SB & Ganapathy V. (2007). Expression of the sodium-coupled monocarboxylate transporters SMCT1 (SLC5A8) and SMCT2 (SLC5A12) in retina. *Investigative ophthalmology & visual science* **48,** 3356-3363.

McMurtrie HL, Cleary HJ, Alvarez BV, Loiselle FB, Sterling D, Morgan PE, Johnson DE & Casey JR. (2004). The bicarbonate transport metabolon. *Journal of enzyme inhibition and medicinal chemistry* **19,** 231-236.

Medrano CJ & Fox DA. (1995). Oxygen consumption in the rat outer and inner retina: light- and pharmacologically-induced inhibition. *Experimental eye research* **61,** 273-284.

Meyertholen EP, Wilson MJ & Ostroy SE. (1986). The effects of hepes, bicarbonate and calcium on the cGMP content of vertebrate rod photoreceptors and the isolated electrophysiological effects of cGMP and calcium. *Vision research* **26,** 521-533.

Millar ID & Brown PD. (2008). NBCe2 exhibits a 3 HCO3(-):1 Na+ stoichiometry in mouse choroid plexus epithelial cells. *Biochemical and biophysical research communications* **373,** 550-554.

Miller SS & Steinberg RH. (1977). Passive ionic properties of frog retinal pigment epithelium. *The Journal of membrane biology* **36,** 337-372.

Milovanova TN, Bhopale VM, Sorokina EM, Moore JS, Hunt TK, Hauer-Jensen M, Velazquez OC & Thom SR. (2008). Lactate stimulates vasculogenic stem cells via the thioredoxin system and engages an autocrine activation loop involving hypoxia-inducible factor 1. *Molecular and cellular biology* **28,** 6248-6261.

Morgan PE, Pastorekova S, Stuart-Tilley AK, Alper SL & Casey JR. (2007). Interactions of transmembrane carbonic anhydrase, CAIX, with bicarbonate transporters. *Am J Physiol Cell Physiol* **293,** C738-748.

Morris ME & Felmlee MA. (2008). Overview of the proton-coupled MCT (SLC16A) family of transporters: characterization, function and role in the transport of the drug of abuse gamma-hydroxybutyric acid. *The AAPS journal* **10,** 311-321.

Nagelhus EA, Mathiisen TM, Bateman AC, Haug FM, Ottersen OP, Grubb JH, Waheed A & Sly WS. (2005). Carbonic anhydrase XIV is enriched in specific membrane domains of retinal pigment epithelium, Muller cells, and astrocytes. *Proceedings of the National Academy of Sciences of the United States of America* **102,** 8030-8035.

Nakazawa T, Hisatomi T, Nakazawa C, Noda K, Maruyama K, She H, Matsubara A, Miyahara S, Nakao S, Yin Y, Benowitz L, Hafezi-Moghadam A & Miller JW. (2007). Monocyte chemoattractant protein 1 mediates retinal detachment-induced photoreceptor apoptosis. *Proceedings of the National Academy of Sciences of the United States of America* **104,** 2425-2430.

Nelson WJ. (2003). Adaptation of core mechanisms to generate cell polarity. *Nature* **422,** 766-774.

Nguyen-Legros J & Hicks D. (2000). Renewal of photoreceptor outer segments and their phagocytosis by the retinal pigment epithelium. *International review of cytology* **196,** 245-313.

Nilius B, Eggermont J, Voets T, Buyse G, Manolopoulos V & Droogmans G. (1997). Properties of volume-regulated anion channels in mammalian cells. *Progress in biophysics and molecular biology* **68,** 69-119.

Okami T, Yamamoto A, Omori K, Takada T, Uyama M & Tashiro Y. (1990). Immunocytochemical localization of Na+,K(+)-ATPase in rat retinal pigment epithelial cells. *J Histochem Cytochem* **38,** 1267-1275.

Okawa H, Sampath AP, Laughlin SB & Fain GL. (2008). ATP consumption by mammalian rod photoreceptors in darkness and in light. *Curr Biol* **18,** 1917-1921.

Olver JM. (1990). Functional anatomy of the choroidal circulation: methyl methacrylate casting of human choroid. *Eye (London, England)* **4 (Pt 2),** 262-272.

Oyster CW. (1999). *The Human Eye: Structure and Function*. Sinauer associates, Inc., Sunderland, MA.

Padnick-Silver L & Linsenmeier RA. (2002). Quantification of in vivo anaerobic metabolism in the normal cat retina through intraretinal pH measurements. *Visual neuroscience* **19,** 793-806.

Panfoli I, Calzia D, Bianchini P, Ravera S, Diaspro A, Candiano G, Bachi A, Monticone M, Aluigi MG, Barabino S, Calabria G, Rolando M, Tacchetti C, Morelli A & Pepe IM. (2009). Evidence for aerobic metabolism in retinal rod outer segment disks. *The international journal of biochemistry & cell biology* **41,** 2555-2565.

Parapuram SK, Chang B, Li L, Hartung RA, Chalam KV, Nair-Menon JU, Hunt DM & Hunt RC. (2009). Differential effects of TGFbeta and vitreous on the transformation of retinal pigment epithelial cells. *Investigative ophthalmology & visual science* **50,** 5965-5974.

Pastor JC. (1998). Proliferative vitreoretinopathy: an overview. *Survey of ophthalmology* **43,** 3-18.

Pellerin L. (2008). Brain energetics (thought needs food). *Current opinion in clinical nutrition and metabolic care* **11,** 701-705.

Pellerin L, Bouzier-Sore AK, Aubert A, Serres S, Merle M, Costalat R & Magistretti PJ. (2007). Activity-dependent regulation of energy metabolism by astrocytes: an update. *Glia* **55,** 1251-1262.

Peter JB, Sawaki S, Barnard RJ, Edgerton VR & Gillespie CA. (1971). Lactate dehydrogenase isoenzymes: distribution in fast-twitch red, fast-twitch white, and slow-twitch intermediate fibers of guinea pig skeletal muscle. *Archives of biochemistry and biophysics* **144,** 304-307.

Pettersen EO, Larsen LH, Ramsing NB & Ebbesen P. (2005). Pericellular oxygen depletion during ordinary tissue culturing, measured with oxygen microsensors. *Cell proliferation* **38,** 257-267.

Philp A, Macdonald AL & Watt PW. (2005). Lactate--a signal coordinating cell and systemic function. *The Journal of experimental biology* **208,** 4561-4575.

Philp NJ, Ochrietor JD, Rudoy C, Muramatsu T & Linser PJ. (2003a). Loss of MCT1, MCT3, and MCT4 expression in the retinal pigment epithelium and neural retina of the 5A11/basigin-null mouse. *Investigative ophthalmology & visual science* **44,** 1305-1311.

Philp NJ, Wang D, Yoon H & Hjelmeland LM. (2003b). Polarized expression of monocarboxylate transporters in human retinal pigment epithelium and ARPE-19 cells. *Investigative ophthalmology & visual science* **44,** 1716-1721.

Philp NJ, Yoon H & Grollman EF. (1998). Monocarboxylate transporter MCT1 is located in the apical membrane and MCT3 in the basal membrane of rat RPE. *The American journal of physiology* **274,** R1824-1828.

Philp NJ, Yoon H & Lombardi L. (2001). Mouse MCT3 gene is expressed preferentially in retinal pigment and choroid plexus epithelia. *Am J Physiol Cell Physiol* **280,** C1319-1326.

Poitry-Yamate CL, Poitry S & Tsacopoulos M. (1995). Lactate released by Muller glial cells is metabolized by photoreceptors from mammalian retina. *J Neurosci* **15,** 5179-5191.

Poitry S, Poitry-Yamate C, Ueberfeld J, MacLeish PR & Tsacopoulos M. (2000). Mechanisms of glutamate metabolic signaling in retinal glial (Muller) cells. *J Neurosci* **20,** 1809-1821.

Praetorius J. (2007). Water and solute secretion by the choroid plexus. *Pflugers Arch* **454,** 1-18.

Pushkin A, Abuladze N, Gross E, Newman D, Tatishchev S, Lee I, Fedotoff O, Bondar G, Azimov R, Ngyuen M & Kurtz I. (2004). Molecular mechanism of kNBC1-carbonic anhydrase II interaction in proximal tubule cells. *The Journal of physiology* **559,** 55-65.

Quinn RH, Quong JN & Miller SS. (2001). Adrenergic receptor activated ion transport in human fetal retinal pigment epithelium. *Investigative ophthalmology & visual science* **42,** 255-264.

Rahner C, Fukuhara M, Peng S, Kojima S & Rizzolo LJ. (2004). The apical and basal environments of the retinal pigment epithelium regulate the maturation of tight junctions during development. *J Cell Sci* **117,** 3307-3318.

Rando RR. (1991). Membrane phospholipids as an energy source in the operation of the visual cycle. *Biochemistry* **30,** 595-602.

Rizzolo LJ. (1990). The distribution of Na+,K(+)-ATPase in the retinal pigmented epithelium from chicken embryo is polarized in vivo but not in primary cell culture. *Experimental eye research* **51,** 435-446.

Rizzolo LJ. (1991). Basement membrane stimulates the polarized distribution of integrins but not the Na,K-ATPase in the retinal pigment epithelium. *Cell regulation* **2,** 939-949.

Rizzolo LJ. (1999). Polarization of the Na+, K(+)-ATPase in epithelia derived from the neuroepithelium. *International review of cytology* **185,** 195-235.

Rizzolo LJ. (2007). Development and role of tight junctions in the retinal pigment epithelium. *International review of cytology* **258,** 195-234.

Rothen-Rutishauser B, Riesen FK, Braun A, Gunthert M & Wunderli-Allenspach H. (2002). Dynamics of tight and adherens junctions under EGTA treatment. *The Journal of membrane biology* **188,** 151-162.

Saika S, Kono-Saika S, Tanaka T, Yamanaka O, Ohnishi Y, Sato M, Muragaki Y, Ooshima A, Yoo J, Flanders KC & Roberts AB. (2004). Smad3 is required for dedifferentiation of retinal pigment epithelium following retinal detachment in mice. *Laboratory investigation; a journal of technical methods and pathology* **84,** 1245-1258.

Saito Y & Wright EM. (1983). Bicarbonate transport across the frog choroid plexus and its control by cyclic nucleotides. *The Journal of physiology* **336,** 635-648.

Saito Y & Wright EM. (1984). Regulation of bicarbonate transport across the brush border membrane of the bull-frog choroid plexus. *The Journal of physiology* **350,** 327-342.

Sawada N, Murata M, Kikuchi K, Osanai M, Tobioka H, Kojima T & Chiba H. (2003). Tight junctions and human diseases. *Med Electron Microsc* **36,** 147-156.

Schlingemann RO. (2004). Role of growth factors and the wound healing response in age-related macular degeneration. *Graefe's archive for clinical and experimental ophthalmology = Albrecht von Graefes Archiv fur klinische und experimentelle Ophthalmologie* **242,** 91-101.

Schultz BD, Singh AK, Devor DC & Bridges RJ. (1999). Pharmacology of CFTR chloride channel activity. *Physiological reviews* **79,** S109-144.

Scozzafava A & Supuran CT. (2002). Carbonic anhydrase activators: human isozyme II is strongly activated by oligopeptides incorporating the carboxyterminal sequence of the bicarbonate anion exchanger AE1. *Bioorganic & medicinal chemistry letters* **12,** 1177-1180.

Semenza GL. (2003). Targeting HIF-1 for cancer therapy. *Nature reviews* **3,** 721-732.

Sheu SJ, Wu SN, Hu DN & Chen JF. (2004). The influence of hypotonicity on large-conductance calcium-activated potassium channels in human retinal pigment epithelial cells. *J Ocul Pharmacol Ther* **20,** 563-575.

Shi G, Maminishkis A, Banzon T, Jalickee S, Li R, Hammer J & Miller SS. (2008). Control of chemokine gradients by the retinal pigment epithelium. *Investigative ophthalmology & visual science* **49,** 4620-4630.

Shimura M, Yuan Y, Chang JT, Zhang S, Campochiaro PA, Zack DJ & Hughes BA. (2001). Expression and permeation properties of the K(+) channel Kir7.1 in the retinal pigment epithelium. *The Journal of physiology* **531,** 329-346.

Shin K, Fogg VC & Margolis B. (2006). Tight junctions and cell polarity. *Annual review of cell and developmental biology* **22,** 207-235.

Sillman AJ, Owen WG & Fernandez HR. (1972). The generation of the late receptor potential: an excitation-inhibition phenomenon. *Vision research* **12,** 1519-1531.

Stamer WD, Bok D, Hu J, Jaffe GJ & McKay BS. (2003). Aquaporin-1 channels in human retinal pigment epithelium: role in transepithelial water movement. *Investigative ophthalmology & visual science* **44,** 2803-2808.

Steinberg RH, Linsenmeier RA & Griff ER. (1983). Three light-evoked responses of the retinal pigment epithelium. *Vision research* **23,** 1315-1323.

Sterling D, Reithmeier RA & Casey JR. (2001). A transport metabolon. Functional interaction of carbonic anhydrase II and chloride/bicarbonate exchangers. *The Journal of biological chemistry* **276,** 47886-47894.

Stewart AK, Kurschat CE & Alper SL. (2007). Role of nonconserved charged residues of the AE2 transmembrane domain in regulation of anion exchange by pH. *Pflugers Arch* **454,** 373-384.

Stone J, Maslim J, Valter-Kocsi K, Mervin K, Bowers F, Chu Y, Barnett N, Provis J, Lewis G, Fisher SK, Bisti S, Gargini C, Cervetto L, Merin S & Peer J. (1999). Mechanisms of photoreceptor death and survival in mammalian retina. *Progress in retinal and eye research* **18,** 689-735.

Stone J, van Driel D, Valter K, Rees S & Provis J. (2008). The locations of mitochondria in mammalian photoreceptors: relation to retinal vasculature. *Brain research* **1189,** 58-69.

Strauss O. (2005). The retinal pigment epithelium in visual function. *Physiological reviews* **85,** 845-881.

Strauss O, Richard G & Wienrich M. (1993). Voltage-dependent potassium currents in cultured human retinal pigment epithelial cells. *Biochemical and biophysical research communications* **191,** 775-781.

Strauss O, Rosenthal R, Dey D, Beninde J, Wollmann G, Thieme H & Wiederholt M. (2002). Effects of protein kinase C on delayed rectifier K+ channel regulation by tyrosine kinase in rat retinal pigment epithelial cells. *Investigative ophthalmology & visual science* **43,** 1645-1654.

Svichar N, Esquenazi S, Waheed A, Sly WS & Chesler M. (2006). Functional demonstration of surface carbonic anhydrase IV activity on rat astrocytes. *Glia* **53,** 241-247.

Svichar N, Waheed A, Sly WS, Hennings JC, Hubner CA & Chesler M. (2009). Carbonic anhydrases CA4 and CA14 both enhance AE3-mediated Cl--HCO3- exchange in hippocampal neurons. *J Neurosci* **29,** 3252-3258.

Takahashi K, Dixon DB & Copenhagen DR. (1993). Modulation of a sustained calcium current by intracellular pH in horizontal cells of fish retina. *The Journal of general physiology* **101,** 695-714.

Terry S, Nie M, Matter K & Balda MS. (2010). Rho signaling and tight junction functions. *Physiology (Bethesda, Md* **25,** 16-26.

Thiemann A, Grunder S, Pusch M & Jentsch TJ. (1992). A chloride channel widely expressed in epithelial and non-epithelial cells. *Nature* **356,** 57-60.

Ullah MS, Davies AJ & Halestrap AP. (2006). The plasma membrane lactate transporter MCT4, but not MCT1, is up-regulated by hypoxia through a HIF-1alpha-dependent mechanism. *The Journal of biological chemistry* **281,** 9030-9037.

Valtink M & Engelmann K. (2009). Culturing of retinal pigment epithelium cells. *Developments in ophthalmology* **43,** 109-119.

Vince JW, Carlsson U & Reithmeier RA. (2000). Localization of the Cl-/HCO3- anion exchanger binding site to the amino-terminal region of carbonic anhydrase II. *Biochemistry* **39,** 13344-13349.

Vince JW & Reithmeier RA. (2000). Identification of the carbonic anhydrase II binding site in the Cl(-)/HCO(3)(-) anion exchanger AE1. *Biochemistry* **39,** 5527-5533.

Virkki LV, Wilson DA, Vaughan-Jones RD & Boron WF. (2002). Functional characterization of human NBC4 as an electrogenic Na+-HCO cotransporter (NBCe2). *Am J Physiol Cell Physiol* **282,** C1278-1289.

Vogh BP, Godman DR & Maren TH. (1987). Effect of AlCl3 and other acids on cerebrospinal fluid production: a correction. *The Journal of pharmacology and experimental therapeutics* **243,** 35-39.

Vogh BP & Maren TH. (1975). Sodium, chloride, and bicarbonate movement from plasma to cerebrospinal fluid in cats. *The American journal of physiology* **228,** 673-683.

Vollrath D, Feng W, Duncan JL, Yasumura D, D'Cruz PM, Chappelow A, Matthes MT, Kay MA & LaVail MM. (2001). Correction of the retinal dystrophy phenotype of the RCS rat by viral gene transfer of Mertk. *Proceedings of the National Academy of Sciences of the United States of America* **98,** 12584-12589.

Vugler A, Carr AJ, Lawrence J, Chen LL, Burrell K, Wright A, Lundh P, Semo M, Ahmado A, Gias C, da Cruz L, Moore H, Andrews P, Walsh J & Coffey P. (2008). Elucidating the phenomenon of HESC-derived RPE: anatomy of cell genesis, expansion and retinal transplantation. *Experimental neurology* **214,** 347-361.

Waisbren SJ, Geibel JP, Modlin IM & Boron WF. (1994). Unusual permeability properties of gastric gland cells. *Nature* **368,** 332-335.

Wang L, Kondo M & Bill A. (1997a). Glucose metabolism in cat outer retina. Effects of light and hyperoxia. *Investigative ophthalmology & visual science* **38,** 48-55.

Wang L, Tornquist P & Bill A. (1997b). Glucose metabolism in pig outer retina in light and darkness. *Acta physiologica Scandinavica* **160,** 75-81.

Wangsa-Wirawan ND & Linsenmeier RA. (2003). Retinal oxygen: fundamental and clinical aspects. *Archives of ophthalmology* **121,** 547-557.

Weintraub WH & Machen TE. (1989). pH regulation in hepatoma cells: roles for Na-H exchange, Cl-HCO3 exchange, and Na-HCO3 cotransport. *The American journal of physiology* **257,** G317-327.

Weng TX, Godley BF, Jin GF, Mangini NJ, Kennedy BG, Yu AS & Wills NK. (2002). Oxidant and antioxidant modulation of chloride channels expressed in human retinal pigment epithelium. *Am J Physiol Cell Physiol* **283,** C839-849.

Wetzel P, Hasse A, Papadopoulos S, Voipio J, Kaila K & Gros G. (2001). Extracellular carbonic anhydrase activity facilitates lactic acid transport in rat skeletal muscle fibres. *The Journal of physiology* **531,** 743-756.

Wickham L & Charteris DG. (2009). Glial cell changes of the human retina in proliferative vitreoretinopathy. *Developments in ophthalmology* **44,** 37-45.

Wickham L, Sethi CS, Lewis GP, Fisher SK, McLeod DC & Charteris DG. (2006). Glial and neural response in short-term human retinal detachment. *Archives of ophthalmology* **124,** 1779-1782.

Wills NK, Weng T, Mo L, Hellmich HL, Yu A, Wang T, Buchheit S & Godley BF. (2000). Chloride channel expression in cultured human fetal RPE cells: response to oxidative stress. *Investigative ophthalmology & visual science* **41,** 4247-4255.

Winkler BS, Arnold MJ, Brassell MA & Puro DG. (2000). Energy metabolism in human retinal Muller cells. *Investigative ophthalmology & visual science* **41,** 3183-3190.

Winkler BS, Starnes CA, Sauer MW, Firouzgan Z & Chen SC. (2004). Cultured retinal neuronal cells and Muller cells both show net production of lactate. *Neurochemistry international* **45,** 311-320.

Winkler BS, Starnes CA, Twardy BS, Brault D & Taylor RC. (2008). Nuclear magnetic resonance and biochemical measurements of glucose utilization in the cone-dominant ground squirrel retina. *Investigative ophthalmology & visual science* **49,** 4613-4619.

Wolfensberger TJ. (1999). The role of carbonic anhydrase inhibitors in the management of macular edema. *Documenta ophthalmologica* **97,** 387-397.

Wolfensberger TJ, Chiang RK, Takeuchi A & Marmor MF. (2000). Inhibition of membrane-bound carbonic anhydrase enhances subretinal fluid absorption and

retinal adhesiveness. *Graefe's archive for clinical and experimental ophthalmology = Albrecht von Graefes Archiv fur klinische und experimentelle Ophthalmologie* **238,** 76-80.

Wolfensberger TJ, Mahieu I, Jarvis-Evans J, Boulton M, Carter ND, Nogradi A, Hollande E & Bird AC. (1994). Membrane-bound carbonic anhydrase in human retinal pigment epithelium. *Investigative ophthalmology & visual science* **35,** 3401-3407.

Wright A, Brearey S & Imray C. (2008). High hopes at high altitudes: pharmacotherapy for acute mountain sickness and high-altitude cerebral and pulmonary oedema. *Expert opinion on pharmacotherapy* **9,** 119-127.

Xiong H, Li C, Garami E, Wang Y, Ramjeesingh M, Galley K & Bear CE. (1999). ClC-2 activation modulates regulatory volume decrease. *The Journal of membrane biology* **167,** 215-221.

Xu J, Peng Z, Li R, Dou T, Xu W, Gu G, Liu Y, Kang Z, Tao H, Zhang JH, Ostrowski RP, Lu J & Sun X. (2009). Normoxic induction of cerebral HIF-1alpha by acetazolamide in rats: role of acidosis. *Neuroscience letters* **451,** 274-278.

Yamamoto F, Borgula GA & Steinberg RH. (1992). Effects of light and darkness on pH outside rod photoreceptors in the cat retina. *Experimental eye research* **54,** 685-697.

Yang D, Pan A, Swaminathan A, Kumar G & Hughes BA. (2003). Expression and localization of the inwardly rectifying potassium channel Kir7.1 in native bovine retinal pigment epithelium. *Investigative ophthalmology & visual science* **44,** 3178-3185.

Yang D, Swaminathan A, Zhang X & Hughes BA. (2008a). Expression of Kir7.1 and a novel Kir7.1 splice variant in native human retinal pigment epithelium. *Experimental eye research* **86,** 81-91.

Yang D, Zhang X & Hughes BA. (2008b). Expression of inwardly rectifying potassium channel subunits in native human retinal pigment epithelium. *Experimental eye research* **87,** 176-183.

Yau KW & Hardie RC. (2009). Phototransduction motifs and variations. *Cell* **139,** 246-264.

Yu DY & Cringle SJ. (2001). Oxygen distribution and consumption within the retina in vascularised and avascular retinas and in animal models of retinal disease. *Progress in retinal and eye research* **20,** 175-208.

Yu DY & Cringle SJ. (2002). Outer retinal anoxia during dark adaptation is not a general property of mammalian retinas. *Comparative biochemistry and physiology* **132,** 47-52.

Yuan Y, Shimura M & Hughes BA. (2003). Regulation of inwardly rectifying K+ channels in retinal pigment epithelial cells by intracellular pH. *The Journal of physiology* **549,** 429-438.

Zeidel ML, Silva P & Seifter JL. (1986). Intracellular pH regulation in rabbit renal medullary collecting duct cells. Role of chloride-bicarbonate exchange. *The Journal of clinical investigation* **77,** 1682-1688.

Zeuthen T. (2000). Molecular water pumps. *Reviews of physiology, biochemistry and pharmacology* **141,** 97-151.

Zeuthen T, Hamann S & la Cour M. (1996). Cotransport of H+, lactate and H2O by membrane proteins in retinal pigment epithelium of bullfrog. *The Journal of physiology* **497 (Pt 1),** 3-17.

Zhi CG, Wang FE, Banzon T, Jalickee S, Fariss R, Maminishkis A & Miller SS. (2007). Membrane-Bound Carbonic Anhydrases in Human Fetal Retinal Pigment Epithelial Cells (hfRPE). In *ARVO 2007*. Fort Lauderdale, FL.

Zieker D, Schafer R, Glatzle J, Nieselt K, Coerper S, Kluba T, Northoff H, Konigsrainer A, Hunt TK & Beckert S. (2008). Lactate modulates gene expression in human mesenchymal stem cells. *Langenbeck's archives of surgery / Deutsche Gesellschaft fur Chirurgie* **393,** 297-301.